TECHNISCHE UNIVERSITÄT MÜNCHEN

TUM SCHOOL OF LIFE SCIENCES

Monitoring tree vitality by terrestrial laser scanning (TLS): reaction pattern of stem, crown and defoliation

Martin Jacobs

Vollständiger Abdruck der von der TUM School of Life Sciences der Technischen Universität München zur Erlangung des akademischen Grades eines

Doktors der Naturwissenschaften (Dr. rer. nat.)

genehmigten Dissertation.

Vorsitzender:	Prof. Dr. Thomas Knoke
Prüfende der Dissertation:	1. Prof. Dr. Dr. h.c. Hans Pretzsch
	2. Prof. Dr. Wolfgang Weisser

Die Dissertation wurde am 16.05.2022 bei der Technischen Universität München eingereicht und durch die TUM School of Life Sciences am 03.11.2022 angenommen.

Acknowledgements

I would like to express my deepest gratitude to everyone who supported me during my doctoral studies.

First of all, I want to express my gratitude to Prof. Dr. Dr. h.c. Hans Pretzsch, my supervisor, for his continuous encouragement and inspiring mentoring. He believed in me and gave me this opportunity. Furthermore, I thank Prof. Dr. Wolfgang Weisser for serving as examiner, as well as Prof. Dr. Thomas Knoke for chairing the examination committee. I want to thank my colleagues at the Chair of Forest Growth and Yield Science at the Technical University of Munich for many helpful and interesting conversations. Special thanks are due to Dr. Andreas Rais, my mentor, who guided me in the right direction when I did not know what to do, to Dr. Peter Biber for his valuable support of the statistical evaluation, and to Enno Uhl for his organizational support. In particular, I also thank Beate Felsl for her warm and helpful support in the secretary's office.

Furthermore, I thank the Federal Ministry of Education and Research (BMBF, Bundesministerium für Bildung und Forschung) who funded the FORSENSE project (grant agreement no. 033RK046A) within the "KMU-innovativ" call. Additional funding was received from the European Union's Horizon 2020 Research and Innovation Programme under the Marie Skłodowska-Curie (grant agreement no. 778322). Furthermore, the research was funded by grant number Z073 administered by the Bavarian State Ministry for Food, Agriculture and Forests (Bayerischen Staatsministerium für Ernährung, Landwirtschaft und Forsten).

Finally, I want to thank my family and close friends. My gratitude goes to my wife, my love, Carlotta for having my back at all times, and to our son Ron. I dedicate this work to my father, who has supported me since I was born.

Table of contents

Abstract

Tree vitality is one of the most important indicators for describing forest conditions. In temperate forests, stress factors such as insect infestation, diseases, competition, and climate have strong effects on tree growth and survival. Monitoring tree vitality and developing new indicators is important for detecting early-stage tree stress and identifying rapid environmental changes. In addition, most indicators, especially those involving crown and stem form characteristics, have been estimated rather than measured. Consequently, there is a need for more empirical and accurate methods that can detect, quantify, and apply tree characteristics and, therefore, potential indicators of tree vitality. The main objective of this dissertation is to contribute to a more objective forest inventory and tree vitality monitoring, thus improving our understanding of the reaction pattern of tree stems, crowns and defoliation.

Using terrestrial laser scanning (TLS), innovative methods are demonstrated for the efficient monitoring of tree vitality by investigating the reaction pattern of tree shape to stress for species like Norway spruce (*Picea abies* (L.) H. Karst), European beech (*Fagus sylvatica* L.) and oak trees (*Quercus* L.). Competition, drought, and insect-induced defoliation led to stem form changes, decreasing crown size and stem growth, respectively.

Using TLS, the stem shape of 868 *Picea abies* trees from a long-term spacing and thinning experiment in Germany were measured (Jacobs et al. 2020, Appendix B.1. Article I). The plots cover a broad density range. The effect of competition was analysed and the TLS with conventionally determined stem volume estimates were compared. TLS-based volume estimations showed that the lower the competition, the lower the tree volume with a given diameter at breast height ($d_{1.3}$) and height (h). Commonly used functions underestimate the volume stock overall by 4.2 %, disregarding any levels. At plot level, underestimation varies from 0.7 to 7.0 %. At tree level, the volume was underestimated and overestimated by –10 to +10 %. The more precise the examination, the more suitable the application of TLS for enhancing volume estimation.

The unique drought stress experiment, “Kranzberg Forest Roof Experiment” (KROOF), was used as a basis for scanning and analyzing the growth of Norway spruce (*Picea abies* (L.) H.Karst.) and European beech (*Fagus sylvatica* L.) under progressively limiting water reserves (Jacobs et al. 2021, Appendix B.2. Article II). Before the start of the experiment in the winter of 2012/2013, TLS was performed and repeated in the winter of 2018/2019. One group of 21 trees was trenched and roofed (treatment), while another group of 26 trees acted as reference

(control). Using TLS point clouds from the two subsequent surveys, structural tree modifications within the 6-year period can be directly visualized, computed, and linked to drought stress. Drought stress led to significantly smaller crown size and lower height growth for both tree species. Under drought conditions, the crown projection area changed by –0.74 m^2 yr^{-1} and –0.42 m^2 yr^{-1} for spruce and beech trees, respectively, whereas the control trees showed a growth of 0.17 m^2 yr^{-1} and 0.62 m^2 yr^{-1} respectively. This means that crowns became considerably smaller under dry conditions. Under drought, the pai_{height} was 0.09 m yr^{-1} less for spruce and 0.17 m yr^{-1} less for beech compared with normal growing conditions.

Using on a large-scale field experiment in German oak and mixed oak forests affected by gypsy moths (*Lymantria dispar*), the use of TLS for detecting inter-annual foliation and growth losses at the individual tree level caused by the gypsy moth was tested (Jacobs et al. 2022, Appendix B.3. Article III). The experiment comprised two levels of gypsy moth defoliation risk – high (H) and low (L) – as well as two pest control treatment levels: spraying with the insecticide Mimic (M) or unsprayed control (C). The factorial design consisted of four treatment combinations (HC, HM, LC and LM), applied to 11 spatial blocks with a total of 44 plots. The TLS approach detected defoliation caused by the gypsy moth, which was calculated in terms of leaf area and crown perforation parameters. For the first time, TLS-derived tree foliation was evaluated based on inter-annual stem growth. Leaf area and crown perforation showed a correlation of +0.6 and –0.35, respectively, with basal area increments. Furthermore, this study revealed subsequent growth losses in the same year due to defoliation.

The findings of this dissertation suggest that TLS can offer new opportunities for identifying structural features and developing new indicators that can monitor stem form, crown shape, and foliation at the individual tree level. It is demonstrated that iterative TLS surveys might improve measuring campaigns on common long-term experimental plots in order to obtain a thorough picture of tree vitality. Accurate measurements of crown dimensions are also essential for modelling tree growth. For example, crown shapes may change due to the impacts of climate change. Therefore, crown models contained within tree growth models must be questioned, as must the derived allometries. The increasing frequency of extreme and extensive drought events makes it even more important to consider drought stress effects or insect-induced defoliation in forest practice and ecological modelling.

Zusammenfassung

Die Vitalität der Bäume ist einer der wichtigsten Indikatoren zur Beschreibung des Waldzustands. In gemäßigten Wäldern haben Stressfaktoren wie Insektenbefall, Krankheiten, Konkurrenz und Klima starke Auswirkungen auf das Wachstum und Überleben der Bäume. Die Überwachung der Baumvitalität und die Entwicklung neuer Indikatoren sind wichtig und sollten fortgesetzt werden, um Baumstress frühzeitig zu erkennen, auch im Hinblick auf die schnellen Umweltveränderungen. Darüber hinaus wurden die meisten Indikatoren, insbesondere diejenigen, die die Merkmale der Krone und der oberen Stammform betreffen, eher geschätzt als gemessen. Folglich besteht ein Bedarf an rationalen und genaueren Methoden, mit denen Baummerkmale und damit potenzielle Indikatoren für die Vitalität von Bäumen erkannt, quantifiziert und in der Praxis angewendet werden können. Das Hauptziel dieser Dissertation war ein Schritt in Richtung einer objektiveren Waldinventur sowie eines umfassenderen Monitorings der Baumvitalität und damit ein besseres Verständnis der Reaktionsmuster von Stamm, Krone und Entlaubung.

Anhand terrestrischem Laserscanning (TLS) werden innovative Methoden zur effizienten Überwachung der Baumvitalität demonstriert und das Reaktionsmuster der Baumform auf Stress für Arten wie Fichte (*Picea abies* (L.) H. Karst), Rotbuche (*Fagus sylvatica* L.) und Eiche (*Quercus* L.) untersucht. Konkurrenz, Trockenheit und Insekten-induzierte Entlaubung führten zu Veränderungen der Stammform, zur Abnahme der Kronengröße und des Stammwachstums.

Mit Hilfe von TLS wurde die Stammform von 868 Fichten gemessen, die aus einem Standraum- und Durchforstungsversuch in Deutschland stammen (Jacobs et al. 2020, Anhang B.1. Artikel I). Die Parzellen decken einen breiten Dichtebereich ab. Es wurden die TLS- mit den konventionell ermittelten Stammvolumenschätzungen verglichen und die Auswirkungen der lokalen Konkurrenz pro Baum analysiert. Die TLS-basierten Volumenschätzungen zeigten, dass das Baumvolumen bei gleichem Brusthöhendurchmesser ($d_{1.3}$) und gleicher Höhe (h) umso geringer ist, je geringer die lokale Konkurrenz ist. Die traditionellen Funktionen unterschätzen den gesamten Volumenbestand insgesamt um 4,2 %. Auf Parzellenebene schwankt die Unterschätzung zwischen 0,7 und 7,0 %. Auf Baumebene wurde das Volumen um –10 bis +10 % unter- und überschätzt. Je genauer die Untersuchung ist, desto besser eignet sich die Anwendung von TLS zur Verbesserung der Volumenschätzung.

Das Trockenstress-Experiment "Kranzberg Forest Roof Experiment" (KROOF) diente als Grundlage für die Erfassung und Analyse des Wachstums von Fichte (*Picea abies* (L.) H.Karst.) und Rotbuche (*Fagus sylvatica* L.) unter progressiv begrenzten Wasserreserven (Jacobs et al. 2021, Anhang B.2. Artikel II). Vor Beginn des Versuchs im Winter 2012/2013 wurden Messungen mittels TLS durchgeführt und im Winter 2018/2019 wiederholt. Die hier analysierte Stichprobe von 21 Bäumen wurde am Stamm überdacht und vom Niederschlag abgeschnitten (Behandlung), während weitere 26 Bäume als unbehandelte Referenz (Kontrolle) dienten. Anhand der TLS-Punktwolken der beiden Erhebungen können strukturelle Baumveränderungen innerhalb des 6-Jahres-Zeitraums direkt visualisiert, berechnet und mit Trockenstress in Verbindung gebracht werden. Trockenstress führte bei beiden Baumarten zu einer signifikant kleineren Kronengröße und einem signifikant geringeren Höhenwachstum. Unter Trockenheitsbedingungen veränderte sich die Kronenschirmfläche bei Fichten und Buchen um –0,74 m² pro Jahr bzw. –0,42 m² pro Jahr, während die Kontrollbäume einen Zuwachs von 0,17 m² pro Jahr bzw. 0,62 m² pro Jahr aufwiesen.

Auf der Grundlage eines groß angelegten Feldexperiments in deutschen Eichen-Mischwäldern, die vom Schwammspinner (*Lymantria dispar*) befallen sind, wurde TLS zur Ermittlung der Belaubungs- und Wachstumsverluste auf Einzelbaumebene eingesetzt (Jacobs et al. 2022, Anhang B.3. Artikel III). Der Versuch umfasste zwei Stufen des Entlaubungsrisikos durch den Schwammspinner - hoch (H) und niedrig (L) - sowie zwei Behandlungsstufen der Schädlingsbekämpfung: Bekämpfen mit dem Insektizid Mimic (M) oder ungespritzte Kontrolle (C). Das faktorielle Design bestand aus vier Behandlungskombinationen (HC, HM, LC und LM), die auf 11 räumliche Blöcke mit insgesamt 44 Parzellen angewandt wurden. Mit dem TLS-Ansatz wurde die durch den Schwammspinner verursachte Entlaubung ermittelt und durch die Parameter Blattfläche und Kronenperforation berechnet. Zum ersten Mal wurde die von TLS abgeleitete Baumbelaubung auf der Grundlage des zwischenjährlichen Stammwachstums referenziert und validiert. Die Blattfläche und die Kronenperforation korrelierten mit +0,6 und –0,35 mit den Zuwächsen der Grundfläche. Außerdem zeigte diese Studie, dass es im selben Jahr der Entlaubung zu Wachstumseinbußen am Stamm kam.

Die Ergebnisse dieser Arbeit deuten darauf hin, dass TLS neue Möglichkeiten zur Identifizierung von Strukturmerkmalen bietet und zur Entwicklung neuer Vitalitätsindikatoren geeignet ist. Es können Stammform, Kronenform und Belaubung auf Einzelbaumebene überwacht werden. Auf der Grundlage der analysierten Veränderungen der Baumformparameter hat TLS das Potenzial, ein rationales und geeignetes Instrument zur

Erfassung von Indikatoren für die Bewertung des Waldzustands zu sein. Es hat sich gezeigt, dass iterative TLS-Erhebungen die Messkampagnen auf langfristigen Versuchsflächen verbessern könnten, um ein umfassendes Bild der Baumvitalitätsüberwachung zu erhalten. Solch genaue Daten beispielsweise über die Kronendimension sind auch für die Modellierung des Baumwachstums unerlässlich. So kann sich beispielsweise die Kronenform aufgrund der Auswirkungen des Klimawandels verändern. Daher müssen Kronenmodelle innerhalb von Baumwachstumsmodellen hinterfragt werden, ebenso wie die abgeleiteten Allometrien. Die zunehmende Häufigkeit extremer und extensiver Dürreereignisse macht es noch wichtiger, die Auswirkungen von Trockenstress oder Insekten-induzierter Entlaubung in der forstlichen Praxis und ökologischen Modellierung zu berücksichtigen.

Cumulative thesis – publication overview

This dissertation is based on three peer-reviewed publications (Article I – III). For each of these publications, the original abstract, journal information and author's contribution are provided in the following. The full list of all publications and conference contributions prepared by the candidate during his doctoral studies is provided in Appendix A. Original versions of Articles I – III can be found in Appendix B or can be accessed via the respective DOI listed below.

Article I

Jacobs M, Rais A, Pretzsch H (2020) Analysis of stand density effects on the stem form of Norway spruce trees and volume miscalculation by traditional form factor equations using terrestrial laser scanning (TLS). ***Can. J. For. Res.*** **50 (1), 51–64.**

DOI: 10.1139/cjfr-2019-0121.

Journal impact factor: 1.812 (2019)

Abstract: Tree and stand volume estimates are relevant for forest inventories, forest sales and carbon stock evaluations. Forest practice commonly uses generalized, stem wood volume functions. However, such generalized approaches neglect the stem form in detail. Hence, trees of a given species with the same diameter at breast height ($d_{1.3}$) and height (h) are always assumed to have the same form factor and thus the same volume. This case study focuses on stem form variation of *Picea abies* due to competition effects. Using terrestrial laser scanning (TLS), the stem shape of 868 trees from a long-term spacing and thinning experiment in Germany was measured. The plots cover a broad density range. The effect of competition was analyzed and the TLS-based stem volume estimates with conventionally determined stem volume estimates were compared. TLS-based volume estimations showed that the lower the competition, the lower the tree volume with a given $d_{1.3}$ and h. Commonly used functions underestimate the volume stock overall by 4.2 %, disregarding any levels. At plot level, underestimation varies from 0.7 to 7.0 %. At tree level, the volume was over- and underestimated by –10 to +10 %. The more precise the examination, the more suitable the application of TLS for enhancing volume estimation.

Author's contribution: Conceptualisation: M.J., H.P.; data curation: M.J.; formal analysis: M.J.; investigation: M.J.; methodology: M.J.; resources: H.P.; software: M.J.; supervision: H.P., A.R.; validation: M.J., A.R.; visualisation: M.J., A.R.; writing – original draft preparation: M.J., A.R.; writing – review & editing: M.J., A.R., H.P.; percentage M.J. overall: 80 %

Article II

Jacobs M, Rais A, Pretzsch H (2021) How drought stress becomes visible upon detecting tree shape using terrestrial laser scanning (TLS). ***Forest Ecology and Management, 489,*** **118975.**

DOI: 10.1016/j.foreco.2021.118975

Journal impact factor: 3.126 (2018)

Abstract: Due to climate change, the occurrence of drought events with essential effects on trees will arise. The impact of severe drought stress on trees' vitality with regard to growth has often been analyzed using traditional, easy-to-measure variables, such as diameter at breast height ($d_{1.3}$). The focus was on tree dimensions, as potential vitality indicators, that are difficult to measure. The unique drought stress experiment "Kranzberg Forest Roof Experiment" (KROOF) was used as a basis for scanning and analyzing the growth of Norway spruce (*Picea abies* (L.) H.Karst.) and European beech (*Fagus sylvatica* L.) under progressively limiting water reserves. Before the start of the experiment in the winter of 2012/2013, terrestrial laser scanning (TLS) was performed and repeated in the winter of 2018/2019. One sample of 21 trees was trenched and roofed (treatment), while additional 26 trees served as untreated reference (control). Drought stress led to significantly smaller crown size and lower height growth for both tree species. The crowns of Norway spruce trees increased significantly in transparency and roughness. In addition, high competition combined with drought stress significantly reduced the roughness and increased the compactness of the crown. The results show that TLS can offer new opportunities for identifying structural features in trees. Iterative TLS-surveys may extend existing measuring campaigns on common long-term experimental plots, in order to analyze general changes or monitor tree vitality.

Author's contribution: Conceptualisation: M.J., A.R., H.P.; data curation: M.J.; formal analysis: M.J.; investigation: M.J.; methodology: M.J.; resources: H.P.; software: M.J.; supervision: H.P., A.R.; validation: M.J.; visualisation: M.J., A.R.; writing – original draft preparation: M.J., A.R.; writing – review & editing: M.J., A.R., H.P.; percentage M.J. overall: 90 %

Article III

Jacobs M, Hilmers T, Leroy BML, Lemme H, Kienlein S, Müller J, Weisser WW, Pretzsch H (2022) Assessment of defoliation and subsequent growth losses caused by Lymantria dispar using terrestrial laser scanning (TLS). ***Trees.***

DOI: 10.1007/s00468-021-02255-z

Journal impact factor: 2.529 (2020)

Abstract: Foliation strongly determines all tree growth processes but can be reduced by various stress factors. Insect defoliation is time-variable and one stress factor that may affect photosynthetic processes and cause immediate reactions as well a possible refoliation, which are difficult to detect by surveys repeated at one-year-intervals. This study used a large-scale field experiment in German oak/mixed forests affected by gypsy moths (*Lymantria dispar*) to test the use of terrestrial laser scanning (TLS) for detecting inter-annual foliation and growth losses at the individual tree level caused by the gypsy moth. The experiment comprised two levels of gypsy moth defoliation risk – high (H) and low (L) – as well as two pest control treatment levels: spraying with the insecticide Mimic (M) or unsprayed control (C). The factorial design consisted of four treatment combinations (HC, HM, LC and LM), applied to 11 spatial blocks with in total of 44 plots. The TLS approach detected defoliation caused by the gypsy moth, calculated as leaf area and crown perforation parameters. For the first time, TLS-derived tree foliation was evaluated, based on inter-annual stem growth. Leaf area and crown perforation showed a correlation of +0.6 and –0.35, respectively, with basal area increments. Furthermore, this study revealed subsequent growth losses in the same year due to defoliation. The results show that TLS can offer new opportunities to develop new indicators that monitor foliation at the individual tree level. The crown perforation can describe defoliation or the tree vitality based on one scanning campaign, whereas the leaf area needed at least two.

Author's contribution: Conceptualisation: M.J., T.H., B.L., S.K., H.L., J.M., W.W., H.P.; data curation: M.J., T.H.; formal analysis: M.J.; investigation: M.J.; methodology: M.J.; resources: J.M., W.W., H.P.; software: M.J.; supervision: J.M., W.W., H.P.; validation: M.J.; visualisation: M.J., T.H.; writing – original draft preparation: M.J; writing – review & editing: M.J., T.H., B.L., H.L., J.M., W.W., H.P.; percentage M.J. overall: 75 %

1. Introduction

1.1. Motivation

Tree vitality is one of the most essential indicators for describing the state of a forest (Innes 1993). In temperate forests, stress factors such as insect infestation, diseases, competition, and climate have strong effects on tree growth and survival (Cortini and Comeau 2020). Forest monitoring is used to investigate these stress factors and their effects on forest condition (Lorenz et al. 2004). Monitoring tree vitality and developing new indicators is important in order to detect tree stress at an early stage (Dobbertin et al. 2009) and identify rapid environmental changes (IPCC 2012). In addition, most indicators, especially those involving crown and upper stem characteristics, have been estimated rather than measured. Consequently, there is a need for more accurate empirical methods that can detect and quantify tree characteristics and, therefore, potential indicators of tree vitality. Terrestrial laser scanning (TLS) was used to fill gaps in conventional inventory data (Calders et al. 2020). In this dissertation, I show innovative methods for the efficient monitoring of tree vitality under stress for common German tree species like Norway spruce (*Picea abies* (L.) H. Karst)**,** European beech (*Fagus sylvatica* L.) and oak (*Quercus* L.).

Due to climate change, drought events will become more widespread, extensive, and extreme in the future (IPCC 2012), and thus the frequency and intensity of forest disturbances caused by insects will increase (Seidl et al. 2011). Furthermore, climate change is likely to accelerate tree mortality (Anderegg et al. 2013), where large trees are potentially at the greatest risk, putting crucial environmental, economic, and social benefits at risk (Stovall et al. 2019). In addition to mortality, tree growth has also been affected by recent droughts (Pretzsch et al. 2020). With regard to insect-induced disturbances and defoliation, the condition of trees will be affected, causing significantly reduced timber production (Piper et al. 2015). Defoliation can result in reduced growth (Naidoo and Lechowicz 2001), reduced root biomass production (Thomas et al. 2002), and increased tree mortality (Elling et al. 2007). Here, tree mortality depends on the frequency, intensity, duration, and combination of defoliation, the vitality of the infested trees, and biotic or abiotic stresses (Elling et al. 2007). In summary, stress factors like insect infestation, diseases, competition, and climate can have strong effects on the growth and survival of trees, thus affecting tree vitality (Cortini and Comeau 2020).

The terms vitality and vigor describe the condition of trees. They are close in meaning, but vigor refers specifically to the capacity to resist strain. It is a genetic factor linked to the capacity

to withstand a new source of stress (Shigo 1990). Vitality, by contrast, is often taken to refer to the ability to grow under present conditions (Shigo 1990) —but diverse definitions can be found in the literature. According to Gehrig (2004), plant vitality is in a triangle between stress tolerance, longevity/growth and reproduction. Brang (1998) stated, that vitality is the capacity of an organism to assimilate carbon, to resist stress, to adapt to changing environmental conditions, and to reproduce.

Although widely used, the term "vitality" is difficult to define. Loosely, vitality is meant to quantify the health of an organism (Gehrig 2004) —although “health” is difficult to describe too, and is often defined in the negative as the absence of illness (Gehrig 2004). The World Health Organization (WHO), however, defines health as a state of complete physical, mental, and social well-being and not merely the absence of disease or infirmity (World Health Organization 2008). This definition presupposes an individual's awareness of his or her condition, and therefore, a person can also say whether they are healthy or not. If this awareness is not present, or if this cannot be communicated, changes in external behavior or shape must lead to the conclusion that there is a deviation from the normal state (Gehrig 2004). Thus, to assess tree vitality it is necessary to quantify external changes.

In this dissertation, the definition and the concept of tree vitality monitoring are based on and tie in with the work of Dobbertin (2005). In order to assess tree vitality, it is important to evaluate the effect of external stress, as stress resistance is an important criterion in all vitality concepts. Unfortunately, the hypothetical optimal tree vitality is not known. In most cases, only tree mortality, the minimum tree vitality, can be clearly identified. Therefore, only changes in certain indicators of tree vitality can be observed. So although tree vitality is an important forest monitoring variable (Innes 1993), it is qualitative, which means it cannot be measured directly. Therefore, various tree vitality indicators should serve to describe vitality for a more comprehensive assessment (Gehrig 2004). There are a number of observable characteristics that could serve as tree vitality indicators. For example, height compared to other trees, crown length, crown projection area (*cpa*), crown density in relation to the total height of the tree and to its diameter, social position in the stand, branching form, shoot length and diameter, needle length or leaf size, and needle or leaf color (Gehrig 2004). Other characteristics may not be immediately visible, such as root density (ratio of fine to coarse roots), annual ring width and annual ring structure (ratio of early to late wood), nutrient level values of needles and leaves, and suction tension (water potential) (Gehrig 2004). The difficulty in field studies is first to identify and measure the appropriate vitality indicator, secondly to assess the strength and

duration of the stress, and thirdly to determine the absolute or relative level of the vitality indicator (Dobbertin 2005). Field-ready and cost-effective methods are needed. Biochemical indicators at the plant cell level, such as phytohormones or enzymes, can reflect the response of trees to various environmental stresses (Scherer 1995). Unfortunately, many of these indicators cannot be readily obtained locally or are very expensive. According to Dobbertin et al. (2009), practical field methods are important for long-term monitoring and include assessment of crown foliation or transparency (Eichhorn 1998), crown morphology (Roloff 1987), measurement of stem growth (Waring et al. 1980) and other internal stem and leaf characteristics that are not externally detectable. Here, I concentrate on external indicators, since they can be assessed non-destructively. The two most common external indicators to describe tree vitality are crown transparency, defoliation, and stem growth (Dobbertin et al. 2009). In order to assess the long-term development of tree vitality, it is often necessary to select easy-to-measure indicators for forest inventories. Since a tree loses its needles or leaves before it dies, crown transparency has been suggested as an indicator, expressed as the percentage of a fully foliated tree crown (Müller and Stierlin 1990). According to Dobbertin et al. (2009) , the traditional indicators of crown transparency and stem growth could be used as indicators for the vitality of a single tree, with certain limitations. Stem diameter at breast height ($d_{1.3}$) or the width of tree rings can be useful growth indicators. Much more difficult to measure are stem diameters at different heights, the tree height itself, branch and leaf growth, including the crown size, and the total aboveground biomass. For this reason, I use stem growth as an indicator of stress in general (Dobbertin 2005). Crown transparency and stem growth alone do not paint a full picture, however. Thus, there is no universal indicator for the vitality of a single tree (Dobbertin et al. 2009). Therefore, research on traditional and potential tree vitality indicators is important to detect environmental stress. Whereas stem growth at breast height is easy to measure, stem form, crown size, leaf area, crown transparency, or any other crown morphological parameter determination is more challenging. In practice, it is rarely feasible to measure these parameters destructively, so they are usually visually estimated or predicted via parameters that are measurable from the ground. The visual assessment of tree crowns and their classification into transparency or defoliation classes is a standard procedure in many parts of the world and can be carried out cost-effectively and relatively quickly in field surveys (Müller-Edzards et al. 1997). However, crown transparency assessments have been criticized as overly subjective (Dobbertin et al. 2009). Furthermore, they require intensive training courses and repeated control assessments (Wulff 2002). No absolute reference is known, so site-specific reference trees are used (Innes 1993). Consequently, there is a need for new measurement

methods with a fast and easily understandable procedure for determining a tree's crown morphology, leaf area, and crown transparency. Because crown conditions can be highly dynamic over the course of a year, new methods should seek to accommodate taking objective measurements several times a year to record seasonal changes in crown condition. The crown foliation of a tree is also dynamic during the vegetation period. Besides the leaf growth at the beginning of the vegetation period, the temporally variable onset of insect feeding can also lead to leaf regrowth depending on the intensity of insect feeding. This makes an objective estimation of leaf area or foliage condition difficult, especially if only one measurement is made per year.

Terrestrial laser scanning (TLS) has been used to address numerous information gaps in traditional inventory data (Calders et al. 2020) and can measure detailed stand and individual tree information (Liang et al. 2018). Regarding stem information, the advantages of TLS are that no tree has to be cut and manual surveys can be avoided. With TLS and automated methods, numerous measurements of diameters with different heights distributed over a large part of the tree stem can be made, instead of only one measurement at breast height. In addition, TLS offers much more than just the stem form as information, but also the three-dimensional occupation of the trees in space, as well as information on crown width, length, inclination, and curvature of the respective tree. Ground-based LiDAR (light detection and ranging) measurements can serve as an alternative to airborne LiDAR observations, depending on the information needed, especially at the single-tree level (Hilker et al. 2010). In particular, it is possible to determine the structural crown properties of trees independently of tree species (Bayer et al. 2013). TLS has the potential and ability to scan and reach the canopy area successfully (Seidel et al. 2015). When, for instance, TLS-derived tree heights and traditional measured heights have been cross-checked against true tree heights obtained using destructive techniques, TLS was found to be more accurate (Calders et al. 2015). Furthermore, several studies have already shown how to detect single tree defoliation at tree and stand level via TLS (Huo et al. 2019; Kaasalainen et al. 2010). However, determining leaf area and classification of biomass into wood and leaf material is challenging even with TLS. Leaf-wood separation approaches based on spectral information from TLS return intensity or machine learning are complex and expensive (Calders et al. 2020), making them difficult to reproduce. Therefore, robust and simple methods are required that are reproducible.

So far, in traditional forest monitoring, an objective assessment of stem form, crown morphology, and crown foliation is lacking. The reason for this is that those parameters are

difficult to measure non-destructively and thus are mostly estimated from the ground. Especially for tree vitality monitoring, more indicators might enable higher precision and reliability. Previous research on indicators is incomplete, and TLS has the potential to deliver more insights into the reaction patterns of stem, crown, and defoliation. Thus, it is important to develop a strong empirical foundation based on long-term plots, unique experiments, and large-scale field experiments —particularly those with practical relevance —using consistent and comprehensible modelling approaches.

In this dissertation, I develop new methods and analyze TLS acquisitions to assess tree vitality. Measurements of crown foliation, crown size, and tree stem growth under environmental stress were analyzed to derive their potential as tree vitality indicators. I focused on the most common commercial conifer and broadleaved tree species in Germany: Norway spruce (*Picea abies* (L.) H. Karst), European beech (*Fagus sylvatica* L.) and oak trees (*Quercus* L.). (BMEL - Bundesministerium für Ernährung und Landwirtschaft 2014).

1.2. Objectives and outline

The main objective of this dissertation is to contribute to the development of a more objective forest inventory and tree vitality monitoring techniques, thus improving our understanding of the reaction pattern of tree stems, crowns, and defoliation due to stress. This work aims to provide generalisable and easily transferrable knowledge that supports today's forest professionals in their challenging endeavor of adapting forest ecosystems to climate change and providing sustainable forest production systems for future generations by using new techniques such as TLS.

Figure 1 shows the conceptual framework of this dissertation and the relationships between the three articles. The TLS symbolizes the rational measurement and was the main tool used for tree monitoring during this doctorate. On the left side of Figure 1, the TLS encloses the tree monitoring architecture of this dissertation. All three research topics are embedded within the tree monitoring architecture. In this dissertation, the main objective of the tree monitoring component is to continuously measure aboveground tree shape (which encompasses both stem and crown attributes) in order to form a basis for assessing tree vitality. Tree vitality represents the core focus of this dissertation (Topic II). I examine tree vitality indicators encompassing stem and crown attributes. The first and third publications complement the tree vitality focus and concentrate on stem and crown attributes, respectively.

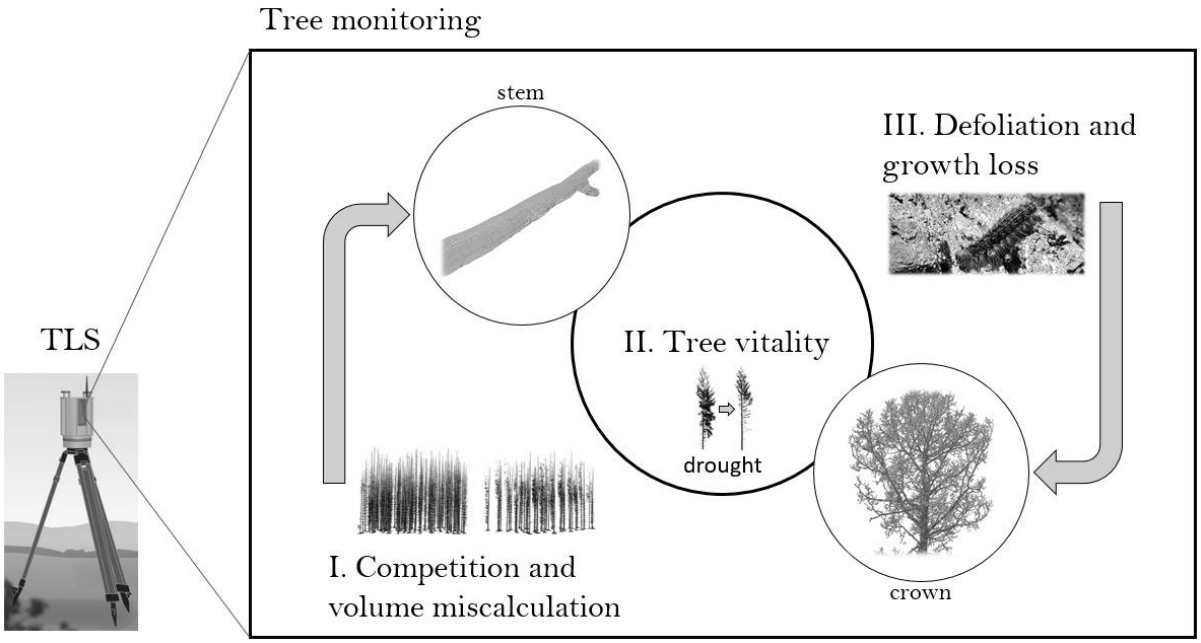

Figure 1 The conceptual framework of this dissertation. In the first publication, stem form variation and volume miscalculation of Norway spruce trees due to competition effects were analyzed (Topic I). The second publication evaluates the usefulness of tree variables and growth measurements as indicators of either vitality or stress in Norway spruce and European beech (Topic II). The third publication examines the relationship between growth, leaf area, and defoliation (Topic III). All work and analysis was based on terrestrial laser scanning (TLS) data to obtain unbiased and objective information (RIEGL 2019).

The central theme was developed over the course of the dissertation. The doctorate also represents a development process, which is also reflected in the topic. Articles II and III, in particular, deal centrally with tree vitality indicators. It should be mentioned that Article I, with the topic of stem form and competition, fits less into the topic of vitality but was necessary as a developmental step regarding the holistic analysis of tree shape and the development of algorithms. Therefore, the order of the articles also reflects the methodological progress of the dissertation to extract various tree parameters from terrestrial laser scanning data. First, I concentrated on new methods and focused on stem form variation and volume miscalculation of Norway spruce trees due to competition effects. I developed algorithms enabling automated stem detections, isolations, and measurements (Article I). With the isolated stems as a basis, I then developed semi-automated algorithms to isolate the crowns and thus measure the crown size parameters. It was evaluated whether growth measurements or stem and crown characteristics under drought stress might serve as useful indicators of either vitality or physiological stress (Article II). Once single trees are isolated, new developed methods enable leaf area calculation. It was analyzed how stem growth of oak trees is related to defoliation immediately following insect feeding (Article III).

The dissertation aims for three research questions:

QI: How does competition modify the stem form of trees with the same height and diameter at breast height, thereby influencing volume miscalculation by traditional form factor equations?

QII: How does severe drought stress affect potential tree vitality indicators consisting of stem and crown attributes?

QIII: How does insect defoliation caused by Lymantria dispar affect stem growth?

Each research question (*QI* – *QIII*) led to an individual study whose results were reported separately in peer-reviewed research articles (Article I – Article III, Figure 1).

2. Material and methods

2.1. Material

2.1.1. Spacing and thinning experiment (Topic I)

Study site and data

For Article I, a case study was carried out on trees from pure Norway spruce treatment plots located in Fürstenfeldbruck (FFB612) in southern Germany. The spacing and thinning experiment is part of long-term trials established in 1974 on the initiative of the International Union of Forest Research Organizations IUFRO (Krutzsch 1974). They cover stands with a broad range of stand density, including initial and final densities. Table 1 summarizes the most relevant characteristics; for more detailed information, see Pretzsch (2006), Rötzer and Pretzsch (2010), and Huang and Pretzsch (2010).

Table 1 Stand and site characteristics as average values.

	Fürstenfeldbruck FFB612
Location	
Altitude above sea level (m)	550
Coordinates	N 48°14'02.5" E 11°05'01.6"
Climate 1988 – 2017 (average values)*	
Year	
Temperature (°C)	8.8
Precipitation (mm yr-1)	952
Soil	
Initial substrate	Loess
Soil type	lessivé soil
Stand characteristics 2017 (average values)	
n (ha^{-1})	689
dq (cm)	30
hq (m)	27.5
BA (m² ha^{-1})	39.8
Standing volume (m³ ha^{-1})	553.3

*from climate data center (2019)

Note: n (ha^{-1}) = trees per hectare, dq = quadratic mean diameter (cm), hq = height corresponding to dq, BA = basal area (m²).

Figure 2 illustrates the layout of the experimental trial. In total, 14 out of 21 plots were scanned. The remaining 7 plots were removed either because they were too similar in treatment or because the sample size (trees) of the plots would have been extremely uneven. The RIEGL LMS-Z420i (RIEGL 2010) laser-scanning system was used for data acquisition in January

2018. Five scan positions were realized per plot. For each scan position, two scans (horizontal and vertical) were performed. The scan positions formed an approximate rectangle around each plot, with four scan positions at each corner and one central scan position in the middle of the plot. The vertical and horizontal angular resolutions were set to 0.05° in order to achieve a reasonable trade-off between scan-time and the risk of disturbances due to tree movement through wind. Due to the angular measurement scheme of the scanner that operates from the ground, the point density naturally decreases to the top of the trees. Furthermore, the laser beam is usually not able to penetrate tree compartments in order to perform measurements behind obstacles. These two effects result in rather sparse measurement densities in the upper crown and stem regions, especially if the crown parts near the scanner are dense, like those of conifers (Hilker et al. 2010). I attempted with the RIEGL distance-measurement mode called "last-pulse" or "last-target" to counteract these effects by recording the deepest points within a footprint, thus gaining a higher proportion of returns from inner crown regions compared to the first-pulse mode. Using the software RiSCAN PRO, all scan positions per plot were co-registered. The co-registration was based on artificial targets (reflectors). The result was a "Plot Point Cloud Raw" (PPC-R).

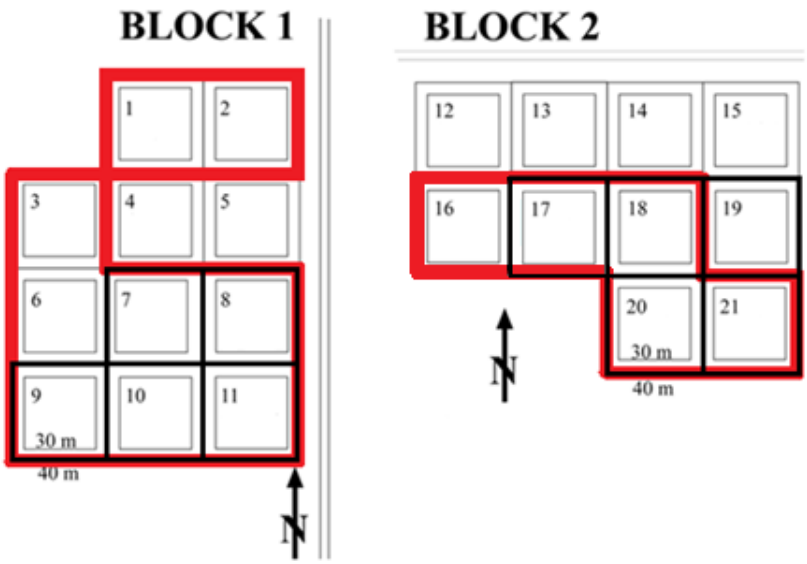

Figure 2 Experimental design of the spacing and thinning experiment in Fürstenfeldbruck (FFB612). The experiment consists of two blocks. Each block comprises plots of 30 m x 30 m (900 m²) on which different types of silvicultural treatment were applied in terms of spacing and thinning. In total, 14 of the 21 plots have been selected. The red-bordered plots were scanned. The spacing experiment represents Treatment 1 and the thinning experiment Treatment 2. The plots where the thinning experiment (Treatment 2) took place were additionally black-bordered in bold. The rest of the plots were black-bordered in thin lines and belong to the spacing experiment Treatment 1.

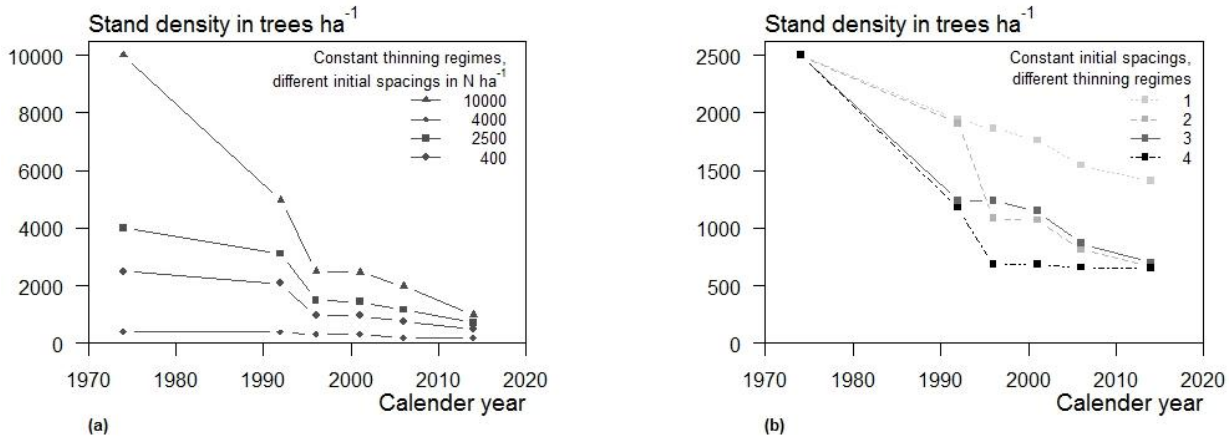

Figure 3 Characteristics of the spacing and thinning experiment FFB612. The spacing experiment (a) represents Treatment 1 and the thinning experiment (b) Treatment 2. (a) There are some plots of varying establishment spacings (and same thinning regime) and (b) others of varying thinning regimes (and same establishment spacings). Thinning regime 1 was never thinned. Thinning regime 2 was late thinned. Thinning regime 3 was moderately thinned. Thinning regime 4 early thinned.

The treatment of the plots differs either in establishment spacing (Figure 3a) or thinning regime (Figure 3b). Each thinning regime has been simplified by time of thinning. Thinning regime 1 was control (null thinning). Thinning regime 2 was late thinned. Thinning regime 3 was moderately thinned. Thinning regime 4 early thinned. Detailed information on treatment and thinning interventions as well as a complete yield overview over time per plot is given in Appendix C Supplementary A (Table A1 – A3). All $d_{1.3}$ were recorded in September 2017 – TLS data acquisition took place in January 2018 (Table 2) – and were measured manually for all trees in the plots. For each plot, total tree height was measured on a subsample of 50 % of the trees randomly selected, using a Haglöf Vertex. The height of all non-measured trees was estimated from a diameter-height function fitting for each plot (Petterson 1955). The stem-wood volume was estimated by common general-form factor equations (Kennel 1969).In spring 2018, a thinning intervention took place. From the 55 felled trees, several diameters along the stem axis were measured with a caliper in two perpendicular directions. A tape either on logs or on complete trees measured length. Tree inclination – detected by TLS – was considered when transforming length into total height. Finally, Smalian function was applied for volume calculation (Hush et al. 1982). A mensurational overview of the 55 felled trees is provided in Table 2.

Table 2 Range, mean and number of all sampled trees in 2017 and the trees that were harvested for destructive sampling during thinning in spring 2018.

Sampled and scanned trees	**Range**	**Mean**	**N**
$d_{1.3}$ (cm)	9.0 – 59.1	28.3	868
Height (m)	12.3 – 31.3	24.7	868
Volume (m³)	0.05 – 2.7	0.8	868
Harvested trees (validation)			
$d_{1.3}$ (cm)	10.2 – 38.7	22.7	55
Total tree height (m)	14.6 – 27.0	22.6	28
Volume (m³)	0.07 – 1.4	0.5	55

Note: The diameter at breast height ($d_{1.3}$), the height (h) and the volume of the sampled trees were measured by traditional forest inventory. Diameters at breast height ($d_{1.3}$) were measured by caliper and the height of the felled trees was measured by tape. Total tree heights were calculated for trees that had not been sawn into sections by the harvester (28 trees) to avoid measuring mistakes.

2.1.2. Drought stress experiment (Topic II)

Experimental design

The experimental plot Kranzberger Forst (FRE 813/1) with a size of 0.5 ha and is located in the southern part of Bavaria, approximately 35 km northeast of Munich. On this site, the "Kranzberg Roof Project" ("KROOF") was initiated in spring 2013 (Pretzsch et al. 2014). Table 3 summarizes the relevant site and plot characteristics.

Table 3 Site, plot and tree characteristics of the experimental plot Kranzberger Forst FRE 813/1 are given for 2014, i.e. before the start of the drought stress experiment.

Location					
Altitude above sea level	m	490			
Coordinates		11°39'42"E, 48°25'12"N			
Climate[1)]					
Mean annual temperature	°C	7.5			
Annual precipitation	mm yr^{-1}	750-800			
Soil					
Initial substrate		Loess			
Soil type		Luvisol			
Trees[2)] scanned / mean (± SE)					
Species		European beech		Norway spruce	
Group		Control	Treatment	Control	Treatment
Trees per group and species *n*		13	11	13	10
Stand density index *SDI*		851 (44)	823 (43)	777 (73)	816 (35)
Diameter at breast height $d_{1.3}$	cm	32.5 (8.7)	30.9 (7.4)	35.9 (5.6)	37.7 (9.5)
Height *h*	m	29.3 (1.6)	29.2 (3.1)	31.8 (2.1)	31.6 (2.0)
Crown radius *cr*	m	3.1 (1.1)	3.3 (1.3)	2.3 (0.4)	2.4 (0.2)
Crown base height *cbh*	m	16.7 (3.6)	16.5 (2.4)	16.5 (4.8)	17.4 (4.3)
Crown projection area *cpa*	m^2	33.4 (26.6)	39.0 (33.1)	16.6 (5.8)	18.0 (2.6)

1) Climate reference period 1988-2017
2) Data from the survey in 2014

The plot was specially selected for the KROOF experiment (Pretzsch et al. 2014). The mixed stand, which consists of European beech and Norway spruce, was never thinned and is fully stocked. Both tree species share the same soil resources and form a common closed canopy. Within the site, large groups of beech grow surrounded by spruce. In 2014, the tree age within the mixed stand was assessed to be 63 ±2 years for spruce and 83 ±4 years for beech (Pretzsch et al. 2016). Conditions such as growth stage, stand density, basal area, or stem volume of mono-specific spruce, mono-specific beech, and beech/spruce mixture are similar across the control and treatment plots (Pretzsch et al. 2014).

In 2013, the experimental area was subdivided into six groups that were not roofed ("Control") and six groups that were roofed ("Treatment"). Each plot had four to six beech trees on one side and the same number of spruce trees on the opposite side, enabling a broad contact zone in between the two. Plot sizes ranged between 110 m^2 and 200 m^2, amounting to 868 m^2 and 862 m^2 in total for control and drought treatments, respectively (Pretzsch et al. 2016). On treatment plots, special houses were installed underneath the canopy, three meters above the ground. The roof of each house automatically closes during rainfall. During the construction process, the forest floor was covered with wooden pallets to avoid compaction of the soil from construction work (Grams et al. 2021). Vegetation cover at the forest floor was almost entirely absent due to the high density of the tree crowns. To prevent throughfall, each roof extends approximately 40 cm beyond the borders of the treatment plots (Grams et al. 2021). The novelty of roof construction is the automated closure during rain by means of water-impermeable, tile-composed roller blinds, which are electrically motorised (Pretzsch et al. 2014). The roof-intercepted quantities of water are channeled out of the study site. This design prevents a greenhouse effect when there is no rain. The stationary portions of the roof are secured around individual trees and are permanently closed. Stem flow is negated via perforation hoses encircling each tree stem above the roof, and the thus-collected water is directed to the roof gutters (Grams et al. 2021). All the rain that is held off is transported off the experimental site via plastic hoses attached to gutters on each side of the roofs. Additionally, the roofed plots are hydraulically isolated to avoid lateral soil water access. Hence, a durable cover, preventing penetration by water or roots, is placed in the dug trenches around the roofed plots. In 2010, the 12 experimental plots were trenched to a soil depth of 1 m, where the layer of sandy loam hardly allows deeper root growth. As such preparation causes root injury, trenching was performed four years before the actual beginning of the drought experiment (Pretzsch et al. 2016). Due to the good water and nutrient supply along with the high water storage capacity of the soil, it was possible to concentrate on the effects of experimentally induced drought without the

interference of other limiting factors. The drought phase of the KROOF experiment started in March 2014 and continued until November 2018. During this phase, the roofs were automatically closed during rainfall during the growing season and on average withheld 69 ±7 % of the annual rainfall (Grams et al. 2021). The water was kept away in summer, while in winter the forest ecosystem of the treated plots was allowed to recover.

An overview of the classical growth and yield-related variables of all scanned sample trees is provided in Table 4. More detailed information on the experimental design can be found in Pretzsch et al. (2014), Goisser et al. (2016), and Grams et al. (2021).

2.1.3. Gypsy moth experiment (Topic III)

Experimental design

The experiment took place in mixed oak forests in different stands in Franconia-Bavaria in Germany (Leroy et al. 2021). The experimental design area consisted of 11 blocks (A, B, D, F, G, H, J, M, N, O, and S), varying spatially and dominated by oak trees. Each block was subdivided into four plots with similar forest structures, stand ages, and tree species composition within the block. Each plot had a mean size of 0.05 km2 (± SD 0.20). Within each block, two of the four plots had a high (H) defoliation risk, while the other two had a low (L) defoliation risk. For this classification, a defoliation risk index was used, which calculation was based primarily on gypsy moth egg mass density (Leroy et al. 2021). The survey of egg mass density was conducted by regional forest offices in 2018 (Leroy et al. 2021). In each block, an insecticide treatment (Mimic; M) was randomly assigned to one plot per defoliation risk level, while the second plot was left unsprayed and used as a control (C). The treatment plots were sprayed with the insecticide tebufenozide as Mimic® (Spiess-Urania Chemicals, Hamburg, Germany; 240 g L^{-1} active ingredient) between May 3rd and May 23rd (124 – 144 days of the year, DOY) 2019 at the maximal legal rate of 750 ml ha-1. The treatments were applied by helicopter under conditions of dry and less-than-windy weather. In total, 44 plots were sampled, which had been selected to represent 11 weak and strong infestations, and 11 remained with and without control.

At each plot, 20 six-tree samples, including one central oak tree and the following five neighboring trees with a diameter at breast height ($d_{1.3}$) greater than or equal to seven cm, were sampled, so that 880 central trees and 4400 neighboring trees were used to describe the stand characteristics such as basal area, standing volume, etc. for each block (Table 1). Single tree

volume was calculated based on basal area, total tree height, and species-specific form factors for all six-tree sample trees. The single tree volumes were summed up to standing volume for block level. For stand characteristics, the total tree heights and basal area were retrieved from TLS. To estimate the variables per ha, the expansion factor was calculated. For this, the distance between the central oak tree and the fifth neighboring tree was measured via TLS for all 80 six-tree samples per block. After that, the circular area for each six-tree sample was calculated using the measured distances as the radius. All the areas of one block were summed up, and then this area was divided by 10,000 to get the expansion factor to calculate the variables per ha. A more detailed description of the stand characteristics per plot can be found in Table A1 in the Appendix C Supplementary A. The 20 six-tree samples were established along transects in the four main cardinal directions (Figure 1), starting from the center of each sampling plot. Six-tree samples were taken at 25, 50, 75, 100, and 125 m from the center of each plot (origin of the coordinate system in Figure 1). More detailed information on the experiment and its design can be found in (Leroy et al. 2021).

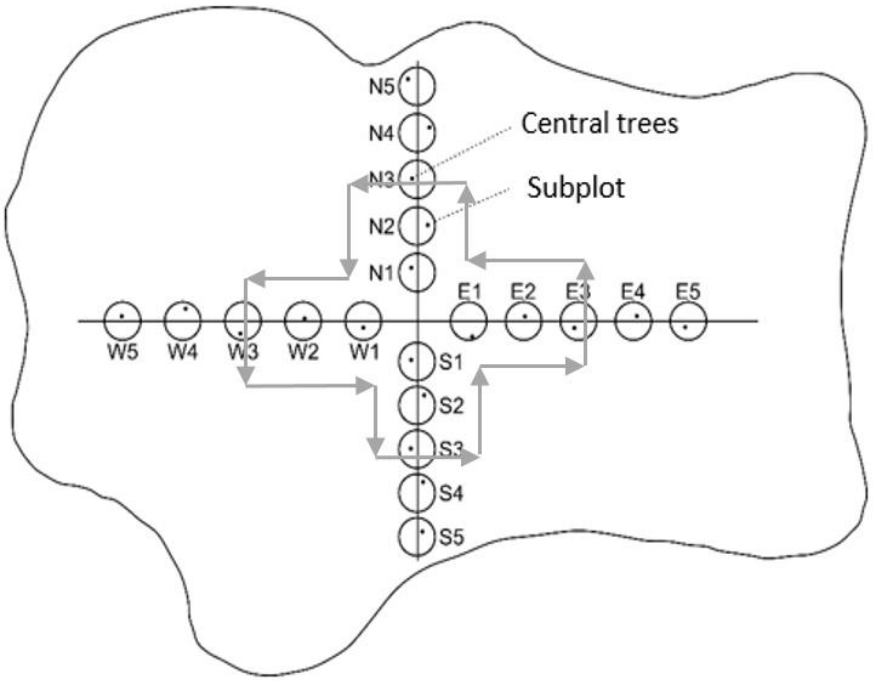

Figure 4 An overview of a plot with 20 six-tree subplots along transects in the main cardinal directions, starting from the center of the infested area For the detailed analysis, each six-tree subplot yields one central tree and five neighboring trees with $d_{1.3}$ greater than or equal to seven cm. The surveys were carried out along the transect using TLS in the winter. The gray arrows signify the scanning direction of TLS campaigns two and three in summer in relation to leaf area detection.

Table 4 The stand characteristics of the 11 blocks in Franconia-Bavaria, Germany. The parameters were calculated based on TLS point clouds using 5280 trees (six-tree subplots).

Block	n (ha^{-1})	dq (cm)	hq (m)	BA (m^2 ha^{-1})	SV (m^3 ha^{-1})
A	**493** (339-713)	**23.0** (7.1-71.5)	**17.6** (5.2-26.6)	**26.8** (23.5-30.1)	**235.3** (218.3-265.0)
B	**424** (314-622	**25.5** (7.6-61.6)	**19.8** (6.3-27.4)	**26.0** (22.5-30.5)	**256.8** (211.1-313.5)
D	**563** (357-753)	**23.0** (7.0-76.0)	**17.4** (6.1-29.2)	**34.0** (27.7-40.1)	**296.6** (258.0-364.6)
F	**260** (200-467)	**33.3** (7.6-85.7)	**22.9** (6.0-33.1)	**28.0** (22.7-36.4)	**319.2** (240.3-373.3)
G	**415** (261-632)	**24.7** (7.0-69.8)	**17.8** (3.1-30.6)	**28.6** (27.7-30.1)	**254.3** (230.5-301.0)
H	**517** (437-640)	**26.3** (7.0-66.9)	**20.6** (6.2-30.1)	**32.1** (29.0-34.3)	**329.7** (300.7-369.5)
J	**434** (294-718)	**26.2** (7.3-97.6)	**20.8** (4.5-34.4)	**30.5** (25.8-35.2)	**316.9** (281.3-356.5)
M	**411** (323-512)	**28.8** (7.3-78.2)	**20.9** (4.1-31.1)	**35.2** (28.7-41.7)	**367.9** (317.8-443.0)
N	**377** (293-474)	**26.2** (7.2-78.2)	**18.5** (4.4-28.1)	**26.8** (24.9-30.1)	**247.8** (228.1-272.5)
O	**287** (190-672)	**29.4** (8.0-83.7)	**20.3** (5.9-31.1)	**24.8** (20.5-36.1)	**252.1** (230.4-309.2)
S	**307** (305-350)	**29.9** (7.1-78.8)	**22.2** (5.0-33.0)	**29.0** (26.3-32.6)	**321.9** (305.4-349.7)

Note: Data from TLS survey in 2019, **mean** (range); n, number of trees; dq, quadratic mean diameter; hq, height corresponding to dq; BA, basal area; SV, standing volume.

2.2. Methods

2.2.1. Scanner types

Scanner types

Two different laser-scanning systems were used. The RIEGL LMS-Z420i (RIEGL 2010) for Article I and II. The RIEGL VZ-400i (RIEGL 2019) for Article II and III. An overview of the two scanners, summarizing their main characteristics, is provided in Table 5.

Table 5 Overview of both scanners, RIEGL LMS-Z420i (RIEGL 2010), and RIEGL VZ-400i (RIEGL 2019).

Laser Measurement System (LMS)		**RIEGL Z420i**	**RIEGL VZ-400i**
Range[1)]	m	1000	800
Effective measurement rate[2)]	meas./s	11000	500000
Accuracy[3)4)]	mm	10	5
Precision[4)5)]	mm	4	3
Vertical field of view	°	80	100
Pulse mode		last-pulse	multiple target capability
Registration		artificial	automatic
Laser beam divergence	Mrad[6)]	0.25	0.35

Note: 1) Typical values for average conditions. Maximum range is specified for flat targets with a size in excess of the laser beam diameter, perpendicular angle of incidence, and for atmospheric visibility of 23 km. In bright sunlight, the maximum range is shorter than under overcast sky. 2) Rounded values. 3) Accuracy is the degree of conformity of a measured quantity to its actual (true) value. 4) One sigma at 100 m range under RIEGL test conditions. 5) Precision, also called reproducibility or repeatability, is the degree to which further measurements show. 6) Measured at the 1/e2 points. 0.25/0.35 mrad corresponds to an increase of 25/35 mm of beam diameter.

2.2.2. Analysis of stand density effects on the stem form and investigation of subsequent volume miscalculations (Topic I)

QI: How does competition modify the stem form of trees with the same height and diameter at breast height and thus influence volume miscalculation by traditional form factor equations?

TLS workflow: scan acquisition

The following demonstrates the different steps of the TLS method applied in Article I. A detailed description of the workflow can be found in the Appendix C Supplementary A. 1. Laser-scanning system RIEGL LMS-Z420i (RIEGL 2010) scan acquisition. 2. Stem detection. 3. The x- and y-coordinates were determined at each stem base (stem position). 4. Acquisition

of the cylindrical subset around the stem position (1 m radius). 5. On the cylindrical-subset data, stem isolation was made and the total tree heights were calculated. 6. From the isolated stem data, stem diameters were calculated. In order to identify the trees in both the field database and the TLS point cloud, I manually rotated and merged the two tree spatial maps obtained from the field database and the stem detection method.

Quantification of competition

The competition was expressed by modifying the index introduced by Hegyi (1974), using Function (1). The original Hegyi-index builds the ratio between the diameters of competitor trees and the reference tree, considering concurrently the distances of all the competitors. The spatial positions of all trees were available because the trial is part of a network of long-term growth and yield research plots.

$$HgCI_i = \sum_{j=1}^{n} \frac{d_{1.3\,j}}{d_{1.3\,i}} \frac{1}{Abst_{ij}} \quad (1)$$

Where $HgCI_i$ is the competition index for reference tree$_i$, $d_{1.3\,j}$ is the $d_{1.3}$ of competitor tree$_j$ (cm), $d_{1.3\,i}$ the $d_{1.3}$ of reference tree (cm), $Abst_{ij}$ the distance between reference tree$_i$ and competitor tree$_j$ (m) and *n* the number of competitor trees. The competition zone radius (CZR) defined the radius in which competitors were searched around the reference tree (Function 2). It was calculated for each plot and time. The competition zone of border trees was mostly outside the plot in relative size. To counteract this problem, the external surface was calculated. With this value, it was then possible to extrapolate the calculated competition for the partial area to the total area.

$$CZR = k * \sqrt{\frac{10000}{N}} \quad (2)$$

The variable *k* is a constant defining the radius of the competition zone ($2 < k < 4$) and *N* the number of trees per hectare (Lee and Gadow 1997). The competition was calculated three times during the stand's history: at the beginning of planting, after 27 years, and at present (44 years

since establishment). For the purpose of calculation, the following Function (3) for each tree was used, which was weighted according to time:

$$Competition = \frac{\frac{HgCI_{i_{t0}} + HgCI_{i_{tm}}}{2} * tm + \frac{HgCI_{i_{tm}} + HgCI_{i_{t1}}}{2} * (t1 - tm)}{t1} \quad (3)$$

Where $HgCI_{i_{t0}}$ is the Hegyi index at time 0 (planting time), $HgCI_{i_{tm}}$ = Hegyi index at mid-age of stand and $HgCI_{i_{t1}}$ = Hegyi index at the present age. The parameter t_0 is the age at the beginning of stand, t_m is the mid-age of the stand and t_1 is the complete age of the stand.

Individual TLS-data-fitted stem curve by Pain function

The diameters at the higher sections of the stem that were not gathered by the laser scanner were determined by the two-parameter taper Function (4) of Pain and Boyer (1996). The two parameters α and β were calculated for each individual tree using all the diameter measurements of the visible stem sections. The Pain function was fitted for each individual tree with, α, β, and stem radius in relative stem height, obtained by TLS, and reconstructs the whole stem curve.

$$r(h_{rel}) = \alpha * (1 - h_{rel}^3) + \beta * (ln(h_{rel})) \quad (4)$$

Where $r(h_{rel})$ is the stem radius in relative stem height h_{rel}. The parameter α is the dimension-describing parameter, while β is the form-describing parameter.

Types of volume determination

Three different calculations of the volume were used, which vary in both input parameters and methods (Table 6).

Table 6 Types of stem volume calculations. The types differ in source of input parameters (TLS or traditional forest inventory TFI) and in the method applied (stem curve Function (4) and traditional form factor equation (Kennel 1969).

Type	**1**	**2**	**3**
Height (h)	TLS	TLS	TFI
Diameter at breast height $(d_{1.3})$	TLS	TLS	TFI
Diameters along the stem (d_{all}, h)	TLS	-	-
Volume function (f_i)	$f_1(d_{all}, h)$	$f_2(d_{1.3}, h)$	$f_2(d_{1.3}, h)$

Note: Type 1: terrestrial laser scanner (TLS) measurement of height (h) and diameters along the stem in 0.1 m height intervals (d_{all}). The stem curve function 4 was used as volume function (f_1) Type 2: TLS input of height (h) and diameter at breast height ($d_{1.3}$). The traditional form factor equation (Kennel 1969) was used as volume function (f_2) Type 3: Traditional forest inventory (TFI) measurements of height (h) and diameter at breast height ($d_{1.3}$). The traditional form factor equation was used as the volume function (f_2).

The volume computation according to type 1 is exclusively based on TLS, i.e. Function (4) was used (Pain and Boyer 1996) to derive total tree volume. Type 3 volume estimation used traditional forest inventory data and conventional form factor equations (Kennel 1969). The volume calculation of type 2 was a composite method of types 1 and 3. It was based on TLS data, but only the height and the diameter at breast height were taken and inserted into the conventional form factor equation (Kennel 1969). The goal of type 2 was to determine whether any differences between types 1 and 2 were due to the volume calculation method. The main focus was on type 1, which was always the reference to the other types because they were more realistic estimations. Type 1 was compared with type 2 (volume ratio 1) and type 3 (volume ratio 2) by forming ratios to determine differences per tree as a percentage. Type 1 was the numerator in both cases, and types 2 and 3 were the denominators.

2.2.3. Investigation of tree shape responses to drought stress (Topic II)

QII: How does severe drought stress affect potential tree vitality indicators consisting of stem and crown attributes?

TLS workflow: scan acquisition

In winter 2012/2013, before the start of the drought stress experiment, terrestrial laser scanning (TLS) was carried out and repeated in the winter of 2018/2019. Using TLS-point clouds from the two surveys, structural tree modifications within the six-year period were directly visualized, computed, and linked to water limitation. Two different laser-scanning systems were used for the two surveys: the RIEGL LMS-Z420i (RIEGL 2010) for the winter of

2012/2013 and the RIEGL VZ-400i (RIEGL 2019) for the winter of 2018/2019. A detailed description of the scan acquisition can be found in Appendix C Supplementary B. In the winter of 2018/2019, the resolution was chosen so that the scans were comparable to the TLS recordings in the winter of 2012/2013. Due to the angular measurement scheme of the scanners, which operate from the ground, the point density naturally decreases towards the top of the canopy. Furthermore, the laser beam is usually unable to penetrate tree compartments in order to perform measurements behind obstacles. These two effects result in rather sparse measurement densities in the upper crown and stem regions, especially if the crown parts near the scanner are dense (Hilker et al. 2010). Regarding the RIEGL LMS-Z420i, I attempted – with the RIEGL distance-measurement mode called “last-pulse” or “last-target” – to counteract these effects and record the deepest points within a footprint, thus gaining a higher proportion of returns from inner-crown regions compared to the first-pulse mode. Using the pulsed time-of-flight method for laser range measurements, the RIEGL LMS VZ-400i determines the range to all targets with which a single laser pulse interacts ("multi-target capability"). Depending on the measurement program used, the maximum number of targets that can be detected varies. In summary, the RIEGL LMS-Z 420i in the last-target setting generates one deep point per laser beam, while the RIEGL LMS-VZ-400i can generate 4 – 15 points per laser beam. Due to this difference between the two scanners, I did not focus on three-dimensional tree features. Instead, the crown target variables (*cpa*, transparency, and roughness) were two-dimensional to take into account the ability of the newer scanner to generate more points inside the crown space. This was done to exclude errors occurring in the three-dimensional analysis due to non-scanned areas of the upper crown region, respectively. In winter 2012/13, artificial reference targets (reflectors) distributed in the scanned forest scenes enabled the co-registration of the scans. Using the software RiSCAN PRO version 2.0.2 (http://www.riegl.com/products/software-packages/riscan-pro/), all scan positions per plot were co-registered. In winter 2018/19, the new automatic registration of the LMS VZ-400i was used so that artificial reference targets were no longer needed. Automatic registration and filtering were performed using the software RiSCAN PRO version 2.8.2. The entire point cloud was reduced using an octree to enable fast point-cloud processing without accuracy loss (Elseberg et al. 2013). This distributes the data evenly in space, whereby each cube with an edge length of 5 cm contains on average only one measuring point, which is set according to the center of gravity of the original points in the cube. Both point clouds, from winter 2012/2013 and winter 2018/2019, were post-processed via the software Cloudcompare, using the fine registration feature to register both clouds in the same project coordinate system.

Tree characteristics

Several tree characteristics, describing both stem and crown properties, were extracted from the TLS data. Only the measurements for $d_{1.3}$ were taken manually with a girth tape. The isolation of the single tree from the TLS point cloud was performed using a preprocessing algorithm within the R programming environment (R Core Team 2016). After this step, each tree was visually checked for completeness. If necessary, unrecognised tree parts were added manually, and artifacts that did not belong to the tree were removed using the software RiSCAN PRO version 2.0.2 (http://www.riegl.com/products/software-packages/riscan-pro/).

Stem properties – diameter, height and taper

The diameter at breast height ($d_{1.3}$) was measured for all trees, using a girth tape, in the winter of 2012/2013 and winter of 2018/2019. The periodic annual diameter increment ($pai_{d1.3}$ in cm yr^{-1}) was calculated as the difference between the two dates divided by the time range of six years. Based on the TLS data, tree height was calculated as the difference between the highest and lowest z-axis points of the isolated tree. The periodic annual height increment (pai_{height} in m yr^{-1}) was computed as the difference between the heights from the two consecutive surveys, divided by six years. Generally, taper is the diameter change per unit of length. Modern log measurement systems determine the taper as the slope of a linear regression between different diameters and their axial positions (ÖNORM L 1021 2013). The procedure applied here was as follows: Firstly, the stem was isolated from the TLS-data using the method developed by Jacobs et al. (2020). Secondly, the stem was separated into 0.1 m intervals, from 1.3 m to 10.0 m. Thirdly, within this stem section, the taper was calculated as the slope of the linear regression between diameter and axial position. Finally, the periodic annual taper change (pac_{taper} in mm m^{-1} yr^{-1}) was the difference between the taper in the winter of 2012/2013 and the winter of 2018/2019, divided by six years.

Crown properties – projection area, transparency and roughness

Based on point clouds from TLS scanning, crown properties were calculated using the R package “alphahull” (Rodriguez-Casal and Pateiro-Lopez 2019). This package enables the determination of the area and bordering line of a sample of points in a plane. By varying the α-value, the tightness of the bordering line around the point cloud can be adjusted. Very low α-values even recognize areas without any points in the middle of a two-dimensional point set.

Choosing an α-value of 1, the TLS points were framed with a slack polygon (Figure 5a). The area inside this polygon was used as a proxy for the crown projection area ($cpa_{tradition}$), which

closely resembles the traditional crown projection area that is recorded in the field from the ground. Subtracting the two subsequent crown projection areas from each other and then dividing the difference by six years, the periodic annual change of the crown projection area (pac_{cpa} in m^2 yr^{-1}) was obtained. Without claiming to have calculated the actual $cpa_{tradition}$, it was important to choose the same alpha values for the scans of winter 2012/13 and winter 2018/19, to ensure the comparability of the two measurements (*ceteris paribus* conditions).

The crown projection area (Figure 5a) also served to assess crown transparency. For this, a polygon was created surrounding the two-dimensional point cloud per tree, choosing an α-value of 0.1. Consequently, the polygon fitted tightly to the points (Figure 5b). The resulting area of the tight polygon (Figure 5b) was normalised by the $cpa_{tradition}$ first and then subtracted by 1. Analogous to the previous definitions, the difference in crown transparency on two different dates was divided by six years to obtain the periodic annual change in crown transparency ($pac_{transparency}$ in % yr^{-1}). The calculated crown transparency is not the replication of the conventionally calculated parameter (Müller and Stierlin 1990). The calculation is based on the two-dimensional top view perspective, whereas conventional crown transparency is estimated based on lateral perspectives.

The tight polygon (α = 0.1, Figure 5b) can be used not only for the derivation of an area but also of the polygon length to determine the crown roughness. To eliminate the size effect, the perimeter of a circle was calculated, which had the same area as the polygon of $cpa_{tradition}$ (α = 1, Figure 5a). The perimeter of the tight polygon (α = 0.1, Figure 5b) was finally divided by the perimeter of the circle (Function 5). By analogy with the previous definitions, the difference in the crown roughness on two different dates was divided by six years, to obtain the periodic annual change of crown roughness ($pac_{roughness}$ in % yr^{-1}).

$$pac_{roughness} = \frac{\left(\frac{P_{length_{cpa\,\propto 0.1}}}{2*\sqrt{cpa_{tradition\,\propto 1}*\pi}}\right)_{2018/19} - \left(\frac{P_{length_{cpa\,\propto 0.1}}}{2*\sqrt{cpa_{tradition\,\propto 1}*\pi}}\right)_{2012/13}}{6} \quad (5)$$

$pac_{roughness}$ = periodic annual change of crown roughness
P = Polygon
cpa = crown projection area
$\propto$ = alpha-values

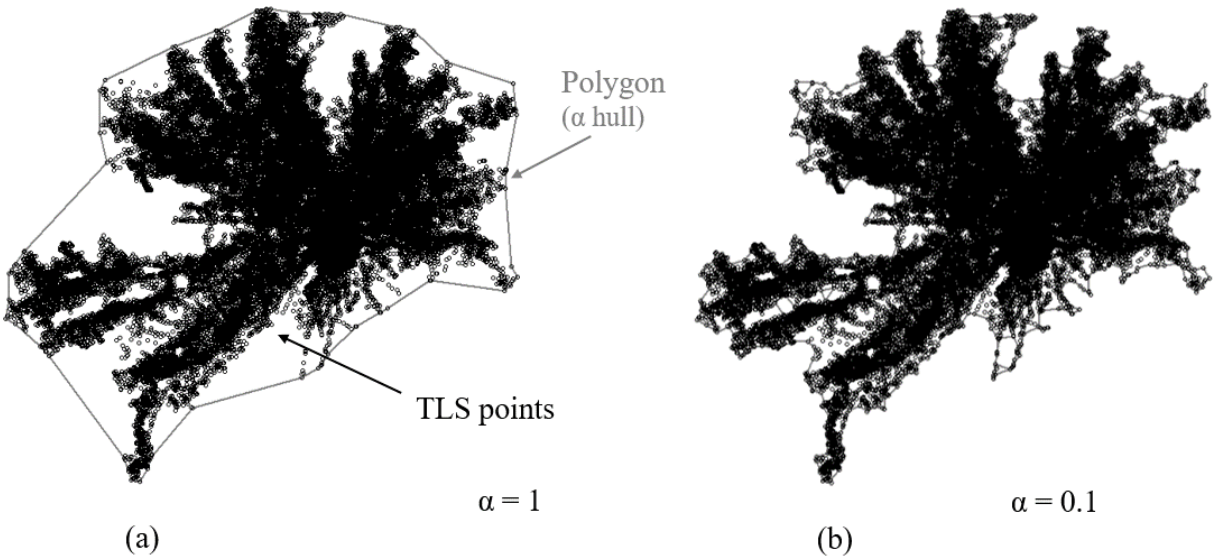

Figure 5 Top view of tree number 89, by way of illustration of the different methods for calculating the crown projection area within the R package "alphahull". Choosing an α-value of 1 (a), a projection area similar to the traditional crown projection area was derived. Choosing an α-value of 0.1 (b), the polygon framed the crown tightly. The crown transparency was calculated based on both crown projection areas.

The *cpa* varies with different α-values, but at value 1, the difference in *cpa* between the two measurements was stable (Figure 6).

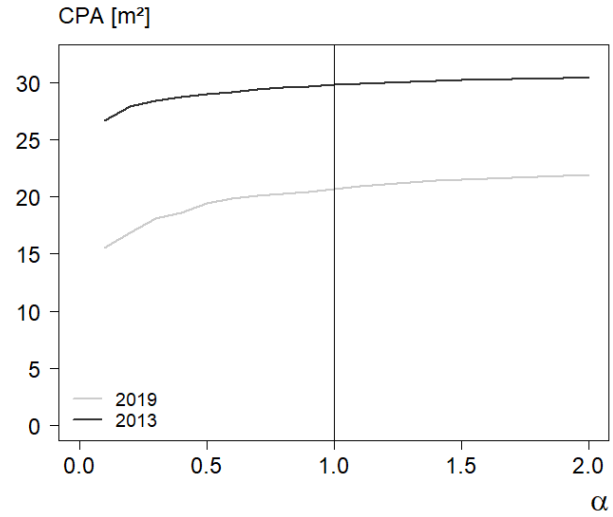

Figure 6 Comparison of different α-values for α-hulls determining the *cpa* of tree number 89.

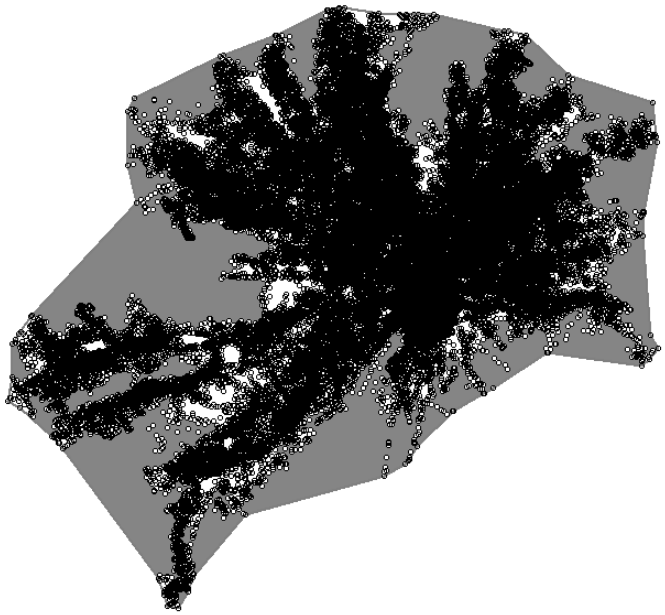

Figure 7 Two-dimensional top view of a Norway spruce tree (number 89) in winter 2012/13. The gray area shows what was considered to be the transparent parts of the crown projection area. The black points are TLS points.

Finally, the focus was on the investment pattern between stem and crown. The allometry exponent β of the allometric Function (6) was determined. The slope β indicated the change in *cpa* at the growth rate of the $d_{1.3}$ (Bertalanffy 1951). If β > 1, a positive allometry is present, where *cpa* changes more than $d_{1.3}$. Vice versa, with negative allometry (β < 1), $d_{1.3}$ changes more than *cpa*. Isometry prevails if the initial proportions remain constant over time (Pretzsch 2001).

$$\ln(cpa) = t + \beta_{cpa,\, d1.3} \times \ln(d_{1.3}) \qquad (6)$$

cpa = crown projection area
$d_{1.3}$ = diameter at breast height
t = offset
$\beta_{cpa,d1.3}$= allometry exponent

Quantification of competition

The competition was expressed by the index introduced by Hegyi (1974), using Function (1) that already served to calculate the local competition for research Topic I, where stem form variation and volume miscalculation due to competition were analyzed. The original Hegyi-

index forms the ratio between the diameters of neighbouring trees and the reference tree, considering concurrently the distance from all the competitors. The spatial positions of all trees were taken from terrestrial laser scans.

The competition zone radius (CZR) proposed by Lee and Gadow (1997), defined as the radius in which competitors were searched around the reference tree, is a function of the number of trees per hectare, and was determined only once, so that the radius was the same for every investigated tree. For this Function (2) was used that also served to calculate the competition zone radius and thus the local competition for research Topic I. The competition zone of border trees was mostly outside the plot in relative size. To counteract this problem, the calculated competition for the partial area inside the plot was extrapolated to the total area of the competition zone.

2.2.4. Assessment of defoliation and analysis of subsequent growth losses (Topic III)

QIII: How does insect defoliation caused by Lymantria dispar affects stem growth?

TLS workflow: scan acquisition

For Article III, the RIEGL VZ-400i (RIEGL 2019) was used. An overview of the scanner, summarizing the main characteristics, is provided in Table 5. For all scanning campaigns, multiple scans were taken consecutively around the plots. The number of scan positions varied between the plots depending on the stand density of the plots. The higher the stand density, the more scan positions were needed. The number of scan positions between the scanning campaigns t_2 and t_3 was always the same to ensure the comparability of the measurements (*ceteris paribus* conditions).

A laser pulse repetition rate of 1200 kHz was used. One horizontal 360° scan was performed for each scan position with a 100° vertical field of view. In my practical experience, the horizontal angular resolution was set to 0.04°, which in our practical experience, achieves a reasonable trade-off between scan-time (45 seconds per scan) and the risk of disturbances due to tree movement through wind. Due to the angular measurement scheme of the scanner, which operates from the ground, the point density naturally decreases towards the top of the canopy. Furthermore, the laser beam is usually unable to penetrate tree compartments in order to perform measurements behind obstacles. These two effects result in rather sparse measurement

densities in the upper crown and stem regions, especially if the crown parts near the scanner are dense (Hilker et al. 2010). Using the pulsed time-of-flight method for laser range measurements, the RIEGL LMS VZ-400i determines the range to all targets with which a single laser pulse interacts ("multi-target capability"). Depending on the measurement program used, the maximum number of targets that can be detected varies. The RIEGL LMS VZ-400i can generate 4 – 15 points per laser beam. I did not focus on three-dimensional tree features. Instead, the crown target variables (leaf area and crown perforation) were two-dimensional. This was done to exclude errors occurring in the three-dimensional analysis due to non-scanned areas of the upper crown region, respectively. Using the software RiSCAN PRO version 2.0.2 (http://www.riegl.com/products/software-packages/riscan-pro/), all scan positions per plot were co-registered.The new automatic registration of the LMS VZ-400i was used so that artificial reference targets were no longer needed. Automatic registration and filtering were performed using the software RiSCAN PRO version 2.8.2.

TLS data post-processing

The automatic registration of the LMS VZ-400i was applied so that artificial reference targets were not needed in the field. The automatic registration, filtering, and multi-station adjustment (MSA), which were used to refine the overall registration, were performed using the RiSCAN PRO version 2.8.2 software (http://www.riegl.com/products/software-packages/riscan-pro/). By using the automatic registration feature and since I started each scan at approximately the same position where I finished the previous scanning campaign at the specific plot, it was possible to register all the point clouds of each scanning campaign (TLS_1 – TLS_3) into one project coordinate system. To include all the foliage, stems, and branches (sometimes hidden by foliage) on t_2 and t_3, each point cloud from TLS_2 and TLS_3 was merged with the point clouds from TLS_1, before using an octree. This means that structural tree modifications within the scanning campaigns t_1 to t_3 can be directly visualized (Figure 2). Every point cloud was reduced using an octree to enable fast point-cloud processing without accuracy loss (Elseberg et al. 2013). This way, the data is evenly distributed in space, whereby each cube with an edge length of 5 cm contains only one measuring point on average, set according to the center of gravity of the cube's original points.

The complete processing was carried out within the programming environment of R (R Core Team 2016). For this purpose, the rlas package (Roussel and Boissieu 2019) was applied. Each central tree was marked with a reflector in the field during scanning. This made it possible to detect central trees in all point clouds due to their higher reflectance values (> 1) compared to

the rest of the points. After tree detection, the isolation of each central tree from the TLS point cloud of t_1, t_2, and t_3 was performed using a preprocessing algorithm. Following this step, each tree was visually checked for completeness. If necessary, unrecognised tree parts were added manually, and artifacts that did not belong to the tree were removed.

Foliation-describing parameter

Leaf area

The difference between a tree's winter state and a tree's summer state after defoliation was used to calculate insect impact on foliation in insecticide-treated and control plots. Based on the TLS point clouds, total leaf area was calculated using the "alphahull" R package (Rodriguez-Casal and Pateiro-Lopez 2019). This package permitted the determination of the area and borderline of a sample of points in a plane, and it had also been successfully used in previous research to determine crown attributes (Jacobs et al. 2021). By varying the α-value, it was possible to adjust the tightness of the borderline around the point cloud. Very low α-values can even recognize areas without any points in the middle of a two-dimensional point set. When a uniform α-value of 0.1 was chosen, the polygon fitted tightly to the points (Figure 9). Subtracting each of the two subsequent areas from winter and summer, the periodic change of leaf area ($pc_{leaf\ area}$ in m^2) was obtained. It was essential to choose the same alpha values for the scans in leaf-off and leaf-on conditions to ensure the comparability of the measurements (*ceteris paribus* conditions). Repeated scanning campaigns of the same plots in 2019 made it possible to calculate the $pc_{leaf\ area}$ at the individual tree level. Via the difference between the *horizontal projection area* of the respective summer scanning campaign t_2 or t_3 and t_1 (Figure 8), the $pc_{leaf\ area}$ of the individual tree could thus be calculated objectively in m^2 (Function 7 and 8).

$$pc_{leaf\ area}, t_2 = horizontal\ projection\ area_{\alpha=0.1,\ t2} - horizontal\ projection\ area_{\alpha=0.1,\ t1} \quad (7)$$

$$pc_{leaf\ area}, t_3 = horizontal\ projection\ area_{\alpha=0.1,\ t3} - horizontal\ projection\ area_{\alpha=0.1,\ t1} \quad (8)$$

The $leaf\ area_i$ as the arithmetic mean of the periodic change for the individual tree is determined by Function (9):

$$leaf\ area_i = (pc_{leaf\ area}, t_2 + pc_{leaf\ area}, t_3)/2 \quad (9)$$

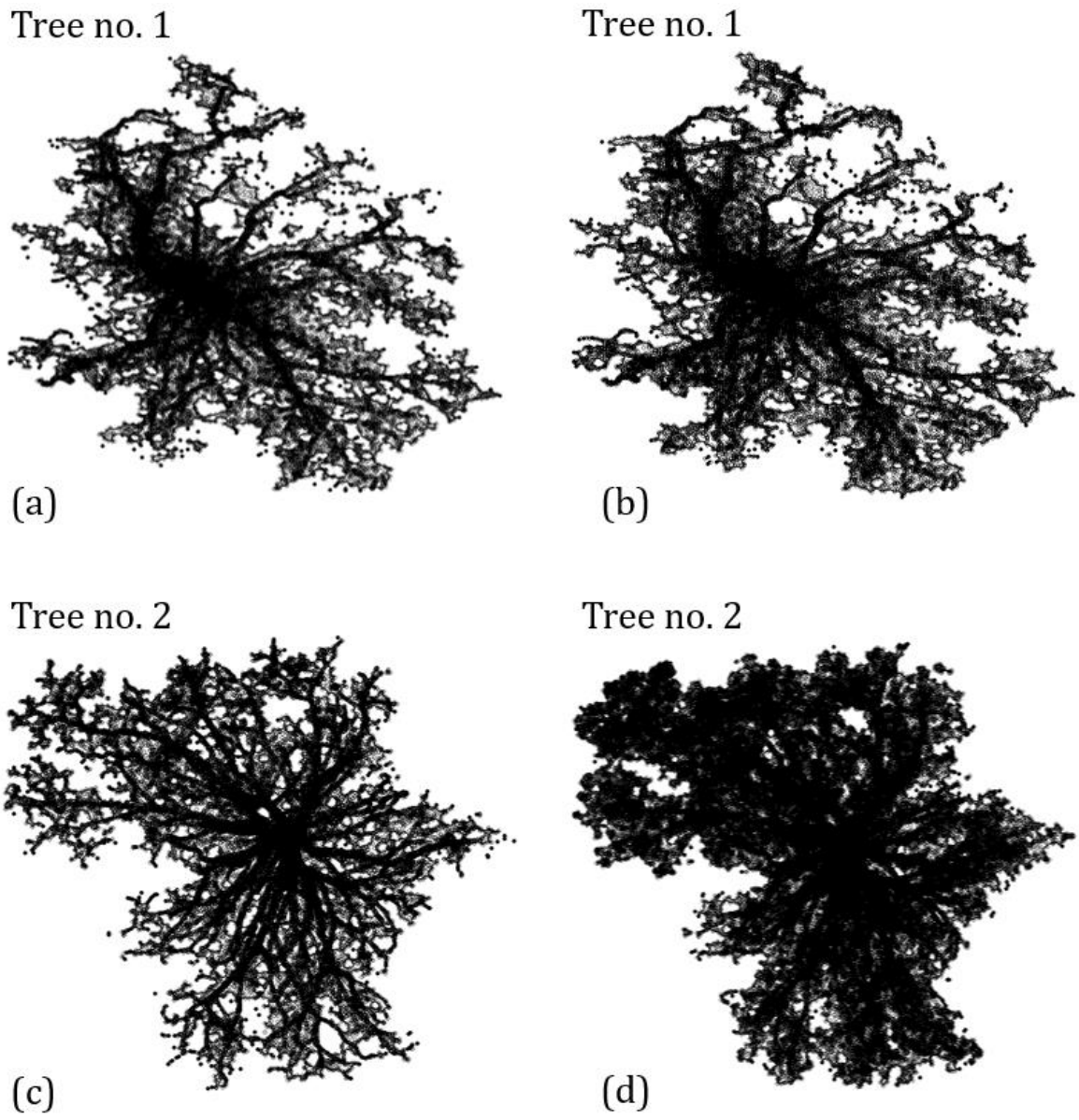

Figure 8 A top view of two sample trees extracted from the TLS point cloud (a), (c) in winter without leaves; (b), (d) in summer during peak feeding. Tree no. 1 is a tree from a plot with a high defoliation risk and no treatment (HC, i.e., control); Tree no. 2 is a tree from an area with a high defoliation risk and treated with Mimic (HM). Tree no. 1 has a calculated leaf area of 5.9 m^2 and tree no. 2 has a leaf area of 38.3 m^2.

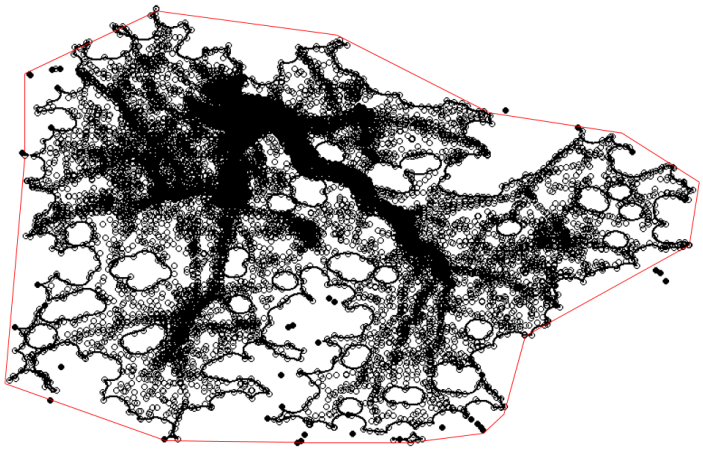

Figure 9 Top view of an oak tree, by way of illustration of the different methods for calculating the leaf area and crown perforation within the R package "alphahull". Choosing an α-value of 1 (red polygon), a projection area similar to the traditional crown projection area was derived. Choosing an α-value of 0.1 (black polygon), the polygon framed the crown tightly.

Crown perforation

In addition to total leaf area also crown perforation was calculated from the data. The polygon can not only be used to derive an area but also to determine its length. Firstly, the polygon length (α = 0.1) was divided by the crown projection area (*cpa*) area with α = 1 to eliminate the size effect. This result was finally divided by the polygon length of the *cpa* with α = 1 and multiplied by 100 (Function 10) to obtain the crown perforation as a percentage. The length of the polygon (α = 0.1) primarily determines the perforation of the crown. The higher the polygon length (always in relation to crown size), the higher the perforation because more holes within the crown can then be found. The crowns are less compact in the profile.

$$Crown\ perforation_{t2} = \frac{\left(\frac{Pl_{0.1}}{Pa_1}\right)}{Pl_1} * 100 \quad (10)$$

t2 = scanning campaign at high peak gypsy moth
$Pl_{0.1}$ = Polygon length of the crown projection calculated with alpha = 0.1
Pa_1 = Polygon area of the crown projection calculated with alpha = 1
Pl_1 = Polygon length of the crown projection calculated with alpha = 0.1

2.2.5. Modelling approach and evaluation

In this dissertation, generalized additive mixed models and linear mixed-effects models were used to consider nesting in the data. Random effects included in the models address the inter-correlation of samples caused by spatial and temporal clustering. All statistical testing was conducted by the use of the R-function gamm and lme from the package mgcv (Zuur 2009). In the following, models are described in accordance with the main research questions (*QI – QIII*) outlined in chapter 1.2. These models were formulated to test specific hypotheses in the associated publications (Article I – III).

QI: How does competition modify the stem form of trees with the same height and diameter at breast height and thus influences volume miscalculation by traditional form factor equations?

Generalised additive mixed model (GAMM)

The data was nested on tree- and plot-level, which means that there were several observations per tree on different plots. Therefore, a generalized additive mixed model (GAMM) was required. In Table 7 three GAMM Functions (12) – (16) were formulated to answer the question *QI*. Volume ratios 1 and 2 were set as response variables. All models explain the response variable as a function of different linear predictors like $d_{1.3}$, h, treatment (Figure 2a), thinning regime (Figure 2b), initial planting density (plants per hectare) and competition as a non-linear predictor. Detailed information on treatment and thinning regime per plot is given in Appendix C Supplementary A (Table A1 – A3). Function (11) shows the general structure of the model that was used:

$$Y_{ij} = a_0 + a_1 * X_{1,i} + a_2 * X_{2,j} + \ldots + a_n * X_{n,ij} + f(Competition_i) + b_j + \varepsilon_{ij} \qquad (11)$$

Throughout each model, the variable Y is the response variable, the variables $X_1 \ldots X_n$ are the linear predictors, the variable i indexes the tree, and the variable j the plot. The variable a represents the model's intercept, the variable b represents the random effect related to the plots, and the symbol ε represents the remaining errors. The variable f is a non-linear smoother, which covers non-linear relationships. Zuur et al. (2009) described the technical details (mgcv

package). Here, smoother f is based on competition and is intended to cover the effects of unobservable influence variables. The parameters $d_{1.3}$ and h were set as linear predictors to analyze the effect of competition on trees with the same $d_{1.3}$ and h. The competition was tested on its own while other variables were set to the mean. This was also done for Function (14), with stem taper as the response variable. The log class (butt, middle, and top log) differentiates the stem into three parts and was added as a linear predictor to see which part of the stem is affected by changes in shape due to competition.

Table 7 GAMM Functions (12) – (16) regarding ***QI***.

Response variable	Linear predictors	Smoother	Function
TLS volume	$d_{1.3}$+h+Treatment+Thinning+PD	f(Competition)	(12)
Form factor	Treatment+Thinning+PD	f(Competition)	(13)
Stem taper	$d_{1.3}$+h+Treatment+Thinning+PD+Log class	f(Competition)	(14)
Volume ratio 1	Treatment+Thinning+PD	f(Competition)	(15)
Volume ratio 2	Treatment+Thinning+PD	f(Competition)	(16)

Note: Generalized additive mixed model (GAMM); TLS volume = volume obtained by terrestrial laser scanning (TLS) method, diameter at breast height = $d_{1.3}$, h = total tree height, PD = planting density, Log class = log classes per tree (butt, mid and top log), D_1 = lower diameter at the beginning of the stem section, D_2 = upper diameter at the end of the stem section, L = length of stem section, Stem taper = $\frac{(D_1-D_2)}{L}$, Form factor = $\frac{\text{TLS Volume}}{((\frac{pi}{4} * d_{1.3}) * h)}$.

Evaluation of TLS method

The automated TLS method's performance was assessed in terms of correct tree detection and deviation of $d_{1.3}$ diameters along the stems d_{all} and the total heights of the harvested trees due to the values obtained using manual measurement methods as reference (e.g., caliper, tape, and vertex). A key assumption in applying ordinary least squares (OLS) is that the independent variable is measured without error (Harper 2014) or that the magnitude of the error in the response variable is much larger than that in the independent (explanatory) variable (Legendre and Legendre 1988), which is not the case for this analysis. The measured diameters (TLS and manual measurement) contain some components of error. For those variables, Legendre (1998) recommends a major axis (MA) regression instead of an ordinary least squares regression. For this evaluation, the lmodel2 package (Legendre 2018) was used. The automated estimations were compared with the reference measurements at the tree level. The accuracy of the estimations was evaluated in terms of the bias and root mean squared error (RMSE) by using

the R package SimDesign (Chalmers 2018). To validate the tree detection, the proportion of detected trees in the plots to all trees in the plots ($\frac{detected\ trees}{trees\ in\ the\ dataset}$) was calculated.

The processing was done within the programming environment of R (R Core Team 2016). The R packages used for the automated method were rlas, dbscan, TreeLS, and conicfit. The exact description of the R packages used for the respective tasks is given in Appendix C Supplementary A.

QII: How does severe drought stress affect potential tree vitality indicators consisting of stem and crown attributes?

T-test

To visualize possible differences between control and treatment plots regarding drought stress, boxplots were created for all the analyzed parameters regarding. A t-test was used to determine whether there was a significant difference between the means of the two groups: the control group (no water limitation) and the treatment group (water limitation).

Mixed Effect Regression Model

The data was nested at the group level, which means that there were several trees in one group. Therefore, a mixed effect regression model with random effects at plot level was required. I started with a complex model using a generalized mixed-effects model (GAMM) with smoother expecting a non-linear relationship between the interaction of drought and competition. Instead, the relationship turned out to be linear. Thus, a linear mixed-effects model (LMM) was used. Seven LMM functions were formulated to answer *QII* regarding the stem property parameters (Function 18 – 20), regarding crown property parameters (Function 21 – 23) and regarding their allometry exponents (Function 24). All parameters were set as response variables to analyze the effects of species, drought, competition and the interaction effects between competition and drought (Table 8). All models explain the response variable as a function of different linear predictors like drought, species and competition. Function (17) shows the general structure of the model that was used for all LMM functions:

$$Y_{ij} = a_0 + a_1 * X_{1,i} + a_2 * X_{2,j} + a_3 * X_{3,j} + a_4 * X_{2,ij} * X_{3,ij} + b_j + \varepsilon_{ij} \quad (17)$$

Throughout each model, the variable Y is the response variable, the variables $X_1 \ldots X_3$ (X_1 = Species, X_2 = Drought and X_3 = Competition) are the linear predictors, the variable i indexes the tree, and the variable j the plot. The variable a_o represents the model's intercept, the variables $a_1 \ldots a_4$ represent the slope coefficients, the variable b represents the random effect related to the plots, and the symbol ε represents the remaining errors.

Table 8 LMM Functions regarding ***QII***. All Functions (18) – (24) differ only in the response variable. The linear predictors and the interaction effects are the same for each Function.

Response variable	Linear predictors	Interaction effects	Function
$pai_{d1.3}$	Species Drought Competition	Drought Competition	(18)
pai_{height}			(19)
pac_{taper}			(20)
pac_{cpa}			(21)
$pac_{transparency}$			(22)
$pac_{roughness}$			(23)
$\beta_{cpa,d1.3}$			(24)

Note: Linear mixed model (LMM); The $pai_{d1.3}$ (cm yr^{-1}) is the periodic annual diameter at breast height increment, pai_{height} (m yr^{-1}) is the periodic annual total tree height increment, pac_{taper} (yr^{-1}) the periodic annual change of taper, pac_{cpa} ($m^2\ yr^{-1}$) the periodic annual change of crown projection area, $pac_{transparency}$ (% yr^{-1}) the periodic annual change of crown transparency, $pac_{roughness}$ (% yr^{-1}) the periodic annual change of crown roughness, $\beta_{cpa,d1.3}$ the tree allometry exponent.

Whether using the t-test or the mixed effect regression model, the significance level for the tests is considered statistically significant when the p-value is lower than 5 %. The processing was performed within the programming environment of R (R Core Team 2016). The R packages used for the evaluation were stats and graphics, which are both part of R (R Core Team 2016). Zuur et al. (2009) described the technical details (mgcv package (Wood 2017)).

QIII: How does insect defoliation caused by Lymantria dispar affects stem growth?

Linear mixed-effects models (LMM)

The linear mixed-effects models were used to estimate the parameters for functions predicting leaf area, crown perforation, and basal area that formed the basis for subsequent tests for the effect of gypsy moths on defoliation and tree growth. To analyze wheter the leaf area and crown perforation calculated using TLS differ between trees attacked by gypsy moths and trees without damage, Functions (25) and (27) were created, which used the foliation values of all 352 oak trees scanned at t_2 and t_3. Those 352 trees served as the basis for Functions (26) and (28) to predict (*pred()*) leaf area and crown perforation for all 880 central oak trees as linear predictors to analyze the relationship between leaf area/crown perforation and basal area

increment modified by the gypsy moth. The basal area increment was calculated via the long-term girth tapes measured at the interval after defoliation (June 2019) until the end of the growing season 2019.

$$ln(Leaf\ area_{ijk}) = a_0 + a_1 * ln(Basal\ area) + a_2 * Defoliation\ risk + a_3 * Treatment + b_k + \varepsilon_{ijk} \quad (25)$$
$$ln(Basal\ area\ increment_{ijk}) = a_0 + a_1 * ln(Basal\ area) + a_2 * pred(Leaf\ area) + b_k + \varepsilon_{ijk} \quad (26)$$
$$ln(Crown\ perforatrion_{ijk}) = a_0 + a_1 * ln(Basal\ area) + a_2 * Defoliation\ risk + a_3 * Treatment + b_k + \varepsilon_{ijk} \quad (27)$$
$$ln(Basal\ area\ increment_{ijk}) = a_0 + a_1 * ln(Basal\ area) + a_2 * pred(Crown\ perforation) + b_k + \varepsilon_{ijk} \quad (28)$$

Throughout each Function, the variable *i* indexes the tree, the variable *j* the plot, and the variable *k* the block. The variable a_o represents the model's intercept, the variables a_1 and a_2 represent the slope coefficients, while the variable b_k represents the random effect related to the blocks. All random effects were assumed to be normally distributed, with an expected mean of zero. The uncorrelated remaining errors are ε_{ijk}.

Descriptive statistics

Boxplots were used to illustrate the differences in the distribution of the leaf area and crown perforation calculated using TLS between trees attacked by gypsy moths and trees without damage. Then correlation analyses were performed to determine whether leaf area and crown perforation were related to stem increment within the same year. I decided to focus on the strength of the relationship between TLS foliation measurements and inter-annual stem growth because no accurate reference for the leaf area status was available. With Functions (29) and (30), linear models of tree growth were compared. The tree growth was expressed as an inter-annual increment in the trees' basal area, which includes the time from defoliation until the end of the growing season.

$$Basal\ area\ increment_i = a_0 + a_1 * Leaf\ area + \varepsilon_i \quad (29)$$
$$Basal\ area\ increment_i = a_0 + a_1 * Crown\ perforation + \varepsilon_i \quad (30)$$

3. Results

By the application of new techniques like TLS, this dissertation contributes to enhancing forest inventory and tree vitality monitoring, thus expanding our understanding of the reaction patterns of stems, crowns, and defoliation to environmental stress. It argues that TLS data can facilitate greater objectivity in vitality monitoring, which typically relies on subjective judgments. All three research topics are embedded within the tree monitoring architecture. Tree vitality is the focus of this dissertation (Topic II). Research Topics I and III complement this focus by exploring stem and crown attributes, respectively. Together, these attributes serve as key indicators of tree vitality. This work investigates the reaction patterns of the stem attributes due to competition (Topic I) and drought (Topic II), as well as the reaction patterns of the crown attributes due to drought (Topic II) and defoliation (Topic III). Each Topic (I – III) explores a specific research question (*QI* – *QIII*). The results are reported separately in peer-reviewed research Articles (I – III), and are summarized in this section. The research questions are:

QI: How does competition modify the stem form of trees with the same height and diameter at breast height, thereby influencing volume miscalculation by traditional form factor equations?

QII: How does severe drought stress affect potential tree vitality indicators consisting of stem and crown attributes?

QIII: How does insect defoliation caused by Lymantria dispar affect stem growth?

3.1. Stem form variation and volume miscalculation due to competition (Topic I)

***QI**: How does competition modify the stem form of trees with the same height and diameter at breast height, thereby influencing volume miscalculation by traditional form factor equations?*

The effect of competition was significant on all three dependent variables – stem volume, form factor, and stem taper (Table 9 Functions 12 – 14). The lower the competition, the lower the volume and form factor of a single tree with the same $d_{1.3}$ and h (Figure 10a and Table 9). Figure 10cde shows interaction (competition:log) effects.

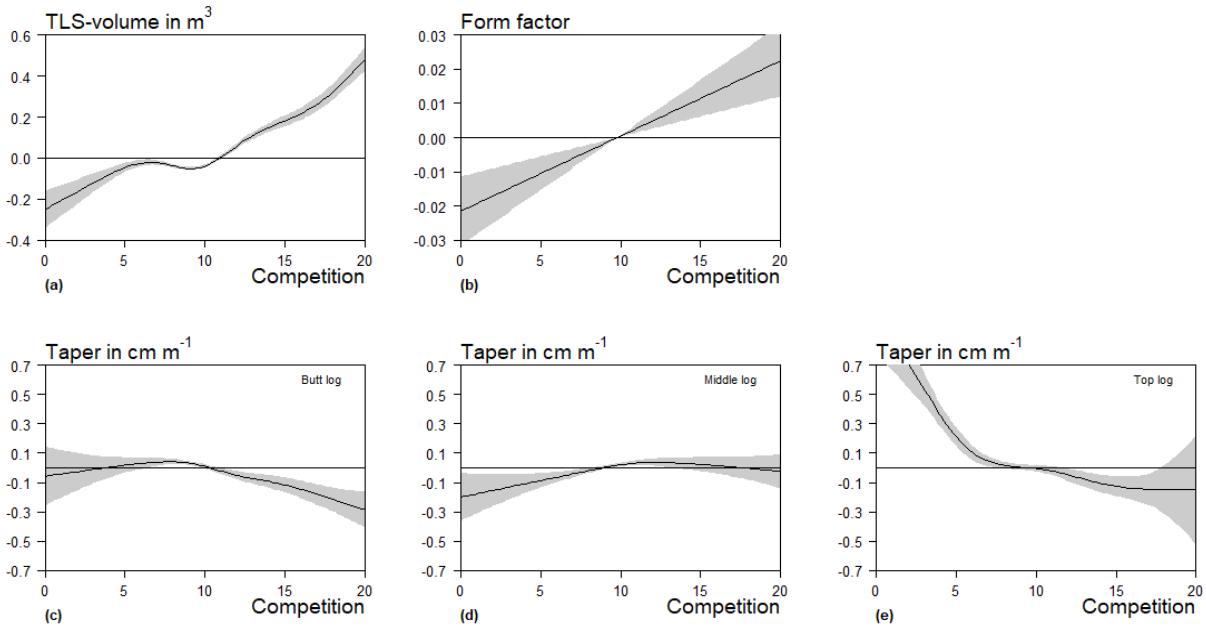

Figure 10 Effects of competition on **(a)** TLS volume, **(b)** form factor per tree, **(c)** stem taper of butt log, **(d)** stem taper of mid log and **(e)** stem taper of top log. Competition was tested on its own while other variables were set to the mean. Each Y-axis shows the deviation from the mean for that variable.

The effect of competition on the stem taper varied according to the log class but was significant for all log classes (Table 9). The butt logs of trees of the same size ($d_{1.3}$ and h) decreased in taper given increasing competition (Figure 10c), while the stem taper of the mid log increased with competition (Figure 10d). The stem taper of the top log decreased with increasing competition (Figure 10e). The competition, the log class itself, and the interaction of both had a significant influence on stem taper (Table 9).

Traditional volume functions neglect, or at least do not respect, the dependency of volume on competition, as they are designed to be simple, fast, and efficient for the purpose of practical applications. Even though competition had a statistically significant influence on deviations expressed by ratio 1, the total variability explained by Functions (15) and (16) was low (Table 9).

Table 9 GAMM statistics of Functions (12) – (16) for ***QI***. For volume ratio 1, the TLS volume calculation (numerator) was compared with the composite method of the volume calculation that uses the conventional form factor equation and TLS-determined input parameters (denominator). For volume ratio 2, the TLS volume calculation (numerator) was compared with the volume estimation that used traditional forest inventory data and conventional form factor equations (denominator). Both ratios were formed to determine differences per tree as a percentage.

	(12) TLS-volume (m^3)	**(13) Form factor**	**(14) Stem taper ($cm^{-1}\ m$)**	**(15) Volume ratio 1**	**(16) Volume ratio 2**
Intercept a_0	-1.01×10^{0}***	$+4.98 \times 10^{-1}$***	$+1.88 \times 10^{0}$***	$+1.01 \times 10^{0}$***	$+1.05 \times 10^{0}$***
$d_{1.3}$ (m)	$+5.84 \times 10^{0}$***		$+3.92 \times 10^{0}$***		
h (m)	$+9.39 \times 10^{-3}$***		-8.95×10^{-2}***		
Treatment2	$+4.92 \times 10^{-3}$	-1.14×10^{-2}***	-1.71×10^{-2}	-2.75×10^{-2}***	-2.63×10^{-2}
Thinning2	$+6.18 \times 10^{-3}$	-1.48×10^{-2}***	-1.02×10^{-2}	-6.47×10^{-3}	-2.71×10^{-2}
Thinning3	$+1.03 \times 10^{-2}$	-1.60×10^{-2}***	-5.34×10^{-3}	-7.01×10^{-3}	-5.09×10^{-4}
Thinning4	-6.13×10^{-3}	-9.89×10^{-3}***	-4.33×10^{-3}	$+2.87 \times 10^{-3}$	-1.56×10^{-2}
PD	-2.23×10^{-3}***	-6.59×10^{-7}	$+6.72 \times 10^{-6}$	$+1.22 \times 10^{-5}$***	$+1.49 \times 10^{-7}$
Log Class2			-5.54×10^{-2}***		
Log Class3			$+1.04 \times 10^{0}$***		
f(Comp)	***	***	***	***	***
f(Comp):Log Class1			***		
f(Comp):Log Class2			***		
f(Comp):Log Class3			***		
R-sq. (adj)	0.95	0.03	0.89	0.11	0.01

Note: General additive mixed model (GAMM); significance values: '***' $p < 0.001$, '**' $p < 0.01$, '*' $p < 0.05$. PD = initial planting density (trees per hectare), $d_{1.3}$ = diameter at breast height, h = total tree height, f = Smoother, Comp = Competition, Log Class = log classes per tree (butt-, mid- and top log), coefficient of determination = R-sq., Form factor = $\frac{TLS\ Volume}{((\frac{pi}{4} * d_{1.3}) * h)}$, D_1 = lower diameter at the beginning of the stem section, D_2 = upper diameter at the end of the stem section, L = length of stem section (log class), Stem taper = $\frac{(D_1 - D_2)}{L}$.

This suggests that, in addition to the effects of treatment, initial planting density, and competition, a significant portion of the deviations caused by the use of traditional volume functions (Table 10) were unrelated to competition effects.

Table 10 Volume differences by treatment. The spacing experiment represents Treatment 1 and the thinning experiment Treatment 2. For thinning, regime 1 was never thinned, regime 2 was thinned late, regime 3 was moderately thinned, and regime 4 early thinned. Planting density (PD) varied between 400 and 10000 trees/ha. For volume ratio 1, the TLS volume calculation (numerator) was compared with the composite method of the volume calculation that uses the conventional form factor equation and TLS-determined input parameters (denominator). For volume ratio 2, the TLS volume calculation (numerator) was compared with the volume estimation that used traditional forest inventory data and conventional form factor equations (denominator). Both ratios were formed to determine differences per tree as a percentage.

	Volume ratio (1) (%)	Volume ratio (2) (%)	Forest inventory volume stock (m^3)	Corrected volume stock (m^3) ratio (2)
Total	+4.2	+2.0	553	564
Treatment1	+5.4	+2.7	447	459
Treatment2	+3.8	+1.6	612	622
Thinning1	+3.1	+3.2	808	834
Thinning2	+4.0	+0.7	583	587
Thinning3	+2.8	+2.5	580	595
Thinning4	+4.6	+1.4	660	669
PD400	+6.1	+7.0	331	354
PD2500	+8.3	+5.0	455	478
PD4000	+4.0	+0.7	484	487
PD10000	+3.4	+3.5	513	531

Note: The percent volume differences were calculated for volume ratios 1 and 2. The values of the volume stocks were determined by traditional forest inventory methods. Volume ratio 2 was used to correct these values, because stem volume is traditionally calculated using form factor equations with taper and vertex as the input parameters. The more accurate TLS volumes are the reference. Volume ratio 2 deals exactly with these two procedures. Volume ratio 1 uses the same TLS data input to compare TLS against forest inventory methods. The red numbers highlight particularly strong changes or adjustments between treatments.

However, the investigation demonstrates how competition affects the stem form of trees of the same $d_{1.3}$ and h. The results show that stem taper decreased with increasing competition and vice versa (Figure 10ab). In particular, the lowest stem section (butt log) becomes more cylindrical the higher the competition (Figure 10c). The ratio of volume miscalculation decreased with increasing competition (Figure 11).

Since the butt log contains the most volume, it accounts for a large share of the overall volume difference. Competition, planting density, and treatment all influenced stem form, but these variables alone do not fully account for differences in stem form (Table 9 Functions 15 and 16). The high level of unexplained stem form variability suggests that other, unidentified plot- or tree-level factors are also at work.

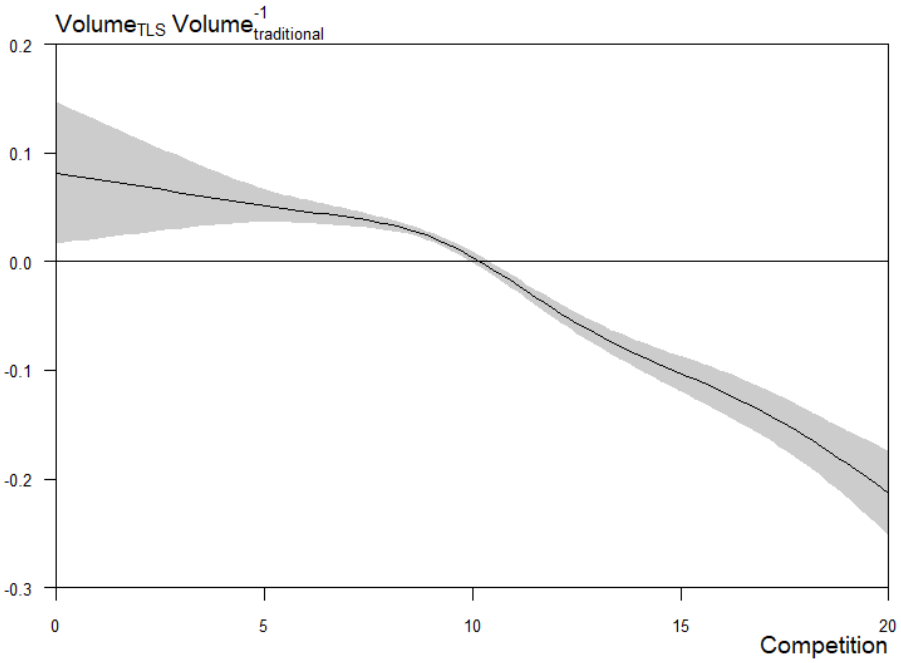

Figure 11 Effect of competition on volume ratio 1. For volume ratio 1, the TLS volume calculation (numerator) was compared with the composite method of the volume calculation that uses the conventional form factor equation and TLS-determined input parameters (denominator). Competition was tested on its own while other variables were set to the mean. The y-axis shows the deviation from the mean of the respective variable.

When focusing on the distribution (Figure 11), deviations that increase and decrease apart from the average can be observed. This may be explained by changing forest management strategies. The experimental area was heavily thinned and the degree of competition may have changed significantly over time. Stem shape may reflect the legacy of past stand structures. Hence, older samples may have been limited to trees coming from less structured stands, which were lightly thinned from below. This suggests that traditional volume functions are particularly suitable for homogeneous single-layer stands featuring medium competition. The more heterogeneous and complex the stand structure, the less suitable these functions are.

Accuracy of TLS method

The $d_{1.3}$ obtained from TLS is plotted against field measurements (Figure 12a).

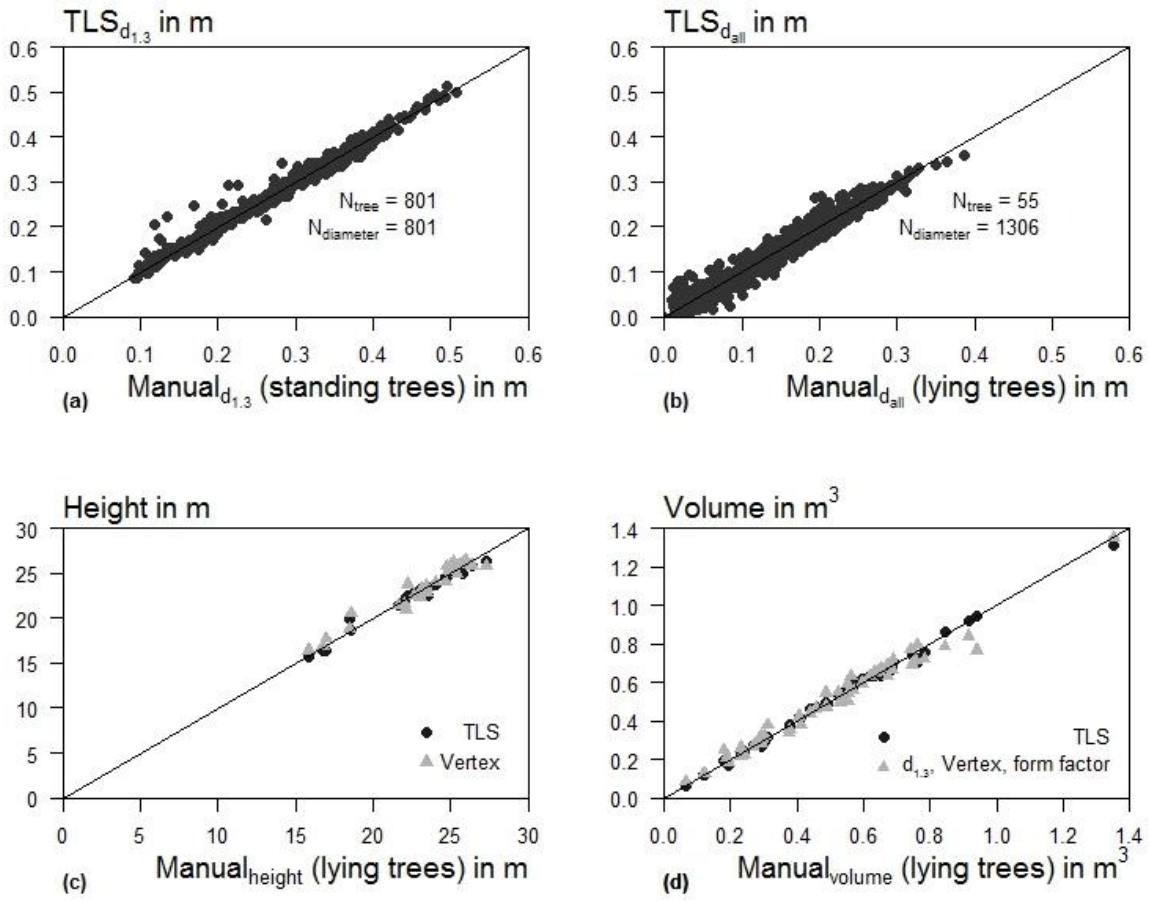

Figure 12 (a) Comparison of $d_{1.3}$ measurements between TLS and manual measurement using diameter tape. **(b)** Diameters of the 55 logged trees were measured by a caliper. **(c)** Comparison of all 28 heights across measurement types. *Type 1*: automated TLS method. *Type 2:* traditional height measurement by vertex. **(d)** Stem volumes by measurement type. *Type 1*: automated TLS method. *Type 2:* traditional volume function using forest inventory parameters. The lines represent a 1:1 relationship.

The automated TLS method yielded good diameter estimates with RMSE values of 1.15 cm for $d_{1.3}$ and 1.36 cm for diameters of all heights. TLS outperformed field measurements in terms of RMSE, bias, and linear correlation (Table 11). The heights estimated using the automated TLS method were plotted against heights that were calculated from field measurements (Figure 12b). The automated TLS method delivered good estimates of total heights overall, with RMSE values of 0.52 m for total tree height (Table 11). The traditional height estimation error with manual measurement input was 0.8 m (Table 11). The estimated volumes from the automated TLS method were plotted against volumes that were calculated from field measurements and

the Smalian (Hush et al. 1982) volume function (Figure 12c). The automated TLS method had good estimates of volumes overall, with RMSE values of 0.018 m³ for stem-wood volume (Table 11). The traditional volume estimation error with TLS $d_{1.3}$ and h input was 0.055 m³, and with manual measurement input 0.042 m³ (Table 11).

Table 11 Root mean square error (RMSE), bias and coefficient of determination (R-sq.) of the diameters at breast height ($d_{1.3}$) and diameter along the stem (d_{all}) obtained from TLS, where manual measurement was the reference.

	Mean	**RMSE**	**Bias**	**R-sq.**
Diameter (m)				
Reference $d_{1.3}$-856 trees	0.2891			
TLS $d_{1.3}$-856 trees	0.2884	0.0115	–0.0007	0.9902
Reference d_{all}-55 trees	0.1516			
TLS d_{all}-55 trees	0.1497	0.0136	0.0019	0.9807
Total height (m) – 28 trees				
Reference	22.9872			
TLS	22.9458	0.5192	–0.0343	0.9854
Traditional	23.1145	0.7942	–0.2031	0.9677
Volume (m³) – 55 trees				
Reference	0.5305			
TLS	0.5311	0.0180	–0.0006	0.9975
TLS-Traditional	0.5087	0.0547	0.0218	0.9815
Traditional	0.5263	0.0417	0.0042	0.9870

Note: Mean, RMSE, Bias and R-sq. of total tree heights calculated by TLS and by traditional forest inventory (Traditional), where manual measurement of the felled tree was the reference. Mean, RMSE, Bias and R-sq. of volumes calculated by TLS, traditional volume function with TLS data input (TLS - Traditional) and traditional volume function with input of traditional forest inventory (Traditional) where manual measurement and volume computation by Smalian (Hush et al. 1982) was the reference.

3.2. Tree vitality indicator responses to severe drought stress (Topic II)

QII: *How does severe drought stress affect potential tree vitality indicators consisting of stem and crown attributes?*

Drought stress led to a significantly smaller crown size as well as lower stem and height growth. In addition, high competition combined with drought stress resulted in crowns that were less rough and thus more compact.

It can be observed that despite random effects on plot level, drought stress affected pai_{height}, pac_{cpa} and $pac_{roughness}$ regardless of the tree species (Table 11 Functions 19, 20, and 23), which is demonstrated by the estimate values of –0.14, –1.43, and +15.9 for treated trees respectively. Furthermore, local competition had an effect on the $pai_{d1.3}$ and pac_{cpa} of the control trees (Table 12 Functions 18 and 21), which is shown by the estimate values of –0.07 and –0.27 if

competition increases by one unit, respectively. The lower the competition, the higher the growth in *cpa* and $d_{1.3}$ for the control trees. The $pac_{roughness}$ is the only parameter that is affected by local competition under drought stress, which is demonstrated by the estimate value of –9.5 for treated trees if competition increases by one unit. The lower the competition, the higher the roughness of the crowns for trees under drought stress, and vice versa. In terms of species, the variables pai_{height}, pac_{cpa} and $pac_{roughness}$ differ (Table 11 Functions 19, 21, and 23), which is demonstrated by the estimate values of +0.10, +0.52, and +7.73, respectively, for beech trees.

The results cannot prove an effect of drought stress on stem form. Only a trend towards cylindrical stem forms occurred (Table 12 Function 20). This work showed that lower competition might have the potential to improve the growth performance of trees in response to drought if the whole stem is considered (Table 12 Function 20). Due to the low model performance (R^2), drought, species and local competition may not be the only root causes of the observed stem-form differences (Table 12 Function 20).

The height growth was affected by drought stress for each individual tree species and was lower in comparison to the control trees (Figure 13b). In Table 12 (Function 19), height growth was affected by drought, which is demonstrated by the estimate value of –0.14 for all treated trees. For Douglas fir, height growth response to drought stress was observed to be an even more sensitive indicator than basal area (Rais et al. 2014).

Table 12 LMM statistics of Functions (18) – (24) for ***QII***.

Function	(18)	(19)	(20)	(21)	(22)	(23)	(24)
Response variable	$\boldsymbol{pai_{d1.3}}$	$\boldsymbol{pai_{height}}$	$\boldsymbol{pai_{taper}}$	$\boldsymbol{pac_{cpa}}$	$\boldsymbol{pac_{transparency}}$	$\boldsymbol{pac_{roughness}}$	$\boldsymbol{B_{cpa,d1.3}}$
Intercept a_0	**+0.34*** **	**+0.29*** **	**–0.07***	**+0.55** **	+0.58	+2.01	+6.63
Species (European beech)	+0.01 b	**+0.10 b** **	+0.04 b	**+0.52 b*** **	–0.08 b	**+7.73 b** **	+7.7 b
Drought (Treatment)	–0.12 b	**–0.14 b***	–0.06 b	**–1.43 b** **	+1.2 b	**+15.9 b***	–21.57 b
Competition	**–0.07** **	–0.03	–0.005	**–0.27** **	+0.05	–1.16	–5.47
Drought:Competition (Treatment)	–0.02 b	–0.003 b	–0.08 b	+0.3 b	–0.3 b	**–9.5 b***	+3.74
R^2 (adjusted)	0.33	0.43	–0.03	0.61	0.1	0.25	0.16

Note: Linear mixed-effects model (LMM); R^2 (adjusted) is the coefficient of multiple determination; all significance values and trends were bold: **'***' p < 0.001, '**' p < 0.01, '*' p < 0.05**; The $pai_{d1.3}$ (cm yr^{-1}) is the periodic annual diameter at breast height increment, pai_{height} (m yr^{-1}) is the periodic annual total tree height increment, pac_{taper} (mm m^{-1} yr^{-1}) the periodic annual change of taper, pac_{cpa} (m^2 yr^{-1}) the periodic annual change of crown projection area, $pac_{transparency}$ (% yr^{-1}) the periodic annual change of crown transparency, $pac_{roughness}$ (% yr^{-1}) the periodic annual change of crown roughness, $\beta_{cpa,d1.3}$ the tree allometry exponent. Competition is the local index by Hegyi (1974). Within a given category of drought (control vs. treatment) and species (Norway spruce vs European beech).

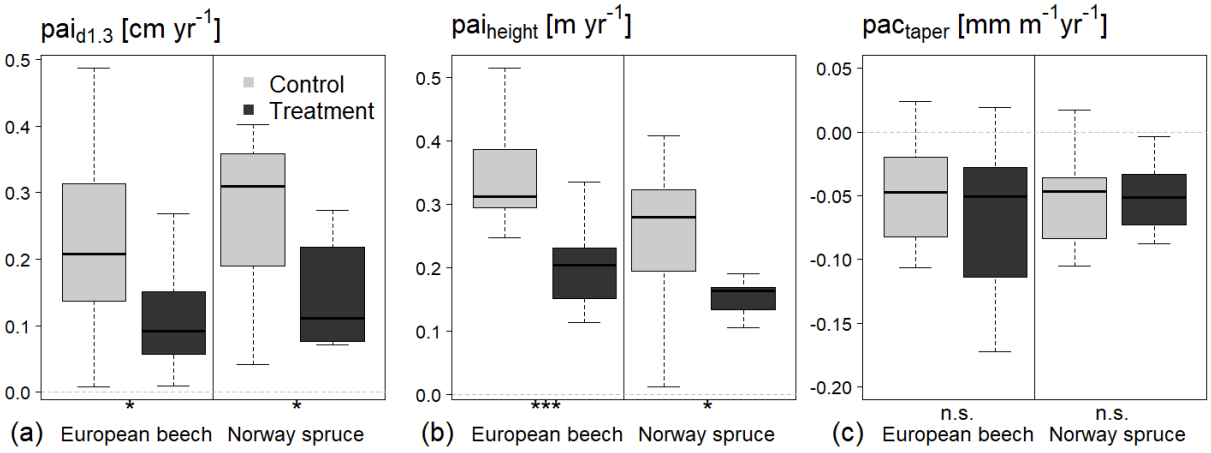

Figure 13 Effects of drought stress on stem properties ***QII***, (a) $pai_{d1.3}$ periodic annual $d_{1.3}$ increment in cm yr^{-1}, (b) pai_{height} periodic annual height increment in m yr^{-1}, (c) pac_{taper} periodic annual change of taper in mm m^{-1} yr^{-1}, yr is the year. Significance values: **'***' p < 0.001, '**' p < 0.01, '*' p < 0.05, 'n.s.' not significant.**

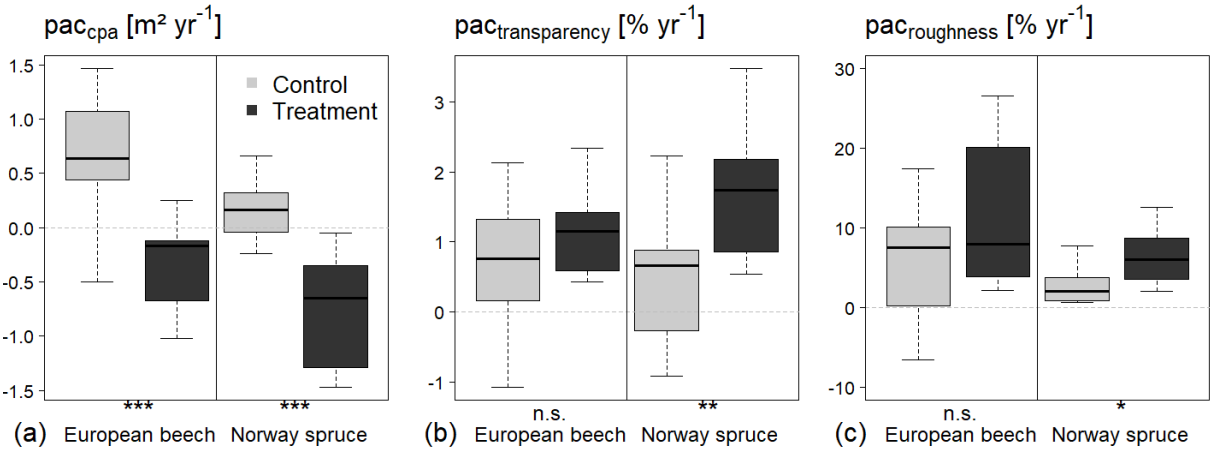

Figure 14 Effects of drought stress on crown properties ***QII***, (a) pac_{cpa} the periodic annual change of *cpa* in m^2 yr^{-1}, (b) $pac_{transparency}$ the periodic annual change of crown transparency in % yr^{-1}, (c) $pac_{roughness}$ the periodic annual change of crown roughness in % yr^{-1}. The variable *cpa* is the crown projection area (m^2) and yr is year. Significance values: '***' p < 0.001, '**' p < 0.01, '*' p < 0.05, 'n.s.' not significant.

Drought stress led to a significantly smaller crown size for each individual tree species (Figure 14a). In Table 12 (Function 18), this is demonstrated by the estimate value of –1.43 for all treated trees. The crowns of Norway spruce trees also increased in transparency and roughness on the treatment plots (Figure 14bc). The TLS scans were performed after the vegetation period, and thus the beech trees had no leaves. Lower crown transparency in beech trees could only have resulted from branch loss. Overall, almost all trees became more transparent, with trees under drought stress showing more transparent crowns (Figure 14b).

3.3. Tree growth responses to insect induced defoliation (Topic III)

QIII*: *How does insect defoliation caused by Lymantria dispar affects stem growth?

Defoliation detection by TLS

The TLS approach detected defoliation and introduced the novel parameters of leaf area and crown perforation that can be used for further studies (Figure 15ab, Table 13 Functions 25 and 27). Using this approach in an experimental setting with plots differing in outbreak condition and pest control measures, it was possible to show that leaf area was significantly higher in plots that were sprayed with Mimic that protected the trees against defoliation by gypsy moth (Figure 15a, Table 13 Function 25), while crown perforation was significantly lower on these plots, resulting in fewer perforated and more compact crowns in leaf-on (t_2) condition (Figure 15b, Table 13 Function 27).

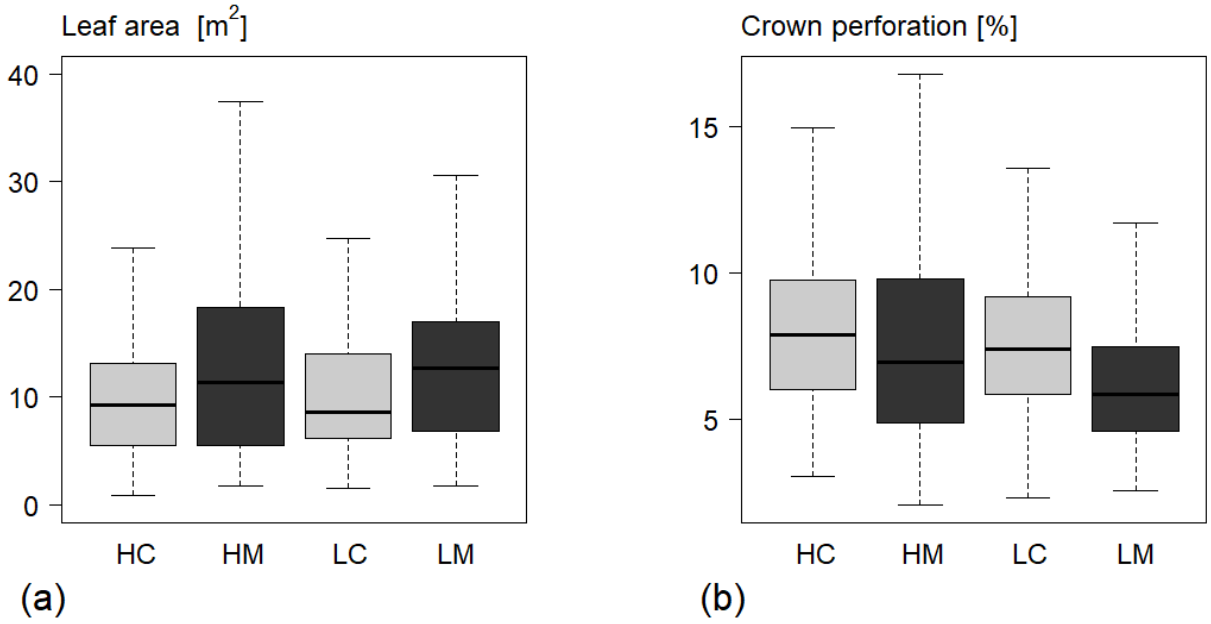

Figure 15 Descriptive statistics boxplot of (a) leaf area ($(t_2 + t_3)/2$) in m^2 and (b) crown perforation (t_2) as a percentage per tree, depending on treatment and defoliation risk, measured using raw data after defoliation until the end of the growing season. The experiment comprised two defoliation risk levels, high (H) or low (L), and two treatment types, sprayed with Mimic (M) to protect the trees against defoliation or unsprayed control (C). The factorial design comprised the four combination types (HC, HM, LC, and LM).

Both of the foliation-describing parameters correlated with basal area increment, which was calculated within the same year directly after defoliation had taken place. As expected, leaf area was significantly and positively (Figure 16a, correlation = +0.6, R^2 = 0.35), and crown

perforation significantly and negatively (Figure 16b, correlation = –0.35, R^2 = 0.12) related to basal area increment. The reason for the lower correlation is probably that the crown perforation calculation was based on only one scanning campaign, whereas the leaf area determination method needed at least two and thus contained more information.

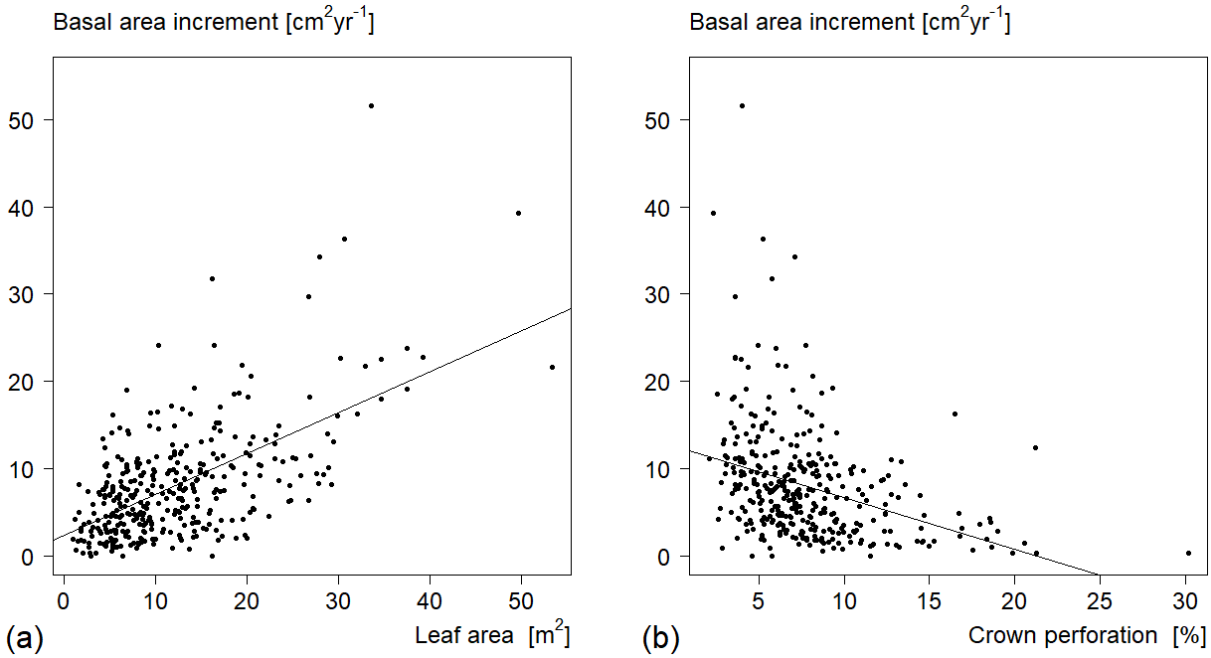

Figure 16 Comparison of basal area increment in cm^2 $year^{-1}$ measured by long-term girth tapes between June 2019 (after defoliation) and the end of the growing season 2019, with (a) leaf area in m^2 measured after defoliation, and (b) crown perforation in %. Every dot is a single tree, and every line represents the regression line of Functions (29) and (30).

In summary, it was possible to detect defoliation with the TLS approach introduced and the two parameters (Figure 15ab). The leaf area was the more suitable parameter for determining the foliation. The correlation with basal area increment showed better results (Figure 16ab). Still, the crown perforation parameter was able to describe defoliation and showed subsequent growth losses due to defoliation. Nevertheless, crown perforation seems to have a greater effect on stem growth, as shown by the significance and R^2 of Function (28) (Table 13). In addition, Function (27) shows that crown perforation, in contrast to the leaf area, was significantly lower on plots where a low defoliation risk with a low density of gypsy moth eggs was found. Thus, the assessment of defoliation risk based on egg-mass density before the outbreak occurred was relatively accurate.

Defoliation and subsequent growth loss

Oaks with a lower leaf area and higher crown perforation showed significant losses in the estimation of the basal area increment parameter compared to non-defoliated trees (Figure 17ab, Table 13 Functions 26 and 28). The growth losses depended in an almost linear way on crown perforation for trees at the lower end of the diameter range. However, non-linear effects occurred for trees at the upper end of the diameter range. Therefore, higher increment losses due to defoliation are expected for trees with a higher basal area (Figure 17a, Table 13 Function 26). As for leaf area, higher increment losses due to higher crown perforation are expected for trees with a higher basal area (Figure 17b, Table 13 Function 28). The curves of leaf area and crown perforation, from Functions (26) and (28), differ in intercept and slope. The slope of the leaf area curves is higher, while the curves of the crown perforation are separated from each other by a greater distance. Overall, they cover the same stem growth range. To create the curves, the first quartile, median, and third quartile values of all leaf area and crown perforation values were used to set them as leaf area and crown perforation parameters in Functions (26) and (28), respectively (Figure 17).

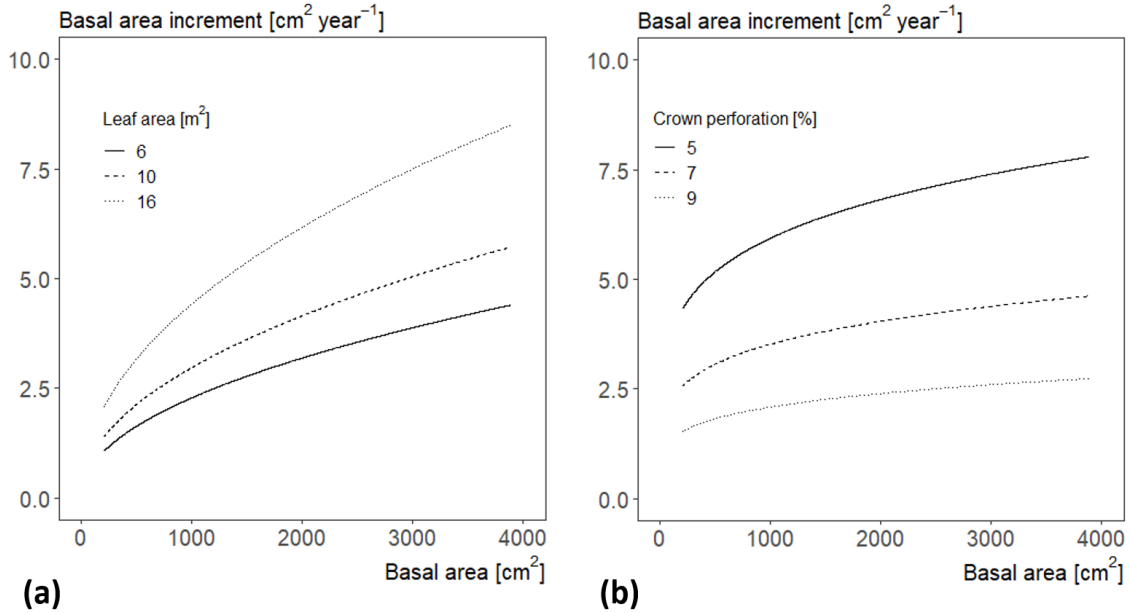

Figure 17 Three curves for (a) leaf area (m^2) from Function (26) and (b) crown perforation (%) from Function (28) each (first quartile = solid, median = dashed and third quartile = dotted) depending on basal area increment in cm^2 year^{-1} and basal area in cm^2.

Table 13 Statistics from linear mixed-effects models for ***QIII*** (Functions 25 – 28).

Function	(25)	(26)	(27)	(28)
Response variable	***Ln(leaf area)***	***Ln(basal area increment)***	***Ln(crown perforation)***	***Ln(basal area increment)***
Intercept	**–2.70*****	**–2.91****	**–4.45*****	+1.71
Ln (basal area)	**+0.67*****	**+0.48****	**–0.33*****	+0.20
Defoliation risk (low)	+0.02		**–0.11***	
Treatment (Mimic)	**+0.2*****		**–0.14****	
Pred (leaf area)		**+0.07***		
Pred (crown perforation)				**–0.26*****
R^2 (adjusted)	0.33	0.19	0.23	0.21

Note: Ln() is the logarithmic transformation, and *pred* means predicted. The category of defoliation risk is divided into high vs. low and treatment is in control vs. Mimic; R^2 (adjusted) is the coefficient of multiple determination; Estimates and significance values are given, while all significance values are in bold type: **'***' p < 0.001, '**' p < 0.01, '*' p < 0.05.**

4. Discussion

4.1. QI: How does competition modify the stem form of trees with the same height and diameter at breast height and thus influences volume miscalculation by traditional form factor equations?

Topics II and III, which involve vitality indicator responses to severe drought stress and growth responses to insect-induced defoliation, are directly related to the core issue of vitality monitoring and index assessment. The connection to Topic I, which examines stem form as a result of competition effects, is less direct. However, Topic I provided an essential step in tree shape assessment and stem detection algorithm development. The isolated stem also served as a starting point for identifying the crown belonging to it.

In general, stem form depends on genetics, silviculture, and site characteristics (Karlsson 2000). According to Assmann (1968) and Larson (1963), the diameter increment changes along the stem depending on stand density. The reduction of density-stress promotes the diameter increment at the bottom part of the stem. As a result, the lowering of stand density can cause a decrease in form factors ($f_{1.3}$), an increase in taper rates, and a decline in slenderness ($h/d_{1.3}$), making the single tree more resistant to wind throw. In other words, with decreasing stand density, the lower part of the stem begins to appear more conic rather than cylindrical (Jonsson 1995). Social status also affects stem shape. Trees free from competition with unrestricted crown development increased in stem taper, while dominated trees in closed stands produced smaller crowns with less stem taper (Gray 1956). My investigation reveals that competition also affects the stem form of trees of the same $d_{1.3}$ and h. These results go beyond the findings obtained by Assmann (1968) and Larson (1963). The results also identified competition as a relevant stand property responsible for volume miscalculation. Like Calama and Montero (2006), I conclude that there is still a high level of non-explained random variability regarding stem form shaping that indicates the presence or interaction of factors that act at plot and tree level. According to Schneider (2018), further main factors were biomechanical or hydraulic constraints. Both factors highlight the important influence of crown dimensions on stem form (Schneider 2018). Zakrzewski (1999) pointed out, considering crown dynamics that were related to stand density could improve the research of stem form changes. In addition, stem form variation is influenced by climatic variables (Schneider 2018). Future research might focus on the effect of these factors on stem form. Since TLS records stem, crown shape and branch structures three-dimensionally, this additional information should be included in future investigations. The use of TLS systems designed for surveying by the ecological research

community has generated new interest, experimentation, and the development of tools and approaches. This virtuous circle of instruments, measurement, and processing is fast progressing, opening up new fields of research in relation to tree structure and function at all scales along the way (Disney 2019).

It is important to identify and analyze the inaccuracy that traditional stem form factor equations cause, besides the ecological question of how local competition effects stem form. As a result, the precision of the measurement tools used is important. Individual tree characteristics such as crown projection area are estimated visually from the ground in traditional forest inventories, while stem form or volume of a stem is traditionally estimated using two parameters ($d_{1.3}$ and h) and a tree species-specific form factor. Determining the volume of standing trees is challenging due to the difficult accessibility of measurement features such as tree height and diameter. Increasing the accuracy usually involves a higher workload. Several types of volume equations have been developed to predict the stem volume of a tree across varying geographical regions and different tree species: Merchantable volume functions, taper functions, and general form factor equations (West 2015). In forest practice and science, general form factor equations are commonly used. The error that results from neglecting the stem form in detail is largely unknown. According to Stinglwagner et al. (2016) a calculation error of up to 15 % occurs, despite error-free measurements of the input variables (h and $d_{1.3}$).

TLS is considered to be a precise measurement tool (RIEGL 2019). In addition to completeness, handling, and the level of detail of the measurement, TLS confers significant cost-effectiveness advantages. Traditional techniques from hand surveying to tacheometric surveying are slow and carry the potential for error. With the laser scanner, which measures statically with millimeter accuracy, it is unlikely that details will be overlooked, and the need to examine and measure the same object several times for the purpose of redensification is usually completely eliminated (Studnicka et al. 2019). Still, TLS as a measurement tool, the applied method, and calculation must be evaluated. This leads to the lack of a reference measurement, i.e. finding suitable reference measurements to evaluate the tree parameters obtained from TLS point clouds or traditional measurement methods was challenging. Regarding the stem form, destructive measurements were made to compare the performance of the presented TLS and the old technique. During the thinning operation, the trees were felled and measured manually. The TLS volume determination and traditional volume determination methods were both validated using this time-consuming manual measurement as a reference. Whether the manual measurement using a caliper is actually more accurate than the TLS estimate is open to debate.

However, it was chosen as a reference because it is quick and widely accepted in traditional forest inventories. As a “true” reference, a high-precision three-dimensional laser measurement in a sawmill would have been a better choice.

According to the results of this dissertation the stem volumes estimated by conventional form factor equations increase and decrease apart from the average competition situation. This may be explained by changing forest management strategies, which might have increased the variety of trees and stem shapes in the study area. Different competition situations were observed over time, and the experimental area was heavily thinned. As a result, the current stand structure probably differs from past ones, with potential implications for stem shape. Hence, the previous sampling may have been more limited to trees coming from less structured stands, which were lightly thinned from below. This suggests that traditional volume functions are particularly suitable for homogeneous single-layer stands with a medium competition situation. The suitability of these functions likely declines with increasing stand complexity and heterogeneity. However, in this study, competition could not fully explain all differences in stem shape, as Functions 15 and 16 show (Table 9). Furthermore, it must be questioned whether a competition index over time (as calculated in this work) could summarize the structural changes over time generated by all thinning regimes. Since the competition values were averaged over time, inaccuracies may occur over the course of time regarding the respective competitive situation; the formula does not consider whether the competitive situation was low or high at the beginning or towards the end.

However, the miscalculation of volume gets more obvious with a decreasing abstraction level. Pooling all trees (n = 868) and computing the total stock, relatively small deviations of +2.0 % or +4.2 % were observed, depending on the method applied. Volume differences were larger for smaller stands. The differences between plots, treatments, thinning regimes, or planting densities varied from +0.7 % to +7.0 % (Table 10). Finally, at tree level, the absolute mean deviation per tree varied from –10 % to +10 %. Thus, in a rough investigation, such as the determination of the total stock, traditional volume functions may be sufficient. For more precise (especially tree-level) measurements, TLS is likely preferred. In a worst-case scenario, scientific results could be misinterpreted and suboptimal recommendations could be given based on traditional volume calculation (Meng 1981). To classify these results, it should be mentioned that the spacing and thinning experiments presented here have a special design. These extremes are more extreme than the extremes you would usually find in the typical temperate forest. The extreme areas of the blocks are divided into very dense, non-thinned plots

and also plots with solitary trees. The experiment thus served as a very good basis for the question of how competition effects affect stem form. If no deviations had been found here, they would not have been noticeable in practice. Although these are extreme competitive situations, this study demonstrates the suitability and accuracy of the TLS measurement that will be needed in future scientific work to learn more about the effects of stress factors such as drought on tree shape.

Regarding Topic I, volume miscalculations by classical form factor equations due to competition were discovered. The focus was on the stem forms of trees, with the same $d_{1.3}$ and h, and how they reacted to competition. Trees tend to adopt cylindrical stem forms with increasing competition, whereas stem form tapering increased with decreasing competition. The logical next step was to see how they behaved to other stress factors, such as drought, either alone or in combination. Since TLS is able to scan not only the stem form, other tree shape parameters should also be provided to analyze the reaction pattern of the entire external shape caused by stress.

4.2. *QII*: *How does severe drought stress affect potential tree vitality indicators consisting of stem and crown attributes?*

It was feasible to analyze the effects of drought stress on both stem and crown properties due to automated stem detection (Topic I) and the development of semi-automatic methods to isolate the crowns and thus quantify the crown size parameters (Topic II). I evaluated (1) the usefulness of stem and crown characteristics of Norway spruce and European beech trees, and (2) also their growth measurements under drought stress, as indicators of either vitality or physiological stress. There are a number of different indicators used to describe the vitality of an individual tree. The two most common ones are crown transparency (which describes defoliation) and diameter growth (Dobbertin et al. 2009). In order to assess the long-term development of tree vitality, it is often necessary to select easy-to-measure indicators for forest inventories. This is where research Topic II intends to contribute to future forest inventories and tree vitality assessments. The results show that drought stress led to a significantly smaller crown size (Figure 14a). The magnitude of the change in the crown, which shrank dramatically due to drought, supports the conclusion that the change in crown projection area (*cpa*) should be employed alongside metrics like stem growth and crown transparency in the future in forest inventories to better assess tree vitality.

The impact of drought on the crown has been critically discussed, and assumptions regarding all strategies vis-à-vis drought were summarized in the review by Bréda et al. (2006). The potential acclimatisation strategies were cavitation and cladoptosis. Due to drought-induced branch die-off, fewer branches lose water through transpiration, which enables the remaining shoots to maintain a favourable water balance, although this results in smaller and more transparent crowns (Rood et al. 2000). In addition to the die-off of branches, there is also the deliberate, active process of shedding branches (cladoptosis). This mechanism enables trees to adjust root-shoot ratios after drought-induced declines in root system extent and efficiency. Branch shedding and dying were observed for oak, birch, and poplar (Rood et al. 2000; Rust and Roloff 2002) Both strategies imply that crown size should decrease in response to drought stress. The scans were performed in winter, when beech trees were free of foliage. Using the *cpa* as a rather simple crown attribute, it was possible to prove significant crown shrinkage per year, which was observed over a time span of only six years. Beech trees may have suffered from drought stress and shed parts of their branches. The assumed effects of branch shedding and dying were measurable in terms of *cpa*, crown transparency, and crown roughness using TLS. No other study has previously been able to confirm these results. Three-dimensional data is likely to play a key role in monitoring and understanding the responses of terrestrial ecosystems to climate change (Calders et al. 2020). The use of TLS in this work provides strong empirical support for theories about drought stress reactions (Bréda et al. 2006).

It can be hypothesised that crown properties like *cpa*, transparency, and roughness are linked to each other when analyzing the interaction effects of drought and competition. Trees suffering from drought stress and high competition reduced their already-small crown dimensions to the lowest possible size at which they could efficiently survive. Roughness and transparency decrease as a follow-on effect of smaller and more compact crowns. This contrasts with the increasing roughness and transparency of trees under drought stress without competition. Since changes in crown roughness and transparency in response to drought are dependent on the competition situation, these crown properties should not be used in isolation to detect drought stress. In comparison, *cpa* reacted more strongly to drought and should represent a good indicator for tree vitality monitoring.

The height growth was affected by drought stress for each individual tree species and was lower in comparison to the control trees (Figure 13b). For the Douglas fir, height growth response to drought stress was observed to be an even more sensitive indicator than basal area (Rais et al. 2014). In the past, only a few drought-related studies have focused on the height growth of

mature trees, as the accurate measurement of height increments requires the felling of trees (Hasenauer and Monserud 1997). Setting aside technical issues surrounding measurement accuracy, the height growth of most species is a complex multi-seasonal process from an ecophysiological point of view (Bréda et al. 2006). Since annual mean increments were computed using six years of experimental data, seasonal fluctuations were likely averaged out.

Besides the short observation period, another criticism of this work is the sample size. It is possible that effects for some parameters were identified because of the short time period or small sample size (n = 47); a larger experiment might have been able to detect finer differences between roofed and control plots. Due to the low model performance (R^2), drought, species and local competition may not be the only root causes of the observed stem-form differences, for example (Table 12 Function 20). Another point of criticism is the design of the drought stress experiment. The experimental design is an extreme example using contrived conditions in which the treatment area is exposed to absolute drought due to precipitation withdrawal; such conditions are unlikely to exist in nature.

Another challenge involved finding the "true" reference measurement to validate vitality indicators. For *QII*, the presented tree vitality indicators obtained by TLS were not evaluated against a reference, although they may include errors. Wang et al. (2019) reported, for instance, that TLS underestimated the height of big trees, which may be due to occlusion of crown and stem parts. The occlusion problem might be mainly resolved by choosing a sufficient number of different scan positions. On the other side, TLS height measurements on Norway spruce trees in forest stands that covered a broad density range were found to be more accurate than common height measurements with the Vertex, a hand-held device based on trigonometric calculations (Jacobs et al. 2020). It may be even more difficult to find a suitable true reference for crown projection. Seidel et al. (2015) showed that crown attributes obtained from TLS were more closely related to preceding tree growth than those measured in the field. For research Topic III, where tree growth responses to insect-induced defoliation were analyzed, the calculated foliation parameters were evaluated based on inter-annual stem growth since stem growth and foliation are correlated (Rolland et al. 2001). However, the question of what should be used as a direct reference for abstract parameters such as crown transparency or roughness remains. What highlights the TLS measurements in comparison to the conventional measurement of *cpa*, transparency and roughness is the objectivity of the procedure, which does not rely on the forester's subjective judgments. Tree-vitality monitoring could be developed towards more quantitative methods by application of TLS as traditional recording of crown transparency in

the field has some disadvantages. Despite the photo comparison with reference images, there is a risk of systematic or random observer deviations, which require intensive training and standardization exercises (Dobbertin et al. 2009). In addition, crown thinning is not cause-specific, i.e. it can be difficult to differentiate between drought effects and defoliation by insects. Further, it is also not clear whether the crown transparency of a tree is the result of a loss of vitality, or whether the tree is possibly recovering from stress. Reference values are therefore required to classify the characteristic. Roughness, on the other hand, represents a TLS-derived indicator that could be considered in future research. The development of new indicators based on TLS enables to analyze several indicators and evaluate them together. In this study, it was shown that TLS could be appropriate for measuring crown transparency and roughness of tree crowns. If multiple vitality indicators are in agreement, this may be taken as confirmation of the influence of drought on tree properties (Dobbertin et al. 2009).

Furthermore, drought stress effects on trees could have an impact on the results of the modern and rapid estimation approach of estimating the $d_{1.3}$ using the crown diameter computed by drone data (UAV). Due to the significantly smaller *cpa* caused by drought stress, errors in estimating the crown-diameter-based $d_{1.3}$ measured from above using UAV could occur. Thus, $d_{1.3}$ would be underestimated. This is made clear in Table 12 Function (24), which shows the calculated allometry coefficient regarding *cpa* and $d_{1.3}$. It demonstrates how drastically the investment behavior of the tree can change under drought stress. The control trees showed a positive allometry ($\beta > 1$), indicating that the *cpa* grows faster than $d_{1.3}$. Conversely, the treated trees, suffering under drought, had a negative allometry ($\beta < 0$). Here, $d_{1.3}$ grows while the *cpa* shrinks. Crown shapes may change due to the impacts of climate change. Therefore, crown models within tree growth models must be questioned, as must the derived allometries. The higher frequency of extreme and extensive drought events (IPCC 2012) makes it even more important to consider drought stress effects in forest practice and ecological modelling. This is particularly true for the analysis of crowns because of their spontaneous reaction to environmental changes.

In summary, Topic II focused on tree dimensions as potential vitality indicators that are difficult to measure. A three-dimensional change in tree shape due to drought stress is revealed by the innovative approach for efficient monitoring of tree vitality presented here. Still, a need was found to validate future results of difficult-to-measure variables against a reference. After examining stem attributes for Topic I and both stem and crown attributes for Topic II, the dissertation should be completed by examining defoliation and its relationship to stem growth.

In contrast to the common defoliation studies, the calculated foliation parameters of research Topic III were evaluated based on inter-annual stem growth since stem growth and foliation are correlated (Rolland et al. 2001). In addition, stem growth is easy to accurately measure in the field on the same tree that was used to calculate foliation.

4.3. *QIII*: *How does insect defoliation caused by Lymantria dispar affects stem growth?*

Leaf growth is the most critical tree growth process (Waring 1987) and it is closely related to stem growth (Rolland et al. 2001). Precise foliation surveys have high potential for better scientific understanding and modelling. For example, the leaf area index (LAI) is an important factor for estimating the primary productivity of a forest stand and thus important for forecasting the productivity of terrestrial ecosystems (Sato et al. 2007). Furthermore, LAI may increase in mixed (Forrester et al. 2019) and fertilised forest stands (Smethurst et al. 2003). Assessing defoliation is important to predict damage via pest-growth-models (Dietze and Matthes 2014). According to Dobbertin and Brang (2001), including defoliation can considerably improve the prediction accuracy of models that predict tree mortality based solely on competition indicators and tree size.

The reaction patterns of the stem (Topic I and II) and crown (Topic II) due to external influences and stress factors were analyzed. Whereas stem growth is easy to measure, the exact calculation of tree foliation is difficult. There is also no suitable reference for evaluation. Traditional defoliation assessments, e.g. by eye or by using fisheye photographs, have been criticized as being highly subjective (Dobbertin 2005), while current foliation determination approaches based on spectral information from TLS return intensity or machine learning are complex and expensive (Calders et al. 2020). To address this gap, I developed a simple and reliable procedure and compared it to a suitable reference. In contrast to previous approaches, the foliation parameters were evaluated based on inter-annual stem growth since stem growth and leaf area are correlated (Rolland et al. 2001).

Severe insect defoliation as a stress factor directly affects photosynthetic processes and indirectly reduces stem growth (Dobbertin 2005). Ferretti et al. (2021) suggest that mild to moderate variations in defoliation may have a significant impact on tree and forest growth. Even lightly defoliated trees showed significant growth reduction (Ferretti et al. 2021). According to the results of this dissertation, oaks with a decreasing leaf area and an increasing

crown perforation revealed significant losses in basal area stem increment. These results are in line with the findings of Waring (1987), Dobbertin (2005), and Ferretti et al. (2021). The growth losses identified in this dissertation were observed immediately after defoliation towards the end of the growing season. The plots examined in this study had not suffered substantial defoliation in previous years. Perhaps there are some long-term effects and the growth losses became even higher in the year after defoliation occurred. Gieger and Thomas (2002) show for both *Quercus robur* L. and *Quercus petraea* (Matt.) Liebl. that defoliation – solely or in combination with drought – and subsequent growth loss result in a detoriated water supply after embolism, reducing the tree's vitality. When several damaging factors coincide, oak mortality increases (Gieger and Thomas 2002). Trees face a wide variety of naturally-occurring biotic and abiotic stress factors (Larcher 2003), and silvicultural treatments can also lead to stress by altering conditions in the immediate environment (Gehrig 2004). Thus, besides defoliation, more stress factors need to be identified and analyzed in combination in order to better understand oak dieback and growth loss. According to (Gehrig 2004), a stress reaction only occurs to avoid permanent damage when a certain resistance minimum is exceeded, which may require several simultaneous stress factors to affect the physiological functioning of the tree.

To detect defoliation, I employed a TLS approach and introduced the novel parameters leaf area and crown perforation, which may be used in future research. As a result, structural tree crown differences could be shown and linked to tree growth over the year. Using the approach in an experimental setting with plots differing in outbreak condition and pest control measures, the results (Table 13 Functions 25 and 27) show that leaf area was significantly higher in plots that were sprayed with Mimic, which protected the trees against defoliation by gypsy moth (Table 13 Function 25), while crown perforation was significantly lower on these plots (Table 13 Function 27), resulting in fewer perforated and more compact crowns in leaf-on (t_2) condition. These results were unsurprising. The intention here is just to show that with TLS it is possible to detect and identify this defoliation. Previous studies into foliation detection via TLS have so far largely focused on the development of validation methodologies (Calders et al. 2020), but these have not been used so far to identify stress-induced defoliation. However, some studies were able to show that TLS can detect defoliation at both the tree and stand level (Huo et al. 2019; Kaasalainen et al. 2010).

The evaluation of new automated approaches with an appropriate reference for validation is important in all cases. It would be ideal to measure each individual leaf of the crown, which is not possible due to time requirements and the difficulty of accessibility. Most studies use visual

defoliation assessment as a reference for the validation of their estimated parameters (Huo et al. 2019; Kaasalainen et al. 2010). However, visual defoliation assessments may be subjective (Dobbertin et al. 2009). They require intensive training courses and repeated control assessments (Wulff 2002). Even thorough training cannot fully eliminate observer bias when multiple operators perform the assessment, and thus they are not a suitable reference. Other ground-based measurement methods are also not ideal since the resulting foliation is only estimated. Nonetheless, ground-level imaging methods require an exact delineation of the tree and do not operate directly on the raw image (Borianne et al. 2017). Tree delineation can be a difficult process that often relies on imperfect user inputs (e.g., isolating trees in images of dense stands is a common source of error). Similarly, the widely-used ground-based optical instrument, the LAI-2000 or LAI-2200 plant canopy analyser (PCA) (Li-Cor 1992) was designed to calculate the leaf area index by measuring the canopy gap. To ensure accurate leaf area index estimation, measurements must be made at the exact same places each time to remove any spatial variability from the results. Estimations at the individual tree level were only possible if the tree was sufficiently isolated, which is challenging in dense forest stands (Li-Cor 1992). Satellite-based approaches for forest canopy condition monitoring may provide insights into broad-scale forest health dynamics with a relatively fine spatial and temporal resolution (Pasquarella et al. 2018), but not at the individual tree level. Two-dimensional analysis based on viewing from above certainly does not consider every single leaf within the crown (Figure 14). In contrast, utilizing the pulsed time-of-flight method for laser range measurements, the RIEGL LMS VZ-400i (RIEGL 2019) enables the determination of the range to all targets a single laser pulse is interacting with ("multi-target capability"). Depending on the measurement program used, the maximum number of targets that can be detected varies (typically 4 – 15). The advantage of the method is the additional information that can be obtained from digitized pulse trains in multi-echo analysis. Thus, more information can be generated in dense heterogeneous stands, especially in the canopy.

However, critically reflecting, it becomes clear that working with TLS nevertheless has disadvantages. It can only be used in calm conditions without rain and fog, which reduces its temporal flexibility. This is especially the case when you want to capture the exact moment of peak defoliation. Some studies state that TLS underestimates the heights of big trees, which may be due to the occlusion of the crown and stem parts (Wang et al. 2019). The occlusion problem can be largely resolved by choosing a sufficient number of different scan positions (Wilkes et al. 2017). However, this problem shows that it is even more difficult to scan every single leaf of a tree crown that is shaded or covered by other trees in a dense stand. The situation

is comparable to the recording of the LAI: it is always estimated, but practically never measured. Finally, there is also a very large amount of data that needs to be processed. Robust and ready-to-use software is not available, so the ability to program is necessary.

I developed new, objective TLS-based measurement methods to determine the foliation of a tree with a fast and easy-to-understand procedure. Two foliation parameters were developed and successfully tested in a large-scale field experiment in gypsy moth-infested oak-mixed forests in Germany, evaluating the results based on stem growth to demonstrate their performance.

However, there are a few limitations to the methods. Calculating the leaf area parameter is time consuming because at least two scanning campaigns are required, one in a leaf-off condition and one in a leaf-on condition. Branch growth between scanning campaigns one and two could result in overestimating leaf area. Nevertheless, temporal monitoring of three-dimensional structures via repeated TLS scanning showed the potential to deliver time-varying defoliation data. Crown perforation, which only requires one scanning campaign, is not as strongly correlated with basal area increment as leaf area (Figure 16). Furthermore, the leaf area parameter is only applicable to deciduous trees because one scanning campaign without leaves is necessary. This is clearly not possible with evergreen trees. The next steps towards scaling up would be to test other age stages, size dimensions, other species, other pests, or stress factors, and to find a solution to calculate leaf area for evergreen trees.

5. Conclusion

The main objective of this dissertation was to bring us closer to a more objective forest inventory and a more empirical tree vitality monitoring, and thereby improve our understanding of the reaction patterns of tree shape due to environmental stress. The aboveground tree shape consists of stem and crown attributes that can be measured via TLS. Each research question (*I – III*) evaluates the response of different sets of these attributes to stress.

QI: How does competition modify the stem form of trees with the same height and diameter at breast height and thus influences volume miscalculation by traditional form factor equations?

The results show that stem taper decreased with increasing competition and vice versa. In particular, the lowest stem section (butt log) decreased in taper given increasing competition. Since this stem segment contains the most volume, the overall volume differences per tree can be explained by the behavior of the butt log. This change in taper is valid for trees with the same $d_{1.3}$ and h.

Traditional form-factor equations or individual tree-volume functions are usually constructed and applied within a local area and are up to 50 years old in some cases. The use of these functions is problematic, because site characteristics and ecological conditions vary geographically while silvicultural treatment has changed over time. A generally valid volume function that considers all influential factors and adapts to changes in forest management over time is difficult to realize. Additionally, traditional volume functions (*species*, $d_{1.3}$, h) are applied using estimated height values for a larger number of trees rather than using exact measurements of individual trees. As shown in this study, less accurate estimations can be expected in field inventories using volume models and generalized predictors. The results of this work show that the measurement of stem volume using TLS data yields an accurate estimation using tree features that are automatically retrieved. In a rough investigation, such as the determination of the total stock, common volume functions can be sufficient. The more precise the examination, the more suitable the application of TLS. For homogeneous and single-layer stands with a uniform competition situation, common volume functions are still a fast and easy choice.

QII: How does severe drought stress affect potential tree vitality indicators consisting of stem and crown attributes?

Drought stress led to a significantly smaller crown size as well as lower stem and height growth. In addition, high competition combined with drought stress resulted in crowns that were less rough and thus more compact.

In the past, tree attributes like total tree height and crown size have been difficult to measure. TLS has proved to be a powerful tool for measuring physical crown dimensions and can be more reliable than conventional field methods (Seidel et al. 2015). Trees do not have to be cut; manual, time-consuming, and costly surveys can be avoided. So far, the effects of drought stress have been evaluated based on visual observation from the ground or the laborious collection of broken branches and leaves (Rust and Roloff 2002). With this research topic, it is demonstrated that iterative TLS surveys may enhance the information gathered during measuring campaigns on common long-term experimental plots, generating a more thorough picture of changes in growth patterns induced by changing management or climate. According to Binkley et al. (2013), crown size is an important factor that is closely related to light absorption and productivity. Such precise tree-crown dimensions are also required for tree-growth modeling (Houllier et al. 1995; Poschenrieder et al. 2016).

QIII: How does insect defoliation caused by Lymantria dispar affects stem growth?

The leaf area and crown perforation parameters calculated using TLS successfully differentiated between trees attacked by gypsy moths and trees without damage. Defoliation by the gypsy moth had an immediate impact on the relationship between leaf area, crown perforation and basal area increment; stem growth was reduced in the same year as the moth attack.

Precise foliation surveys have high potential to improve modelling and scientific understandings of plant-environment-herbivore interactions. For example, LAI is an important factor for estimating the primary productivity of a forest stand and thus important for forecasting the productivity of terrestrial ecosystems (Sato et al. 2007). Furthermore, other modelling approaches show that LAI may increase in mixed (Forrester et al. 2019), and fertilised forest stands (Smethurst et al. 2003). Accurate defoliation assessment is important to predict damage via pest-growth-models (Dietze and Matthes 2014), while leaf area is an important component for determining light absorption, whose accurate prediction is critical for many process-based forest growth models (Forrester et al. 2014). According to Dobbertin and

Brang (2001), including defoliation can considerably improve the prediction accuracy of models that predict tree mortality based solely on competition indicators and tree size.

6. Research perspectives and methological considerations

Research perspectives

Understanding how and why trees adopt the various shapes they do, as well as the consequences for understanding their function, is an interesting and important topic. The key to improving this understanding is to capture tree form in a full, quantitative, and reproducible way (Disney 2019). TLS has already made a significant contribution to our ability to measure three-dimensional structure from stem to crown. This three-dimensional data will play a key role in monitoring and understanding functional changes in terrestrial ecosystems in response to climate change (Calders et al. 2020). In addition to the detailed measurements of individual organisms presented here, TLS data also has useful applications at a global scale. Using detailed field measurements of forest structural complexity derived from TLS and taking the structural complexity of primary forests as benchmark, Ehbrecht et al. (2021) provided a global estimate of the potential structural complexity across biomes. Their results highlight the need to integrate forest structural complexity in modeling climate change impacts on biodiversity and ecosystem functions. Furthermore, TLS is likely to be key to calibrating and validating new satellite estimates, for example tracking the temporal dynamics of defoliation (Bae et al. 2021). Beyond the applications of TLS in the fields of forest measurement and management, there is a wide range of new application areas where tree architectural information, at a range of scales, may provide the key to new scientific insights (Disney 2019). These new insights prompt us to ask challenging new questions about our data (Calders et al. 2020). Unmanned aerial systems, aircraft, and satellite remote sensing are providing additional opportunities to exploit these measurements. TLS is moving from the fringes to the mainstream, and has the potential to revolutionise our understanding of the three-dimensional ecology of trees (Disney 2019).

This dissertation demonstrates that repeated TLS scanning campaigns with high resolution temporal monitoring have the potential to uncover important structure-function relationships, such as correlations between defoliation and stem growth loss (Jacobs et al. 2022). Furthermore, the study of Bogdanovich et al. (2021) shows that multitemporal TLS is promising for monitoring even small changes in crown dimensions, and is a valuable tool for conducting vegetation dynamics studies and quantifying management effects. According to Calders et al. (2020), developing methods to combine high-resolution three-dimensional data with spectral information will open up new opportunities for the research of structure-function correlations, trait-based analysis, and more. This will require new methods for collecting and integrating data on a regular basis, with a focus on occlusions and point cloud quality. However, TLS systems

and procedures are already entering a new era in four-dimensional measurement (Calders et al. 2020).

Methological considerations

In this work tree shape parameters were developed and it was documented how they changed over time. Future research along these lines might benefit from the following methodological considerations.

In addition to the effects of stress factors solely or in combination, the temporal observation period in which stress has an effect also plays a role. This is particularly true for the analysis of crowns because of their spontaneous reaction to environmental changes. Therefore, depending on the type of stress, suitable indicators should be chosen. If stress, e.g., competition, has an effect over the entire life cycle and the changes occur slowly, the stem form or the stem growth at breast height is the more suitable choice for recording changes and assessing vitality. For research Topic I, where stem form variation and volume miscalculation due to competition were analyzed, the stem form was scanned with TLS to capture the stem form that had developed over time. The local competition was recorded retrospectively and averaged on the basis of three different points in time (Function 3). This was possible thanks to a long term spacing and thinning experiment. However, this competition calculation might not fully explain all differences in stem form. Furthermore, it must be questioned whether a competition index over time, as calculated in this work, could summarize the structural changes over time generated by all thinning regimes. Because the competition values were averaged over time, competition situations could only be described approximately: the formula did not respect, for instance, whether the competitive situation was low or high at the beginning or towards the end. Ideally, the competition plots should have been scanned several times with TLS not only to track the competition situation but also in order to detect the change in stem form or additionally crown shape over time in detail.

In the future, long term forestry plots should be scanned regularly for scientific purposes to track changes. In particular, research Topic II, where tree vitality indicator responses to severe drought stress were analyzed, demonstrated that iterative TLS surveys may enhance the information gathered during measuring campaigns on common long-term experimental plots by obtaining a more thorough picture of growth patterns due to climate change or management plans. Research Topic III, in which tree growth responses to insect-induced defoliation were investigated, also showed the usefulness of repeated scanning campaigns. In shorter study periods, especially crown parameters should be considered as indicators. In future scientific

research, a suitable amount of vitality indicators should be chosen in order to generate a holistic picture of changing tree vitality in response to different stress factor combinations. The change in the size of the *cpa* should definitely be included in future tree vitality research, as the reaction to drought was very clear in my investigations. However, a longer observation period should also be pursued in order to record more visible changes and possible adaptations in response to prolonged exposure to stress. Gehrig (2004) describes how physiological function adapts to changing environmental conditions, supplemented by structural and morphological changes. This kind of adaptation differs from short-term stress reactions because it produces a new stable normal state, at least until a new stress necessitates a response. In general, making a conclusion about the stress load and reaction to a change in the vitality state is only possible with a longer observation period and must always be considered in relation to the other vitality elements: growth/reproduction, and longevity. Of course, the influence of the environment and its development must be taken into account as well (Gehrig 2004).

TLS: range of application (problems, limitations and advantages)

Over the last 20 years, both the public and private sectors have been increasingly aware of the potential impacts of TLS in forest applications (Calders et al. 2020). Even though there has been a significant advancement in hardware, as demonstrated by vastly reduced equipment size and weight, continuously improved data quality, and significantly reduced hardware costs, data processing sophistication has not kept pace with the hardware surge, resulting in a very limited application of TLS in practical operations (Liang et al. 2018). Addressing these shortcomings to capitalize on the advantages of TLS can improve its scope of applicability. However, disadvantages should also be critically evaluated to guide future scientific work. The main problem that occurs while working with TLS is the amount of data that is created. There is always a trade-off between the number of scan positions and the occlusion problem. A higher number of scan positions per plot can mitigate occlusion; but the higher the number of scan positions, the higher the amount of data. Point cloud filtering is essential to handle point clouds with a high number of points. Therefore, the octree filter enables fast point-cloud processing without accuracy loss (Elseberg et al. 2013). Furthermore, an appropriate file format should be chosen, such as .LAS, a binary file format for the fast interchange of three-dimensional data between data users. Theoretically, TLS has the potential to support more objective forest inventory and tree vitality monitoring. Practically, the user is confronted with several problems in the field and during post-processing. The higher number of scan positions results not only in a larger amount of data but also in an increased amount of work, because the RIEGL VZ-400i

(RIEGL 2019) is a heavy measuring device (approximately 20 kg with camera and tripod). Furthermore, taking good measurements depends on the weather. Scanning should not be carried out during storms, windy conditions, snowfall, rain, or fog. This limits the temporal flexibility considerably, especially if peak defoliation has to be recorded in several areas simultaneously. Another disadvantage is the programming ability that a TLS user must have. There are already various software solutions, including open source software (Hackenberg et al. 2015; Trochta et al. 2017). However, in my experience, these are limited in terms of the amount of data, point cloud quality, or do not work with every forest stand type depending on heterogeneity and density.

In its current form, the use of TLS has its raison d'être primarily in science. Due to the high accuracy of the TLS data, new insights can be gained that are particularly advantageous for modelling. Such accurate data of tree-crown dimensions are essential for tree-growth modelling (Houllier et al. 1995; Poschenrieder et al. 2016). In practice, such as forest inventories, it will take some time before the technology can be used quickly and easily by everyone. Lighter and even faster pulse scanners are needed that provide accurate and in-depth information about the crowns. Mobile scanning is already a step in this direction. When it comes to surveying large areas and assessing forest stands, TLS is at a disadvantage compared to airborne laser scanning (ALS) or unmanned air vehicle (UAV). Whereas TLS provides the more accurate data, in the end, a combination of TLS and ALS is probably a good compromise. The TLS is only used selectively with regard to the area, and tree parameters are calculated precisely. Using this data and the airborne data taken over a large area, estimates via the *cpa* for $d_{1.3}$ can be made for the entire area.

7. References

Anderegg WRL, Kane JM, Anderegg LDL (2013) Consequences of widespread tree mortality triggered by drought and temperature stress. Nature Clim Change 3: 30–36. https://doi.org/10.1038/nclimate1635.

Assmann E (1968) Zur "Theorie der Grundflächenhaltung". Forstw Cbl 87: 321–330. https://doi.org/10.1007/BF02735874.

Bae S, Müller J, Förster B, Hilmers T, Hochrein S, Jacobs M, Leroy BML, Pretzsch H, Weisser WW, Mitesser O (2021) Tracking the temporal dynamics of insect defoliation by high-resolution radar satellite data. Methods in Ecology and Evolution. https://doi.org/10.1111/2041-210X.13726.

Bayer D, Seifert S, Pretzsch H (2013) Structural crown properties of Norway spruce (*Picea abies* [L.] Karst.) and European beech (*Fagus sylvatica* [L.]) in mixed versus pure stands revealed by terrestrial laser scanning. Trees 27: 1035–1047. https://doi.org/10.1007/s00468-013-0854-4.

Bertalanffy L von (ed) (1951) Theoretische Biologie: II: Band, Stoffwechsel, Wachstum, 2nd edn, vol 2. A Francke AG, Bern.

Binkley D, Campoe OC, Gspaltl M, Forrester DI (2013) Light absorption and use efficiency in forests: Why patterns differ for trees and stands. Forest Ecology and Management 288: 5–13. https://doi.org/10.1016/j.foreco.2011.11.002.

BMEL - Bundesministerium für Ernährung und Landwirtschaft (2014) Forests In Germany - BWI - Selected Results of the Third National Forest Inventory, Berlin.

Bogdanovich E, Perez-Priego O, El-Madany TS, Guderle M, Pacheco-Labrador J, Levick SR, Moreno G, Carrara A, Pilar Martín M, Migliavacca M (2021) Using terrestrial laser scanning for characterizing tree structural parameters and their changes under different management in a Mediterranean open woodland. Forest Ecology and Management 486: 118945. https://doi.org/10.1016/j.foreco.2021.118945.

Borianne P, Subsol G, Caraglio Y (2017) Automated efficient computation of crown transparency from tree silhouette images. Computers and Electronics in Agriculture 133: 108–118. https://doi.org/10.1016/j.compag.2016.12.011.

Brang P (1998) Sanasilva-Bericht 1997: Zustand und Gefährdung des Schweizer Waldes-eine Zwischenbilanz nach 15 Jahren Waldschadenforschung. Bundesamt für Umwelt Wald und Landschaft; Eidgenössische Forschungsanstalt.

Bréda N, Huc R, Granier A, Dreyer E (2006) Temperate forest trees and stands under severe drought: A review of ecophysiological responses, adaptation processes and long-term consequences. Ann. For. Sci. 63: 625–644. https://doi.org/10.1051/forest:2006042.

Calama R, Montero G (2006) Stand and tree-level variability on stem form and tree volume in *Pinus pinea* L.: a multilevel random components approach. Invest Agrar: Sist Recur For 15: 24–41.

Calders K, Adams J, Armston J, Bartholomeus H, Bauwens S, Bentley LP, Chave J, Danson FM, Demol M, Disney M, Gaulton R, Krishna Moorthy SM, Levick SR, Saarinen N, Schaaf C, Stovall A, Terryn L, Wilkes P, Verbeeck H (2020) Terrestrial laser scanning in forest ecology: Expanding the horizon. Remote Sensing of Environment 251: 112102. https://doi.org/10.1016/j.rse.2020.112102.

Chalmers P (2018) SimDesign: Structure for organizing Monte Carlo simulation designs. R package version 1.

Cortini F, Comeau PG (2020) Pests, climate and competition effects on survival and growth of trembling aspen in western Canada. New Forests 51: 175–190. https://doi.org/10.1007/s11056-019-09726-9.

Dietze MC, Matthes JH (2014) A general ecophysiological framework for modelling the impact of pests and pathogens on forest ecosystems. Ecol Lett 17: 1418–1426. https://doi.org/10.1111/ele.12345.

Disney M (2019) Terrestrial LiDAR: a three-dimensional revolution in how we look at trees. New Phytologist 222: 1736–1741. https://doi.org/10.1111/nph.15517.

Dobbertin M (2005) Tree growth as indicator of tree vitality and of tree reaction to environmental stress: A review. Eur J Forest Res 124: 319–333. https://doi.org/10.1007/s10342-005-0085-3.

Dobbertin M, Brang P (2001) Crown defoliation improves tree mortality models. Forest Ecology and Management 141: 271–284. https://doi.org/10.1016/S0378-1127(00)00335-2.

Dobbertin M, Hug C, Waldner P (2009) Kronenverlichtung, Sterberaten und Waldwachstum in Langzeitstudien – Welche Indikatoren beschreiben den Waldzustand am besten? Forum für Wissen:7–20.

Ehbrecht M, Seidel D, Annighöfer P, Kreft H, Köhler M, Zemp DC, Puettmann K, Nilus R, Babweteera F, Willim K, Stiers M, Soto D, Boehmer HJ, Fisichelli N, Burnett M, Juday G, Stephens SL, Ammer C (2021) Global patterns and climatic controls of forest structural complexity. Nat Commun 12: 519. https://doi.org/10.1038/s41467-020-20767-z.

Eichhorn J (ed) (1998) Manual on methods and criteria for harmonized sampling, assessment, monitoring and analysis of the effects of air pollution on forests. Part II. Visual assessment of crown condition and submanual on visual assessment of crown condition on intensive monitoring plots.

Elling W, Heber U, Polle, A. Beese, F. (2007) Schädigung von Waldökosystemen: Auswirkungen anthropogener Umweltveränderungen und Schutzmaßnahmen. Elsevier, Spektrum Akad. Verlag.

Elseberg J, Borrmann D, Nüchter A (2013) One billion points in the cloud – an octree for efficient processing of 3D laser scans. ISPRS Journal of Photogrammetry and Remote Sensing 76: 76–88. https://doi.org/10.1016/j.isprsjprs.2012.10.004.

Ferretti M, Bacaro G, Brunialti G, Calderisi M, Croisé L, Frati L, Nicolas M (2021) Tree canopy defoliation can reveal growth decline in mid-latitude temperate forests. Ecological Indicators 127:107749. https://doi.org/10.1016/j.ecolind.2021.107749.

Forrester DI, Guisasola R, Tang Xea (2014) Using a stand-level model to predict light absorption in stands with vertically and horizontally heterogeneous canopies. For. Ecosyst.

Forrester DI, Rodenfels P, Haase J, Härdtle W, Leppert KN, Niklaus PA, Oheimb G von, Scherer-Lorenzen M, Bauhus J (2019) Tree-species interactions increase light absorption and growth in Chinese subtropical mixed-species plantations. Oecologia 191: 421–432. https://doi.org/10.1007/s00442-019-04495-w.

Gehrig M (2004) Methoden zur Vitalitätsbeurteilung von Bäumen: Vergleichende Untersuchungen mit visuellen, nadelanalytischen und bioelektrischen Verfahren, ETH Zürich.

Goisser M, Geppert U, Rötzer T, Paya A, Huber A, Kerner R, Bauerle T, Pretzsch H, Pritsch K, Häberle KH, Matyssek R, Grams T (2016) Does belowground interaction with *Fagus*

sylvatica increase drought susceptibility of photosynthesis and stem growth in *Picea abies*? Forest Ecology and Management 375: 268–278. https://doi.org/10.1016/j.foreco.2016.05.032.

Grams T, Hesse, B., Gebhardt, T., Weikl F, Rötzer T, Kovacs B, Hikino K, Hafner, B., Brunn, M., Bauerle T, Häberle K, Pretzsch H, Pritsch K (2021) The Kroof experiment - realization and efficacy of a recurrent drought experiment plus recovery in a beech/spruce forest. Ecosphere. https://doi.org/10.1002/ecs2.3399.

Gray HR (1956) The form and taper of forest-tree stems. Imperial Forestry Institute, University of Oxford Oxford.

Hackenberg J, Spiecker H, Calders K, Disney M, Raumonen P (2015) SimpleTree —An Efficient Open Source Tool to Build Tree Models from TLS Clouds. Forests 6: 4245–4294. https://doi.org/10.3390/f6114245.

Harper WV (2014) Reduced major axis regression. Wiley StatsRef: Statistics Reference Online:1–6.

Hasenauer H, Monserud RA (1997) Biased predictions for tree height increment models developed from smoothed 'data'. Ecological modelling:pp 13-22.

Hegyi F (1974) A simulation model for managing jack-pine standssimulation. RoyalColl. For, Res. Notes 30: 74–90.

Hilker T, van Leeuwen M, Coops NC, Wulder MA, Newnham GJ, Jupp DLB, Culvenor DS (2010) Comparing canopy metrics derived from terrestrial and airborne laser scanning in a Douglas-fir dominated forest stand. Trees 24: 819–832. https://doi.org/10.1007/s00468-010-0452-7.

Houllier F, Leban J-M, Colin F (1995) Linking growth modelling to timber quality assessment for Norway spruce. Forest Ecology and Management 74: 91–102. https://doi.org/10.1016/0378-1127(94)03510-4.

Huang P, Pretzsch H (2010) Using terrestrial laser scanner for estimating leaf areas of individual trees in a conifer forest. Trees 24: 609–619.

Huo L, Zhang N, Zhang X, Wu Y (2019) Tree defoliation classification based on point distribution features derived from single-scan terrestrial laser scanning data. Ecological Indicators:782–790.

Hush B, Miller CI, Beers TW (1982) Forest mensuration.(3 ra Ed.).

Innes JL (1993) Forest health: its assessment and status. CAB international.

IPCC (2012) Managing the Risks of Extreme Events and Disasters to Advance Climate Change Adaptation: A Special Report of Working Groups I and II of the Intergovernmental Panel on Climate Change. Cambridge University Press, Cambridge, UK, and New York, NY, USA:582 pp.

Jacobs M, Rais A, Pretzsch H (2020) Analysis of stand density effects on the stem form of Norway spruce trees and volume miscalculation by traditional form factor equations using terrestrial laser scanning (TLS). Can. J. For. Res. 50: 51–64. https://doi.org/10.1139/cjfr-2019-0121.

Jacobs M, Rais A, Pretzsch H (2021) How drought stress becomes visible upon detecting tree shape using terrestrial laser scanning (TLS). Forest Ecology and Management 489: 118975. https://doi.org/10.1016/j.foreco.2021.118975.

Jacobs M, Hilmers T, Leroy BML, Lemme H, Kienlein S, Müller J, Weisser WW, Pretzsch H (2022) Assessment of defoliation and subsequent growth losses caused by *Lymantria dispar* using terrestrial laser scanning (TLS). Trees. https://doi.org/10.1007/s00468-021-02255-z.

Jonsson B (1995) Thinning response functions for single trees of *pinus sylvestris* L. and *picea abies* (L.) karst. Scandinavian Journal of Forest Research 10: 353–369. https://doi.org/10.1080/02827589509382902.

Kaasalainen S, Hyyppä J, Karjalainen M, Krooks A, Lyytikäinen-Saarenmaa P, Holopainen M, Jaakkola A (2010) Comparison of terrestrial laser scanner and synthetic aperture radar data in the study of forest defoliation.

Karlsson K (2000) Stem Form and Taper Changes After Thinning and Nitrogen Fertilization in *Picea abies* and *Pinus sylvestris* Stands. Scandinavian Journal of Forest Research 15: 621–632. https://doi.org/10.1080/02827580050216879.

Kennel R (1969) Formzahl-und Volumentafeln für Buche und Fichte. Institut für Ertragskunde.

Krutzsch P (1974) The IUFRO 1964/68 provenance test with Norway spruce (*Picea abies* (L.) Karst.). Silvae genetica 23: 58–62.

Larcher W (2003) Physiological plant ecology: ecophysiology and stress physiology of functional groups. Springer Science & Business Media.

Larson PR (1963) Stem form development of forest trees. Forest Science 9:a0001-42.

Lee WK, Gadow K von (1997) Iterative bestimmung der konkurrenzbäume in *Pinus densiflora* beständen. Allgemeine Forst- und Jagdzeitung: 41–45.

Legendre P (1998) Model II regression user's guide, R edition. R Vignette 14.

Legendre P (2018) lmodel2: Model II Regression. R package version 1.7-3. https. CRAN. R-poject. org/pachage = lmodel2.

Legendre P, Legendre L (eds) (1988) Structure spatio-temporelle des variables en odanographie: Problemes d'analyse numerique et methodes d'analyse spatiale.

Leroy BML, Lemme H, Braumiller P, Hilmers T, Jacobs M, Hochrein S, Kienlein S, Müller J, Pretzsch H, Stimm K, Seibold S, Jaworek J, Hahn WA, Müller-Kroehling S, Weisser WW (2021) Relative impacts of gypsy moth outbreaks and insecticide treatments on forest resources and ecosystems: An experimental approach. Ecological Solutions and Evidence 2. https://doi.org/10.1002/2688-8319.12045.

Liang X, Hyyppä J, Kaartinen H, Lehtomäki M, Pyörälä J, Pfeifer N, Holopainen M, Brolly G, Francesco P, Hackenberg J (2018) International benchmarking of terrestrial laser scanning approaches for forest inventories. ISPRS Journal of Photogrammetry and Remote Sensing 144: 137–179.

Li-Cor D (1992) Plant canopy analyser operating manual. Li-Cor Inc., Lincoln, NE, USA.

Meng CH (1981) Detection of stem form change after stand treatment. Can. J. For. Res. 11: 105–111.

Müller E, Stierlin HR (1990) Sanasilva-Kronenbilder mit Nadel- und Blattverlustprozenten, 2nd edn. Eidgenössische Forschungsanstalt für Wald, Schnee und Landschaft. S 129, Birmensdorf.

Müller-Edzards C, Vries WD, & Erisman JW (1997) Ten years of monitoring forest condition in Europe. Studies on temporal development, spatial distribution and impacts of natural and anthropogenic stress factors. UN/ECE.

Naidoo R, Lechowicz MJ (2001) Effects of gypsy moth on radial growth of deciduous trees. Forest Science:338–348.

Pain O, Boyer E (1996) A whole individual tree growth model for Norway spruce. In Proceedings of the Second Workshop "Connection Between Silviculture and Wood Quality Through Modelling Approaches and Simulation Software", Berg-en-Dal, Kruger National Park, South Africa, August 26–31, 1996. Publication Equipe de Recherches sur la Qualité des Bois. INRA-Nancy.

Pasquarella VJ, Elkinton JS, Bradley BA (2018) Extensive gypsy moth defoliation in Southern New England characterized using Landsat satellite observations. Biol Invasions 20: 3047–3053. https://doi.org/10.1007/s10530-018-1778-0.

Petterson H (1955) Die Massenproduktion des Nadelwaldes. 0369-2167.

Piper FI, Gundale MJ, Fajardo A (2015) Extreme defoliation reduces tree growth but not C and N storage in a winter-deciduous species. Ann Bot 115: 1093–1103. https://doi.org/10.1093/aob/mcv038.

Poschenrieder W, Rais A, van de Kuilen J-WG, Pretzsch H (2016) Modelling sawn timber volume and strength development at the individual tree level – essential model features by the example of Douglas fir. Silva Fenn. 50. https://doi.org/10.14214/sf.1393.

Pretzsch H (ed) (2001) Modellierung des Waldwachstums. Parey Buchverlag, Berlin.

Pretzsch H (2006) Von der Standflächeneffizienz der Bäume zur Dichte-Zuwachs-Beziehung des Bestandes. Beitrag zur Integration von Baum-und Bestandesebene. Allgemeine Forst- und Jagdzeitung 177: 188–199.

Pretzsch H, Rötzer T, Matyssek R, Grams TEE, Häberle K-H, Pritsch K, Kerner R, Munch J-C (2014) Mixed Norway spruce (*Picea abies* [L.] Karst) and European beech (*Fagus sylvatica* [L.]) stands under drought: From reaction pattern to mechanism. Trees 28: 1305–1321. https://doi.org/10.1007/s00468-014-1035-9.

Pretzsch H, Bauerle T, Häberle KH, Matyssek R, Schütze G, Rötzer T (2016) Tree diameter growth after root trenching in a mature mixed stand of Norway spruce (*Picea abies* [L.] Karst) and European beech (*Fagus sylvatica* [L.]). Trees 30: 1761–1773. https://doi.org/10.1007/s00468-016-1406-5.

Pretzsch H, Ammer C, Wolf B, Steckel M, Rukh S, Heym M (2020) Zuwachsniveau, Zuwachstrend und episodische Zuwachseinbrüche. Ein zusammenfassendes Bild vom aktuellen Zuwachsgang in Rein- und Mischbeständen aus Fichte, Kiefer, Buche und Eiche. AFJZ.

R Core Team (2016) R: a language and environment for statistical computing. R Foundation for Statistical Computing, Vienna, Austria.

Rais A, van de Kuilen J-WG, Pretzsch H (2014) Growth reaction patterns of tree height, diameter, and volume of Douglas-fir (*Pseudotsuga menziesii* [Mirb.] Franco) under acute drought stress in Southern Germany. Eur J Forest Res 133: 1043–1056. https://doi.org/10.1007/s10342-014-0821-7.

RIEGL (2010) DataSheet RIEGL Z420i 30-05-2010. http://www.riegl.com/uploads/tx_pxpriegldownloads/10_DataSheet_Z420i_03-05-2010.pdf.

RIEGL (2019) Datasheet RIEGL VZ-400i 22-11-2019. http://www.riegl.com/uploads/tx_pxpriegldownloads/RIEGL_VZ-400i_Datasheet_2019-11-22.pdf.

Rodriguez-Casal A, Pateiro-Lopez B (2019) alphahull: Generalization of the Convex Hull of a Sample of Points in the Plane. R package version 2.2. https://CRAN. R-project.org/package=alphahull.

Rolland C, Baltensweiler W, Petitcolas V (2001) The potential for using *Larix decidua* ring widths in reconstructions of larch budmoth (*Zeiraphera diniana*) outbreak history: dendrochronological estimates compared with insect surveys. Trees 15: 414–424. https://doi.org/10.1007/s004680100116.

Roloff A (1987) Morphologie der Kronenentwicklung von *Fagus sylvatica* L.(Rotbuche) unter besonderer Berücksichtigung neuartiger Veränderungen: I. Morphogenetischer Zyklus, Anomalien infolge Prolepsis und Blattfall. Flora 179: 355–378.

Rood SB, Patiño S, Coombs K, Tyree MT (2000) Branch sacrifice: cavitation-associated drought adaptation of riparian cottonwoods. Trees: 248–257.

Rötzer T, Pretzsch H (2010) Stem water storage of Norway spruce and its possible influence on tree growth under drought stress-application of ct-scannings. Berichte des Meteorologischen Instituts der Albert-Ludwigs-Universität Freiburg 153.

Roussel JR, Boissieu F de (2019) rlas: Read and Write 'las' and 'laz' Binary File Formats Used for Remote Sensing Data. R package version 1.3.4.

Rust S, Roloff A (2002) Reduced photosynthesis in old oak (*Quercus robur*): The impact of crown and hydraulic architecture. Tree Physiol 22: 597–601. https://doi.org/10.1093/treephys/22.8.597.

Sato H, Itoh A, Kohyama T (2007) A new Dynamic Global Vegetation Model using a spatially explicit individual-based approach. Ecological modelling 200: 279–307. https://doi.org/10.1016/j.ecolmodel.2006.09.006.

Scherer HW (1995) Larcher, W. (Hrsg.): Ökophysiologie der Pflanzen. Ulmer Verlag, Stuttgart 1994; 360 S., DM 78,- (ISBN 3-8252-8074-8). Zeitschrift für Pflanzenernährung und Bodenkunde 158: 207. https://doi.org/10.1002/jpln.19951580214.

Schneider R (2018) Understanding the factors influencing stem form with modelling tools. Progress in Botany Vol. 80: 295–316.

Seidel D, Schall P, Gille M, Ammer C (2015) Relationship between tree growth and physical dimensions of *Fagus sylvatica* crowns assessed from terrestrial laser scanning. iForest 8: 735–742. https://doi.org/10.3832/ifor1566-008.

Seidl R, Schelhaas M-J, Lexer MJ (2011) Unraveling the drivers of intensifying forest disturbance regimes in Europe. Global Change Biology 17: 2842–2852. https://doi.org/10.1111/j.1365-2486.2011.02452.x.

Shigo AL (1990) Die neue Baumbiologie. Bernhard Thalacker Verlag, Braunschweig.

Smethurst P, Baillie C, Cherry M, Holz G (2003) Fertilizer effects on LAI and growth of four Eucalyptus nitens plantations. Forest Ecology and Management 176: 531–542. https://doi.org/10.1016/S0378-1127(02)00226-8.

Stinglwagner G, Haseder I, Erlbeck R (2016) Das Kosmos Wald-und Forstlexikon. Kosmos.

Stovall AEL, Shugart H, Yang X (2019) Tree height explains mortality risk during an intense drought. Nat Commun 10: 4385. https://doi.org/10.1038/s41467-019-12380-6.

Studnicka N, Groiss B, Fürst C, Ganspöck M (2019) Effiziente Aufnahme und orthogonale Darstellung von Laserscans zur Erstellung von Bestandsplänen historischer Gebäude. AGIT – Journal für Angewandte Geoinformatik:S. 338-345.

Thomas FM, Blank R, & Hartmann G (2002) Abiotic and biotic factors and their interactions as causes of oak decline in Central Europe. Forest Pathol 32: 277–307. https://doi.org/10.1046/j.1439-0329.2002.00291.x.

Trochta J, Krůček M, Vrška T, Král K (2017) 3D Forest: An application for descriptions of three-dimensional forest structures using terrestrial LiDAR. PLoS ONE 12:e0176871. https://doi.org/10.1371/journal.pone.0176871.

Wang Y, Pyörälä J, Liang X, Lehtomäki M, Kukko A, Yu X, Kaartinen H, Hyyppä J (2019) In situ biomass estimation at tree and plot levels: What did data record and what did algorithms derive from terrestrial and aerial point clouds in boreal forest. Remote Sensing of Environment 232: 111309. https://doi.org/10.1016/j.rse.2019.111309.

Waring RH, Thies WG, Muscato D (1980) Stem growth per unit of leaf area: a measure of tree vigor. Forest Science 26: 112–117.

Waring RH (1987) Characteristics of Trees Predisposed to Die. Bioscience: 569–574.

Wilkes P, Lau A, Disney M, Calders K, Burt A, Gonzalez de Tanago J, Bartholomeus H, Brede B, Herold M (2017) Data acquisition considerations for Terrestrial Laser Scanning of forest plots. Remote Sensing of Environment 196: 140–153. https://doi.org/10.1016/j.rse.2017.04.030.

Wood SN (2017) Generalized Additive Models: An Introduction with R (2nd edition). Chapman and Hall/CRC.

World Health Organization (2008) International health regulations (2005). World Health Organization.

Wulff S (2002) The accuracy of forest damage assessments–Experiences from Sweden. Environmental Monitoring and Assessment: pp. 295–309.

Zakrzewski WT (1999) A mathematically tractable stem profile model for jack pine in Ontario. Northern Journal of Applied Forestry 16: 138–143.

Zuur AF, Ieno EN, Walker NJ, Saveliev AA, and Smith GM (2009) GLM and GAM for count data. In Mixed effects models and extensions in ecology with R. Springer, New York.:pp. 209–243.

Appendix

A. List of all publications

A.1. Lead-authorship

1. Jacobs M, Rais A, Pretzsch H (2020) Analysis of stand density effects on the stem form of Norway spruce trees and volume miscalculation by traditional form factor equations using terrestrial laser scanning (TLS). In: Can. J. For. Res. 50 (1), S. 51–64. https://doi.org/10.1139/cjfr-2019-0121.

2. Jacobs M, Rais A, Pretzsch H (2021) How drought stress becomes visible upon detecting tree shape using terrestrial laser scanning (TLS). In: Forest Ecology and Management 489, S. 118975. https://doi.org/10.1016/j.foreco.2021.118975.

3. Jacobs M, Hilmers T, Leroy BML, Lemme H, Kienlein S, Müller J, Weisser WW, Pretzsch H (2022) Assessment of defoliation and subsequent growth losses caused by *Lymantria dispar* using terrestrial laser scanning (TLS). Trees. https://doi.org/10.1007/s00468-021-02255-z.

A.2. Co-authorship

1. Rais A, Jacobs M, van de Kuilen J-WG, Pretzsch H (2020) Crown structure of European beech (*Fagus sylvatica*): a noncausal proxy for mechanical–physical wood properties. Canadian Journal of Forest Research. 51(6): 834-841. https://doi.org/10.1139/cjfr-2020-0382.

2. Leroy BML, Lemme H, Braumiller P, Hilmers T, Jacobs M, Hochrein S, Kienlein S, Müller J, Pretzsch H, Stimm K, Seibold S, Jaworek JW, Hahn A, Müller-Kroehling S, Weisser WW (2021) Relative impacts of gypsy moth outbreaks and insecticide treatments on forest resources and ecosystems: An experimental approach. In: *Ecological Solutions and Evidence* 2 (1). https://doi.org/10.1002/2688-8319.12045.

3. Rais A, Bacher M, Khaloian-Sarnaghi A, Zeilhofer M, Kovryga A, Fontanini F, Hilmers T, Westermayr M, Jacobs M, Pretzsch H, van de Kuilen J-WG (2021) Local 3D fibre orientation for tensile strength prediction of European beech timber, Construction and Building Materials, Volume 279, 2021, 122527, ISSN 0950-0618, https://doi.org/10.1016/j.conbuildmat.2021.122527.

4. Bae S, Müller J, Förster B, Hilmers T, Hochrein S, Jacobs M, Leroy BML, Pretzsch H, Weisser WW, Mitesser O (2021) Tracking the temporal dynamics of insect defoliation by high-resolution radar satellite data. Methods in Ecology and Evolution, 00, 1– 12. https://doi.org/10.1111/2041-210X.13726.

5. Pretzsch H, Ahmed S, Jacobs M, Schmied G, Hilmers T (2022) Linking crown structure with tree ring pattern: methodological considerations and proof of concept. Trees. https://doi.org/10.1007/s00468-022-02297-x.

A.3. Conference contributions

Jacobs M (2021) Erfassung von Entlaubung und anschließenden Wachstumsverlusten durch Lymantria dispar mittels terrestrischem Laserscanning (TLS). Forstwissenschaftliche Tagung FOWITA, Freising, 13. - 15. September 2021.

B. Original research articles (Article I – III)

B.1. Article I

Title: Analysis of stand density effects on the stem form of Norway spruce trees and volume miscalculation by traditional form factor equations using terrestrial laser scanning (TLS)

Authors: Martin Jacobs, Andreas Rais, Hans Pretzsch

Journal: Canadian Journal of Forest Research

Submitted: 4. April 2019

Accepted: 20. October 2019

NRC Research Press

ARTICLE

Analysis of stand density effects on the stem form of Norway spruce trees and volume miscalculation by traditional form factor equations using terrestrial laser scanning (TLS)

Martin Jacobs, Andreas Rais, and Hans Pretzsch

Abstract: Tree and stand volume estimates are relevant for forest inventories, forest sales, and carbon stock evaluations. Forest practice commonly uses generalized stem-wood volume functions; however, such generalized approaches neglect the stem form in detail. Hence, trees of a given species with the same diameter at breast height ($d_{1.3}$) and height (h) are always assumed to have the same form factor and thus the same volume. This case study focused on stem form variation of Norway spruce (*Picea abies* (L.) Karst.) due to competition effects. Using terrestrial laser scanning (TLS), we measured the stem shape of 868 trees from a long-term spacing and thinning experiment in Germany. The plots covered a broad density range. We analysed the effect of competition and compared the TLS-determined stem volume estimates with those determined conventionally. TLS-based volume estimations showed that the lower the competition was, the lower the tree volume was with a given $d_{1.3}$ and h. Commonly used functions underestimated the volume stock overall by 4.2%, disregarding any levels. At plot level, underestimation varied from 0.7% to 7.0%. At tree level, the volume was under- and over-estimated by −10% to +10%, respectively. The more precise the examination was, the more suitable the application of TLS was for enhancing volume estimation.

Key words: tree and stand volume, stem wood, volume function, form factor, competition.

Résumé : L'estimation du volume des arbres et des peuplements est pertinente pour les inventaires forestiers, les ventes forestières et l'évaluation des stocks de carbone. Des équations généralisées du volume de bois des tiges sont couramment utilisées dans la pratique forestière; cependant, ces approches généralisées négligent les détails de la forme de la tige. Par conséquent, les arbres d'une espèce donnée ayant le même diamètre à hauteur de poitrine ($d_{1.3}$) et la même hauteur (h) sont toujours présumés avoir le même facteur de forme et donc le même volume. Cette étude de cas s'est intéressée à la variation de la forme de la tige de *Picea abies* (L.) Karst. due aux effets de la concurrence. À l'aide du balayage laser terrestre (BLT), nous avons mesuré la forme de la tige de 868 arbres provenant d'une expérience à long terme d'éclaircie et d'espacement en Allemagne. Les parcelles couvraient un large éventail de densités. Nous avons analysé l'effet de la concurrence et comparé le BLT à des estimations conventionnelles du volume de la tige. Les estimations du volume fondées sur le BLT ont montré que plus la concurrence est faible, plus le volume de l'arbre est faible pour un $d_{1.3}$ et un h donnés. Les fonctions couramment utilisées ont sous-estimé le volume total de 4,2 %, indépendamment des niveaux d'analyse. À l'échelle de la parcelle, la sous-estimation variait de 0,7 à 7,0 %. À l'échelle des arbres, le volume a été sous-estimé ou sur-estimé ou de −10 à +10 %, respectivement. Plus l'examen est précis plus l'utilisation du BLT est appropriée pour améliorer l'estimation du volume. [Traduit par la Rédaction]

Mots-clés : volume des arbres et du peuplement, bois de la tige, équation de volume, facteur de forme, compétition.

1. Introduction

In forest practice and science, a more precise determination of the volume is important. Forest landowners are interested in the volume available for the wood industry, subdivided into categories such as sawlogs, pulpwood, and plywood (Calama and Montero 2006). In a time of climate change, the ability of forests to store CO_2 becomes more relevant. Therefore, a more accurate determination of the accumulated biomass in the forest system is required (Montero et al. 2002). Furthermore, an important criterion for the plan and implementation of silvicultural treatments is their superiority or inferiority in terms of wood production, for which a precise assessment of stand volume is advantageous as well (Tasissa and Burkhart 1998).

Determining the volume of standing trees is challenging due to the difficult accessibility of measurement features such as tree height and diameter. Increasing the accuracy usually involves a higher logistical input. Several types of volume equations have been developed to predict the stem volume of a tree across varying geographical regions and different tree species: merchantable volume functions, taper functions, and general form factor equations (West 2015). In forest practice and science, general form factor equations are commonly used. These volume functions estimate the volume of a tree as a function of the diameter at breast height ($d_{1.3}$) and the total height (h) of the tree. Assuming the geometric shape of a cylinder, the form factor $f_{1.3}$ is additionally needed for the cylinder volume to correlate to the stem volume (Prodan 1965). The form factor is routinely derived from a general form function of the type $f_{1.3} = f_1(d_{1.3}, h)$. This is the common method for calculating individual stem volume in traditional forest inventory; however, this determination of tree volume, based

Received 4 April 2019. Accepted 20 October 2019.

M. Jacobs, A. Rais, and H. Pretzsch.* Chair of Forest Growth and Yield Science, TUM School of Life Sciences Weihenstephan, Technical University of Munich, Hans-Carl-v.-Carlowitz-Platz 2, 85354 Freising, Germany.

Corresponding author: Martin Jacobs (email: martin.jacobs@tum.de).

*Hans Pretzsch currently serves as an Associate Editor; peer review and editorial decisions regarding this manuscript were handled by Peter Newton.

Can. J. For. Res. **50**: 51–64 (2020) dx.doi.org/10.1139/cjfr-2019-0121

Published at www.nrcresearchpress.com/cjfr on 22 October 2019.

on height (h), diameter at breast height ($d_{1.3}$), and generalized form factors, contains errors due to stem-form variation (Socha and Kulej 2007). According to Stinglwagner et al. (2016), a calculation error of up to 15% can occur, despite error-free measurements of the input variables (h and $d_{1.3}$).

In general, a tree species's stem form depends on genetics, silviculture, and site characteristics (Karlsson 2000). According to Assmann (1968) and Larson (1963), the diameter increment changed along the stem depending on stand density. The reduction of density stress promoted the diameter increment at the bottom part of the stem. As a result, the lowering of stand density can cause a decrease in form factors ($f_{1.3}$), an increase in taper rates, and a decline in the slenderness ($h/d_{1.3}$), making the single tree more resistant to wind throw. In other words, with decreasing stand density, the lower part of the stem is conic instead of cylindrical (Jonsson 1995). Next to the impact of stand density, the social status also affected stem shape: trees free from competition with unrestricted crown development increased in stem taper while dominated trees in closed stands produced smaller crowns with less stem taper (Gray 1956).

Models for the estimation of tree volume tried to implement the dependency of stem shape on stand density and social status. Zakrzewski (1999) derived a rational function to describe the inside-bark cross-sectional area of tree stems with $d_{1.3}$ and h as input. He developed a variable-form, stand density specific, inside-bark stem profile equation for commercial jack pine trees in Ontario. In addition, Meng (1981) showed statistical procedures for detecting stem form changes after stand treatment. He pointed out, using the form factor, that it was a disadvantage that the exponents of $d_{1.3}$ and h were fixed. Consequently, stem form changes due to the changes of exponents of $d_{1.3}$ and h cannot be detected. For those approaches, stand-level metrics were used as surrogate measures of density-dependent effects and were explicitly incorporated into the tree-level taper equations to yield composite-tree stand-level functions. Depending on the functional form of these composite equations, such taper functions can be integrated (or via numeric integration) to yield stem volume estimates. To date, there is a lack of knowledge on how the stem form of trees with the same $d_{1.3}$ and h is affected by the individual competition situation inside the stand. The stem shape between the breast height and the top is unclear. Instead of stand-level metrics, we analysed tree-level metrics to improve stem volume estimation research. According to Calama and Montero (2006), trees growing free from competition were less tapered than trees growing under large stocking densities. Their results conflicts with those of Assmann (1968) and Larson (1963), confirming the idea that the reduction of stand or stem density, and thus decreasing competition, increased taper rates (Peltola et al. 2002). Calama and Montero (2006) pointed out that the high level of unexplained random variability regarding stem form shaping indicated the presence of factors that acted at plot and tree levels such as silvicultural treatment and local competition, respectively.

Due to heterogeneous silviculture and climate change, stem shape variation will rise in future. Changing silvicultural treatments with an increased focus on multilayered, mixed forests with low densities and irregular horizontal patterns may increase the crown form and thus the stem form variance. In a current study on five North American tree species, Schneider (2018) concluded that stem form variation was more influenced by climatic variables than by wind speed. There is an ongoing debate whether climate-induced stem form is determined by biomechanical or hydraulic constraints; both approaches highlight the important influence of crown dimensions on the stem form (Schneider 2018).

Terrestrial laser scanning (TLS) can measure detailed stand and individual-tree information (Liang et al. 2018). The advantages of TLS are that no tree has to be cut and that manual surveys can be avoided. Via TLS and automated methods, it is possible to get numerous measurements of height and diameter distributed over a large part of the tree stem. Electronic dendrometers such as the Criterion RD1000 (Laser Technology, Inc., Centennial, Colorado, USA) are also able to measure the stem shape in a nondestructive way; however, TLS is faster and more precise in data acquisition and offers not only the stem form as information, but also the three-dimensional (3D) occupation of the trees in space, as well as information on crown width, crown length, tree inclination, and stem curvature. Studies on TLS and automatic detection of tree characteristics have often focused on the development of a methodology (e.g., Hackenberg et al. (2014), Olofsson et al. (2014) and Cabo et al. (2018)). Their aim was to validate the introduced approaches under varying circumstances: homogenous vs. heterogeneous stands, sparse vs. dense stands, and stands of different species. Many of these methods for the estimation of height and diameter distributed over the entire tree stem have proven that TLS-based methods were accurate (Liang et al. 2014); however, few studies used these validated and automatic methods to evaluate specific ecological hypotheses.

In this study, we make use of automated TLS methods — a combination of tested algorithms and our own developed algorithms — to calculate the whole stem form by means of individually fitted stem curves for each tree to improve volume estimation. The proposed TLS approach could lead to improvements in the estimation of the stem volume compared with traditional methods such as those using standardized volume equations in combination with localized height–diameter functions. This study presents the benefits of TLS in forest inventory and contributes to the associated measurable estimation of individual-tree metrics (diameter, height, stem shape, and volume). The experimental design of the study area as a long-term trial provides an optimal basis for investigating the impact of competition effects on the stem form. It is designed for the current and future situation in terms of competition situations.

Furthermore, we developed a method in R (R Core Team 2016) for the automated stem form estimation of softwood. Different calculations of the volume were applied, which vary in both input parameters and procedure. One volume computation (type 1) was based exclusively on TLS (see also Table 3). Contrary to this, we applied the volume by the traditional forest inventory method (type 3). The volume calculation of type 2 was a composite of the type 1 and type 3 methods. It was based on TLS data but only h and $d_{1.3}$ were taken and inserted into the general form factor equation. We analysed the accuracy of the methods compared with manual measurement as reference in terms of diameter and volume estimation. Applying the methods, we focused on the stem form variability of Norway spruce (*Picea abies* (L.) Karst.) and its dependency on silvicultural treatment (plot level) and competition (tree level). We addressed the following questions.

(Q1) How does competition modify the stem form and thus the volume, form factor, and stem taper of trees with the same h and $d_{1.3}$?

(Q2) What kinds of deviations occur when comparing more realistic volume estimates with those obtained using general form factor equations with only h and $d_{1.3}$ as input parameters?

(Q3) Which TLS procedure will improve volume estimation and reduce measurement error?

2. Material and methods

2.1. Material

2.1.1. Study site and data

The case study was carried out on trees from pure Norway spruce treatment plots located in Fürstenfeldbruck (FFB612) in southern Germany. The spacing and thinning experiment is part of long-term trials established in 1974 on the initiative of the International Union of Forest Research Organizations (IUFRO) (Krutzsch 1974). The plots covered stands with a broad range of stand densities, initial densities, and final densities. Table 1 sum-

Table 1. Stand and site characteristics as mean values.

	Fürstenfeldbruck FFB612
Stand characteristics 2017 (mean values)	
n (ha^{-1})	689
dq (cm)	30
hq (m)	27.5
BA (m^2·ha^{-1})	39.8
Standing volume (m^3·ha^{-1})	553.3
Location	
Elevation (m above sea level)	550
Coordinates	48°14′02.5″ N, 11°05′01.6″ E
Climate 1988–2017 (annual mean values)*	
Temperature (°C)	8.8
Precipitation (mm)	952
Soil	
Initial substrate	Loess
Soil type	Lessivé soil

Note: n, number of trees; dq, quadratic mean diameter; hq, height corresponding to dq; BA, basal area.
*From climate data center (Deutscher Wetterdienst (DWD) 2019).

marizes the most relevant characteristics; more detailed information can be found in Pretzsch (2006), Rötzer and Pretzsch (2010), and Huang and Pretzsch (2010).

Figure 1 illustrates the layout of the experimental trial. In total, 14 of 21 plots were scanned. The remaining seven plots were removed because either they were too similar in treatment or the sample size (trees) of the plots would have been extremely uneven. The RIEGL LMS-Z420i (RIEGL 2010) laser-scanning system was used for data acquisition in January 2018. Five scan positions were realised per plot. For each scan position, two scans (horizontal and vertical) were performed. The scan positions formed an approximate rectangle around each plot, with four scan positions at each corner and one central scan position in the middle of the plot. The vertical and horizontal angular resolution were set to 0.05° to achieve a reasonable trade-off between scan time and risk of disturbances due to tree movement through wind. Because of the angular measurement scheme of the scanner, the point density naturally decreases to the top of the trees. Furthermore, the laser beam usually is not able to penetrate the tree compartments to perform measurements behind obstacles. These two effects result in rather sparse measurement densities in the upper crown and stem regions, especially if the crown parts near the scanner are dense such as those of conifers (Hilker et al. 2010). Using the RIEGL distance-measurement mode called "last-pulse" or "last-target," we attempted to counteract these effects to record the deepest points within a footprint, thus gaining a higher proportion of returns from inner crown regions compared with first-pulse mode. The data of all scan positions per plot were co-registered by the software RiSCAN PRO version 2.0.2 (http://www.riegl.com/products/software-packages/riscan-pro/). The co-registration was based on artificial targets (reflectors). The result was a "plot point cloud raw" (PPC-R).

The treatment of the plots differed in either establishment spacing (Fig. 2*a*) or thinning regime (Fig. 2*b*). Each thinning regime was simplified by time of thinning. Thinning regime 1 was the control (null thinning), thinning regime 2 was thinned late, thinning regime 3 was thinned midway between thinning regimes 2 and 4, and thinning regime 4 was thinned early. Detailed information of treatment and thinning interventions, as well as a complete yield overview over time per plot, are given in Appendix A (Tables A1–A3).

All $d_{1.3}$ were recorded in September 2017 — TLS data acquisition took place in January 2018 (Table 2) — and measured manually for all trees in the plots. For each plot, total tree height was measured with a Haglöf Vertex IV (http://www.haglofcg.com/index.php/en/products/instruments/height/341-vertex-iv) on a subsample of 50% of the trees randomly selected. The height of all non-measured trees was estimated from a diameter–height function fitted for each plot (Petterson 1955). The stem-wood volume was estimated by common general form factor equations (Kennel 1969).

In spring 2018, a thinning intervention took place. From the 55 felled trees, several diameters were measured with a caliper along the stem axis in two perpendicular directions. A tape measured the length of logs or complete stems. Tree inclination — detected by TLS — was considered when transforming length into (total) height. Finally, Smalian's formula was applied for volume calculation (Husch et al. 1982). A mensurational overview of the 55 felled trees is provided in Table 2.

2.2. Methods

2.2.1. Workflow: Stem detection, stem isolation, and diameter calculation

The following demonstrates the different steps of the TLS method applied. A detailed description of the workflow can be found in Appendix A: section 1, stem detection; section 2, the x and y coordinates were determined at each stem base (stem position); section 3, acquisition of the cylindrical subset around the stem position (1 m radius); section 4, stem isolation was made using the cylindrical-subset data and the total tree heights were calculated; and section 5, stem diameters were calculated using the isolated stem data. To identify the trees in the field database and in the TLS point cloud, we manually rotated and merged the two tree spatial maps obtained from the field database and the stem detection method.

2.2.2. Competition

The competition was expressed by modifying the index introduced by Hegyi (1974) using eq. 1. The original Hegyi index builds the ratio between diameters of neighbouring trees and the reference tree concurrently considering the distance of all competitors. The spatial positions of all trees were available.

$$\text{HgCI}_i = \sum_{j=1}^{n} \frac{d_{1.3j}}{d_{1.3i}} \frac{1}{\text{Abst}_{ij}} \quad (1)$$

where HgCI_i is the competitor index for reference tree i, $d_{1.3j}$ is the $d_{1.3}$ of competitor tree j (cm), $d_{1.3i}$ is the $d_{1.3}$ of reference tree i (cm), Abst_{ij} is the distance between reference tree i and competitor tree j (m) and n is the number of competitor trees. The competition zone radius (CZR) defined the radius in which competitors were searched around the reference tree (eq. 2). It was calculated for each plot and time and was dependent on the number of trees per hectare (N). The competition zone of border trees was mostly outside the plot in relative size. To counteract this problem, the external surface was calculated (mirror image). With this value, it was then possible to extrapolate the calculated competition for the partial area to the total area.

$$\text{CZR} = 3 \times \sqrt{\frac{10000}{N}} \quad (2)$$

The competition was calculated three times during the stand history, at the time of planting (t_0), 27 years after establishment (t_m, middle age), and at the present (t_1, 44 years after establishment). We used eq. 3 for each tree:

$$\text{Competition} = \frac{\frac{\text{HgCI}_{i_{t_0}} + \text{HgCI}_{i_{t_m}}}{2} \times t_m + \frac{\text{HgCI}_{i_{t_m}} + \text{HgCI}_{i_{t_1}}}{2} \times (t_1 - t_m)}{t_1} \quad (3)$$

Fig. 1. Experimental design. The experiment consists of two blocks. Each block comprises plots of 30 m × 30 m (900 m²) on which different types of silvicultural treatment were applied in terms of spacing and thinning. In total, 14 of 21 plots have been selected. The grey-bordered plots were scanned. The plots where the thinning experiment (treatment 2) took place were additionally bordered in black. The rest of the plots belong to the spacing experiment treatment 1.

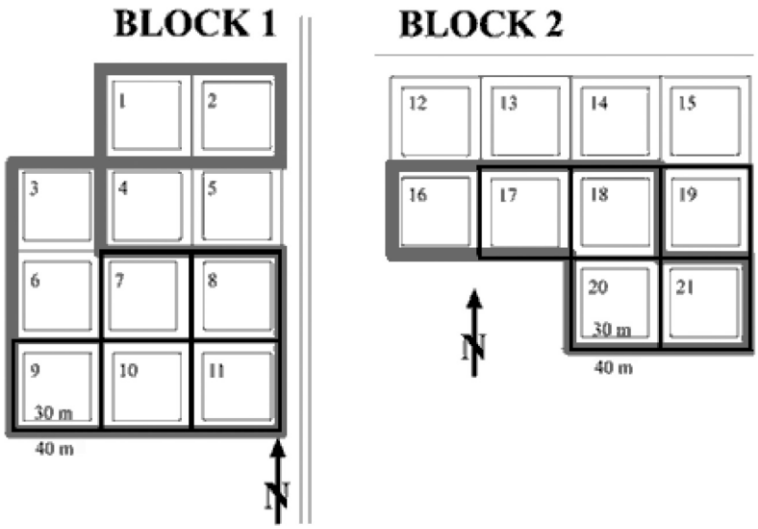

Fig. 2. Characteristics of the spacing and thinning experiment FFB612. The spacing experiment (*a*) represents treatment 1, and the thinning experiment (*b*) represents treatment 2. (*a*) There are some plots of varying establishment spacings (and same thinning regime) and (*b*) others of varying thinning regimes (and same establishment spacings). Thinning regime 1 was control (null thinning). Thinning regime 2 was thinned late. Thinning regime 3 was thinned midway between thinning regimes 2 and 4. Thinning regime 4 was thinned early.

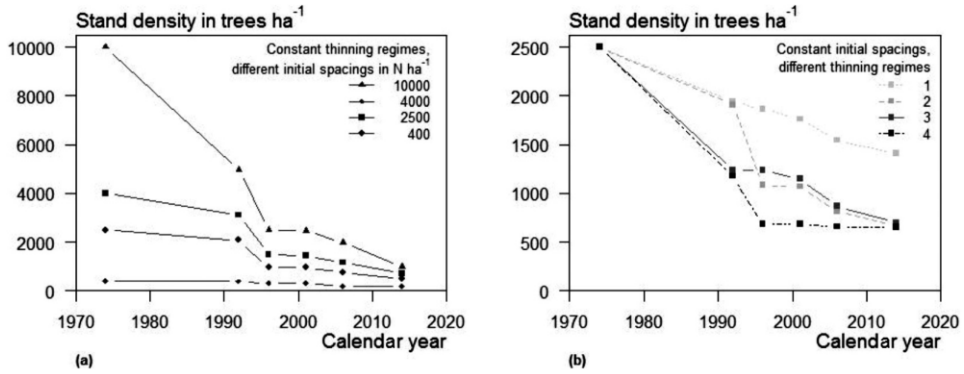

where the parameters $HgCI_{i_{t_0}}$, $HgCI_{i_{t_m}}$, and $HgCI_{i_{t_1}}$ describe the Hegyi indices at times t_0, t_m, and t_1, respectively.

2.2.3. Individual TLS data fitted stem curve by the Pain function

Some diameters at higher sections of the stem were not gathered by the laser scanner and so were determined by the two-parameter taper function (eq. 4) of Pain and Boyer (1996). Based on all diameter measurements of the visible stem sections, the Pain function was fitted for each individual tree, with α, β, and stem radius in relative stem height obtained by TLS, and reconstructs the whole stem curve.

$$(4) \qquad r(h_{rel}) = \alpha\left(1 - h_{rel}^3\right) + \beta(\ln(h_{rel}))$$

where parameter $r(h_{rel})$ is the stem radius in relative stem height (h_{rel}), parameter α is the dimension-describing parameter, and β is the form-describing parameter.

Table 2. Range, mean, and number (*N*) of all sampled trees in 2017 and the trees that were harvested for destructive sampling during thinning in spring 2018.

	Range	Mean	*N*
Sampled and scanned trees			
$d_{1.3}$ (cm)	9.0–59.1	28.3	868
h (m)	12.3–31.3	24.7	868
Volume (m³)	0.05–2.7	0.8	868
Harvested trees (validation)			
$d_{1.3}$ (cm)	10.2–38.7	22.7	55
Total *h* (m)	14.6–27.0	22.6	28
Volume (m³)	0.07–1.4	0.5	55

Note: Diameter at breast height ($d_{1.3}$), height (*h*), and stem volume of the sampled trees were measured by traditional forest inventory. Diameters at breast height ($d_{1.3}$) were measured by caliper, and the height of the felled trees was measured by tape. Total tree heights were calculated for trees that had not been sawn into sections by the harvester (28 trees) to avoid measuring mistakes.

Table 3. Types of stem volume calculations.

	Type 1	Type 2	Type 3
Height (h)	TLS	TLS	TFI
Diameter at breast height ($d_{1.3}$)	TLS	TLS	TFI
Diameters along the stem (d_{all}, h)	TLS	—	—
Volume function (f_i)	f_1 (d_{all}, h)	f_2 ($d_{1.3}$, h)	f_2 ($d_{1.3}$, h)

Note: Type 1: terrestrial laser scanner (TLS) measurement of height (h) and diameters along the stem in 0.1 m height intervals (d_{all}); the stem curve function (eq. 4) was used as volume function (f_1). Type 2: TLS input of height (h) and diameter at breast height ($d_{1.3}$); the traditional form factor equation (Kennel 1969) was used as volume function (f_2). Type 3: traditional forest inventory (TFI) measurements of height (h) and diameter at breast height ($d_{1.3}$); the traditional form factor equation was used as volume function (f_2).

2.2.4. Types of volume determination

The volume calculations used varied in both input parameters and methods (Table 3).

The volume computation according to type 1 was exclusively based on TLS, i.e., we used eq. 4 of Pain and Boyer (1996) to derive total tree volume. Volume estimation of type 3 was based on traditional forest inventory data and conventional form factor equations (Kennel 1969). Type 2 volume calculation was a composite of the methods used for types 1 and 3. It was based on TLS data but only the height and the diameter at breast height were inserted into the conventional form factor equation (Kennel 1969). With type 2, we aimed to analyse possible differences between types 1 and 2 that were due to the method for the volume calculation. The focus was on type 1, which was always the reference to the other types, because they were more realistic estimations. Type 1 was compared with type 2 (volume ratio 1) and type 3 (volume ratio 2) by forming ratios to determine differences per tree as a percentage. Type 1 was the numerator in both cases and types 2 and 3 each were the denominators.

2.2.5. Generalized additive mixed model (GAMM)

The data were nested on tree and plot levels, i.e., there were several observations per tree on different plots. Therefore, a generalized additive mixed model (GAMM) was required. In Table 4, we formulated three GAMM functions 5–7 and two GAMM functions 8 and 9 addressing Q1 and Q2. All models explain the response variable as a function of different linear predictors such as $d_{1.3}$, h, treatment (Fig. 2*a*), thinning regime (Fig. 2*b*), and initial planting density, with competition as a nonlinear predictor. Additional information on treatment and thinning regime per plot is given in Appendix A (Tables A1–A3). The general structure of the model is

$$Y_{ij} = a_0 + a_1X_{1,i} + a_2X_{2,j} + \ldots + a_nX_{n,ij} + f(\text{competition}_i) + b_j + \varepsilon_{ij}$$

where variable Y is the response variable, variables X_1, ..., X_n are the linear predictors, variable i indexes the tree, and variable j indexes the plot. Variable a represents the model's intercept, variable b represents the random effect related to the plots, and symbol ε represents the remaining errors. Variable f is a nonlinear smoother, which covered nonlinear relationships. Zuur et al. (2009) described the technical details of the R package mgcv. Here, smoother f was based on the competition and was intended to cover the effects of unobservable influence variables. The parameters $d_{1.3}$ and h were set as linear predictors to analyse the effect of competition on trees with the same $d_{1.3}$ and h. The competition was tested on its own, while other variables were set to the mean. This was also done for function 7, with stem taper as the response variable, i.e., Table 4. The log class (butt, middle, and top log) differentiated the stem into three parts and was added as a linear predictor to see which part of the stem was affected by changes in shape due to competition.

2.2.6. Evaluation

The performance of the automated TLS method (Q3) was assessed in terms of correct tree detection, deviation of $d_{1.3}$, diameters along the stems (d_{all}), and the total heights of the harvested trees due to the values obtained using manual measurement methods as reference (i.e., caliper, tape, and vertex). A key assumption in applying ordinary least squares (OLS) is that the independent variable is measured without error (Harper 2014) or that the magnitude of the error in the response variable is much larger than the magnitude of the error in the independent (explanatory) variable (Legendre and Legendre 1988), which is not the case for our analysis. In our study, both measured diameters — TLS and manual measurement — contained some components of error. For those variables, Legendre (1998) recommended a major axis (MA) regression instead of an ordinary least squares regression and introduced the package lmodel2 (Legendre 2018). The automated estimations were compared with the reference measurements at the tree level. The accuracy of the estimations was evaluated in terms of the bias and root mean squared error (RMSE) with the R package SimDesign (Chalmers 2018). To validate the tree detection, the proportion of detected trees in the plots to all trees in the plots $\left(\frac{\text{detected trees}}{\text{trees in the dataset}}\right)$ was calculated.

The processing was done within the programming environment of R (R Core Team 2016). The R packages used for the automated method were rlas, dbscan, TreeLS, and conicfit. Exact descriptions of the R packages used for the respective tasks are given in Appendix A.

3. Results

Q1: How does competition modify the stem form and thus the volume, form factor, and stem taper of trees with the same h and $d_{1.3}$?

The effect of the competition was significant on all three dependent variables — stem volume, form factor, and stem taper (Table 5).

The lower the competition was, the lower the single tree volume was with the same $d_{1.3}$ and h. The effects of competition generated volume variations from –25% to 60% in comparison with the mean value (Fig. 3*a* and Table 5). The $d_{1.3}$, h, and planting density had a significant influence on the volume (Table 5).

The effect of competition on the form factor of a single tree was also significant. The lower the competition was, the lower the form factor of a single tree was. The form factor variation ranged from –2% to 2.5% in comparison with the mean form factor (Fig. 3*b* and Table 5). Both treatment and thinning regimes had a significant influence on the form factor (Table 5). Figures 3*c*, 3*d*, and 3*e* show interaction (competition × log class) effects. The effect of competition on the stem taper varied according to the log class but was significant for each log class (Table 5). The butt logs of trees of the same size ($d_{1.3}$ and h) decreased in taper given increasing competition (Fig. 3*c*), while the stem taper of the mid log increased with competition (Fig. 3*d*). The stem taper of the top log decreased with increasing competition (Fig. 3*e*). The competition, the log class itself, and the interaction of both had a significant influence on the stem taper (Table 5).

Q2: What kinds of deviations occur when comparing more realistic volume estimates with those obtained using general form factor equations with only h and $d_{1.3}$ as input parameters?

The effect of competition on the volume ratios was significant. For volume ratio 1, the lower the competition was, the higher the underestimation of the traditional volume of a single tree was. Deviations from –22% to a maximum of 8% around the mean value of the volume ratio occurred (Fig. 4 and Table 5). Both the treatment and planting density had a significant influence on volume ratio 1 (Table 5). The volume differences per treatment form can

Table 4. GAMM functions 5–9 for Q1 and Q2.

	Response variable	Linear predictors	Smoother	Function
Q1	TLS volume	$d_{1.3}$ + h + treatment + thinning + PD	f(competition)	5
	Form factor	Treatment + thinning + PD	f(competition)	6
	Stem taper	$d_{1.3}$ + h + treatment + thinning + PD + log class	f(competition)	7
Q2	Volume ratio 1	Treatment + thinning + PD	f(competition)	8
	Volume ratio 2	Treatment + thinning + PD	f(competition)	9

Note: GAMM, general additive mixed model; TLS volume, stem volume obtained by terrestrial laser scanning (TLS) method; $d_{1.3}$, diameter at breast height; h, total tree height; PD, planting density; log class, log classes per tree (butt, mid, and top log); stem taper = $\frac{(D_1 - D_2)}{L}$, where D_1 is the lower diameter at the beginning of the stem section (log class), D_2 is the upper diameter at the end of the stem section (log class), L is the length of the stem section (log class); form factor = $\frac{\text{TLS volume}}{\left(\left(\frac{\text{pi}}{4} \times d_{1.3}\right) \times h\right)}$.

Table 5. GAMM statistics of models 5–9 for Q1 and Q2.

	(5) TLS volume (m^3)	(6) Form factor	(7) Stem taper ($cm \cdot m^{-1}$)	(8) Volume ratio 1	(9) Volume ratio 2
Intercept a_0	$-1.01 \times 10^{0***}$	$+4.98 \times 10^{-1***}$	$+1.88 \times 10^{0***}$	$+1.01 \times 10^{0***}$	$+1.05 \times 10^{0***}$
$d_{1.3}$ (m)	$+5.84 \times 10^{0***}$		$+3.92 \times 10^{0***}$		
h (m)	$+9.39 \times 10^{-3***}$		$-8.95 \times 10^{-2***}$		
Treatment 2	$+4.92 \times 10^{-3}$	$-1.14 \times 10^{-2***}$	-1.71×10^{-2}	$-2.75 \times 10^{-2***}$	-2.63×10^{-2}
Thinning 2	$+6.18 \times 10^{-3}$	$-1.48 \times 10^{-2***}$	-1.02×10^{-2}	-6.47×10^{-3}	-2.71×10^{-2}
Thinning 3	$+1.03 \times 10^{-2}$	$-1.60 \times 10^{-2***}$	-5.34×10^{-3}	-7.01×10^{-3}	-5.09×10^{-4}
Thinning 4	-6.13×10^{-3}	$-9.89 \times 10^{-3***}$	-4.33×10^{-3}	$+2.87 \times 10^{-3}$	-1.56×10^{-2}
PD	$-2.23 \times 10^{-3***}$	-6.59×10^{-7}	$+6.72 \times 10^{-6}$	$+1.22 \times 10^{-5***}$	$+1.49 \times 10^{-7}$
Log class 2			$-5.54 \times 10^{-2***}$		
Log class 3			$+1.04 \times 10^{0***}$		
f(comp)	***	***	***	***	***
f(comp):log class 1			***		
f(comp):log class 2			***		
f(comp):log class 3			***		
R^2 (adjusted)	0.95	0.03	0.89	0.11	0.01

Note: GAMM, general additive mixed model. Significance: ***, $p < 0.001$; **, $p < 0.01$; *, $p < 0.05$. PD, initial planting density (trees per hectare); $d_{1.3}$, diameter at breast height; h, total tree height; f, smoother; comp, competition; log class, log classes per tree (butt, mid, and top log); R^2, coefficient of multiple determination; form factor = $\frac{\text{TLS volume}}{\left(\left(\frac{\text{pi}}{4} \times d_{1.3}\right) \times h\right)}$; stem taper = $\frac{(D_1 - D_2)}{L}$, where D_1 is the lower diameter at the beginning of the stem section (log class), D_2 is the upper diameter at the end of the stem section (log class), and L is the length of the stem section (log class).

be seen in Table 6. The differences (in percentage) were calculated for volume ratios 1 and 2. The values of the volume stocks were determined by the traditional forest inventory using conventional form factor equations. These were then corrected using volume ratio 2. Volume ratio 2 included manual input for the classic volume function. Depending on the volume ratio, different deviations from the TLS-calculated volume occurred.

Q3: Which TLS procedure will improve volume estimation and reduce measurement error?

All features detected as trees were actual trees. With this aspect in mind, the correctness of the algorithm was 100% on all plots. For evaluation purposes, RMSE, r, and bias were calculated.

The $d_{1.3}$ obtained from TLS is plotted against field measurements (Fig. 5*a*). The automated TLS method had overall good estimates of diameters, with RMSE values of 1.15 cm for $d_{1.3}$ and 1.36 cm for d_{all}. It performed better in RMSE, bias, and linear correlation to field measurements of $d_{1.3}$ (Table 7). The heights estimated using the automated TLS method are plotted against heights calculated from field measurements (Fig. 5*b*). The automated TLS method delivered good estimates of total heights overall, with RMSE values of 0.52 m for total tree height (Table 7), whereas the traditional height estimation error with manual measurement input was 0.8 m (Table 7). The estimated volumes from the automated TLS method are plotted against volumes calculated from field measurements and the Smalian volume function (Husch et al. 1982) (Fig. 5*c*). The automated TLS method had good estimates of volumes overall, with RMSE values of 0.018 m^3 for stem-wood volume (Table 7). The traditional volume estimation error was 0.055 m^3 with TLS $d_{1.3}$ and h input and 0.042 m^3 with manual measurement input (Table 7).

4. Discussion

4.1. Stem form variation influenced by competition

Traditional volume functions neglect, or at least do not respect, the dependency of volume on competition, as they are designed to be simple, fast, and efficient for the purpose of practical applications. Even though competition had a statistically significant influence on deviations expressed by ratio 1, total variability explained by models 8 and 9 was low (Table 5). Beyond the effects of treatment, of initial planting density, and of competition, a considerable part of the deviations caused by the use of traditional volume functions (Table 6) was not related to competition effects; however, our investigation exhibited how competition affects the stem form of trees of the same $d_{1.3}$ and h. According to our results, trees tended to become cylindrical with increasing competition, whereas tapering increased with decreasing competition (Figs. 3*a*, 3*b*). In particular, the higher the competition was, the more cylindrical the lowest stem section (butt log) became (Fig. 3*c*). Because this stem segment contained the most volume, the overall volume differences per tree could be explained by the behaviour of the butt log. The results presented went beyond the findings obtained by Assmann (1968) and Larson (1963), as the

Fig. 3. Effects of competition on (*a*) TLS volume, (*b*) form factor per tree, (*c*) stem taper of butt log, (*d*) stem taper of mid log, and (*e*) stem taper of top log. Competition was tested on its own, while other variables were set to the mean. Each *y* axis shows the deviation from the mean of the respective variables.

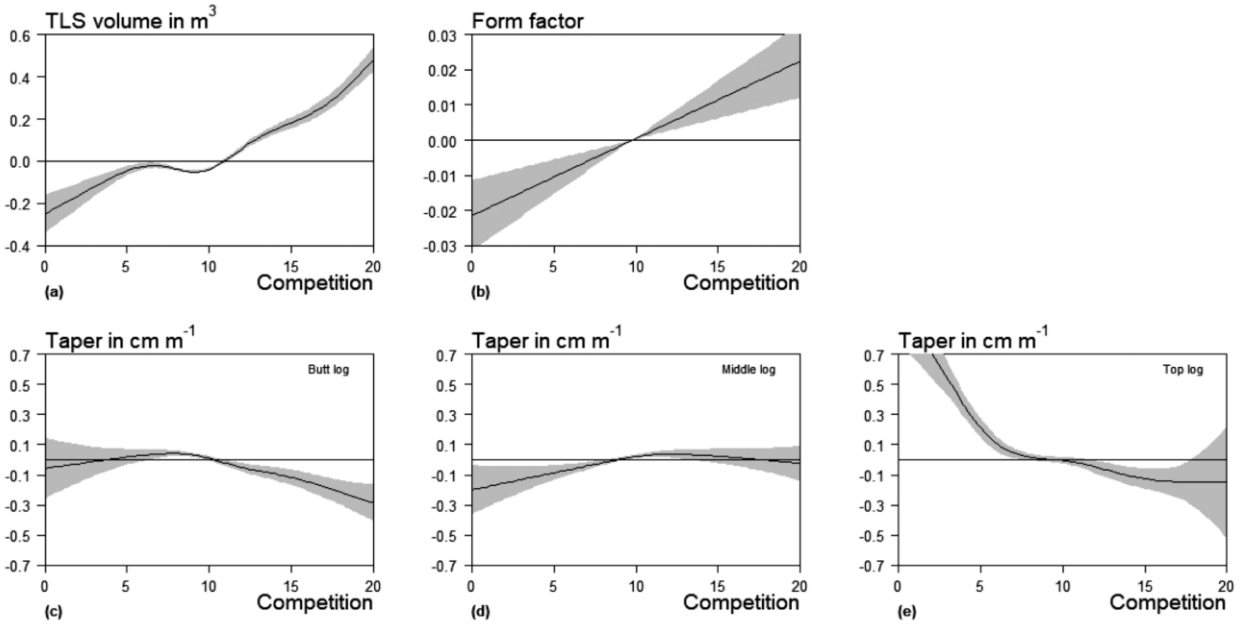

Fig. 4. Effect of competition on volume ratio 1. Competition was tested on its own, while other variables were set to the mean. The *y* axis shows the deviation from the mean of the respective variables.

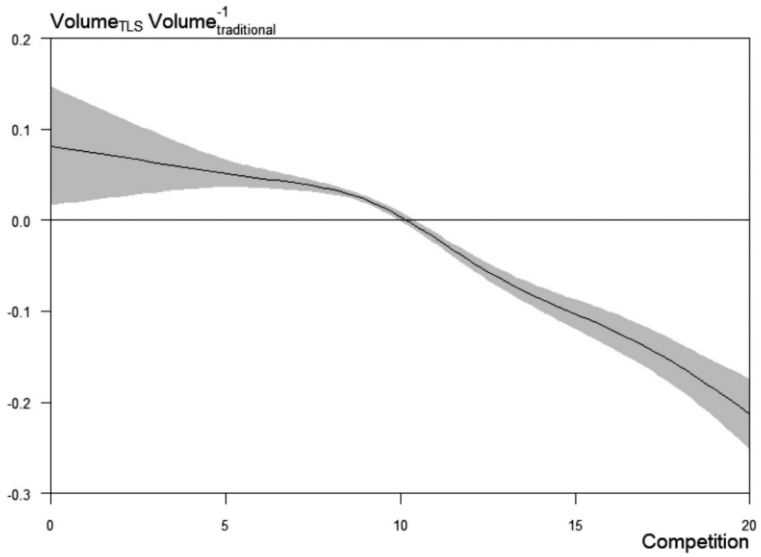

change in taper was valid for trees with the same $d_{1.3}$ and h. The study identified competition as a relevant stand property responsible for volume miscalculation. Both planting density and thinning treatment showed an influence on the stem form. Nevertheless, our results indicated that competition, planting density, and treatment cannot be the only causes of the stem form differences due to the difference in the performance of the models. As in Calama and Montero (2006), we now also conclude that there is still a high level of unexplained random variability regarding stem-form shaping. This variability indicated the presence or interaction of factors that acted at plot and tree levels. According to Schneider (2018), further main factors were biomechanical or hydraulic constraints. Both factors highlighted the important influence of crown dimensions on the stem form (Schneider 2018). Crown dynamics, which were related to stand density, could improve the research of stem-form changes (Zakrzewski 1999). In addition, the stem-form variation was influenced by climatic variables (Schneider 2018). Future research might focus on the effect of these factors on the stem form. Because TLS is able to record stem, crown shape, and branch structures three-dimensionally,

Table 6. Volume differences per treatment form.

	Volume ratio 1 (%)	Volume ratio 2 (%)	Forest inventory volume stock (m^3)	Corrected volume stock (m^3) ratio 2
Total	+4.2	+2.0	553	564
Treatment 1	+5.4	+2.7	447	459
Treatment 2	+3.8	+1.6	612	622
Thinning 1	+3.1	+3.2	808	834
Thinning 2	+4.0	+0.7	**583**	**587**
Thinning 3	+2.8	+2.5	**580**	**595**
Thinning 4	+4.6	+1.4	660	669
PD 400	+6.1	+7.0	331	354
PD 2500	+8.3	+5.0	**455**	**478**
PD 4000	+4.0	+0.7	**484**	**487**
PD 10 000	+3.4	+3.5	513	531

Note: The differences (in %) were calculated for volume ratios 1 and 2. The values of the volume stocks were determined by the traditional forest inventory using conventional form factor equations. These were then corrected using volume ratio 2. This ratio compares TLS and forest inventory method while data input is different (TLS and forest inventory). Volume ratio 1 compares TLS and forest inventory method while data input is the same (TLS). All values in bold type highlight particularly strong changes or adjustments between the treatments. PD, planting density (number of trees per hectare).

this additional information should be included in the future investigation of stem-form changes.

According to our results, the ratio of volume (volume ratio 1) miscalculation decreased with increasing competition (Fig. 4). We only dealt with volume ratio 1, because this ratio compared TLS and forest inventory methods while data input was the same. When focusing on the distribution (Fig. 4), we observed deviations that increased and decreased, apart from the mean. This may be explained by changing forest management strategies. Consequently, the variety of trees and their stem shapes seems to be larger today. Different competition situations were observed over time and the experimental area was heavily thinned. As a result, the stand structure probably differed from past ones, which again influenced the stem shape of trees. Hence, the sampling used for the deviation of the traditional form equations (factors) may have been more limited to trees coming from less structured stands, which were rather weakly thinned (thinning from below). This suggests that traditional volume functions are particularly suitable for homogeneous single-layer stands with a medium competition situation. The more heterogeneous and complex the stands are, the less suitable these functions are. However, competition might not fully explain all differences in stem shape. Furthermore, it must be questioned whether a competition index over time, as calculated in this work, could summarize the structural changes over time generated by all thinning regimes. Because the competition values were averaged over time, inaccuracies may occur over the course of time, i.e., describing the respective competitive situation approximately. Because of the averaging, the formula did not respect, for instance, whether the competitive situation was low or high at the beginning or towards the end.

4.2. Shortcomings of traditional volume calculation

The outcome of this study may be relevant for silviculture. Stand volume is important and to a large extent determines the stand value for forest sales. Planning silvicultural measures or analysing the CO_2 storage capacity of forests are other applications in which knowledge about tree volume is relevant. Moreover, common forest inventories use traditional volume functions. All those approaches use $d_{1.3}$ and have input variables for stem volume estimation. Generally, the height is measured only on a smaller sample of trees. Missing height values are generated using a diameter–height function. Finally, forest owners can determine the tree or stand volume by means of the volume function. If we compared the volume calculated using the aforementioned approach (type 3) with the volume based on TLS (type 1), the traditionally calculated volume stock was lower by 2.0%. TLS volume can be assumed to be accurate according to the following validation. Based on the 55 trees, we showed the superiority (in terms of bias, precision) of the TLS method in comparison with the common method using volume functions, although the validation did not include the complete range of trees in terms of their size (Table 2). This is because those 55 trees were harvested in a thinning (from above) campaign in spring 2018. Future crop trees remained in the stand. The volume stock underestimation was even greater if we only focused on the other method of calculation (4.2%). Therefore, we inserted the height and the diameter at breast height — detected by TLS — in the traditional volume function (type 2). In this way, we were able to identify the part of the effect that was exclusively caused by the method, i.e., utilising the Pain function (eq. 2) with many diameters along the stem axis on the one side, versus applying a simplified volume function on the other.

The aforementioned difference in volume between ratio 1 (4.2%) and ratio 2 (2.0%) could be rooted solely in diameter and height, as the form factor was not changed. The study made use of two different sources for diameter and height, coming from TLS on one hand and from the traditional forest inventory on the other. Looking at the diameter comparison between TLS and the manual method (Table 7 and Figs. 5*a*, 5*b*), we observed only a small bias and a small RMSE. This is caused by the fact that the laser scanner was standing at ground level. The diameters at breast height were much easier to calculate because the point density was much higher at ground level than in dense crown regions. These results were rendered possible using the Hough transformation, as spruce trees are generally straight and, therefore, the stem cross sections parallel to the ground are well approximated by circular shapes in the *x* and *y* planes (Olofsson et al. 2014). Consequently, the input parameter causing the volume differences was the measured tree height (Fig. 5*c*). The heights measured by the traditional forest inventory were higher than those of the TLS. This dampened the volume difference compared with the correct volume from 4.2% to 2.0%. There are findings available in which TLS-derived tree height has been compared with true tree height measured using destructive techniques (Calders et al. 2015) confirming that TLS reaches the top of the canopy easily. This was also the case for our study. Contrary to these findings, several articles concluded that TLS tends to underestimate tree height (Kankare et al. 2013; Liang and Hyyppä 2013; Liang et al. 2018). This was caused by occlusion. A higher number of scan positions per plot can reduce this phenomenon; therefore, the occlusion problem might be mainly a consequence of a reduced number of scans.

4.3. Abstraction level: enterprise, stand, tree

The miscalculation of volume became more obvious with a decreasing abstraction level. In pooling all trees (n = 868) and computing the total stock, relatively small deviations of 2.0% or 4.2% were observed, depending on the method applied. Regarding smaller stands, the volume differences became larger. The differences per plot, treatment, thinning regime, or planting density varied from 0.7% to 7.0% (Table 6). Finally, at the tree level, the absolute mean deviation per tree varied from −10% to +10%. In other words, in a rough investigation such as the determination of the total stock, traditional volume functions may be sufficient. The more precise the examination is, however, especially at tree level, the more suitable the application of TLS may become. In a worst-case scenario, scientific results could be misinterpreted, and wrong recommendations could be given based on traditional volume calculations (Meng 1981). As shown in Table 6, a superiority of 3 $m^3 \cdot ha^{-1}$ in terms of stock volume of thinning regime 2 vs. regime 3 was reversed to an inferiority of 8 $m^3 \cdot ha^{-1}$ based on

Fig. 5. (*a*) Comparison of $d_{1.3}$ measurement types between TLS and manual measurement. All $d_{1.3}$ were measured by tape. (*b*) All diameters of the 55 logged trees were measured by calliper. (*c*) Comparison of all 28 heights depending on measurement type. Type 1, automated TLS method, and type 2, traditional height measurement. (*d*) Comparison of all 55 stem volumes depending on measurement type. Type 1, the automated TLS method, and type 2, the traditional volume function with parameter input of forest inventory. The lines represent a 1:1 relationship.

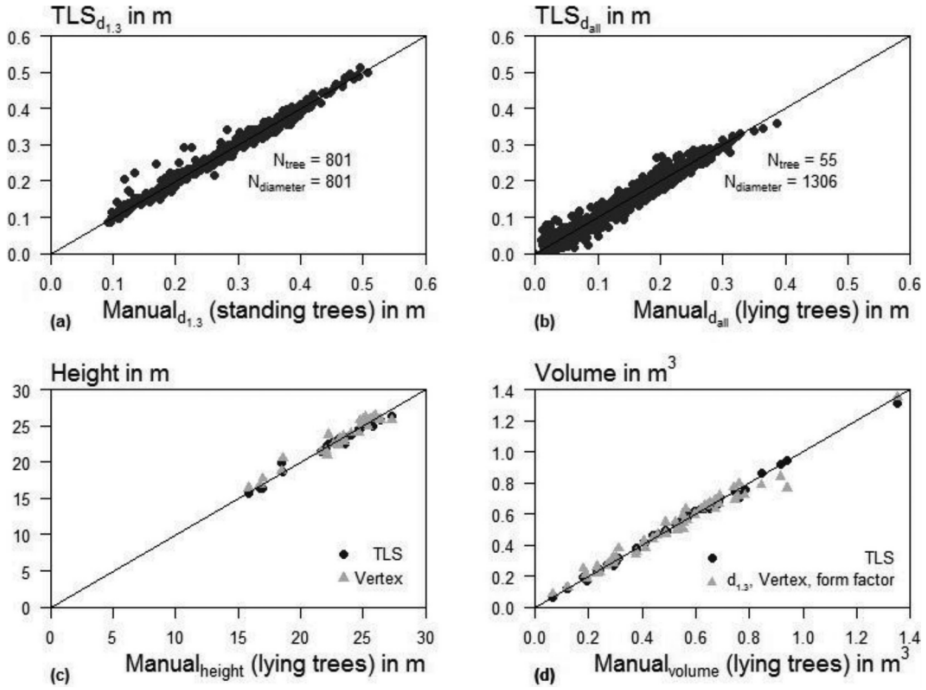

Table 7. Mean, root mean square error (RMSE), bias, and coefficient of multiple determination (R^2) of the diameters at breast height ($d_{1.3}$) and diameter along the stem (d_{all}) obtained from TLS, where manual measurement was the reference.

	Mean	RMSE	Bias	R^2
Diameter (m)				
Reference $d_{1.3}$ – 856 trees	0.2891			
TLS $d_{1.3}$ – 856 trees	0.2884	0.0115	–0.0007	0.9902
Reference d_{all} – 55 trees	0.1516			
TLS d_{all} – 55 trees	0.1497	0.0136	0.0019	0.9807
Total height (m) – 28 trees				
Reference	22.9872			
TLS	22.9458	0.5192	–0.0343	0.9854
Traditional	23.1145	0.7942	–0.2031	0.9677
Volume (m³) – 55 trees				
Reference	0.5305			
TLS	0.5311	0.0180	–0.0006	0.9975
TLS–traditional	0.5087	0.0547	0.0218	0.9815
Traditional	0.5263	0.0417	0.0042	0.9870

Note: Mean, RMSE, bias, and R^2 of total tree heights calculated by TLS and by traditional forest inventory (traditional), where manual measurement of the felled tree was the reference. Mean, RMSE, bias, and R^2 of volumes calculated by TLS, traditional volume function with TLS data input (TLS–traditional), and traditional volume function with input of traditional forest inventory (traditional) where manual measurement and volume computation by the Smalian volume function (Husch et al. 1982) were the references.

correct TLS volume calculation. Comparing plots of different initial planting densities, PD2500 vs. PD4000 (Table 6), the difference in stock volume was traditionally 29 m³·ha⁻¹ and decreased to just 9 m³·ha⁻¹.

A significant contribution to the recording and distribution of the raw material wood in the forest is made by forest inventory. Traditional forest inventory methods, however, do not provide precise information down to a level of variety structure. They only provide information on tree species, diameters, and heights from which the volume and biomass can be determined using model assumptions. The current information basis only permits a resource-efficient use of stem wood to a limited extent. Therefore, TLS with automated methods can be used to calculate the whole stem form using individually fitted stem curves for each tree. More precise information on stem curvature and usable stem length supports a determination of sawn timber assortments even before the harvest of the stand (Seifert et al. 2010). It is precisely this additional information that is decisive for harvest productivity (Labelle et al. 2016) and for the allocation of the raw material to the optimum transport chain (Maness and Adams 2007).

5. Conclusion

Traditional form factor equations or individual-tree volume functions were usually constructed and applied within a local area and were up to 50 years old in some cases. The use of these functions is problematic, because site characteristics and ecological conditions vary geographically while silvicultural treatment has changed over time. A generally valid volume function that considers all influential factors and adapts to changes in forest management over time is difficult to realize. Additionally, traditional volume functions (species, $d_{1.3}$, and h) are applied using estimated height values for a larger number of trees rather than using exact measurements of individual trees. As shown in this study, less accurate estimations can be expected in field inventories using volume models and inaccurate predictors. Our results

showed that the measurement of stem volume with TLS data yielded an accurate estimation. In a rough investigation such as the determination of the total stock, common volume functions can be sufficient; however, the more precise the examination is, the more suitable the application of TLS will be. For homogeneous and single-layer stands with a uniform competition situation, common volume functions are still a fast and easy choice.

Acknowledgements

This study was part of the FORSENSE project (grant agreement no. 033RK046A) within the "KMU-innovativ" call supported by the Federal Ministry of Education and Research (BMBF, Bundesministerium für Bildung und Forschung). Additional funding was received from the European Union's Horizon 2020 Research and Innovation Programme under the Marie Skłodowska-Curie (grant agreement no. 778322). We thank Thomas Seifert and Stefan Seifert from Scientes Mondium UG for supporting the analysis, as well as two anonymous reviewers who also provided comments that improved the manuscript.

References

Assmann, E. 1968. Zur "Theorie der Grundflächenhaltung". Forstwiss. Centralbl. **87**(1): 321–330. doi:10.1007/BF02735874.

Cabo, C., Ordóñez, C., López-Sánchez, C.A., and Armesto, J. 2018. Automatic dendrometry. Tree detection, tree height and diameter estimation using terrestrial laser scanning. Int. J. Appl. Earth Observ. Geoinform. **69**: 164–174. doi:10.1016/j.jag.2018.01.011.

Calama, R., and Montero, G. 2006. Stand and tree-level variability on stem form and tree volume in *Pinus pinea* L.: a multilevel random components approach. For. Syst. **15**(1): 24–41. doi:10.5424/srf/2006151-00951.

Calders, K., Newnham, G., Burt, A., Murphy, S., Raumonen, P., Herold, M., Culvenor, D., et al. 2015. Nondestructive estimates of above-ground biomass using terrestrial laser scanning. Methods Ecol. Evol. **6**(2): 198–208. doi:10.1111/2041-210X.12301.

Chalmers, P. 2018. SimDesign: structure for organizing Monte Carlo simulation designs. R package version 1.9. Available from https://CRAN.R-project.org/package=SimDesign.

Deutscher Wetterdienst (DWD). 2019. Climate data center. Deutscher Wetterdienst. Available from https://www.dwd.de/DE/klimaumwelt/cdc/cdc_node.html.

Gray, H.R. 1956. The form and taper of forest-tree stems. Imperial Forestry Institute, University of Oxford, U.K. pp. 1–79.

Hackenberg, J., Morhart, C., Sheppard, J., Spiecker, H., and Disney, M. 2014. Highly accurate tree models derived from terrestrial laser scan data. A method description. Forests, **5**(5): 1069–1105. doi:10.3390/f5051069.

Harper, W.V. 2014. Reduced major axis regression. Wiley StatsRef: Statistics Reference Online. Available from https://doi.org/10.1002/9781118445112.stat07912.

Hegyi, F. 1974. A simulation model for managing jack-pine stands simulation. Royal Coll. For. Res. Notes, **30**: 74–90.

Hilker, T., van Leeuwen, M., Coops, N.C., Wulder, M.A., Newnham, G.J., Jupp, D.L., and Culvenor, D.S. 2010. Comparing canopy metrics derived from terrestrial and airborne laser scanning in a Douglas-fir dominated forest stand. Trees, **24**(5): 819–832. doi:10.1007/s00468-010-0452-7.

Huang, P., and Pretzsch, H. 2010. Using terrestrial laser scanner for estimating leaf areas of individual trees in a conifer forest. Trees, **24**(4): 609–619. doi:10.1007/s00468-010-0431-z.

Husch, B., Miller, C.I., and Beers, T.W. 1982. Forest mensuration. 3rd ed. John Wiley & Sons, New York.

Jonsson, B. 1995. Thinning response functions for single trees of *Pinus sylvestris* L. and *Picea abies* (L.) Karst. Scand. J. For. Res. **10**(1–4): 353–369. doi:10.1080/02827589509382902.

Kankare, V., Holopainen, M., Vastaranta, M., Puttonen, E., Yu, X., Hyyppä, J., Vaaja, M., et al. 2013. Individual tree biomass estimation using terrestrial laser scanning. ISPRS J. Photogramm. Remote Sens. **75**: 64–75. doi:10.1016/j.isprsjprs.2012.10.003.

Karlsson, K. 2000. Stem form and taper changes after thinning and nitrogen fertilization in *Picea abies* and *Pinus sylvestris* stands. Scand. J. For. Res. **15**(6): 621–632. doi:10.1080/02827580050216879.

Kennel, R. 1969. Formzahl-und Volumentafeln für Buche und Fichte. Institut für Ertragskunde der Forstlichen Forschungsanstalt München. p. 55.

Krutzsch, P. 1974. The IUFRO 1964/68 provenance test with Norway Spruce (*Picea abies* (L.) Karst.). Silvae Genetica, **23**(1–3): 58–62.

Labelle, E.R., Soucy, M., Cyr, A., and Pelletier, G. 2016. Effect of tree form on the productivity of a cut-to-length harvester in a hardwood dominated stand. Croat. J. For. Eng. **37**(1): 175–183.

Larson, P.R. 1963. Stem form development of forest trees. Forest Science, Monograph 5. p. 42.

Legendre, P. 1998. Model II regression user's guide, R edition. R Vignette, 14. Available from https://cran.r-project.org/web/packages/lmodel2/vignettes/mod2user.pdf.

Legendre, P. 2018. lmodel2: Model II Regression. R package version 1.7-3. Available from https://CRAN.R-project.org/package=lmodel2.

Legendre, P., and Legendre, L. 1988. Structure spatio-temporelle des variables en odanographie: Problemes d'analyse numerique et methodes d'analyse spatiale. *In* Biometric et odanographie. *Edited by* S. Frontier. Actes Colloq. Biom. Oceanogr. Sot. Fr. Biom.

Liang, X., and Hyyppä, J. 2013. Automatic stem mapping by merging several terrestrial laser scans at the feature and decision levels. Sensors, **13**(2): 1614–1634. doi:10.3390/s130201614.

Liang, X., Kankare, V., Yu, X., Hyyppa, J., and Holopainen, M. 2014. Automated stem curve measurement using terrestrial laser scanning. IEEE Trans. Geosci. Remote Sens. **52**(3): 1739–1748. doi:10.1109/TGRS.2013.2253783.

Liang, X., Hyyppä, J., Kaartinen, H., Lehtomäki, M., Pyörälä, J., Pfeifer, N., Holopainen, M., et al. 2018. International benchmarking of terrestrial laser scanning approaches for forest inventories. ISPRS J. Photogramm. Remote Sens. **144**: 137–179. doi:10.1016/j.isprsjprs.2018.06.021.

Maness, T.C., and Adams, D.M. 2007. The combined optimization of log bucking and sawing strategies. Wood Fiber Sci. **23**(2): 296–314.

Meng, C.H. 1981. Detection of stem form change after stand treatment. Can. J. For. Res. **11**(1): 105–111. doi:10.1139/x81-014.

Montero, G., Ruiz-Peinado, R., Cañellas, I., Candela, J.A., and Pavón, J. 2002. La fijación de CO_2 por las masas de Pino Piñonero en Andalucía. Forestalia, No. 7.

Olofsson, K., Holmgren, J., and Olsson, H. 2014. Tree stem and height measurements using terrestrial laser scanning and the RANSAC Algorithm. Remote Sens. **6**(5): 4323–4344. doi:10.3390/rs6054323.

Pain, O., and Boyer, E. 1996. A whole individual tree growth model for Norway spruce. *In* Proceedings of the Second Workshop "Connection Between Silviculture and Wood Quality Through Modelling Approaches and Simulation Software", Berg-en-Dal, Kruger National Park, South Africa, August 26–31, 1996. Publication Equipe de Recherches sur la Qualité des Bois. INRA-Nancy, France, 1997/7, December, 450 S.: S. 13–23.

Peltola, H., Miina, J., Rouvinen, I., and Kellomäki, S. 2002. Effect of early thinning on the diameter growth distribution along the stem of Scots pine. Silva Fenn. **36**(4): article id 523. doi:10.14214/sf.523.

Petterson, H. 1955. Die Massenproduktion des Nadelwaldes. Mitt. d. Forstl. Forschungsanst. Schwedens 1955, 45, pp. 1–391.

Pretzsch, H. 2006. Von der Standflächeneffizienz der Bäume zur Dichte-Zuwachs-Beziehung des Bestandes. Beitrag zur Integration von Baum-und Bestandesebene. Allgemeine Forst-und Jagdzeitung, **177**(10): 188–199.

Prodan, M. 1965. Holzmesslehre. Sauerlaender's Verlag, Frankfurt, Germany.

R Core Team. 2016. R: a language and environment for statistical computing. R Foundation for Statistical Computing, Vienna, Austria. Available from https://www.R-project.org/.

RIEGL. 2010. RIEGL LMS-Z420i data sheet. Available from http://www.riegl.com/uploads/tx_pxpriegldownloads/10_DataSheet_Z420i_03-05-2010.pdf.

Rötzer, T., and Pretzsch, H. 2010. Stem water storage of Norway spruce and its possible influence on tree growth under drought stress-application of CT-scannings. Berichte des Meteorologischen Instituts der Albert-Ludwigs-Universität Freiburg, **153**.

Schneider, R. 2018. Understanding the factors influencing stem form with modelling tools. *In* Progress in Botany. Vol. 80. Springer, Cham. pp. 295–316.

Seifert, T., Klemmt, H.J., Seifert, S., Kunneke, A., and Wessels, B. 2010. Integrating terrestrial laser scanning based inventory with sawing simulation. *In* Precision Forestry Symposium Available from https://www.researchgate.net/profile/Asikainen_Antti/publication/235928806_An_evaluation_of_skyline_systems_in_Norwegian_conditions_using_discrete-event_simulation/links/556555e508ae94e957205a02.pdf#page=12.

Socha, J., and Kulej, M. 2007. Variation of the tree form factor and taper in European larch of Polish provenances tested under conditions of the Beskid Sądecki mountain range (southern Poland). J. For. Sci. **53**(12): 538–547.

Stinglwagner, G., Haseder, I., and Erlbeck, R. 2016. Das Kosmos Wald-und Forstlexikon: Mit über 17.000 Stichwörtern. Kosmos.

Tasissa, G., and Burkhart, H.E. 1998. An application of mixed effects analysis to modeling thinning effects on stem profile of loblolly pine. For. Ecol. Manage. **103**(1): 87–101. doi:10.1016/S0378-1127(97)00179-5.

West, P.W. 2015. Tree and forest measurement. Springer, Berlin.

Zakrzewski, W.T. 1999. A mathematically tractable stem profile model for jack pine in Ontario. North. J. Appl. For. **16**(3): 138–143. doi:10.1093/njaf/16.3.138.

Zuur, A.F., Ieno, E.N., Walker, N.J., Saveliev, A.A., and Smith, G.M. 2009. GLM and GAM for count data. *In* Mixed effects models and extensions in ecology with R. Springer, New York. pp. 209–243.

Appendix A

Forest yield overview

Appendix Tables A1–A3 appear on the following pages.

Table A1. Forest yield overview for scanned plots of the stand space test of block 1.

					Remaining stand					Released stand				
Treatment	Plot	Year	Thinning	Thinning regime	N·ha^{-1}	hq	dq	BA	V	N·ha^{-1}	hq	dq	BA	V
Spacing test	1	1974	—	2	4000	—	—	—	—	—	—	—	—	—
Treatment 1		1992	NDF, Z		3110	9.8	11.2	30.9	162	385	9.1	9.3	2.6	14
		1996	NDF, Z		1484	12.5	15.3	27.3	175	1626	11	11.3	16.4	99
		2001	—		1462	15.7	18.9	40.8	317	22	9.2	7.6	0.1	1
		2006	Z		1165	19.3	21.2	41.1	385	297	18.8	19.3	8.7	81
		2014	NDF, Z		703	23	24.8	33.9	369	462	22.4	22.7	18.7	202
Spacing test	2	1974	—	2	400	—	—	—	—	—	—	—	—	—
Treatment 1		1992	—		389	7	14.2	6.2	24	—	—	—	—	—
		1996	Z		311	9.8	22.8	12.7	60	78	7.6	14.3	1.3	5
		2001	—		311	13.1	29.2	20.8	26	—	—	—	—	—
		2006	NDF		200	17.7	36.2	20.6	161	111	16	28.8	7.3	54
		2014	—		200	22	42.5	28.4	267	—	—	—	—	—
Spacing test	3	1974	—	2	10 000	—	—	—	—	—	—	—	—	—
Treatment 1		1992	NDF, Z		4978	10	11.2	30.9	162	385	7.8	9.3	2.6	14
		1996	NDF, Z		2511	12.6	15.3	27.3	175	1626	10.9	11.3	16.4	99
		2001	—		2467	15.5	18.9	40.8	317	22	8.7	7.6	0.1	1
		2006	Z		1978	18.8	21.2	41.1	385	297	18	19.3	8.7	81
		2014	NDF, Z		1000	22.4	24.8	33.9	369	462	20.6	22.7	18.7	202
Spacing test	6	1974	—	2	2500	—	—	—	—	—	—	—	—	—
Treatment 1		1992	—		2080	9.4	12.3	24.7	123	45	1.4	1	—	—
		1996	NDF, Z		966	12.6	16.9	21.8	138	1114	11.5	13	14.8	90
		2001	—		955	15.9	21	33	255	11	4.3	2.2	—	—
		2006	Z		773	19.5	23.9	34.7	322	182	19.2	22.7	7.3	68
		2014	Z		500	23.7	28.8	325	356	273	22.6	24.4	12.8	138

Note: Plots differ in initial planting densities. NDF, thinning from below; Z, thinning from above; N·ha^{-1}, number of trees per hectare; dq, quadratic mean diameter (cm); hq, height corresponding to dq (m); BA, basal area (m^2); V, standing volume (m^3·ha^{-1}). Thinning regime 1 was the control (null thinning); thinning regime 2 was thinned late; thinning regime 3 was thinned midway between thinning regimes 2 and 4; and thinning regime 4 was thinned early.

Table A2. Forest yield overview for scanned plots of the thinning test of block 1.

					Remaining stand					Released stand				
Treatment	Plot	Year	Thinning	Thinning regime	N·ha^{-1}	hq	dq	BA	V	N·ha^{-1}	hq	dq	BA	V
Thinning test	7	1974	—	1	2500	—	—	—	—	—	—	—	—	—
Treatment 2		1992	—		1943	9	12.9	25.6	122	46	1.3	1	—	—
		1996	—		1864	11.9	15.8	36.5	221	79	4.4	3.9	0.1	—
		2001	—		1761	15	18.3	46.3	346	103	7.6	6	0.3	1
		2006	—		1545	18.7	21	53.5	488	216	12.3	8.6	1.3	9
		2014	—		1409	22	23.7	62.3	657	136	16.6	2.1	1.6	14
Thinning test	8	1974	—	3	2500	—	—	—	—	—	—	—	—	—
Treatment 2		1992	—		1614	8.8	13.3	22.4	104	68	1.3	1	—	—
		1996	NDF, Z		886	12	17.3	20.9	126	728	11.5	15.4	13.5	80
		2001	—		830	15.4	22.1	31.8	237	56	6.5	5.4	0.1	1
		2006	NDF, Z		670	19.1	25.1	33.2	300	160	18.7	23.3	6.8	61
		2014	Z		602	23	29.6	41.4	439	68	18.3	17.6	1.7	16
Thinning test	9	1974	—	2	2500	—	—	—	—	—	—	—	—	—
Treatment 2		1992	NDF, Z		1195	10.5	14.4	19.5	106	680	9.6	11.5	7.1	38
		1996	NDF, Z		680	13.8	19.3	19.9	135	515	12.1	15.1	9.3	60
		2001	—		680	17	24	30.8	248	—	—	—	—	—
		2006	—		636	20.9	27.6	37.9	368	44	19.1	20.8	1.5	14
		2014	—		636	24.2	31.2	48.7	537	—	—	—	—	—
Thinning test	10	1974	—	4	2500	—	—	—	—	—	—	—	—	—
Treatment 2		1992	NDF, Z		1216	9.9	14.3	19.6	100	409	9.3	12.1	4.7	24
		1996	—		1216	13	18.1	31.4	204	—	—	—	—	—
		2001	—		1136	16.7	21.8	42.3	341	80	7.1	6.2	0.2	1
		2006	Z		875	20.3	24.4	41.1	396	261	19.7	22.1	10.1	96
		2014	Z		705	23.6	27.6	42	463	170	23.6	27.4	10.1	111
Thinning test	11	1974	—	4	2500	—	—	—	—	—	—	—	—	—
Treatment 2		1992	NDF, Z		1261	9.8	14.1	19.8	100	421	9.1	11.5	4.4	21
		1996	—		1261	12.4	17.4	30.1	189	—	—	—	—	—
		2001	—		1170	16	21.2	41.5	325	91	4.9	5.5	0.2	1
		2006	Z		864	19.9	23.4	37.1	354	301	19.5	21.8	11.5	109
		2014	Z		693	23.9	27	39.8	445	171	23.4	25.3	8.5	95

Note: Plots differ in thinning regimes. NDF, thinning from below; Z, thinning from above; N·ha^{-1}, number of trees per hectare; dq, quadratic mean diameter (cm); hq, height corresponding to dq (m); BA, basal area (m^2); V, standing volume (m^3·ha^{-1}). Thinning regime 1 was the control (null thinning); thinning regime 2 was thinned late; thinning regime 3 was thinned midway between thinning regimes 2 and 4; and thinning regime 4 was thinned early.

Table A3. Forest yield overview for scanned plots of the thinning test of block 2.

					Remaining stand					Released stand				
Treatment	Plot	Year	Thinning	Thinning regime	N·ha^{-1}	hq	dq	BA	V	N·ha^{-1}	hq	dq	BA	V
Thinning test	16	1974	—	2	2500	—	—	—	—	—	—	—	—	—
Treatment 1		1992	—		2116	9.9	12.7	26.9	141	11	1.3	1	—	—
		1996	NDF, Z		998	12.8	17.4	23.6	151	1118	11.2	12.6	13.9	84
		2001	—		998	16.4	21.4	35.8	284	—	—	—	—	—
		2006	Z		800	19.7	23.9	35.8	338	198	19.6	19.6	8.4	78
		2014	Z		504	235	23.5	31.7	346	296	22.8	22.8	15.6	168
Thinning test	17	1974	—	2	2500	—	—	—	—	—	—	—	—	—
Treatment 2		1992	—		1162	10.4	14.1	18.2	98	867	9	10.4	7.3	37
		1996	NDF, Z		691	13.3	19	19.7	129	471	12.1	15.6	9	56
		2001	—		691	16.9	24	31.4	251	—	—	—	—	—
		2006	NDF, Z		680	20.3	27.1	39.2	370	11	19.7	24.7	0.5	5
		2014	Z		669	23.5	30.5	49	527	11	16.2	9.7	0.1	1
Thinning test	18	1974	—	3	2500	—	—	—	—	—	—	—	—	—
Treatment 2		1992	—		2171	10.4	13	28.7	158	33	5.8	3.7	—	—
		1996	NDF, Z		1228	13.3	16.8	27.2	182	943	12.2	13.4	13.4	87
		2001	—		1228	16.7	20.3	39.7	325	—	—	—	—	—
		2006	Z		877	20.2	22.6	35.2	343	351	20	22	13.3	129
		2014	Z		702	23.5	26.6	39.1	430	175	23	25.2	8.8	95
Thinning test	20	1974	—	3	2500	—	—	—	—	—	—	—	—	—
Treatment 2		1992	—		2116	10.2	12.5	25.9	140	66	7.5	6.6	0.2	1
		1996	NDF, Z		1151	12.9	16.7	25.2	164	965	11.5	12.6	12	74
		2001	—		1151	16.3	20.3	37.4	299	—	—	—	—	—
		2006	Z		877	19.6	22.9	36.1	342	274	18.9	21	9.5	88
		2014	Z		702	23.1	27.4	41.3	447	175	21.5	22.5	7	73
Thinning test	21	1974	—	3	2500	—	—	—	—	—	—	—	—	—
Treatment 2		1992	—		1711	10.2	13.6	24.9	132	54	1.4	1	—	—
		1996	NDF, Z		1064	12.6	17.2	24.6	156	647	12.1	15.7	12.5	78
		2001	—		1064	16.4	20.7	35.8	287	—	—	—	—	—
		2006	NDF, Z		822	19.9	23.9	37	351	242	18.2	18.8	6.7	61
		2014	Z		702	23.5	28.5	44.7	488	120	19.5	17.9	3	30

Note: Plots differ in thinning regimes. NDF, thinning from below; Z, thinning from above; N·ha^{-1}, number of trees per hectare; dq, quadratic mean diameter (cm); hq, height corresponding to dq; BA, basal area (m^2); V, standing volume (m^3·ha^{-1}). Thinning regime 1 was the control (null thinning); thinning regime 2 was thinned late; thinning regime 3 was thinned midway between thinning regimes 2 and 4; and thinning regime 4 was thinned early.

Workflow — technical description

1. Stem detection

All scans per plot were referenced to each other and the data were exported in a .LAS file format. This is a binary file format for the fast interchange of three-dimensional (3D) data between data users. The complete processing was done within the programming environment of R (R Core Team 2016). For this purpose, the rlas package (Roussel and De Boissieu 2018) was used.

1.1. Median-centring in PPC-R

A fast data processing was enabled by selecting random rows of the rough plot point cloud (PPC-R) table. The data of one plot was minimised by random sampling from approximately 50 to exactly one million points. The central position was derived as the median value of x and y coordinates of the five scan positions per plot.

1.2. Square selection of points in the centred PPC-R

The coordinates of the central position were set to 0, i.e., $x = 0$, $y = 0$, and $z = 0$, by subtracting their median values. All points with $x \leq 25$ and $x \geq -25$, and $y \leq 25$ and $y \geq -25$ were kept. The result was a square (50 m × 50 m) plot point cloud (PPC). Although the actual plot size was 30 × 30 m, the larger size of the PPC ensured that all trees of the actual plot were included; otherwise, rotations around the z axis would have been necessary to cut out the exact boundaries of the plots. Finally, the coordinates of the PPC were set back to the initial values to match the coordinates of the PPC-R.

1.3. Data thinning – point density reduction

Density-based clustering algorithms were limited for analysing point patterns, which vary spatially in point density. Therefore, it was useful to create a more homogeneous spatial distribution of the 3D points. To achieve this, the x and y axes were divided into classes with an interval of 1 m. In the end, there were 50 × 50 m classes (2500 squares). Each square was 1 × 1 m in size. To achieve a homogeneous point density, a maximum sample of 15 000 points per square was taken. Fewer points were all captured.

1.4. Density-based spatial clustering algorithm with noise

To detect individual-tree positions, we used the dbscan function in the dbscan package of R (Hahsler and Piekenbrock 2017). The function relied on a density-based notion of clusters, which was designed to discover clusters of arbitrary shape (Ester et al. 1996). Only the x and y axes were used as input data, thereby pushing down all points belonging to the z axis to one height level. The consequence was a higher point density per tree stem. Now dbscan was automatically able to find each tree as a cluster. This meant that each recognized cluster (stem) now received a unique number and could be processed individually. Additionally, non-vertically grown trees were detected at the lower part of the stem. Ground points were recognized by dbscan as noise points because of the horizontal structure in contrast to the vertically grown stems. Figure A1 shows the results of this step. For each stem cluster, stem base points were determined. The median values of the x and y coordinates and the minimum value of the z axis of the stems were calculated. The stem base points now served to extract the original points of the entire stem from the PPC-R in the form of a cylinder. In the filtered and reduced PPC, the stem base points were determined to extract the original information of the stems from the PPC-R.

Fig. A1. Automatically generated output of one plot with the density-based spatial clustering algorithm with noise (DBSCAN). Each recognized coloured (bold) cluster received a unique number. Some trees had the same colour due to the repeating colour sequence. Noise points were coloured black (not bold).

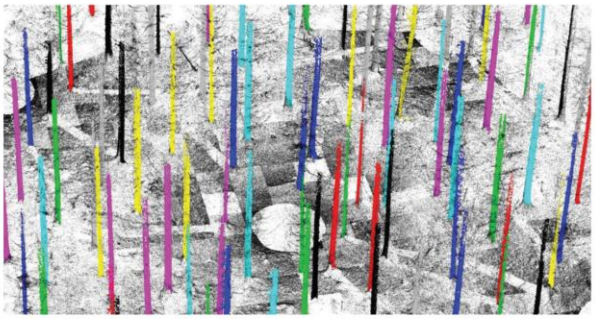

2. Stem isolation

2.1. Cylinder subset

Now the PPC-R served as database. The trees were cut out in a radius of 1 m from the stem base point. The result was a 3D point cloud in the form of a cylinder, which contained all individual-tree information obtained by TLS. The point cloud size per tree differed from 30 000 to 300 000 points due to the scan acquisition, heterogeneous stand densities, shading, and the varying height of the crown base. The studies of DeConto (2016) and Raumonen et al. (2013) suggested that reduced point clouds can already provide precise estimates. DeConto (2016) used point clouds with reduced spatial resolution with not more than 300 000 points per tree, and good accuracy was still achieved. In the mentioned study, this was the maximum size of a point cloud per tree. In our study, the mean size was approximately 70 000 points per tree. Not every detected tree was involved in the estimation of the stem form. Due to the heterogeneous density of the point cloud, a threshold for a minimum amount of points per tree was used. The number of points was determined for each tree silhouette. The lowest 5% were removed, as they were either juvenile or poorly covered by TLS. Some trees were detected but the number of points was too low to precisely measure the stem form. This was caused by occlusion. This phenomenon can be reduced by using more scans per plots. Considering this, the occlusion problem was mainly a consequence of a reduced number of scans.

2.2. Hough transformation for stem isolation

For stem isolation, the Hough transformation, adapted by Olofsson et al (2014), was used. It was already implemented in the R package TreeLS (DeConto 2016). According to DeConto (2016), the Hough transformation presented the best overall performance for most species, including Norway spruce. The result was an isolated stem without ground, branch, and crown points. Figure A2 illustrates the visual results of the stem isolation (blue points).

3. Height determination depending on competition situation

The point density naturally decreased to the top of the trees because the scanner operated from the ground. Furthermore, the laser beam was usually not able to penetrate tree compartments to perform measurements behind obstacles. These effects resulted in rather sparse measurement densities in the upper crown and stem regions, especially if the crown parts near the scanner are dense such as those of conifers (Hilker et al. 2010). Therefore, the isolated stems could not be used to determine the total tree height, as the stems could only be measured up to a limited height (Fig. A2). The cylinder subsets calculated in the previous step (2.1) were used to determine the total tree heights. As already mentioned, each tree was cut out around its stem base point in a radius of 1 m. This cylinder subset included parts of the branches, as well as the uppermost part of the crown. Afterwards the highest point was determined in this cylinder. In addition, the stem isolated in the previous step (2.2) was used to determine the lowest stem point. The difference between the highest and lowest point ($\max(z) - \min(z)$) resulted in the total tree height. However, this form of calculation caused errors regarding the competition situation. In particular, the crowns of dominant trees overshadow small trees underneath them. The cylinder subset contained not only the uppermost crown part, but also parts of crowns of competing trees. As a result, the total tree height was overestimated.

Fig. A2. Visual result of TLS method (plot 3). The black points belong to the cylinder subsets of each tree. The isolated stems are coloured in blue, and the green points, which are circles, are calculated for all height sections for which stem information was not available due to occlusion problems. The circle diameter calculation was done by the stem curve function (Pain and Boyer (1996)). The green circles serve for the three-dimensional stem reconstruction; however, they were calculated up to the height at which the diameter was higher than 7 cm (stem wood).

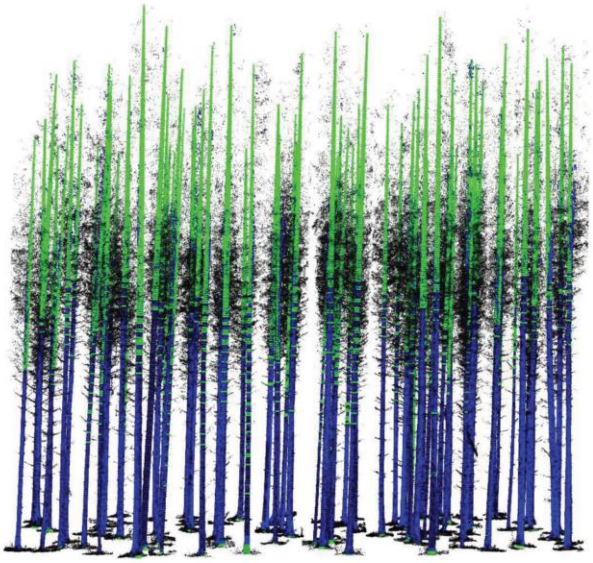

The total height of trees with $d_{1.3}$ greater than 20 cm (more dominant trees) was detected by determining the z axis minimum and maximum points of the cylinder. The minimum value was subtracted from the maximum value and the output was the height.

The height of trees where $d_{1.3}$ was greater than 14 cm and lower than 20 cm was detected by determining the z axis minimum and maximum points of the cylinder. The cylinder had a smaller size due to a radius of 0.1 m. Before this, the highest point of the stem isolation result was set as the central position of the cylinder. The minimum value was subtracted from the maximum value and the output was the height.

The height of trees with $d_{1.3} < 14$ cm was detected by determining the z axis minimum and maximum points of the stem point cloud. Dominant trees surrounded these trees. The advantage was that the stem in the upper region was more visible. The minimum value was subtracted from the maximum value and the output was the height.

According to Calders et al. (2015), TLS easily reaches the top of the canopy. Therefore, TLS-derived tree height had been com-

pared with true tree height measured using destructive techniques.

4. Diameter calculation

At first, each isolated stem was divided into height classes with intervals of 0.1 m. At every 0.1 m, a diameter was measured. To ensure a sufficient number of points per height class for ellipse fitting, every point 0.1 m below and 0.1 m above the certain height was involved in diameter computation. As a result, each section had a vertical size of 20 cm (e.g., 1.30 m = 1.20 m to 1.40 m). After this, the centre of the stem section was calculated by a geometric circle fit (Späth 1996). The distances from the centre to all points were computed. Ellipses were fitted using the method of Fitzgibbon and Fisher (1996), which was extremely robust and efficient. The circle and ellipse fit were implemented in the R package conicfit (Gama and Chernov 2015). Before ellipse fitting, a preparation or filtering of the stem section data was necessary due to possible noise points of branches or needles. Filtering was done using the Hough transformation (refer to step 2.2 on the previous page). Only ellipse fitting without filtering would lead to a deviation comparing manual and TLS measurement, especially for small tree diameters with estimations tending to be more upwardly biased for stem segments smaller than 10 cm in diameter (DeConto 2016).

Afterwards, the ellipse could be fitted and was converted into a polygon. The perimeter was derived by the surface area of the polygon. Finally, the diameter was derived by the perimeter of the stem section. The diameters calculated were used to fit the stem curve function.

5. Tree by tree comparison

The estimations based on TLS data vs. estimations based on traditional inventory data were compared. It was necessary to identify each particular study tree (n = 868) on each PPC. To identify the trees in the field database and in the TLS point cloud, we manually rotated and merged the two tree spatial maps obtained from traditional inventory and TLS.

References

Calders, K., Newnham, G., Burt, A., Murphy, S., Raumonen, P., Herold, M., Culvenor, D., et al. 2015. Nondestructive estimates of above-ground biomass using terrestrial laser scanning. Methods Ecol. Evol. **6**(2): 198–208. doi:10.1111/2041-210X.12301.

DeConto, T. 2016. Performance of tree stem isolation algorithms for terrestrial laser scanning point clouds. Master's thesis in Forest Management, Swedish University of Agricultural Sciences.

Ester, M., Kriegel, H.P., Sander, J., and Xu, X. 1996. A density-based algorithm for discovering clusters in large spatial databases with noise. *In* Proceedings, 2nd International Conference on Knowledge Discovery and Data Mining. Portland, Ore. pp. 226–231. Available from https://www.aaai.org/Papers/KDD/1996/KDD96-037.pdf.

Fitzgibbon, A.W., and Fisher, R.B. 1996. A buyer's guide to conic fitting. DAI Research paper, University of Edinburgh, Edinburgh, U.K.

Gama, J., and Chernov, N. 2015. conicfit: algorithms for fitting circles, ellipses and conics based on the work by Prof. Nikolai Chernov. R package version 1.0.4. Available from https://CRAN.R-project.org/package=conicfit.

Hahsler, M., and Piekenbrock, M. 2017. dbscan: Density Based Clustering of Applications with Noise (DBSCAN) and related algorithms. R package version 1.1-1. Available from https://CRAN.R-project.org/package=dbscan.

Hilker, T., van Leeuwen, M., Coops, N.C., Wulder, M.A., Newnham, G.J., Jupp, D.L., and Culvenor, D.S. 2010. Comparing canopy metrics derived from terrestrial and airborne laser scanning in a Douglas-fir dominated forest stand. Trees, **24**(5): 819–832. doi:10.1007/s00468-010-0452-7.

Legendre, P. 2018. lmodel2: Model II Regression. R package version 1.7-3. Available from https://CRAN.R-project.org/package=lmodel2.

Olofsson, K., Holmgren, J., and Olsson, H. 2014. Tree stem and height measurements using terrestrial laser scanning and the RANSAC algorithm. Remote Sens. **6**(5): 4323–4344. doi:10.3390/rs6054323.

Pain, O., and Boyer, E. 1996. A whole individual tree growth model for Norway spruce. *In* Proceedings of the Second Workshop "Connection Between Silviculture and Wood Quality Through Modelling Approaches and Simulation Software", Berg-en-Dal, Kruger National Park, South Africa, August 26–31, 1996. Publication Equipe de Recherches sur la Qualité des Bois. INRA-Nancy, France, 1997/7, December, 450 S.: S. 13–23.

R Core Team. 2016. R: a language and environment for statistical computing. R Foundation for Statistical Computing, Vienna, Austria. Available from https://www.R-project.org/.

Raumonen, P., Kaasalainen, M., Åkerblom, M., Kaasalainen, S., Kaartinen, H., Vastaranta, M., et al. 2013. Fast automatic precision tree models from terrestrial laser scanner data. Remote Sens. **5**: 491–520. doi:10.3390/rs5020491.

Roussel, J.R., and De Boissieu, F. 2018. rlas: Read and write 'las' and 'laz' binary file formats used for remote sensing data. R package version 1.2.1. Available from https://CRAN.R-project.org/package=rlas.

Späth, H. 1996. Least-squares fitting by circles. Computing, **57**(2): 179–185. doi:10.1007/BF02276879.

B.2. Article II

Title: How drought stress becomes visible upon detecting tree shape using terrestrial laser scanning (TLS)

Authors: Martin Jacobs, Andreas Rais, Hans Pretzsch

Journal: Forest Ecology and Management

Submitted: 27. July 2020

Accepted: 23. January 2021

Forest Ecology and Management 489 (2021) 118975

Contents lists available at ScienceDirect

Forest Ecology and Management

journal homepage: www.elsevier.com/locate/foreco

How drought stress becomes visible upon detecting tree shape using terrestrial laser scanning (TLS)

Martin Jacobs *, Andreas Rais, Hans Pretzsch

Chair of Forest Growth and Yield Science, TUM School of Life Sciences Weihenstephan, Technical University of Munich, Hans-Carl-v.-Carlowitz-Platz 2, 85354 Freising, Germany

ARTICLE INFO

Keywords:
Water retention experiment
Norway spruce
European beech
Allometry
Crown
Competition

ABSTRACT

Due to climate change, the occurrence of drought events with essential effects on trees will arise. The impact of severe drought stress on trees' vitality with regard to growth has often been analysed using traditional, easy-to-measure variables, such as diameter at breast height ($d_{1.3}$). Another commonly used tree-vitality indicator is crown transparency, which is not directly measurable and has to be determined qualitatively by well-trained field experts. In this study, we focused on tree dimensions, as potential vitality indicators, that are difficult to measure. The new approach for the efficient monitoring of tree vitality introduced here revealed three-dimensional change of tree shape due to drought stress.

The unique drought stress experiment "Kranzberg Forest Roof Experiment" (KROOF) was used as a basis for scanning and analysing the growth of Norway spruce (*Picea abies* (L.) H. Karst.) and European beech (*Fagus sylvatica* L.) under progressively limiting water reserves. Before the start of the experiment in the winter of 2012/2013, terrestrial laser scanning (TLS) was performed and repeated in the winter of 2018/2019. One sample of 21 trees was trenched and roofed (treatment), while additional 26 trees served as untreated reference (control). Using the TLS-point clouds of the two subsequent surveys, structural tree modifications within the 6-year period can be directly visualised, computed and linked to drought stress.

Drought stress led to significantly smaller crown size and lower height growth for both tree species. The crowns of Norway spruce trees increased significantly in transparency and roughness. In addition, high competition combined with drought stress significantly reduced the roughness and increased the compactness of the crown. The periodic annual change in crown projection area (pac_{cpa}) as well as the periodic annual height increment (pai_{height}) differed significantly between control and treatment for both tree species. Under drought conditions, pac_{cpa} changed by –0.74 $m^2\ yr^{-1}$ and –0.42 $m^2\ yr^{-1}$ for spruce and beech trees respectively, whereas the control trees showed a growth of 0.17 $m^2\ yr^{-1}$ and 0.62 $m^2\ yr^{-1}$ respectively. This means that crowns became considerably smaller under dry conditions. Under drought, the pai_{height} was 0.09 m yr^{-1} less for spruce and 0.17 m yr^{-1} less for beech compared with normal growing conditions. The periodic annual change in crown roughness ($pac_{roughness}$) was −9.5% yr^{-1} if local competition increased by one.

Our results show that TLS can offer new opportunities for identifying structural features in trees. Iterative TLS-surveys may extend existing measuring campaigns on common long-term experimental plots, in order to analyse general changes or monitor tree vitality.

1. Introduction

Drought events will become more widespread, extensive and extreme in the future (IPCC 2012). Climate change is likely to accelerate tree mortality (Anderegg et al. 2013), where large trees may be potentially most vulnerable, putting crucial environmental, economic and social benefits at risk (Stovall et al. 2019). According to the rapid environmental changes (IPCC 2012), the development and analysis of tree vitality indicators is important and should be continued in order to recognise tree stress at an early stage (Dobbertin et al. 2009). Here, we show innovative methods for the efficient monitoring of tree vitality under climate change, by way of example, for Norway spruce (*Picea abies* (L.) H. Karst) and the European beech (*Fagus sylvatica* L.).

There are a number of different indicators used to describe the

* Corresponding author at: Chair of Forest Growth and Yield Science, Room: 1.2.2.10, Hans-Carl-von-Carlowitz-Platz 2, 85354 Freising, Germany.
E-mail address: martin.jacobs@tum.de (M. Jacobs).

https://doi.org/10.1016/j.foreco.2021.118975
Received 27 July 2020; Received in revised form 15 January 2021; Accepted 23 January 2021
Available online 16 March 2021
0378-1127/

vitality of an individual tree. The two most common ones are crown transparency, describing defoliation, and diameter growth of the individual tree (Dobbertin et al. 2009). In order to assess the long-term development of tree vitality, it is often necessary to select easy to measure indicators for forest inventories. Since a tree loses its needles or leaves before it dies, crown transparency has been recorded as an indicator of tree vitality by the percentage of a fully foliated tree crown (Müller and Stierlin 1990). To determine the growth of a tree, it has proven beneficial to measure the stem diameter at breast height ($d_{1.3}$) or the width of tree rings. Much more difficult to measure are tree height, branch and leaf growth, including the total aboveground biomass. For this reason, stem growth was primarily selected as an indicator of stress in general (Dobbertin 2005). According to Dobbertin et al. (2009), the traditional indicators crown transparency and stem growth could, with certain limitations, be used as indicators for the vitality of a single tree. However, they should not be considered on their own, as this could lead to misinterpretations. There is no universal indicator for the vitality of a single tree (Dobbertin et al. 2009). Therefore, research on traditional and potential tree vitality indicators is important to detect drought stress.

The growth of Norway spruce and European beech, which are the most common commercial conifer and broadleaved tree species in Germany (BMEL - Bundesministerium für Ernährung und Landwirtschaft 2014), has been adversely affected by recent drought events (Pretzsch et al. 2020a). In the drought of 2015, stand growth of Norway spruce decreased by approximately 30% (Pretzsch et al. 2020a). In general, stem increment in Norway spruce has been reduced by high summer temperatures (Seidling et al. 2012). In contrast, European beech has proven to be more drought-resistant in terms of growth (Pretzsch et al. 2018) and to recover better after wetter summers (Seidling et al. 2012). It can generally be assumed that more favourable growth conditions will promote growth at the lower part of the stem, while upper stem regions will grow proportionally better when resources are limited (Larson 1963). Accordingly, the majority of studies have shown that radial growth at breast height is more sensitive to climate-induced growth reductions compared to radial increment measured higher up the stem (Mette et al. 2015). Sterba (1996) showed that stress-induced tree growth declines is more pronounced at the lower third of the stem for softwood species such as Norway spruce, Scots pine (*Pinus sylvestris* L.) and silver fir (*Abies alba* Mill.). Similar growth patterns were observed for Norway spruce under drought stress (Sohn et al. 2012) and even under ozone stress (Pretzsch et al. 2010).

Height growth has been found to respond to severe drought stress even more sensitive than basal area growth (Rais et al. 2014) and should therefore be considered as an indicator of drought stress in future surveys. The behaviour of height growth under drought stress has rarely been investigated on mature trees (Mäkinen 1998; Wang et al. 2012), as the direct and accurate height measurement requires tree felling, which is often not feasible (Hasenauer and Monserud 1997). From an ecophysiological point of view, the height growth of most coniferous species is a complex multi-seasonal process involving the formation of terminal buds during late summer of the first year, and shoot elongation during spring in the second year (Bréda et al. 2006). In contrast, radial growth is primarily driven by current growing season precipitation (Griesbauer and Green 2010) and more precisely by the occurrence of water availability (Taeger et al. 2013).

The effects of drought stress on tree crown development have thoroughly been described by Bréda et al. (2006): If a tree's water supply deteriorates, the water pressure drops. This leads to constraints of water transport from the roots to the crown leaves. In order to prevent a drop in pressure and further drying out, trees close the stomata of their leaves to avoid water losses (McDowell and Sevanto 2010). When stomata are closed, less carbon dioxide can be absorbed, leading to a loss of productive photosynthesis needed for nutrition supply. The crowns of European beech and Norway spruce trees have been observed to be more transparent in hot compared with averagely hot summers (Seidling et al. 2012). The defoliation caused by drought can be reversed when the water supply improves (Eilmann et al. 2013). Dry and warm summers accelerate defoliation, discolouration of foliage, cone formation and mortality. High crown transparency can occur due to increased needle-shedding in the autumn after dry summers (Solberg 2004).

In terms of the impact of drought on crown size, it has been controversially discussed whether branch shedding can be seen acclimatisation to drought stress or not. In this context, Rood et al. (2000) assumed that the susceptibility to cavitation and the death of branches are physiologically linked to each other. In addition, the active process of shedding branches (cladoptosis) enables trees to adjust root-shoot ratios after drought-induced decline in root system extent and efficiency. In line with this natural process of cladoptosis, Bréda et al. (2006) hypothesised that crown thinning and branch shedding could be an acclimatisation to drought stress. In contrast, Rust and Roloff (2004) did not support the widely held assumption that cladoptosis is an immediate reaction to drought stress that reduces transpiring leaf area. Whereas branch shedding and dying was observed for oak, birch and poplar (Rood et al. 2000; Rust and Roloff 2002), evidence regarding this phenomenon is still lacking for the Norway spruce and European beech. Yet, it has not been validated that limited water availability shrinks the crown size, expressed as the crown projection area (*cpa*). In addition, it is not clear if the assumed effects of branch shedding and dying reach an extent, which is measurable via the *cpa*.

Most of the studies regarding drought stress reactions e.g. Bréda et al. (2006) either analysed past drought events (e.g. 2015) or simulated drought stress, to simulate more severe, potential future weather conditions, some studies have been conducted in regions where current weather conditions are assumed to be similar to future conditions in the region of interest. The unique experiment "KROOF" ("Kranzberg Forest Roof Experiment") has been the basis of several previous studies. It has served as a long-term ozone-fumigation experiment (Pretzsch et al. 2010) and as a drought-related intraspecific growth experiment (Pretzsch et al. 2018; Schäfer et al. 2019; Pretzsch et al. 2020b). From 2014 to 2018, the experiment aimed to investigate the effects of recurrent summer droughts on mature Norway spruce and European beech growing in monoculture and mixed-species stands. For this reason, novel precipitation-exclusion roofs were constructed over six of 12 plots, in order to exclude any summer precipitation on the precipitation-exclusion plots. Based on this drought experiment from 2014 to 2018, Pretzsch et al. (2020) stated that the induced water limitation led to a decline in growth in the first year, especially for Norway spruce. A slight acclimatisation to the dry conditions followed. Beech acclimatised and recovered faster than spruce under all growing conditions, while spruce only acclimatised faster in mixture with beech. Both species showed a higher mortality under induced drought compared to the control plots; for spruce, the long-term mortality rate was higher than for beech. Our current investigation is directly linked to this research and concentrated on tree dimensions, which have so far been difficult to measure and thus have not yet been analysed.

Based on terrestrial laser scanning (TLS), the current study focused on the scan and quantification of the variability in stem and crown characteristics caused by drought stress. TLS can measure detailed stand and individual tree information (Trochta et al. 2017) and is a suitable tool for measuring physical crown dimensions (Seidel et al. 2015), without the need for cutting of trees or time-consuming and costly manual surveys. When for instance, TLS derived tree heights and traditional measured heights have been compared with true tree heights using destructive techniques TLS was found to be more accurate (Calders et al. 2015; Jacobs et al. 2020). Our study focused on stem taper as the stem-form-describing variable, and total tree height as the height-describing variable. Regarding crown characteristics, *cpa*, crown transparency and crown roughness were considered. The study addressed the following research questions:

Q1 How does severe drought stress affect stem characteristics ($d_{1.3}$, height, taper)?

Table 1
Site, plot and tree characteristics of the experimental plot Kranzberger Forst FRE 813/1 are given for 2014, i.e. before the start of the throughfall exclusion recorded manually.

Location					
Altitude above sea level	m	490			
Coordinates		11°39′42″E, 48°25′12″N			
Climate[1)]					
Mean annual temperature	°C	7.5			
Annual precipitation	mm yr^{-1}	750–800			
Soil					
Initial substrate		Loess			
Soil type		Luvisol			
Trees[2)]					
Species		European beech		Norway spruce	
Group		Control	Treatment	Control	Treatment
Trees per group and species		13	11	13	10
Stand density index *SDI*		851 (44)	823 (43)	777 (73)	816 (35)
Diameter at breast height $d_{1.3}$	cm	32.5 (8.7)	30.9 (7.4)	35.9 (5.6)	37.7 (9.5)
Height *h*	m	29.3 (1.6)	29.2 (3.1)	31.8 (2.1)	31.6 (2.0)
Crown radius *cr*	m	3.1 (1.1)	3.3 (1.3)	2.3 (0.4)	2.4 (0.2)
Crown base height *cbh*	m	16.7 (3.6)	16.5 (2.4)	16.5 (4.8)	17.4 (4.3)
Crown projection area *cpa*	m^2	33.4 (26.6)	39.0 (33.1)	16.6 (5.8)	18.0 (2.6)

1) Climate reference period 1988–2017.
2) Data from the survey in 2014, mean (±SE)

Q2 How does severe drought stress affect crown characteristics (*cpa*, transparency, roughness)?

Q3 How does the interaction of severe drought stress and competition affect tree allometry ($d_{1.3}$, *cpa*)?

2. Material and methods

2.1. Material

The experimental plot Kranzberger Forst (FRE 813/1) with a size of 0.5 ha is located in the southern part of Bavaria, approximately 35 km northeast of Munich. On this site, the "Kranzberg Roof Project" ("KROOF") was initiated in spring 2013 (Pretzsch et al. 2014). Table 1 summarises relevant site and plot characteristics.

The plot was specially selected for the KROOF experiment (Pretzsch et al. 2014). The mixed stand consists of European beech and Norway spruce, was never thinned and is fully stocked. Both tree species share the same soil resources and form a common closed canopy. Within the site, large groups of beech grow surrounded by spruce. In 2014, tree age within the mixed stand was assessed to be 63 ± 2 years for spruce and 83 ± 4 years for beech (Pretzsch et al. 2016). The conditions such as growth stage, stand density, basal area, or stem volume of mono-specific spruce, monospecific beech, and beech/spruce mixture are similar across the control and treatment plots each (Pretzsch et al. 2014).

In 2013, the experimental area was subdivided into six groups that were not roofed ("Control") and six groups that were roofed ("Treatment"). Each plot had four to six beech trees on one side and the same number of spruce trees on the opposite side, enabling a broad contact zone in between the two. Plot sizes ranged between 110 m^2 and 200 m^2, amounting to 868 m^2 and 862 m^2 in total for control and drought treatments, respectively (Pretzsch et al. 2016). On treatment plots, special houses were installed underneath the canopy three metres above the ground. The roof of each house automatically closes during rainfall. During the construction process, the forest floor was covered with wooden pallets, to avoid compaction of the soil from construction work (Grams et al. 2020). Vegetation cover at the forest floor was almost entirely absent due to the high density of the tree crowns. Each roof extends approximately 40 cm beyond the borders of the treatment plots to prevent throughfall (Grams et al. 2020). The novelty of the roof construction is the automated closure during rain by means of water impermeable, tile-composed roller blinds, which are electrically motorised (Pretzsch et al. 2014). The roof-intercepted quantities of water are channelled out of the study site. This design prevents a greenhouse effect when there is no rain. The stationary portions of the roof are secured around individual trees and permanently closed. Stem flow is negated via perforation hoses encircling each tree stem above the roof, and the thus-collected water directed to the roof gutters (Grams et al. 2020). All rain that is held off is transported off the experimental site via plastic hoses attached to gutters at each side of the roofs. Additionally, the roofed plots are hydraulically isolated to avoid lateral soil water access. Hence, a durable cover, preventing penetration by water or roots, is placed in the dug trenches around the roofed plots. In 2010, the 12 experimental plots were trenched to 1 m soil depth, where the layer of sandy loam hardly allows deeper root growth. As such preparation causes root injury, trenching was performed four years before the actual beginning of the drought experiment (Pretzsch et al. 2016). It was possible to concentrate on the effects of experimentally induced drought without the interference of other limiting factors, due to the good water and nutrient supply along with the high-water storage capacity of the soil. The drought phase of the KROOF experiment started in March 2014 and continued until November 2018. During this phase, the roofs were automatically closed during rainfall in the growing season and on average withheld 69 ± 7% of the annual rainfall (Grams et al. 2020). The water was kept away in summer, whilst in winter the forest ecosystem of the treated plots was allowed to recover.

An overview of classical growth and yield related variables of all scanned sample trees is provided in Table 1. More detailed information on the experimental design can be found in Pretzsch et al. (2014), Goisser et al. (2016) and Grams et al. (2020).

2.2. Methods

2.2.1. Scan acquisition

In winter 2012/2013, before the start of the drought stress experiment, terrestrial laser scanning (TLS) was carried out and repeated in the winter of 2018/2019. Using the TLS-point clouds from the two surveys, structural tree modifications within the six-year period were directly visualised, computed and linked to water limitation. Two different laser-scanning systems were used for the two surveys: RIEGL LMS-Z420i (RIEGL 2010) for the winter of 2012/2013 and RIEGL VZ-400i (RIEGL 2019) for the winter of 2018/2019. A detailed description of the scan acquisition can be found in the appendix.

2.2.2. Tree characteristics

Several tree characteristics, describing both stem and crown properties, were extracted from the TLS data. Only the measurements for $d_{1.3}$

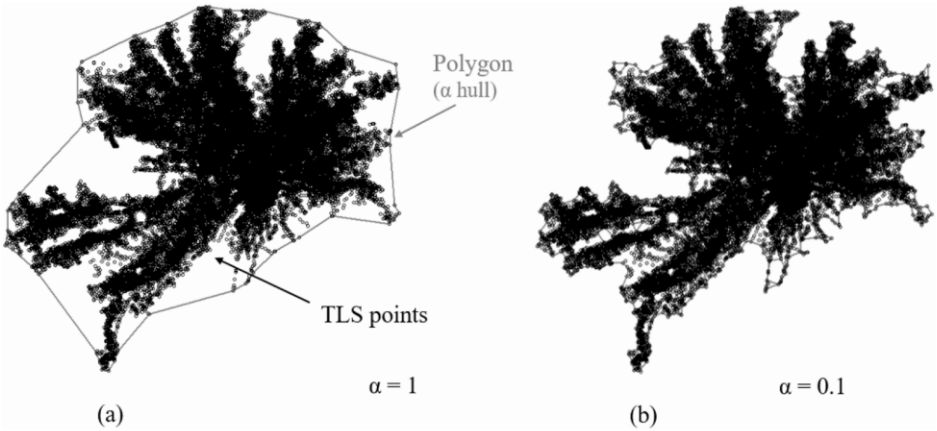

Fig. 1. Top view of tree number 89, by way of illustration of the different methods for calculating the crown projection area within the R package "alphahull". Choosing an α-value of 1 (a), a projection area similar to the traditional crown projection area was derived. Choosing an α-value of 0.1 (b), the polygon framed the crown tightly. The crown transparency was calculated based on both crown projection areas.

were taken manually with a girth tape. The isolation of the single tree from the TLS point cloud was performed using a pre-processing algorithm within the R programming environment (R Core Team 2016). After this step, each tree was visually checked for completeness. If necessary, unrecognised tree parts were added manually, and artefacts, not belonging to the tree, removed using the software RiSCAN PRO version 2.0.2 (http://www.riegl.com/products/software-packages/riscan-pro/).

Stem properties – diameter, height and taper

The diameter at breast height $d_{1.3}$ was measured for all trees, using a girth tape, in the winter of 2012/2013 and winter of 2018/2019. The periodic annual diameter increment ($pai_{d1.3}$ in cm yr^{-1}) was calculated as the difference between the two dates divided by the time range of six years. Based on the TLS data, tree height was calculated as the difference between the highest and lowest Z-axis point of the isolated tree. The periodic annual height increment (pai_{height} in m yr^{-1}) was computed as the difference between the heights from the two consecutive surveys, divided by six years. Generally, taper is the diameter change per unit of length. Modern log measurement systems determine the taper as the slope of a linear regression between different diameters and their axial positions (ÖNORM L 1021 2013). The procedure applied here was as follows: Firstly, the stem was isolated from the TLS-data using the method developed in Jacobs et al. (2020). Secondly, the stem was separated into 0.1 m intervals, from 1.3 m to 10.0 m. Thirdly, within this stem section, the taper was calculated as the slope of the linear regression between diameter and axial position. Finally, the periodic annual taper change (pac_{taper} in mm m^{-1} yr^{-1}) was the difference between the taper in the winter of 2012/2013 and in the winter of 2018/2019, divided by six years.

Crown properties – projection area, transparency and roughness

Based on the point clouds from TLS scanning, the crown properties were calculated using the R package "alphahull"(Rodriguez-Casal and Pateiro-Lopez 2019). This package enabled the determination of the area and bordering line of a sample of points in a plane and was succesfully used to analyse the crown structure (Rais et al. 2020). By varying the α-value, the tightness of the bordering line around the point cloud could be adjusted. Very low α-values even recognise areas without any points in the middle of a two-dimensional point set.

Choosing an α-value of 1, the TLS points were framed with a slack polygon (Fig. 1a). The area inside this polygon was used as a proxy to the crown projection area ($cpa_{tradition}$), which closely resembles the traditional crown projection area that is recorded in the field from the ground. Subtracting the two subsequent crown projection areas from each other and then dividing the difference by six years, we obtained the periodic annual change of the crown projection area (pac_{cpa} in m^2 yr^{-1}). Without claiming to have calculated the actual $cpa_{tradition}$, it was important to choose the same alpha values for the scans of winter 2012/13 and winter 2018/19, to ensure the comparability of the two measurements (*ceteris paribus* conditions).

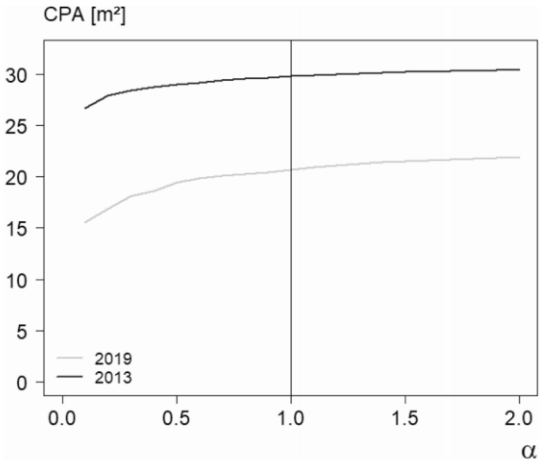

Fig. 2. Comparison of different α-values for α hulls determining the *cpa* of tree number 89.

The crown projection area (Fig. 1a) also served to assess the crown transparency. For this, a polygon was created surrounding the two-dimensional point cloud per tree, choosing an α-value of 0.1. Consequently, the polygon fitted tightly to the points (Fig. 1b). The resulting area of the tight polygon (Fig. 3) was normalised by the $cpa_{tradition}$ first and then subtracted by 1. Analogous to the previous definitions, the difference in the crown transparencies on two different dates were divided by six years to obtain the periodic annual change in crown transparency ($pac_{transparency}$ in % yr^{-1}). The calculated crown transparency is not the replication of the conventionally calculated parameter (Müller and Stierlin 1990). Our calculation is based on the two-dimensional top view perspective whereas the conventional crown transparency is estimated based on lateral perspectives.

The tight polygon (α = 0.1, Fig. 1b) can be used not only for the

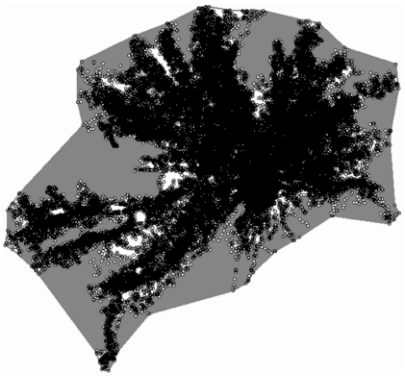

Fig. 3. Two-dimensional bird's-eye view of a Norway spruce tree number 89 scanned with TLS in winter 2012/13. The grey area shows what we considered to be the transparent parts of the crown projection area.

derivation of an area, but also of the polygon length to determine the crown roughness. To eliminate the size effect, we first calculated the perimeter of a circle, which had the same area as the polygon of $cpa_{tradition}$ (α = 1, Fig. 1a). The perimeter of the tight polygon (α = 0.1, Fig. 1b) was finally divided by the perimeter of the circle (Eq. (1)). By analogy with the previous definitions, the difference in the crown roughness on two different dates was divided by six years, to obtain the periodic annual change of crown roughness ($pac_{roughness}$ in % yr^{-1}).

$$pac_{roughness} = \frac{\left(\frac{P_{length_{cpaα0.1}}}{2*\sqrt{cpa_{traditionα1}*\pi}}\right)_{2018/19} - \left(\frac{P_{length_{cpaα0.1}}}{2*\sqrt{cpa_{traditionα1}*\pi}}\right)_{2012/13}}{6} \quad (1)$$

$pac_{roughness}$ = periodic annual change of crown roughness
P = Polygon
cpa = crown projection area
α = alpha-values

The cpa varies with different α-values but at value 1 the difference in cpa between the two measurements was stable (Fig. 2).

Finally, we looked at the investment pattern between stem and crown. The allometry exponent β of the allometric Eq. (2) was determined. The slope β indicated the change in cpa at the growth rate of the $d_{1.3}$ (von Bertalanffy 1951). If β > 1, a positive allometry is present, where cpa changes more than $d_{1.3}$. Vice versa, with negative allometry (β < 1), $d_{1.3}$ changes more than cpa. Isometry prevails if the initial proportions remain constant over time (Pretzsch 2001)

$$\ln(cpa) = t + \beta_{cpa,d1.3} \times \ln(d_{1.3}) \quad (2)$$

cpa = crown projection area
$d_{1.3}$ = diameter at breast height
t = offset
$\beta_{cpa,d1.3}$ = allometry exponent

Competition

The competition was expressed by the index introduced by Hegyi (1974), using Eq. (3). The original Hegyi-index forms the ratio between the diameters of neighbouring trees and the reference tree, considering concurrently the distance from all the competitors. The spatial positions of all trees were taken from the terrestrial laser scans.

$$HgCI_i = \sum_{j=1}^{n} \frac{d_{1.3j}}{d_{1.3i}} \frac{1}{Dist_{ij}} \quad (3)$$

In this formula$HgCI_i$ is the competitor index for reference tree i, $d_{1.3j}$ is the $d_{1.3}$of competitor tree j (cm),$d_{1.3i}$ the $d_{1.3}$of reference tree (cm),$Dist_{ij}$ the distance between reference tree i and competitor tree j (m), and n the number of competitor trees.

The competition zone radius (CZR) proposed by Lee and von Gadow (1997), defined as the radius in which competitors were searched around the reference tree (Eq. (4)), is a function of the number of trees per hectare (N), and was determined only once, so that the radius was the same for every investigated tree. The competition zone of border trees was mostly outside the plot in relative size. To counteract this problem, we extrapolated the calculated competition for the partial area inside the plot to the total area of the competition zone.

$$CZR = k*\sqrt{\frac{10000}{N}} \quad (4)$$

The variable k is a constant defining the radius of the competition zone ($2 < k < 4$) and N the number of trees per hectare (Lee and von Gadow 1997).

Table 2
LMM Functions regarding **Q1**, **Q2** and **Q3**. The $pai_{d1.3}$ (cm yr^{-1}) is the periodic annual diameter at breast height increment, pai_{height} (m yr^{-1}) is the periodic annual total tree height increment, pac_{taper} (yr^{-1}) the periodic annual change of taper, pac_{cpa} (m^2 yr^{-1}) the periodic annual change of crown projection area, $pac_{transparency}$ (% yr^{-1}) the periodic annual change of crown transparency, $pac_{roughness}$ (% yr^{-1}) the periodic annual change of crown roughness, $\beta_{cpa,d1.3}$ the tree allometry exponent.

	Response variable	Linear predictors	Interaction effects	Function
Q1:	$pai_{d1.3}$			(5)
	pai_{height}			(6)
	pac_{taper}	Species	Drought	(7)
Q2:	pac_{cpa}	Drought	Competition	(8)
	$pac_{transparency}$	Competition		(9)
	$pac_{roughness}$			(10)
Q3	$\beta_{cpa,d1.3}$			(11)

2.2.3. Evaluation

T-test

To visualise possible differences between control and treatment plots regarding drought stress, we created boxplots for all analysed parameters. A t-test was used to determine whether there is a significant difference between the means of the two groups: The control group (no water limitation) and the treatment group (water limitation).

Mixed effect regression model

The data was nested at the group level, which means that there were several trees in one group. Therefore, a mixed effect regression model with random effects at plot level was required. We started with a complex model using a generalized mixed-effects model (GAMM) with smoother expecting a non-linear relationship between the interaction of drought and competition. Instead, the relationship turned out to be linear. Thus, we used a linear mixed-effects model (LMM). We formulated seven LMM functions to answer **Q1** regarding the stem property parameters (Function 5 to 7), **Q2** regarding crown property parameters (Function 8 to 10) and **Q3** regarding their allometry exponent (Function 11). All parameters were set as response variables to analyse the effects of species, drought, competition and the interaction effects between competition and drought (Table 2). All models explain the response variable as a function of different linear predictors like drought, species and competition. Here is the general structure of the model we used for all LMM functions:

$$Y_{ij} = a_0 + a_1*X_{1,i} + a_2*X_{2,j} + a_3*X_{3,j} + a_4*X_{2,ij}*X_{3,ij} + b_j + \varepsilon_{ij}$$

Throughout each model, the variable Y is the response variable, the variables $X_1 \ldots X_3$ (X_1 = Species, X_2 = Drought and X_3 = Competition) are the linear predictors, the variable i indexes the tree, and the variable j the plot. The variable a_o represents the model's intercept, the variables $a_1 \ldots a_4$ represent the slope coefficients, the variable b represents the random effect related to the plots and the symbol ε represents the

Table 3
Overview of *t*-test statistics. Mean, standard deviation (in brackets) and p-value are given. The $pai_{d1.3}$ (cm yr^{-1}) is the periodic annual diameter at breast height increment, pai_{height} (m yr^{-1}) is the periodic annual total tree height increment, pac_{taper} (mm m^{-1} yr^{-1}) the periodic annual change of taper, pac_{cpa} (m^2 yr^{-1}) the periodic annual change of crown projection area, $pac_{transparency}$ (% yr^{-1}) the periodic annual change of crown transparency, $pac_{roughness}$ (% yr^{-1}) the periodic annual change of crown roughness, $\beta_{cpa,d1.3}$ the tree allometry exponent.

	European beech			Norway spruce		
	Control	Treatment	p-value	Control	Treatment	p-value
$pai_{d1.3}$	0.22 (0.16)	0.11 (0.08)	**0.049**	0.26 (0.13)	0.14 (0.08)	**0.011**
pai_{height}	0.36 (0.09)	0.19 (0.08)	**0.000**	0.25 (0.12)	0.16 (0.04)	**0.019**
pac_{taper}	−0.05 (0.04)	−0.07 (0.07)	0.472	−0.06 (0.05)	−0.1 (0.14)	0.560
pac_{cpa}	0.62 (0.53)	−0.42 (0.52)	**0.000**	0.17 (0.29)	−0.74 (0.51)	**0.000**
$pac_{transparency}$	0.7 (1.02)	1.27 (0.95)	0.168	0.55 (0.92)	1.67 (0.89)	**0.008**
$pac_{roughness}$	6.18 (7)	13.61 (15)	0.154	2.11 (4.2)	6.35 (3.68)	**0.018**
$\beta_{cpa,d1.3}$	4.26 (25.3)	−10.0 (16.8)	0.113	−0.06 (5.5)	−15.68 (11.4)	**0.002**
Trees per group and species	13	11		13	10	

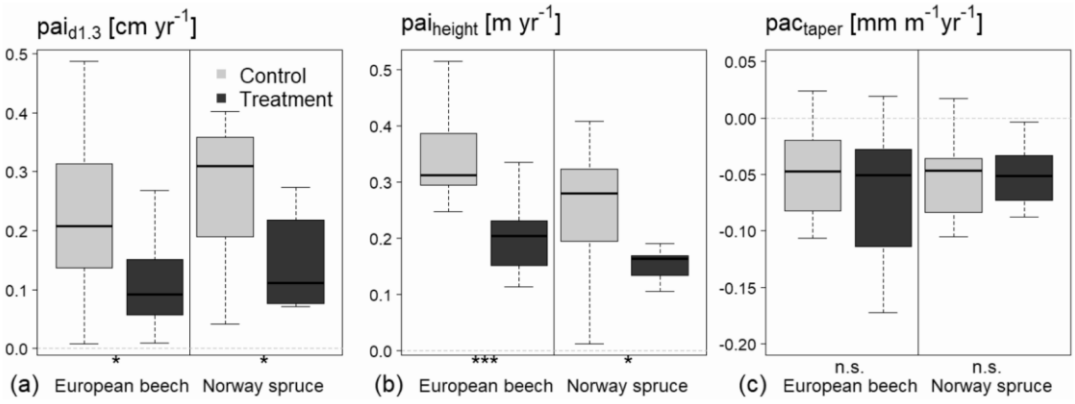

Fig. 4. Effects of drought stress on stem properties **Q1**, (a) $pai_{d1.3}$ periodic annual $d_{1.3}$ increment in cm yr^{-1}, (b) pai_{height} periodic annual height increment in m yr^{-1}, (c) pac_{taper} periodic annual change of taper in mm m^{-1} yr^{-1}, yr is the year. Significance values: '***' $p < 0.001$, '**' $p < 0.01$, '*' $p < 0.05$, 'n.s.' not significant.

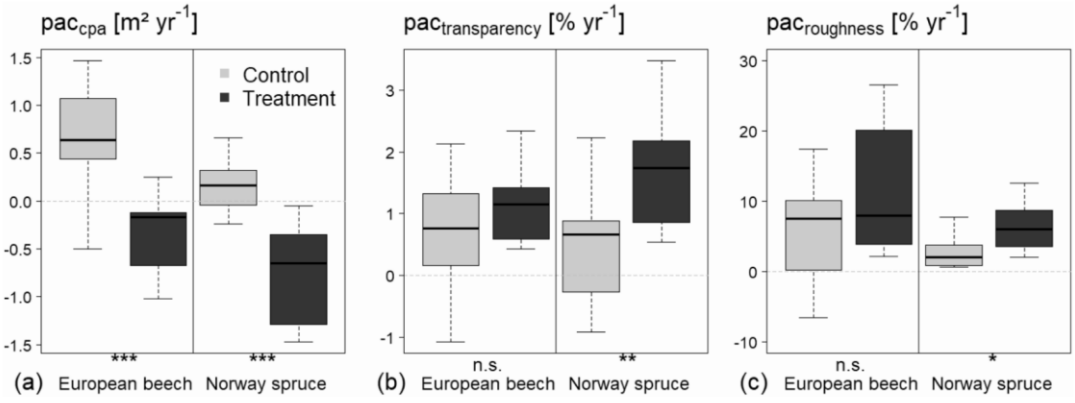

Fig. 5. Effects of drought stress on crown properties **Q2**, (a) pac_{cpa} the periodic annual change of *cpa* in m^2 yr^{-1}, (b) $pac_{transparency}$ the periodic annual change of crown transparency in % yr^{-1}, (c) $pac_{roughness}$ the periodic annual change of crown roughness in % yr^{-1}. The variable *cpa* is the crown projection area (m^2) and yr is year. Significance values: '***' $p < 0.001$, '**' $p < 0.01$, '*' $p < 0.05$, 'n.s.' not significant.

remaining errors.

Whether the *t*-test or the mixed effect regression model, the significance level for our tests is considered statistically significant when the p-value was lower than 5%. The processing was performed within the programming environment of R (R Core Team 2016). The R packages used for the evaluation were stats and graphics, which are both part of R (R Core Team 2016). Zuur et al. (2009) described the technical details (mgcv package (Wood 2017)).

3. Results

An Overview of the *t*-test statistics is provided in Table 3.
The $pai_{d1.3}$ and pai_{height} differ between control and treatment for both tree species (Fig. 4ab, Table 3). In contrast to the control trees, which show growth in $pai_{d1.3}$ of 0.26 cm yr^{-1} for spruce and 0.22 cm yr^{-1} for beech, the treated trees have a lower growth of 0.14 cm yr^{-1} for spruce and 0.11 cm yr^{-1} for beech (Table 3). The pai_{height} of the control trees is

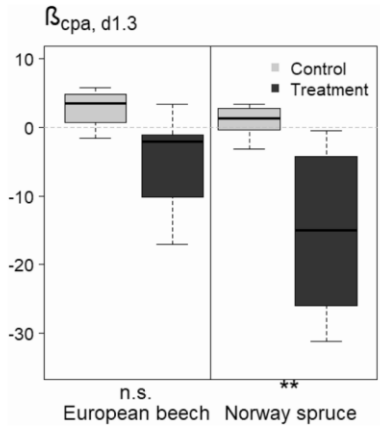

Fig. 6. Effects of drought stress on the allometry exponent $\beta_{cpa,d1.3}$ **Q3**. Significance values: '***' $p < 0.001$, '**' $p < 0.01$, '*' $p < 0.05$, 'n.s.' not significant.

0.25 m yr^{-1} for spruce and 0.36 m yr^{-1} for beech, while the treated spruces (0.16 m yr^{-1}) and beeches (0.19 m yr^{-1}) had lower growth (Table 3).

The pac_{taper} (Fig. 4c, Table 3) does not differ between control and treatment. In contrast to the control trees, which show taper on average by −0.063 mm m^{-1} yr^{-1} for spruce and −0.049 mm m^{-1} yr^{-1} for beech, the taper of the treated trees decreased on average by −0.095 mm m^{-1} yr^{-1} and −0.07 mm m^{-1} yr^{-1} respectively (Table 3).

The crown properties pac_{cpa}, $pac_{transparency}$ and $pac_{roughness}$ are affected by drought stress especially for spruce (Fig. 5abc, Table 3). The crown property pac_{cpa} differs highly significant between control and treatment for both tree species (Fig. 5a, Table 3). The control trees showed growth in pac_{cpa} by 0.17 m^2 yr^{-1} for spruce and 0.62 m^2 yr^{-1} for beech, while the pac_{cpa} of the treated trees changed by −0.74 m^2 yr^{-1} for spruce and −0.42 m^2 yr^{-1} for beech (Table 3).

The $pac_{transparency}$ (Fig. 5b, Table 3) and $pac_{roughness}$ (Fig. 5c, Table 3) differ between control and treatment only for Norway spruce trees. In contrast to the control trees, which show an increment in $pac_{transparency}$ of 0.55% yr^{-1} for spruce and 0.7% yr^{-1} for beech, the $pac_{transparency}$ of the treated trees increased by 1.67% yr^{-1} for spruce and 1.27% yr^{-1} for beech (Table 3). The $pac_{roughness}$ increased by 2.11% yr^{-1} for spruce and 6.18% yr^{-1} for beech, while the $pac_{roughness}$ of the treated trees increased by 6.35% yr^{-1} for spruce and 13.61% yr^{-1} for beech (Table 3).

The allometry exponent $\beta_{cpa,d1.3}$ changed under drought stress (Fig. 6, Table 3). The trend towards crown shrinking and lower growth under drought stress was seen in both tree species (Table 3). Whereas spruce changed its investment behaviour significantly under drought stress, the beech trees experienced the same trend, but the investment behaviour did not change.

Regarding **Q1** and **Q2**, it can be observed that despite random effects on plot level, drought stress affected pai_{height}, pac_{cpa} and $pac_{roughness}$ regardless of the tree species (Table 5, Function 6, 8 and 10), which is demonstrated by the estimate values of −0.14, −1.43 and + 15.9 for treated trees respectively. Furthermore regarding **Q3**, the local competition had an effect on the $pai_{d1.3}$ and pac_{cpa} of the control trees (Table 4, Function 5 and 8), which is shown by the estimate values of −0.07 and −0.27 if competition increases by one unit respectively. The lower the competition, the higher was the growth in cpa and $d_{1.3}$ for the control trees. The $pac_{roughness}$ is the only parameter that is affected by local competition under drought stress, which is demonstrated by the estimate value of −9.5 for treated trees if competition increases by one unit. The lower the competition, the higher the roughness of the crowns for trees under drought stress, and vice versa. In terms of species, the variables pai_{height}, pac_{cpa} and $pac_{roughness}$ differ (Table 5 Function 6, 8 and 10), which is demonstrated by the estimate values of + 0.10, +0.52 and + 7.73 respectively for beech trees.

4. Discussion

Drought stress led to a significantly smaller crown size as well as a lower stem and height growth. In addition, high competition combined with drought stress resulted in crowns that were less rough and thus more compact.

4.1. Tree shape modified by drought

Our results cannot prove an effect of drought stress on the stem form. Only a trend towards cylindrical stem forms occurred (Table 4, Function 7). Sohn et al. (2012) also did not find a combined effect of both drought and competition on radial growth along the stem. Our study showed that lower competition might have the potential to improve growth performance of trees in response to drought if the whole stem is considered (Table 4, Function 7). One reason for the non-significance may be the short time period or the small sample size (N = 47) of our study. Consequently, (relative) differences were probably reduced between roofed and control plots. Due to the low model performance (R^2), drought, species and local competition may not be the only root causes of the observed stem-form differences (Table 4, Function 7).

Table 4
LMM statistics for **Q1**, **Q2** and **Q3**. Estimates and significance values are given. The $pai_{d1.3}$ (cm yr^{-1}) is the periodic annual diameter at breast height increment, pai_{height} (m yr^{-1}) is the periodic annual total tree height increment, pac_{taper} (mm m^{-1} yr^{-1}) the periodic annual change of taper, pac_{cpa} (m^2 yr^{-1}) the periodic annual change of crown projection area, $pac_{transparency}$ (% yr^{-1}) the periodic annual change of crown transparency, $pac_{roughness}$ (% yr^{-1}) the periodic annual change of crown roughness, $\beta_{cpa,d1.3}$ the tree allometry exponent. Competition is the local index by Hegyi (1974). Within a given category of drought (control vs. treatment) and species (Norway spruce vs European beech), numbers within the same column are significantly different at the 0.05 probability level if they are different in all letters (a and b); linear mixed-effects model; R^2 (adjusted) is the coefficient of multiple determination; all significance values and trends were bold: **'***' $p < 0.001$, '**' $p < 0.01$, '*' $p < 0.05$.**

Function	(5)	(6)	(7)	(8)	(9)	(10)	(11)
Response variable	$pai_{d1.3}$	pai_{height}	pai_{taper}	pac_{cpa}	$pac_{transparency}$	$pac_{roughness}$	$B_{cpa,d1.3}$
Intercept	**+0.34*** **	**+0.29*** **	**−0.07***	**+0.55****	+0.58	+2.01	+6.63
Species							
Norway spruce	-a	-a	-a	-a	-a	-a	-a
European beech	+0.01b	**+0.10b****	+0.04b	**+0.52b*****	−0.08b	**+7.73b****	+7.7b
Drought							
Control	-a	-a	-a	-a	-a	-a	-a
Treatment	−0.12b	**−0.14b***	−0.06b	**−1.43b****	+1.2b	**+15.9b***	−21.57b
Competition	**−0.07****	−0.03	−0.005	**−0.27****	+0.05	−1.16	−5.47
Drought:Competition							
Control	-a	-a	-a	-a	-a	-a	-a
Treatment	−0.02b	−0.003b	−0.08b	+0.3b	−0.3b	**−9.5b***	+3.74
R^2 (adjusted)	0.33	0.43	−0.03	0.61	0.1	0.25	0.16

The height growth was affected by drought stress for each individual tree species and was lower in comparison to the control trees (Fig. 4b). In Table 4 (Function 6), the height growth was affected by drought, which is demonstrated by the estimate value of −0.14 for all treated trees. For the Douglas fir, height growth response to drought stress was observed to be an even more sensitive indicator than basal area (Rais et al. 2014). In the past, only a few drought related studies have focused on the height growth of mature trees, as the accurate measurement of height increments requires the felling of trees (Hasenauer and Monserud 1997). As well as the technical issue concerning measuring, the height growth of most species is a complex multi-seasonal process from an ecophysiological point of view (Bréda et al. 2006). Due to the observation of the experiment over six years and computing the annual mean increment, this difficulty was likely averaged out.

Drought stress led to a significantly smaller crown size for each individual tree species (Fig. 5a). In Table 4 (Function 5), this is demonstrated by the estimate value of −1.43 for all treated trees. The crowns of Norway spruce trees also increased in transparency and roughness on the treatment plots (Fig. 5bc). The TLS scans were performed after the vegetation period and thus beech trees had no leaves. The lower crown transparency for beech trees could only have arisen from a loss of branches. Overall, almost all trees become more transparent, with trees under drought stress showing crowns that are more transparent (Fig. 5b). This could be related to actual drought years such as 2015, when control trees also suffered from drought stress.

4.2. Acclimatisation strategies to deal with drought stress and competition

The impact of drought on the crown has been critically discussed and assumptions regarding all strategies vis-à-vis drought were summarised in the review by (Bréda et al. 2006). These potential acclimatisation strategies were cavitation and cladoptosis. Due to drought-induced branch die-off, fewer branches lose water through transpiration, which enables the remaining shoots to maintain a favourable water balance, although resulting in smaller and more transparent crowns (Rood et al. 2000). In addition to the die-off of branches, there is also the deliberate, active process of shedding branches (cladoptosis). This mechanism enables trees to adjust root-shoot ratios after drought-induced decline in root system extent and efficiency. Branch shedding and dying was observed for oak, birch and poplar (Rood et al. 2000; Rust and Roloff 2002). In both two hypotheses of acclimatisation strategies, crown size should get smaller due to drought stress. Our scans were performed in winter, when beech trees were free of foliage. Using the *cpa* as a rather simple crown attribute, we were able to prove significant crown shrinkage per year, which was observed over a time span of only six years. Hence, the fact that drought led not only to losses in needles, can be seen from the significantly smaller non-leaved crowns of beech trees. They may have suffered from drought stress and shed parts of their branches. The assumed effects of branch shedding and dying reached an extent that was measurable in terms of *cpa,* crown transparency and crown roughness using TLS. No other study has previously been able to confirm these results. The theories and assumptions about drought stress reactions (Bréda et al. 2006) have thereby been confirmed, and been clearly demonstrated by the use of TLS.

Trees that are experiencing low levels of competition tend to increase their crown width (Forrester et al. 2013). This is confirmed by our study for all trees (Table 4, Function 8), which is demonstrated by the estimate value of −0.23 if competition increases by one unit. During drought, the competition had no influence on the *cpa*, and this is also the case for the crown transparency (Table 4, Function 9). We assume that the control trees are mainly light-limited, and therefore react more strongly to above ground competition from neighbours than those trees that are water-limited due to water retention. The treatment trees are more water- than light-limited. We hypothesise that the crown properties *cpa*, transparency and roughness are linked to each other when analysing the interaction effects of drought and competition. Therefore, trees suffering from drought stress and high competition reduced their already small crown dimensions to the lowest possible size at which they could efficiently survive. Roughness and transparency decrease as a follow-on effect of smaller and more compact crowns. This contrasts with the increasing roughness and transparency of trees under drought stress without competition. Due to this contrast, the crown properties roughness and transparency are not the ideal variables for detecting drought stress alone. In comparison, *cpa* reacted more strongly to drought, and should represent a good indicator for tree-vitality monitoring.

4.3. Conclusions for monitoring and research

In the past, crown attributes have proven difficult to measure. TLS is proved to be a powerful tool for measuring physical crown dimensions and to be more reliable than conventional field methods (Seidel et al. 2015). Trees do not have to be cut and manual time-consuming and costly surveys can be avoided. So far, the effects of drought stress have been based on visual observation from the ground or the laborious collection of broken branches and leaves (Rust and Roloff 2002). This study demonstrated that iterative TLS surveys may enhance the information gathered during measuring campaigns on common long-term experimental plots by obtaining a more thorough picture of growth patterns due to climate change or management plans. Crown size is an important factor which is closely related to light absorption and productivity (Binkley et al. 2013). Such accurate data of tree-crown dimensions are also essential for tree-growth modelling (Poschenrieder et al. 2016).

The presented tree vitality indicators obtained by TLS were not evaluated against a reference although they may include errors. Wang et al. (2019) reported for instance that TLS underestimated height of big trees, which may be due to occlusion of crown and stem parts. The occlusion problem might be mainly resolved choosing a sufficient of different scan positions. On the other side, TLS height measurements on Norway spruce trees in forests stands that covered a broad density range were found to be more accurate than common height measurements with the Vertex, a hand-held device based on the trigonometrical principle (Jacobs et al. 2020). Regarding crown dimensions, it may be more complex to find a suitable reference. Seidel et al. (2015) showed that crown attributes obtained from TLS were more closely related to preceding tree growth than those measured in the field. The question what should be used as a direct reference for abstract parameters such as crown transparency or roughness remains. What highlights the TLS measurements in comparison to the conventional measurement of *cpa*, transparency and roughness is the purely rational procedure without subjective influence. Still, tree-vitality monitoring could be developed towards more quantitative methods by application of TLS as traditional recording of crown transparency in the field has some disadvantages. Crown transparency is not directly measurable and must instead be carried out by well-trained field experts. Despite the photo comparison with reference images, there is a risk of systematic or random observer deviations, which require intensive training and standardisation exercises (Dobbertin et al. 2009). In addition, crown thinning is not cause-specific, i.e. different reasons cause similarly high crown transparency, for example insect damages. Further, it is also not clear whether the crown transparency of a tree is the result of a loss of vitality, or whether the tree is possibly recovering from stress. Reference values are therefore required to classify the characteristic. Roughness, on the other hand, represents a TLS developed indicator that could be considered in future

research. Tree vitality indicators should not be evaluated individually, as this can easily lead to misinterpretation (Dobbertin et al. 2009). The development of new indicators based on TLS enables to analyse several indicators and evaluate them together. In this study, we showed that TLS could be appropriate for measuring crown transparency and roughness of tree crowns. Taking into account not only one but also several tree vitality indicators, all of them going in the same direction, may confirm the influence of drought on tree properties (Dobbertin et al. 2009).

Furthermore, drought stress effects on trees could have an impact on the results of the modern and rapid estimation approach of estimating the diameter at breast height using the crown diameter computed by drone data (UAV). The significant smaller *cpa*, due to drought stress could lead to errors when estimating the crown-diameter-based $d_{1.3}$ measured from above using UAV. Thus, $d_{1.3}$ would be underestimated. This is made clear in Fig. 6, which shows the calculated allometry coefficient regarding *cpa* and $d_{1.3}$. It demonstrates how drastically the investment behaviour of the tree can change under drought stress. The control trees showed a positive allometry ($\beta > 1$), where *cpa* grows more than $d_{1.3}$. Vice versa, the treated trees, suffering under drought, had a negative allometry ($\beta < 0$). Here $d_{1.3}$ grows while the *cpa* shrinks. Crown shapes may change due to the impacts of climate change. Therefore, crown models within tree growth models must be questioned, as must the derived allometries. The higher frequency of extreme and extensive drought events (IPCC 2012) makes it even more important to consider drought stress effects in forest practice and ecological modelling. This is particularly true for the analysis of crowns, because of their spontaneous reaction to environmental and neighbouring changes.

5. Conclusion

TLS can offer new opportunities in identifying structural features in trees to measure and analyse indicators of tree vitality. Based on changes in tree shape parameters, TLS has the potential to be a rational and suitable tool for capturing indicators to evaluate the condition of a forest. We demonstrated that iterative TLS surveys might improve the measuring campaigns on common long-term experimental plots, in order to obtain a thorough picture of tree-vitality monitoring. The unique experiment "KROOF" combined with the TLS made it possible to get unique results about drought impacts on tree shape.

CRediT authorship contribution statement

Martin Jacobs: Conceptualization, Data curation, Formal analysis, Investigation, Methodology, Resources, Software, Validation, Visualization, Writing - original draft, Writing - review & editing. **Andreas Rais:** Supervision, Conceptualization, Methodology, Visualization, Writing - original draft, Writing - review & editing. **Hans Pretzsch:** Supervision, Conceptualization, Methodology, Resources, Writing - original draft, Writing - review & editing.

Declaration of Competing Interest

The authors declare that they have no known competing financial interests or personal relationships that could have appeared to influence the work reported in this paper.

Acknowledgements

We would like to thank Gerhard Schütze for all traditional measurements and the TLS data acquisition in the winter of 2012/2013.

Funding

This research did not receive any specific grant from funding agencies in the public, commercial, or not-for-profit sectors.

Appendix A

Table A1
Overview of both scanners, RIEGL LMS-Z420i (RIEGL 2010) and RIEGL VZ-400i (RIEGL 2019), summarising the main characteristics.

Laser Measurement System (LMS)		RIEGL Z420i	RIEGL VZ-400i
Range[1)]	m	1000	800
Effective measurement rate[2)]	meas./sec	11,000	500,000
Accuracy[3),4)]	mm	10	5
Precision[4),5)]	mm	4	3
Vertical field of view	°	80	100
Pulse mode		last-pulse	multiple target capability
Registration		artificial targets	automatic
Laser beam divergence	mrad[6)]	0.25	0.35

1) Typical values for average conditions. Maximum range is specified for flat targets with size in excess of the laser beam diameter, perpendicular angle of incidence, and for atmospheric visibility of 23 km. In bright sunlight, the max. range is shorter than under overcast sky.
2) Rounded values.
3) Accuracy is the degree of conformity of a measured quantity to its actual (true) value.
4) One sigma at 100 m range under RIEGL test conditions.
5) Precision, also called reproducibility or repeatability, is the degree to which further measurements show.
6) Measured at the $1/e^2$ points. 0.25/0.35 mrad corresponds to an increase of 25/35 mm of beam diameter.

A.1 Scan acquisition

Two different laser-scanning systems were used for the two surveys: RIEGL LMS-Z420i (RIEGL 2010) for winter 2012/2013 and RIEGL VZ-400i (RIEGL 2019) for winter 2018/2019. An overview of the two scanners, summarising the main characteristics, is provided in Table A1. For both dates, multiple scans were consecutively taken around the plots. In winter 2012/2013, two scans (horizontal and vertical) were performed for each scan position. The vertical and horizontal angular resolution was set to 0.05°, which in our practical experience, achieves a reasonable trade-off between scan-time and risk of disturbances due to tree movement through wind.

In the winter of 2018/2019, the resolution was chosen so that the scans were comparable to the TLS recordings in the winter of 2012/2013. Due to the angular measurement scheme of the scanners, which operate from the ground, the point density naturally decreases towards the top of the canopy. Furthermore, the laser beam is usually unable to penetrate tree compartments in order to perform measurements behind obstacles. These two effects result in rather sparse measurement densities in the upper crown and stem regions, especially if the crown parts near the scanner are dense (Hilker et al. 2010). Regarding the RIEGL LMS-Z420i, we attempted – with the RIEGL distance-measurement mode called "last-pulse" or "last-target" – to counteract these effects and record the deepest points within a footprint, thus gaining a higher proportion of returns from inner-crown regions compared to first-pulse mode. Utilising the pulsed time-of-flight method for laser range measurements, the RIEGL LMS VZ-400i enables the determination of the range to all targets a single laser pulse is interacting with ("multi-target capability"). Depending on the measurement program used, the maximum number of targets, which can be detected, varied (typically 4–15). In summary, the RIEGL LMS Z-420i in the last-target setting generates one deep point per laser beam, while the RIEGL LMS VZ-400i can generate 4–15 points per laser beam. Due to this difference of the two scanners, we did not focus on three-dimensional tree features. Instead, our crown target variables (*cpa*, transparency and roughness) were two-dimensional to take into account the ability of the newer

scanner to generate more points inside the crown space. This was done to exclude errors occurring in the three-dimensional analysis due to non-scanned areas of the upper crown region respectively. In winter 2012/13, artificial reference targets (reflectors) distributed in the scanned forest scenes enabled the co-registration of the scans. The data of all scan positions per plot were co-registered using the software RiSCAN PRO version 2.0.2 (http://www.riegl.com/products/software-packages/riscan-pro/). In winter 2018/19, the new automatic registration of the LMS VZ-400i was used so that artificial reference targets were no longer needed. Automatic registration and filtering were performed using the software RiSCAN PRO version 2.8.2. The entire point cloud was reduced using an octree to enable fast point-cloud processing without accuracy loss (Elseberg et al. 2013). This distributes the data evenly in space, whereby each cube with an edge length of 5 cm contains on average only one measuring point, which is set according to the centre of gravity of the original points in the cube. Both point clouds, from winter 2012/2013 and winter 2018/2019, were post-processed via the software Cloudcompare, using the fine registration feature to register both clouds in the same project coordinate system.

References

Anderegg, W.R.L., Kane, J.M., Anderegg, L.D.L., 2013. Consequences of widespread tree mortality triggered by drought and temperature stress. Nature Clim Change 3 (1), 30–36. https://doi.org/10.1038/nclimate1635.

von Bertalanffy, L. (Ed.), 1951. Theoretische Biologie: II, 2nd edn. A Francke AG (2), Bern.

Binkley, D., Campoe, O.C., Gspaltl, M., Forrester, D.I., 2013. Light absorption and use efficiency in forests. Why patterns differ for trees and stands. For. Ecol. Manage. 288, 5–13. https://doi.org/10.1016/j.foreco.2011.11.002.

BMEL - Bundesministerium für Ernährung und Landwirtschaft (2014): Forests In Germany - BWI - Selected Results of the Third National Forest Inventory, Berlin.

Bréda, N., Huc, R., Granier, A., Dreyer, E., 2006. Temperate forest trees and stands under severe drought. A review of ecophysiological responses, adaptation processes and long-term consequences. Ann. For. Sci. 63 (6), 625–644. https://doi.org/10.1051/forest:2006042.

Calders, K., Newnham, G., Burt, A., Murphy, S., Raumonen, P., Herold, M., Culvenor, D., et al. 2015. Nondestructive estimates of above-ground biomass using terrestrial laser scanning. Methods Ecol. Evol. 6, 2, 198–208. http://doi.org/10.1111/2041-210X.12301.

Dobbertin, M., Hug, C., Waldner, P., 2009. Kronenverlichtung, Sterberaten und Waldwachstum in Langzeitstudien – Welche Indikatoren beschreiben den Waldzustand am besten? In: Forum für Wissen, pp. 7–20.

Dobbertin, M., 2005. Tree growth as indicator of tree vitality and of tree reaction to environmental stress. A review. Eur. J. Forest Res. 124 (4), 319–333. https://doi.org/10.1007/s10342-005-0085-3.

Eilmann, B., Dobbertin, M., Rigling, A., 2013. Growth response of Scots pine with different crown transparency status to drought release. Ann. Forest Sci. 70 (7), 685–693. https://doi.org/10.1007/s13595-013-0310-z.

Elseberg, J., Borrmann, D., Nüchter, A., 2013. One billion points in the cloud – an octree for efficient processing of 3D laser scans. ISPRS J. Photogramm. Remote Sens. 76, 76–88. https://doi.org/10.1016/j.isprsjprs.2012.10.004.

Forrester, D.I., Collopy, J.J., Beadle, C.L., Baker, T.G., 2013. Effect of thinning, pruning and nitrogen fertiliser application on light interception and light-use efficiency in a young Eucalyptus nitens plantation. For. Ecol. Manage. 288, 21–30. https://doi.org/10.1016/j.foreco.2011.11.024.

Goisser, M., Geppert, U., Rötzer, T., Paya, A., Huber, A., Kerner, R., et al., 2016. Does belowground interaction with *Fagus sylvatica* increase drought susceptibility of photosynthesis and stem growth in *Picea abies*? For. Ecol. Manage. 375, 268–278. https://doi.org/10.1016/j.foreco.2016.05.032.

Grams, T., Hesse, B., Gebhardt, T., Weikl, F., Rötzer, T., Kovacs, B., Hikino, K., et al., 2020. The Kroof experiment - realization and efficacy of a recurrent drought experiment plus recovery in a beech/spruce forest. Submitted.

Griesbauer, H.P., Green, D.S., 2010. Regional and ecological patterns in interior Douglas-fir climate–growth relationships in British Columbia, Canada. Can. J. For. Res. 40 (2), 308–321. https://doi.org/10.1139/X09-197.

Hasenauer, H., Monserud, R.A., 1997. Biased predictions for tree height increment models developed from smoothed 'data'. Ecol. Model. 98 (1), 13–22.

Hegyi, F., 1974. A simulation model for managing jack-pine stands simulation. Royal Coll. For. Res. Notes, 30: pp. 74–90.

Hilker, T., van Leeuwen, M., Coops, N.C., Wulder, M.A., Newnham, G.J., Jupp, D.L.B., Culvenor, D.S., 2010. Comparing canopy metrics derived from terrestrial and airborne laser scanning in a Douglas-fir dominated forest stand. Trees 24 (5), 819–832. https://doi.org/10.1007/s00468-010-0452-7.

IPCC (2012): Managing the Risks of Extreme Events and Disasters to Advance Climate Change Adaptation. A Special Report of Working Groups I and II of the Intergovernmental Panel on Climate Change. In: Cambridge University Press, Cambridge, UK, and New York, NY, USA, 582 pp.

Jacobs, M., Rais, A., Pretzsch, H., 2020. Analysis of stand density effects on the stem form of Norway spruce trees and volume miscalculation by traditional form factor equations using terrestrial laser scanning (TLS). Can. J. For. Res. 50 (1), 51–64. https://doi.org/10.1139/cjfr-2019-0121.

Larson, P.R., 1963. Stem form development of forest trees. Forest Science, Monograph 5, 42.

Lee, W.K., von Gadow, K., 1997. Iterative bestimmung der konkurrenzbäume in Pinus densiflora beständen. Allgemeine Forst- und Jagdzeitung 168 (3–4), 41–45.

Mäkinen, H., 1998. The suitability of height and radial increment variation in *Pinus sylvestris* (L.) for expressing environmental signals. For. Ecol. Manage. (112), 191–197.

McDowell, N.G., Sevanto, S., 2010. The mechanisms of carbon starvation: how, when, or does it even occur at all? New Phytol. 186, 264–266. https://doi.org/10.1111/j.1469-8137.2010.03232.x.

Mette, T., Falk, W., Uhl, E., Biber, P., Pretzsch, H., 2015. Increment allocation along the stem axis of dominant and suppressed trees in reaction to drought. - results from 123 stem analyses of Norway spruce, Scots pine and European beech. Austrian J. For. Sci. 4, 185–254.

Müller, E., Stierlin, H.R., 1990. Sanasilva-Kronenbilder mit Nadel- und Blattverlustprozenten. 2. erweiterte Auflage. Birmensdorf: Eidgenössische Forschungsanstalt für Wald, Schnee und Landschaft. p. 129.

Poschenrieder, W., Van de Kuilen, J.W.G., Pretzsch, H., et al., 2016. Modelling sawn timber volume and strength development at the individual tree level - essential model features by the example of Douglas fir. Silva Fennica 50(1), 1–25. https://doi.org/10.14214/sf.1393.

Pretzsch, H.; Ammer, C.; Wolf, B.; Steckel, M.; Rukh, S.; Heym, M. (2020a): Zuwachsniveau, Zuwachstrend und episodische Zuwachseinbrüche. Ein zusammenfassendes Bild vom aktuellen Zuwachsgang in Rein- und Mischbeständen aus Fichte, Kiefer, Buche und Eiche. In: AFJZ.

Pretzsch, H., Bauerle, T., Häberle, K.H., Matyssek, R., Schütze, G., Rötzer, T., 2016. Tree diameter growth after root trenching in a mature mixed stand of Norway spruce (*Picea abies* [L.] Karst) and European beech (*Fagus sylvatica* [L.]). Trees 30 (5), 1761–1773. https://doi.org/10.1007/s00468-016-1406-5.

Pretzsch, H., Grams, T., Häberle, K.H., Pritsch, K., Bauerle, T., Rötzer, T., 2020. Growth and mortality of Norway spruce and European beech in mono-specific and mixed-species stands under natural episodic and experimentally extended drought. Results of the KROOF throughfall exclusion experiment. Submitted.

Pretzsch, H., Rötzer, T., Matyssek, R., Grams, T.E.E., Häberle, K.-H., Pritsch, K., et al., 2014. Mixed Norway spruce (*Picea abies* [L.] Karst) and European beech (*Fagus sylvatica* [L.]) stands under drought. From reaction pattern to mechanism. Trees 28 (5), 1305–1321. https://doi.org/10.1007/s00468-014-1035-9.

Pretzsch, H. (Ed.), 2001. Modellierung des Waldwachstums. Parey Buchverlag, Berlin.

Pretzsch, H., Dieler, J., Matyssek, R., Wipfler, P., 2010. In: Tree and stand growth of mature Norway spruce and European beech under long-term ozone fumigation 1987 (4). Environmental pollution (Barking, Essex), pp. 1581061–1581070. http://doi.org/10.1016/j.envpol.2009.07.035.

Pretzsch, H., Schütze, G., Biber, P., 2018. Drought can favour the growth of small in relation to tall trees in mature stands of Norway spruce and European beech. For. Ecosyst. 5 (1), 227. https://doi.org/10.1186/s40663-018-0139-x.

R Core Team, 2016. R: a language and environment for statistical computing. In: R Foundation for Statistical Computing, Vienna, Austria. Online verfügbar unter Available from https://www.R-project.org/.

Rais, A., Van de Kuilen, J.W.G., Pretzsch, H., 2014. Growth reaction patterns of tree height, diameter, and volume of Douglas-fir (*Pseudotsuga menziesii* [Mirb.] Franco) under acute drought stress in Southern Germany. Eur. J. Forest Res. 133 (6), 1043–1056. https://doi.org/10.1007/s10342-014-0821-7.

Rais, A., Jacobs, M., Van de Kuilen, J.W.G., Pretzsch, H., et al., 2020. Crown structure of European beech (*Fagus sylvatica* L.): a non-causal proxy for mechanical–physical wood properties. Canadian Journal of Forest Research. https://doi.org/10.1139/cjfr-2020-0382.

RIEGL (2010): 10_DataSheet_Z420i_30-05-2010_pdf.cdr. Online verfügbar unter http://www.riegl.com/uploads/tx_pxprieglddownloads/10_DataSheet_Z420i_03-05-2010.pdf.

RIEGL (2019): RIEGL_VZ-400i_Datasheet_2019-11-22.indd 2019. Online verfügbar unter http://www.riegl.com/uploads/tx_pxprieglddownloads/RIEGL_VZ-400i_Datasheet_2019-11-22.pdf.

Rodriguez-Casal, A., Pateiro-Lopez, B., 2019. alphahull: Generalization of the Convex Hull of a Sample of Points in the Plane. R package version 2.2. https://CRAN.R-project.org/package=alphahull.

Rood, S.B., Patiño, S., Coombs, K., Tyree, M.T., 2000. Branch sacrifice: cavitation-associated drought adaptation of riparian cottonwoods. Trees 14, 248–257.

Rust, S., Roloff, A., 2002. Reduced photosynthesis in old oak (*Quercus robur*). The impact of crown and hydraulic architecture. Tree Physiol. 22 (8), 597–601. https://doi.org/10.1093/treephys/22.8.597.

Rust, S., Roloff, A., 2004. Acclimation of crown structure to drought in *Quercus robur* L.—intra- and inter-annual variation of abscission and traits of shed twigs. Basic Appl. Ecol. 5 (3), 283–291.

Schäfer, C., Rötzer, T., Thurm, E.A., Biber, P., Kallenbach, C., Pretzsch, H., 2019. Growth and Tree Water Deficit of Mixed Norway Spruce and European Beech at Different Heights in a Tree and under Heavy Drought. In. Forests 10 (7), 577. http://doi.org/10.3390/f10070577.

Seidel, D., Schall, P., Gille, M., Ammer, C., 2015. Relationship between tree growth and physical dimensions of *Fagus sylvatica* crowns assessed from terrestrial laser scanning. iForest 8 (6), 735–742. https://doi.org/10.3832/ifor1566-008.

Seidling, W., Ziche, D., Beck, W., 2012. Climate responses and interrelations of stem increment and crown transparency in Norway spruce, Scots pine, and common

beech. For. Ecol. Manage. 284, 196–204. https://doi.org/10.1016/j.foreco.2012.07.015.
Sohn, J.A., Kohler, M., Gessler, A., Bauhus, J., 2012. Interactions of thinning and stem height on the drought response of radial stem growth and isotopic composition of Norway spruce (*Picea abies*). Tree Physiol. 32 (10), 1199–1213. https://doi.org/10.1093/treephys/tps077.
Solberg, S., 2004. Summer drought: a driver for crown condition and mortality of Norway spruce in Norway. Forest Pathol. 34(2, 93–104.
Sterba, H., 1996. Forest Decline and Growth Trends in Central Europe - a Review. In: Growth Trends in European Forests (research report 5). Springer, Heidelberg, pp. 149–165.
Stovall, A. E.L., Shugart, H., Yang, X., 2019. Tree height explains mortality risk during an intense drought. Nat. Commun. 10 (1), 4385. https://doi.org/10.1038/s41467-019-12380-6.
Taeger, S., Zang, C., Liesebach, M., Schneck, V., Menzel, A., 2013. Impact of climate and drought events on the growth of Scots pine (*Pinus sylvestris* L.) provenances. For. Ecol. Manage. 307, 30–42. https://doi.org/10.1016/j.foreco.2013.06.053.
Trochta, J., Krůček, M., Vrška, T., Král, K., 2017. 3D Forest. An application for descriptions of three-dimensional forest structures using terrestrial LiDAR. PLoS ONE 12 (5), e0176871. https://doi.org/10.1371/journal.pone.0176871.
Wang, Y., Čufar, K., Eckstein, D., Liang, E., 2012. Variation of maximum tree height and annual shoot growth of Smith fir at various elevations in the Sygera Mountains, southeastern Tibetan Plateau. PLoS ONE 7 (3), e31725. https://doi.org/10.1371/journal.pone.0031725.
Wang, Y., et al., 2019. In situ biomass estimation at tree and plot levels: What did data record and what did algorithms derive from terrestrial and aerial point clouds in boreal forest. Remote Sens. Environ. 232, 111309.
Wood, S. N. (2017): Generalized Additive Models: An Introduction with R (2nd edition). In: Chapman and Hall/CRC.
Zuur, A.F., Ieno, E.N., Walker, N.J., Saveliev, A.A., Smith, G.M., 2009. GLM and GAM for count data. In: Mixed effects models and extensions in ecology with R. Springer, New York, pp. 209–243.

B.3. Article III

Title: Assessment of defoliation and subsequent growth losses caused by *Lymantria dispar* using terrestrial laser scanning (TLS)

Authors: Martin Jacobs, Torben Hilmers, Benjamin M. L. Leroy, Hannes Lemme, Sebastian Kienlein, Jörg Müller, Wolfgang W. Weisser, Hans Pretzsch

Journal: Trees – Structure and Function

Submitted: 4. August 2021

Accepted: 4. December 2021

Trees
https://doi.org/10.1007/s00468-021-02255-z

ORIGINAL ARTICLE

Assessment of defoliation and subsequent growth losses caused by *Lymantria dispar* using terrestrial laser scanning (TLS)

Martin Jacobs[1] · Torben Hilmers[1] · Benjamin M. L. Leroy[2] · Hannes Lemme[6] · Sebastian Kienlein[2,3] · Jörg Müller[4,5] · Wolfgang W. Weisser[2] · Hans Pretzsch[1]

Received: 4 August 2021 / Accepted: 4 December 2021

Abstract

Key message **TLS scans of three surveys before, during and after gypsy moth gradation, allowed high-resolution tracking of defoliation and subsequent inter-annual growth losses on an individual tree level.**

Abstract Foliation strongly determines all tree growth processes but can be reduced by various stress factors. Insect defoliation starts at variable times and is one stress factor that may affect photosynthetic processes and cause immediate reactions like refoliation, which are difficult to detect by surveys repeated at 1-year intervals. This study used a large-scale field experiment in German oak/mixed forests affected by gypsy moths (*Lymantria dispar*) to test the use of terrestrial laser scanning (TLS) for detecting inter-annual foliation and growth losses at the individual tree level caused by the gypsy moth. The experiment comprised two levels of gypsy moth defoliation risk, high (H) and low (L), as well as two pest control treatment levels: spraying with the insecticide Mimic (M) or unsprayed control (C). The factorial design consisted of four treatment combinations (HC, HM, LC, and LM), applied to 11 spatial blocks with a total of 44 plots. The TLS approach detected the defoliation caused by the gypsy moth, estimated as leaf area and crown perforation parameters. For the first time, TLS-derived tree foliation was evaluated based on inter-annual stem growth. Leaf area and crown perforation showed a correlation of + 0.6 and – 0.35, respectively, with basal area increments. Furthermore, this study revealed subsequent growth losses in the same year due to defoliation. Our results show that TLS can offer new opportunities to develop new indicators that monitor foliation at the individual tree level. The crown perforation can describe defoliation or the tree's vitality based on one scanning campaign, whereas the leaf area needed at least two.

Keywords Oak · Crown transparency · Leaf area · Infestation · Crown projection area · Monitoring

Communicated by Camarero.

✉ Martin Jacobs
martin.jacobs@tum.de

[1] Chair of Forest Growth and Yield Science, Department of Life Science Systems, TUM School of Life Sciences, Technical University of Munich, Hans-Carl-von-Carlowitz-Platz 2, 85354 Freising, Germany

[2] Terrestrial Ecology Research Group, Department of Life Science Systems, TUM School of Life Sciences, Technical University of Munich, Freising, Germany

[3] Ecosystem Dynamics and Forest Management Research Group, Department of Life Science Systems, TUM School of Life Sciences, Technical University of Munich, Freising, Germany

[4] Field Station Fabrikschleichach, Department of Animal Ecology and Tropical Biology, Biocenter, University of Würzburg, Rauhenebrach, Germany

[5] Bavarian Forest National Park, Grafenau, Germany

[6] Department of Forest Protection, Bavarian State Institute of Forestry, Freising, Germany

Published online: 21 January 2022

Introduction

The frequency and intensity of insect-induced forest disturbances is set to rise due to climate change and changes in forest structure and composition (Seidl et al. 2011). Consequently, effective methods that can detect and quantify stress factors are needed. One important stress factor is insect defoliation, which causes a significant reduction in tree growth (Piper et al. 2015). Whereas stem growth is easy to measure, the exact calculation of a tree's foliation is difficult. There is no suitable reference for evaluation. Traditional defoliation assessments, e.g., by eye or using fisheye photographs, have been criticised as being highly subjective (Dobbertin 2005), while current foliation determination approaches based on spectral information from TLS return intensity or machine learning are complex and expensive (Calders et al. 2020). As a result, a simple and reliable procedure is required, the results of which were compared to a suitable reference. In contrast to the approaches available, we evaluated our calculated foliation parameters based on inter-annual stem growth since stem growth and leaf area are correlated (Rolland et al. 2001).

With regard to defoliation, the gypsy moth (*Lymantria dispar*) is one of the most critical pest species of hardwood forests in its introduced range in North America and its native range in temperate Europe, North Africa, and Asia (Montgomery and Wallner 1988). Introduced roughly 150 years ago into the eastern part of the United States, the species spread across most of East Canada (Liebhold et al. 1992), causing overall annual damage of $3.4 billion in North America (Bradshaw et al. 2016). In its native range, it can cause severe damage during outbreaks, e.g., in Europe, but it is mostly known for its severe impacts and rapid expansion in North American forests, where it is invasive (McManus and Csóka 2007). Severe defoliation, range expansion, and increasing gypsy moth frequencies, exacerbated by rising temperatures (Logan et al. 2003), have also been reported in Central Europe (McManus and Csóka 2007), Russian Far East and Central Asia (Gninenko and Orlinskii 2003; Orozumbekov et al. 2009) and North Africa (Villemant and Ramzi 1995). However, it is not an invasive species in Europe and Asia yet.

Defoliation can have effects on forest structure and stand development. In addition, defoliation and tree mortality may also affect the community composition of tree regeneration and herbaceous vegetation through interspecies competition effects in the sub-canopies, triggered by the increased light availability in the canopy gaps (Fajvan and Wood 1996). Furthermore, Nakajima (2015) suggested that insect defoliation can dramatically affect forest ecosystem processes, such as the regeneration of host trees and the behavior of wildlife that depend on seed production, by reducing the reproductive potential of host trees. At single-tree level, defoliation affects the condition, causing significantly reduced timber production (Piper et al. 2015). In detail, tree defoliation can result in growth loss (Naidoo and Lechowicz 2001), reduced root biomass production (Thomas et al. 2002), and increased tree mortality compared to non-outbreak situations (Elling et al. 2007). Here, tree mortality depends on the frequency, intensity, duration, and combination of defoliation, the vitality status of the infested trees, and biotic or abiotic stresses (Elling et al. 2007). Severe insect defoliation as a stress factor directly affects the photosynthetic processes and indirectly reduces stem growth (Dobbertin 2005). Defoliation also induces the formation of a light ring consisting of thin-walled latewood tracheids in larch trees, which would affect timber quality (Watanabe and Ohno 2020). This is also proven for oak trees and may also affect tree vitality (Blank 1997). The study by Gieger and Thomas (2002) revealed for both *Quercus robur* L. and *Quercus petraea* (Matt.) Liebl. that defoliation—solely or in combination with drought—and subsequent growth loss result in a deteriorated water supply after embolism, reducing the tree's vitality. When several damaging factors coincide, such as defoliation and late frost or defoliation and drought, this may lead to the death of the oaks (Gieger and Thomas 2002). According to Fajvan et al. (2008), the defoliation of oaks by gypsy moth reduced volume growth increment and wood strength properties more in the upper stem sections than in the lower bole. In summary, defoliation by insects is a critical stress factor affecting the photosynthetic processes, carbon allocation, and thus tree growth (Dobbertin 2005). Tree growth is the increase in size and in the tree's number of vegetative structures, consisting of leaves, stem and roots, while leaf growth is the most critical tree growth process (Waring 1987).

Analysing the relationship between insect defoliation and tree growth is not simple. Insect defoliation has been shown to influence tree growth and can be reconstructed from tree rings (Rolland et al. 2001). For example, periodically reoccurring outbreaks of the larch bud moth (*Zeiraphera diniana* Gn) in the European Alps were shown to lead to reduced ring widths in the European larch (*Larix decidua* Mill) (Rolland et al. 2001). Additionally, the leaf area has been found to correlate well with the sapwood area at breast height (Waring et al. 1981) or with the sapwood area without the latewood (Eckmüllner and Sterba 2000). As the effect of the outbreaks is usually compensated for during non-outbreak periods, the effects of insect defoliation on tree growth cannot be detected in forest inventories carried out in one or 5-year growth intervals (Dobbertin 2005). For that reason, inter-annual stem growth and leaf area should be assessed together (Dobbertin 2005).

Whereas measuring stem growth is simple, determining leaf area is more difficult due to accessibility issues. Because the destructive assessment of a tree's original leaf area size is rarely feasible, the visual assessment of tree crowns and their classification into transparency or defoliation classes is a standard procedure in many parts of the world and can be carried out cost-effectively and relatively quickly in field surveys (Müller-Edzards et al. 1997). However, crown transparency assessments are under criticism due to their high level of subjectivity (Dobbertin et al. 2009). Furthermore, they require intensive training courses and repeated control assessments (Wulff 2002). For crown transparency assessments, no absolute reference is known. Instead, only site-specific reference trees are used (Innes 1993). Satellite-based approaches for forest canopy condition monitoring may provide insights into broad-scale forest health dynamics with a relatively fine spatial and temporal resolution (Pasquarella et al. 2018) but not at individual tree level. Collection of the leaves with leaf trap baskets is laborious and not applicable over a large area. Leaves can also be carried away by wind. Consequently, there is a need for new rational measurement methods with a fast and easily understandable procedure for determining a single tree's foliation. In addition, a method is required that is able to take objective measurements several times a year to record the temporal change in the crown condition. Starting with the beginning of the leaf growth, the temporally variable onset of insect feeding, which, depending on the intensity, also leads to leaf regrowth, a very high dynamic is formed in the vegetation period.

TLS has been used to address numerous information gaps in traditional inventory data (Calders et al. 2020). Ground-based LiDAR measurements can thereby be an alternative to airborne LiDAR observations, depending on the information needed, especially at the single-tree level (Hilker et al. 2010). In particular, it is possible to determine the structural crown properties of trees independently of tree species (Bayer et al. 2013). TLS has the potential and ability to scan and reach the canopy area successfully (Seidel et al. 2015). Several studies have already shown how to detect single tree defoliation at tree and stand level via TLS (Huo et al. 2019; Kaasalainen et al. 2010). The methodology of leaf area determination and classification into wood and leaf material is challenging. Leaf-wood separation approaches based on spectral information from TLS return intensity or machine learning are complex and expensive (Calders et al. 2020), making them difficult to reproduce. Therefore, robust and simple methods are required.

This study shows some simple new methods for the efficient monitoring of foliation at an individual tree level via terrestrial laser scanning (TLS), using the example of oak/mixed forests in Germany. Here, we used a novel approach to assess tree defoliation and link it to tree growth. In contrast to the TLS leaf-wood separation approaches available, we evaluated our calculated foliation parameters based on inter-annual stem growth since stem growth and leaf area are correlated (Rolland et al. 2001). To show the effects of defoliation, we used a large-scale field experiment in gypsy moth-infested oak-mixed forests in Germany (Leroy et al. 2021). The experimental design comprises two defoliation risk levels based on gypsy moth egg-mass occurrence and two treatment types sprayed to protect the trees from defoliation or unsprayed control. Based on TLS and the large-scale field experiment, the current study focused on the scan and quantification of the leaf area status using the TLS point clouds of three subsequent surveys before and after the gypsy moth infestation. We also focused on the development of the parameter crown perforation, which describes the foliation based on only one TLS survey in the growing season.

The study addressed the following research questions:

Q1: Does the leaf area and crown perforation calculated using TLS differ between trees attacked by gypsy moths and trees without damage?

Q2: Are leaf area and crown perforation related to stem increment within the same year?

Q3: Is the relationship between leaf area/crown perforation and basal area increment modified by the gypsy moth?

Material and methods

Experimental design

The experiment took place in mixed oak forests in different stands in Franconia-Bavaria in Germany (Leroy et al. 2021). The experimental design area consisted of 11 blocks (A, B, D, F, G, H, J, M, N, O, and S), varying spatially and dominated by oak trees. Each block was subdivided into four plots with similar forest structures, stand ages, and tree species composition within the block. Each plot had a mean size of 0.05 km^2 ($\pm$SD 0.20). Within each block, two of the four plots had a high (H) defoliation risk, while the other two had a low (L) defoliation risk. For this classification, a defoliation risk index was used, which calculation was based primarily on gypsy moth egg-mass density (Leroy et al. 2021, Appendix). The survey of egg-mass density was conducted by regional forest offices in 2018 (Leroy et al. 2021). In each block, an insecticide treatment (Mimic; M) was randomly assigned to one plot per defoliation risk level, while the second plot was left unsprayed and used as a control (C). The treatment plots were sprayed with the insecticide tebufenozide as Mimic® (Spiess-Urania Chemicals, Hamburg, Germany; 240 g l^{-1} active ingredient) between May 3rd and May 23rd (124–144 days of the year, DOY) 2019 at the maximal legal rate of 750 ml ha^{-1}. The treatments were applied by helicopter under conditions

of dry and less-than-windy weather. In total, 44 plots were sampled, which had been selected to represent 11 weak and strong infestations, and 11 remained with and without control.

At each plot, 20 six-tree samples, including one central oak tree and the following five neighboring trees with a diameter at breast height ($d_{1.3}$) greater than or equal to seven cm, were sampled, so that 880 central trees and 4400 neighboring trees were used to describe the stand characteristics such as basal area, standing volume, etc. for each block (Table 1). Single tree volume was calculated based on basal area, total tree height and species specific form factors for all six-tree sample trees. The single tree volumes were summed up to standing volume for block level. For stand characteristics, the total tree heights and basal area were retrieved from TLS. To estimate the variables per ha, we calculated the expansion factor. For this, we measured the distance between the central oak tree and the fifth neighboring tree via TLS for all 80 six-tree samples per block. After that, we calculated the circular area for each six-tree sample using the measured distances as the radius. We summed up all the areas of one block, and then we divided 10,000 by this area to get the expansion factor to calculate the variables per ha. A more detailed description of the stand characteristics per plot can be found in Table 4 in the Appendix. The 20 six-tree samples were established along transects in the four main cardinal directions (Fig. 1), starting from the centre of each sampling plot. Six-tree samples were taken at 25, 50, 75, 100, and 125 m from the centre of each plot (origin of the coordinate system in Fig. 1). More detailed information on the experiment and its design can be found in (Leroy et al. 2021).

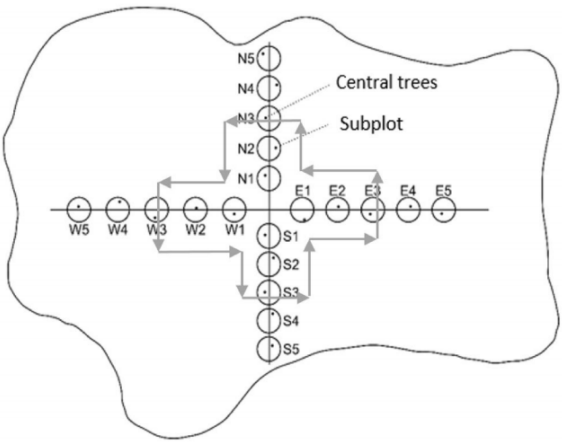

Fig. 1 An overview of a plot with 20 six-tree subplots along transects in the main cardinal directions, starting from the centre of the infested area For the detailed analysis, each six-tree subplot yields one central tree and five neighboring trees with $d_{1.3}$ greater than or equal to seven cm. The surveys were carried out along the transect using TLS in the winter. The grey arrows signify the scanning direction of TLS campaigns two and three in summer in relation to leaf area detection

Methods

The 880 central oak trees of each six-tree sampling were equipped with long-term girth tapes to analyse the interannual stem growth during the 2019 growing season. We measured the tree positions (x- and y-coordinates), the distances between the trees and the total tree heights via TLS. The following demonstrates the different steps of the TLS method applied. A detailed description of the workflow of the TLS procedure can be found in the Appendix: 1. Scanner

Table 1 The stand characteristics of the 11 blocks in Franconia-Bavaria, Germany

Block	n (ha^{-1})	dq (cm)	hq (m)	BA (m^2 ha^{-1})	SV (m^3 ha^{-1})
A	**493** (339–713)	**23.0** (7.1–71.5)	**17.6** (5.2–26.6)	**26.8** (23.5–30.1)	**235.3** (218.3–265.0)
B	**424** (314–622	**25.5** (7.6–61.6)	**19.8** (6.3–27.4)	**26.0** (22.5–30.5)	**256.8** (211.1–313.5)
D	**563** (357–753)	**23.0** (7.0–76.0)	**17.4** (6.1–29.2)	**34.0** (27.7–40.1)	**296.6** (258.0–364.6)
F	**260** (200–467)	**33.3** (7.6–85.7)	**22.9** (6.0–33.1)	**28.0** (22.7–36.4)	**319.2** (240.3–373.3)
G	**415** (261–632)	**24.7** (7.0–69.8)	**17.8** (3.1–30.6)	**28.6** (27.7–30.1)	**254.3** (230.5–301.0)
H	**517** (437–640)	**26.3** (7.0–66.9)	**20.6** (6.2–30.1)	**32.1** (29.0–34.3)	**329.7** (300.7–369.5)
J	**434** (294–718)	**26.2** (7.3–97.6)	**20.8** (4.5–34.4)	**30.5** (25.8–35.2)	**316.9** (281.3–356.5)
M	**411** (323–512)	**28.8** (7.3–78.2)	**20.9** (4.1–31.1)	**35.2** (28.7–41.7)	**367.9** (317.8–443.0)
N	**377** (293–474)	**26.2** (7.2–78.2)	**18.5** (4.4–28.1)	**26.8** (24.9–30.1)	**247.8** (228.1–272.5)
O	**287** (190–672)	**29.4** (8.0–83.7)	**20.3** (5.9–31.1)	**24.8** (20.5–36.1)	**252.1** (230.4–309.2)
S	**307** (305–350)	**29.9** (7.1–78.8)	**22.2** (5.0–33.0)	**29.0** (26.3–32.6)	**321.9** (305.4–349.7)

The parameters were calculated based on TLS point clouds using 5280 trees (six-tree subplots). Data from TLS survey in 2019, **mean** (range)

n number of trees, *dq* quadratic mean diameter, *hq* height corresponding to dq, *BA* basal area, *SV* standing volume

configuration and settings; 2. Data post-processing; 3. Tree detection and isolation; 4. Tree parameter extraction.

Terrestrial laser scanning acquisition

The terrestrial laser scanning (TLS) campaign was conducted to record the six-tree samplings in a leaf-off situation in winter to describe the forest stand characteristics (Table 1) and to determine the different status of forest canopy structures in three dimensions before and after insect defoliation. The RIEGL VZ-400i (RIEGL 2019) was used as a laser measurement system. A detailed description of the scanner configuration and settings can be found in the appendix.

The first scanning campaign (TLS_1) was carried out in early 2019, before the growing season in leaf-off conditions (79–107 DOY; 20th March–17th April, t_1). The second campaign (TLS_2) was conducted during the peak feeding of the gypsy moth between 179 and 200 DOY (28th June–19th July, t_2), and the third campaign (TLS_3) after the end of defoliation between 240 and 249 DOY (27th August–5th September, t_3). TLS_1 covered the total area of the subplots of each plot to describe the stand characteristics (Fig. 1, Table 1). As shown in Fig. 1 and marked by the grey arrows, TLS_2 and TLS_3 covered the area from the plot centre to the second subplot of each transect direction. Since all the plots needed to be scanned roughly simultaneously during the defoliation period, a smaller scan area was chosen for faster acquisition during the second and third campaigns. Consequently, the leaf area status was determined for eight trees per plot, resulting in 352 (44 × 8) trees in total. Their characteristics are described in Table 2. For all scanning campaigns, multiple scans were taken consecutively around the plots. The number of scan positions varied between the plots depending on the stand density of the plots. The higher the stand density, the more scan positions were needed. The number of scan positions per plot between the scanning campaigns t_2 and t_3 was always the same to ensure the comparability of the measurements (*ceteris paribus* conditions).

TLS data post-processing

The automatic registration of the LMS VZ-400i was applied so that artificial reference targets were not needed in the field. The automatic registration, filtering, and multi-station adjustment (MSA), which were used to refine the overall registration, were performed using the RiSCAN PRO version 2.10.1 software (http://www.riegl.com/products/software-packages/riscan-pro/). Using the automatic registration feature and since we started each scan at approximately the same position where we finished the previous scanning campaign at the specific plot, it was possible to register all the point clouds of each scanning campaign (TLS_1 to TLS_3) into one project coordinate system. To include all the foliage, stems, and branches (sometimes hidden by foliage) on t_2 and t_3, we merged each point cloud from TLS_2 and TLS_3 with the point clouds from TLS_1, before using an octree. This means that structural tree modifications within the scanning campaigns t_1 to t_3 can be directly visualised (Fig. 2). Every point cloud was reduced using an octree to enable fast point-cloud processing without accuracy loss (Elseberg et al. 2013). An octree is a tree data structure that is used for indexing three-dimensional data where one node has up to eight children, each responding to one octant of the overlying node. Therefore, the octree data structure is ideally suited to storing and retrieving three-dimensional laser scanner data efficiently (Elseberg et al. 2013). This way, the data are evenly distributed in space, whereby each cube with an edge length of five cm contains only one measuring point on average, set according to the centre of gravity of the cube's original points.

The complete processing was carried out within the programming environment of R (R Core Team 2016). For this purpose, the rlas package (Roussel and Boissieu 2019) was applied to import the .las files into R. Each central tree was marked with a reflector in the field during scanning. This made it possible to detect the central trees in all point clouds due to their higher reflectance values (> 1) compared to the rest of the points. After tree detection, the isolation of each central tree from the TLS point cloud of t_1, t_2, and t_3 was performed using a specifically developed preprocessing algorithm, which is based on the density-based spatial clustering

Table 2 Central oak tree characteristics of the four defoliation risk/treatment groups in Franconia-Bavaria, Germany, were calculated via TLS data where diameter at breast height ($d_{1.3}$) was recorded manually with long-term girth tape

Trees scanned for leaf area determination/mean[a] (± SE)					
Group		High control	High mimic	Low control	Low mimic
Trees per group *n*		88	88	88	88
Diameter at breast height $d_{1.3}$	cm	42.7 (1.4)	42.8 (1.4)	43.4 (1.0)	45.4 (1.4)
Height *h*	m	23.5 (0.4)	24.1 (0.4)	25.0 (0.4)	24.7 (0.3)
Crown projection area *cpa*	m^2	45.9 (2.6)	51.0 (4.1)	49.0 (2.9)	54.2 (3.3)

[a]Data from the survey in 2019

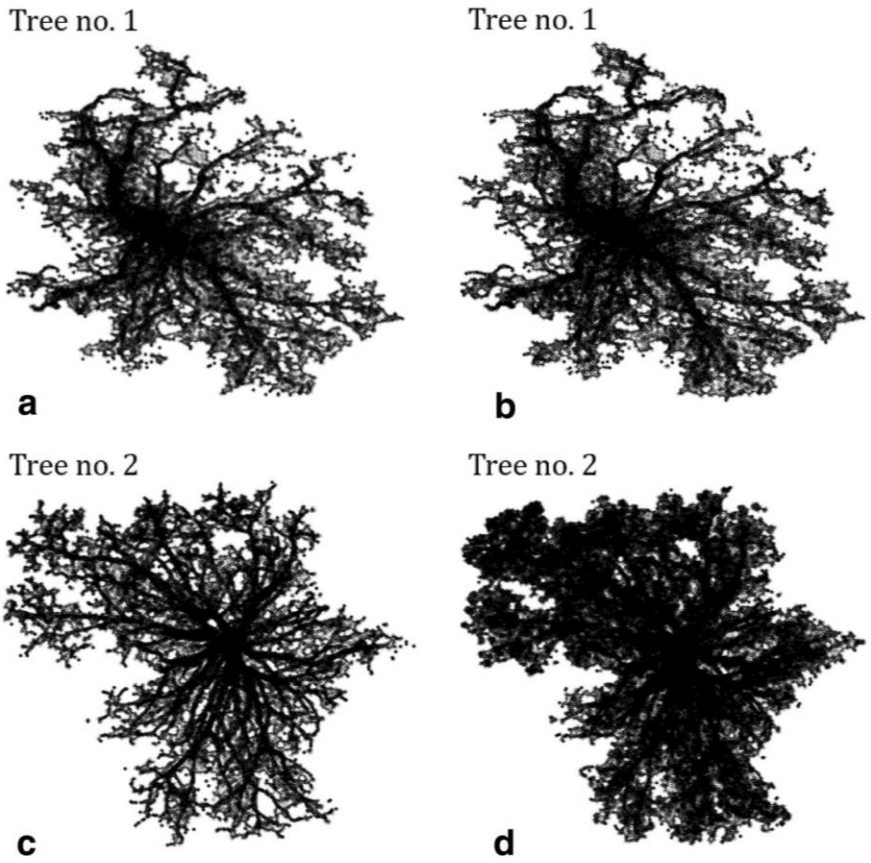

Fig. 2 A bird's-eye view of two sample trees extracted from the TLS point cloud **a**, **c** in winter without leaves; **b**, **d** in summer during peak feeding. Tree no. 1 is a tree from a plot with a high defoliation risk and no treatment (HC, i.e., control); Tree no. 2 is a tree from an area with a high defoliation risk and treated with Mimic (HM). Tree no. 1 has a calculated leaf area of 5.9 m^2 and tree no. 2 has a leaf area of 38.3 m^2

algorithm with noise (dbscan) function (Ester et al. 1996), obtained from the dbscan package of R (Hahsler and Piekenbrock 2019). We also used distance functions from the VoxR package for three-dimensional space (Lecigne et al. 2018). Afterwards, each tree was visually checked for completeness. If necessary, unrecognised tree parts were added manually, and artefacts that did not belong to the tree were removed using the software RiSCAN PRO version 2.10.1 (http://www.riegl.com/products/software-packages/riscan-pro/). Exact descriptions of the R packages used for the respective tasks are given in Appendix.

Foliation-describing parameter

Leaf area We used the difference between a tree's winter state and a tree's summer state after defoliation to calculate insect impact on foliation in insecticide-treated and control plots. Based on the TLS point clouds, total leaf area was calculated using the "alphahull" R package (Rodriguez-Casal and Pateiro-Lopez 2019). This package permitted the determination of the area and borderline of a sample of points in a plane, and it had also been successfully used in previous research to determine crown attributes (Jacobs et al. 2021; Rais et al. 2020). By varying the α-value, it was possible to adjust the tightness of the borderline around the point cloud. Very low α-values can even recognize areas without any points in the middle of a two-dimensional point set. When a uniform α-value of 0.1 was chosen, the polygon fitted tightly to the points (Fig. 6., Appendix). Subtracting each of the two subsequent areas from winter and summer, we obtained the periodic change of leaf area ($pc_{leaf\ area}$ in m^2). It was essential to choose the same alpha values for the scans in leaf-off and leaf-on conditions to ensure the comparability of the measurements (*ceteris paribus* conditions). Repeated scanning campaigns of the same plots in 2019 made it possible to calculate the $pc_{leaf\ area}$ at the individual tree level. Via the difference between the horizontal projection area of the respective summer scanning campaign t_2 or t_3 and t_1 (Fig. 2), the $pc_{leaf\ area}$ of the individual tree could thus be calculated objectively in m^2 (Eqs. 1 and 2).

$$\mathrm{pc}_{\text{leaf area}}, t_2 = \text{horizontal projection area}_{\alpha=0.1, t2} - \text{horizontal projection area}_{\alpha=0.1, t1} \quad (1)$$

$$\mathrm{pc}_{\text{leaf area}}, t_3 = \text{horizontal projection area}_{\alpha=0.1, t3} - \text{horizontal projection area}_{\alpha=0.1, t1} \quad (2)$$

The leaf area$_i$ as the arithmetic mean of the periodic change for the individual tree is determined by Eq. 3:

$$\text{leaf area}_i = \left(\mathrm{pc}_{\text{leaf area}}, t_2 + \mathrm{pc}_{\text{leaf area}}, t_3\right)/2. \quad (3)$$

Crown perforation In addition to the leaf area, we also calculated crown perforation from the data. The polygon can be used not only to derive an area but also to determine its length. To eliminate the size effect, the polygon length (α = 0.1) was divided by the crown projection area (*cpa*) area with α = 1 (Fig. 6). This result was finally divided by the polygon length of the *cpa* with α = 1 and multiplied by 100 (Eq. 4) to obtain the crown perforation as a percentage. The perforation of the crown is primarily determined by the length of the polygon (α = 0.1). The higher the polygon length (always in relation to crown size), the higher the perforation because more holes within the crown can then be found. The crowns are less compact in profile.

$$\text{Crown perforation}_{t2} = \frac{\left(\frac{Pl_{0.1}}{Pa_1}\right)}{Pl_1} * 100, \quad (4)$$

Statistics

Estimating leaf area, basal area increments, and crown perforation

We used the linear mixed-effects models to estimate the parameters for equations predicting leaf area, crown perforation, and basal area that form the basis for subsequent tests for the effect of gypsy moths on defoliation and tree growth (**Q1** and **Q3**). To analyse whether the leaf area and crown perforation calculated using TLS differ between trees attacked by gypsy moths and trees without damage (**Q1**), we created Eqs. 5 and 7, which used the foliation values of all 352 oak trees scanned at t_2 and t_3. Those 352 trees served as the basis for Eqs. 6 and 8 to predict (*pred()*) leaf area and crown perforation for all 880 central oak trees as linear predictors to analyse the relationship between leaf area/crown perforation and basal area increment modified by the gypsy moth (**Q3**). The basal area increment was calculated via the long-term girth tapes measured in the interval after defoliation (June 2019) until the end of the growing season 2019.

$$\ln(\text{leaf area}_{ijk}) = a_0 + a_1 * \ln(\text{basal area}) + a_2 * \text{defoliation risk} + a_3 * \text{treatment} + b_k + \varepsilon_{ijk} \quad (5)$$

$$\ln(\text{basal area increment}_{ijk}) = a_0 + a_1 * \ln(\text{basal area}) + a_2 * \text{pred(leaf area)} + b_k + \varepsilon_{ijk} \quad (6)$$

$$\ln(\text{crown perforatrion}_{ijk}) = a_0 + a_1 * \ln(\text{basal area}) + a_2 * \text{defoliation risk} + a_3 * \text{treatment} + b_k + \varepsilon_{ijk} \quad (7)$$

$$\ln(\text{basal area increment}_{ijk}) = a_0 + a_1 * \ln(\text{basal area}) + a_2 * \text{pred(crown perforation)} + b_k + \varepsilon_{ijk} \quad (8)$$

t2 = scanning campaign at high peak gypsy moth,

$Pl_{0.1}$ = Polygon length of the crown projection calculated with alpha = 0.1,

Pa_1 = Polygon area of the crown projection calculated with alpha = 1,

Pl_1 = Polygon length of the crown projection calculated with alpha = 1.

Throughout each model, the variable *i* indexes the tree, the variable *j* the plot, and the variable *k* the block. The variable a_o represents the model's intercept, the variables a_1 and a_2 represent the slope coefficients, while the variable b_k represents the random effect related to the blocks. All random effects were assumed to be normally distributed, with an expected mean of zero. The uncorrelated remaining errors are ε_{ijk}.

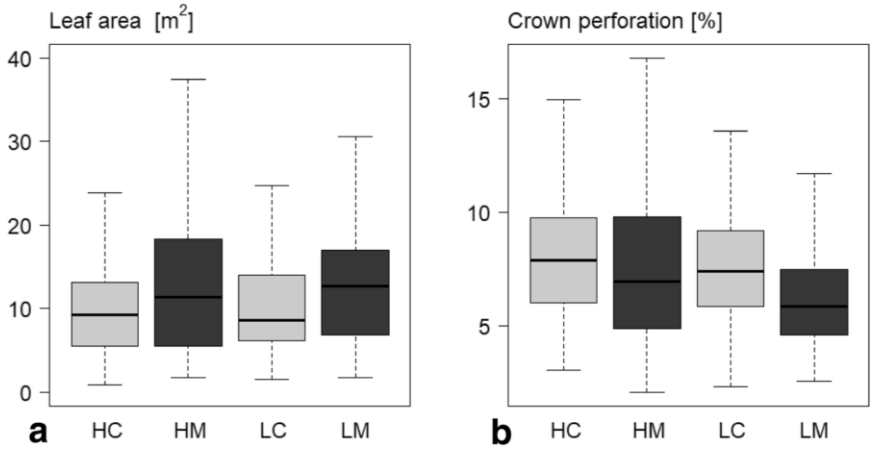

Fig. 3 Descriptive statistics boxplot of **a** leaf area ($(t_2+t_3)/2$) in m^2 and **b** crown perforation (t_2) as a percentage per tree, depending on treatment and defoliation risk, measured using raw data after defoliation until the end of the growing season. The experiment comprised two defoliation risk levels, high (H) or low (L), and two treatment types, sprayed with Mimic (M) to protect the trees against defoliation or unsprayed control (C). The factorial design comprised the four combination types (HC, HM, LC and LM)

Descriptive statistics

We used boxplots to illustrate the distribution of the leaf area and crown perforation depending on treatment and defoliation risk to see the difference between trees attacked by gypsy moths and trees without damage (Q1). We performed correlation analyses to determine whether leaf area and crown perforation are related to stem increment within the same year (Q2). We decided to focus on the strength of the relationship between TLS foliation measurements and inter-annual stem growth because no accurate reference for the leaf area status was available. With Eqs. 9 and 10, we compared linear models of tree growth, expressed as inter-annual increments in the trees' basal area, which includes the time from defoliation until the end of the growing season.

$$\text{basal area increment}_i = a_0 + a_1 * \text{leaf area} + \varepsilon_i \quad (9)$$

$$\text{basal area increment}_i = a_0 + a_1 * \text{crown perforation} + \varepsilon_i \quad (10)$$

Results

Descriptive statistics

For a first graphical overview, the leaf area and crown perforation distribution over the four defoliation risk and treatment groups are displayed as boxplots in Fig. 3. The distribution of the leaf area and the crown perforation differed between the four combination types visually (HC, HM, LC, and LM). The plots sprayed with Mimic had higher median leaf area values and lower median crown perforation values than the control plots (Fig. 3a, b).

Table 3 Statistics from linear mixed-effects models for Q1 and Q3

Function	(5)	(6)	(7)	(8)
Response variable	Ln (leaf area)	Ln (basal area increment)	Ln (crown perforation)	Ln (basal area increment)
Intercept	**− 2.70*****	**− 2.91****	**− 4.45*****	+ 1.71
Ln (basal area)	**+ 0.67*****	**+ 0.48****	**− 0.33*****	+ 0.20
Defoliation risk (low)	+ 0.02		**− 0.11***	
Treatment (Mimic)	**+ 0.2*****		**− 0.14****	
Pred (leaf area)		**+ 0.07***		
Pred (crown perforation)				**− 0.26*****
R^2 (adjusted)	0.33	0.19	0.23	0.21

Ln () is the logarithmic transformation, and *pred* means predicted. The category of defoliation risk is divided into high vs. low and treatment is in control vs. Mimic; R^2 (adjusted) is the coefficient of multiple determination; Estimates and significance values are given, while all significance values are in bold type

*$p < 0.05$

**$p < 0.01$

***$p < 0.001$

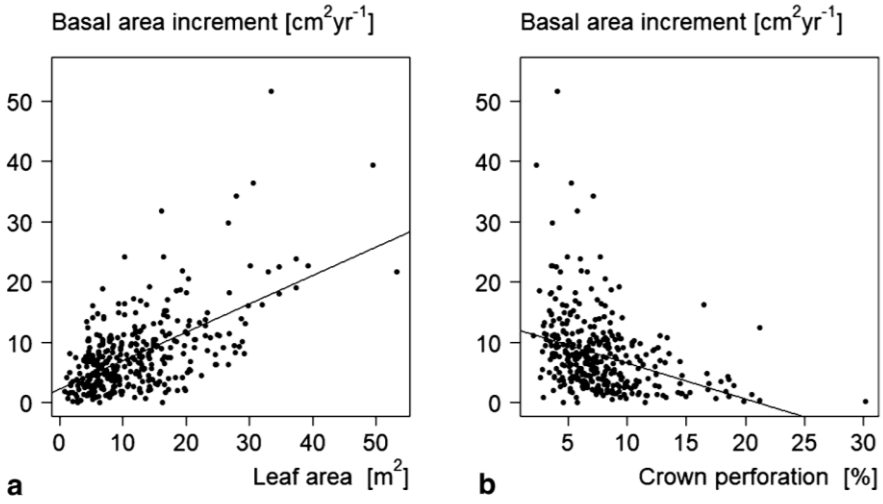

Fig. 4 Comparison of basal area increment in cm^2 $year^{-1}$ measured by long-term girth tapes between June 2019 (after defoliation) and the end of the growing season 2019 with **a** leaf area in m^2 measured after defoliation, and **b** crown perforation in %. Every dot is a single tree, and every line represents the regression line of Eqs. 9 and 10

(Q1) Defoliation detection by TLS parameters

The results of the linear mixed-effects models are shown in Table 3. Regarding the leaf area, the estimation of the insecticide treatment parameter was significant, while the estimation of the defoliation risk parameter was not significant. For the crown perforation, the estimation of the treatment parameter and the defoliation risk parameter were significant. It can be seen that despite random effects on a block level, the estimation of the insect defoliation parameters affected leaf area and crown perforation (Fig. 3a, b, Table 3, Functions 5 and 7). Via TLS, we observed differences in leaf area and crown perforation distribution on sprayed and control trees (Fig. 3a). The TLS-determined leaf area of trees on plots with no treatment was significantly lower than the tree's leaf area in the other treatment alternative (Table 3, Function 5). The estimated value of + 0.2 for treated trees, shown in Table 3, Function 5, demonstrated this. Crown perforation differed significantly between control and treatment plots, as well as between high and low defoliation risk plots, and was higher in control plots and plots with a high defoliation risk (Table 3, Function 7). In Table 3, Function 7, the estimated values of − 0.11 for treated trees and − 0.14 for trees with a low defoliation risk also demonstrated this.

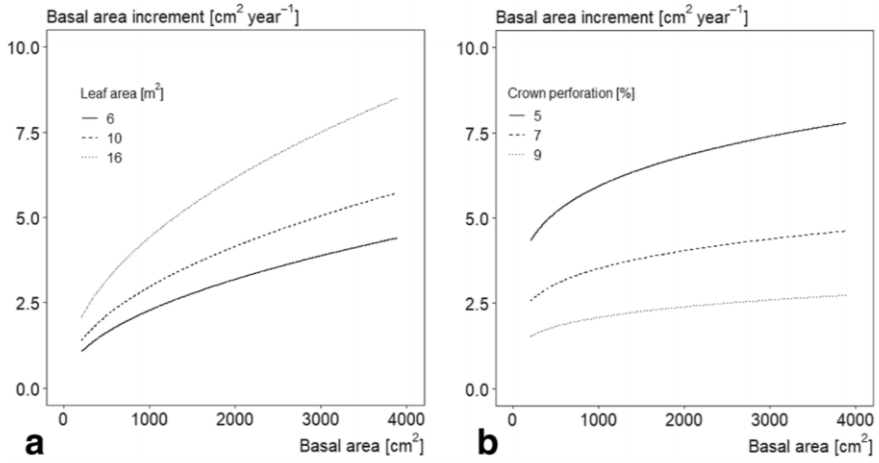

Fig. 5 Three curves for **a**) leaf area (m^2) from Eq. 6 and **b** crown perforation (%) from Eq. 8 each depend on basal area increment in cm^2 $year^{-1}$ and basal area in cm^2. To create the three curves of **a**, the leaf area parameter from Eq. 6 was set to 6, the first quartile (= solid curve), then was set to 10, the median value (= dashed curve), and then was set to 16, the third quartile (= dotted curve) of all leaf area values. For the three curves of **b**, the crown perforation parameter from Eq. 8 was set to 5, the first quartile (= solid curve), then was set to 7, the median value (= dashed curve), and then was set to 9, the third quartile (= dotted curve) of all crown perforation values

(Q2) Correlation of basal area increment and foliation parameters

To answer the question, we decided to focus on the strength of the relationship between TLS foliation measurements and inter-annual stem growth, because no accurate reference for the leaf area status was available. At tree level, leaf area after defoliation was positively related to basal area increment (Fig. 4a, cor = + 0.6, $R^2 = 0.35$, $p < 0.001$), and the crown perforation negatively with basal area increment (Fig. 4b, cor = − 0.35, $R^2 = 0.12$, $p < 0.001$).

(Q3) Influence of defoliation on basal area increment

Oaks with a lower leaf area and higher crown perforation showed significant losses in the estimation of the basal area increment parameter compared to non-defoliated trees (Fig. 5a, b, Table 3, Functions 6 and 8). The growth losses depended in an almost linear way on crown perforation for trees at the lower end of the diameter range. However, non-linear effects occurred for trees at the upper end of the diameter range (Fig. 5a). Therefore, higher increment losses due to defoliation are expected for trees with a higher basal area (Fig. 5a). As for leaf area, higher increment losses due to higher crown perforation are expected for trees with a higher basal area (Fig. 5b). The curves of leaf area and crown perforation, from Functions 6 and 8, differ in intercept and slope. The slope of the leaf area curves is higher, while the curves of the crown perforation are separated from each other by a greater distance. Overall, they cover the same stem growth range. To create the curves, the first quartile, median, and third quartile values of all leaf area and crown perforation values were used to set them as leaf area and crown perforation parameters in Functions 6 and 8, respectively (Fig. 5).

Discussion

Defoliation detection by TLS

The high-resolution temporal monitoring of three-dimensional structures via repeated TLS scanning can deliver unique time-varying four-dimensional data of canopy structural dynamics (Calders et al. 2020). We used a TLS approach to detect defoliation and introduced the novel parameters of leaf area and crown perforation that can be used for further studies. Therefore, the structural tree crown variations could be directly visualised and linked to tree growth over the year. Using our approach in an experimental setting with plots differing in outbreak condition and pest control measures, our linear mixed-effects models (Table 3, Functions 5 and 7) show that leaf area was significantly higher in plots that were sprayed with Mimic, which protected the trees against defoliation by gypsy moth (Table 3, Function 5), while crown perforation was significantly lower on these plots (Table 3, Function 7), resulting in fewer perforated and more compact crowns in leaf-on (t_2) condition. Previous studies into foliation detection via TLS have so far largely focused on the development of a methodology (Calders et al. 2020), with the aim of validating the approaches introduced, but these have not been used so far to identify stress-induced defoliation. On the other hand, some studies were able to show that TLS can detect defoliation at both the tree and stand level (Huo et al. 2019; Kaasalainen et al. 2010).

The evaluation of new automated approaches with an appropriate reference for validation is important in all cases. It would be ideal to measure each individual leaf of the crown, which is not possible due to time requirements and the difficulty of accessibility. Most of the studies used visual defoliation assessment as a reference for the validation of their estimated parameters (Huo et al. 2019; Kaasalainen et al. 2010). Even thorough training may not remove observer bias if multiple operators perform the assessment, and thus visual assessment is not a suitable reference. Any other ground-based measurement method is also not the ideal reference since the resulting foliation is only estimated. In contrast to the common TLS leaf-wood separation approaches and defoliation studies, we evaluated our calculated foliation parameters based on inter-annual stem growth, since stem growth and foliation are correlated (Rolland et al. 2001). In addition, stem growth is easy and accurate to measure in the field on the same tree that we used to calculate the foliation. The results of Ferretti et al. (2021) suggest that even slight and moderate variations in defoliation may have a significant impact on tree and forest growth. They found out that growth was inversely related to defoliation. Even lightly defoliated trees showed a significant reduction in growth (Ferretti et al. 2021). Both of our foliation-describing parameters correlated with the basal area increment, which was calculated within the same year directly after defoliation had taken place. As expected, leaf area was significantly and positively (Fig. 4a, cor = + 0.6, $R^2 = 0.35$, $p < 0.001$), and the crown perforation significantly and negatively (Fig. 4b, cor = − 0.35, $R^2 = 0.12$, $p < 0.001$) related to basal area increment. The reason for the lower correlation is probably that the crown perforation calculation was based on only one scanning campaign, whereas the leaf area determination method needed at least two and thus contained more information.

We cannot compare our results in terms of validation with other studies, as they mostly do visual assessments and do not consider stem growth as a reference. Regarding our results, the leaf area was the more suitable parameter for determining the foliation. The correlation of leaf area and basal area increment showed better results compared to crown perforation and basal area increment (Fig. 4a, b). Still, the crown perforation parameter was able to describe defoliation (Table 3, Function 7). Nevertheless, crown perforation seems to have a greater effect on stem growth, as shown by the significance and R^2 of Function 8 (Table 3). In addition, Function 7 (Table 3) shows

that crown perforation, in contrast to the leaf area, is significantly lower on plots where a low defoliation risk with a low density of gypsy moth eggs was found. Thus, the assessment of the defoliation risk based on egg-mass density, before the outbreak occurred was relatively accurate. The way the crown perforation describes the structure of the crown might give some clues about the current and past tree health. Perhaps the crown perforation not only offers the possibility to estimate foliation but also assess the tree's vitality due to the additional information on the crown's structural properties.

Defoliation and tree growth loss

Oaks with a decreasing leaf area and an increasing crown perforation revealed significant losses in basal area stem increment (Fig. 5a, b, Table 3, Functions 6 and 8). Our results are in line with the findings of Waring (1987), Dobbertin (2005) and Ferretti et al. (2021) who stated that insect defoliation affects the photosynthetic processes and reduces stem growth. Furthermore, due to the varying distances between the curves, we found that the growth losses, with decreasing leaf area and increasing crown perforation, were smaller at the lower end of the diameter range compared to the upper end of the diameter range (Fig. 5a, Table 3, Function 6). Hence, higher increment losses due to defoliation are expected for thicker trees that have a higher basal area (Fig. 5b, Table 3, Function 8).Usually, defoliation by insects initially becomes visible while stem growth reactions occur with a delay (Dobbertin 2005). The growth losses identified in this study were observed immediately after defoliation towards the end of the growing season. The plots integrated in this study did not suffer substantial defoliation in the previous years. Perhaps there are some long-term effects and the growth losses became even higher in the year after defoliation occurred.

Suitability of TLS and foliation-describing parameters

However, after critically reflecting, it becomes clear that working with TLS nevertheless has disadvantages. It can only be used in calm conditions without rain and fog, which reduces its temporal flexibility. This is especially true when capturing the exact time of peak defoliation is crucial. There is also a very large amount of data that needs to be processed. Still, we developed new rational measurement methods to determine the foliation of a tree with a fast and easy-to-understand procedure. However, there are a few limitations to our methods. Calculating the leaf area parameter is time consuming because at least two scanning campaigns are required, one in a leaf-off condition and one in a leaf-on condition. Nevertheless, the temporal monitoring of three-dimensional structures via repeated TLS scanning showed the potential to deliver time-varying defoliation data. The calculated crown perforation, which only requires one scanning campaign, is not as strongly correlated with basal area increment as the calculated leaf area. Furthermore, the leaf area parameter is only applicable to deciduous trees because one scanning campaign without leaves is necessary. This is clearly not possible with evergreen trees. The parameter crown perforation is not limited by the need for only one scanning campaign, but the input has less information and hence is not as accurate in relation to the correlation results with basal area increment (Fig. 4).

The branch growth between scanning campaigns one and two could result in overestimating leaf area. However, this only affects the leaf area parameter since, as mentioned above, at least two scanning campaigns are needed as input, in contrast to the parameter crown perforation, which needs only one measurement.

Another point of criticism is that the two-dimensional analysis based on viewing from above certainly does not consider every single leaf within the crown (Fig. 2). Moreover, some studies state that TLS underestimates the heights of big trees, which may be due to the occlusion of the crown and stem parts (Wang et al. 2019). The occlusion problem can be largely resolved by choosing sufficient different scan positions (Wilkes et al. 2017). However, this problem shows that it is even more difficult to scan every single leaf of a tree crown that is shaded or covered by other trees in a dense stand. Hence, a robust and simple method is required that works even if not all the leaves in the crown are scanned. The situation is comparable to the recording of the LAI. It is always estimated but practically never measured. We developed two foliation describing parameters and successfully tested them in a large-scale field experiment in gypsy moth-infested oak-mixed forests in Germany, evaluating the results based on stem growth to demonstrate their performance. The next steps towards scaling up would be to test other age stages, size dimensions, other species, other pests, or stress factors, and to find a solution to calculate leaf area for evergreen trees.

Summary-applications, recommendations, and implications

Regarding our research questions, the leaf area and crown perforation calculated using TLS differed between trees attacked by gypsy moths and trees without damage. Within the same year, leaf area and crown perforation are related to stem increment. The relationship between leaf area/crown perforation and basal area increment was modified by the gypsy moth, causing foliation and stem growth loss.

Precise foliation surveys have high potential for better scientific understanding and modelling. For example, the leaf area index (LAI) is an important factor for estimating the primary productivity of a forest stand and thus important for forecasting the productivity of terrestrial ecosystems (Sato et al. 2007). Furthermore, other modelling approaches show that LAI may increase in mixed (Forrester et al. 2019) and fertilised forest

stands (Smethurst et al. 2003). The determination of defoliation is important to predict damage via pest-growth-models (Dietze and Matthes 2014), while leaf area is an important component for determining light absorption, whose accurate prediction is critical for many process-based forest growth models (Forrester et al. 2014). According to Dobbertin and Brang (2001), including defoliation can considerably improve the prediction accuracy of models that predict tree mortality based solely on competition indicators and tree size.

Conclusions

Our results show that TLS can offer new opportunities for calculating foliation at the individual tree level. On the one hand, this study could be a step forward towards a more objective and personal independent foliation estimation, which is easier to understand in comparison to other TLS approaches. On the other hand, our results demonstrated that iterative TLS surveys might enhance the information gathered during measuring campaigns on common long-term experimental plots by obtaining a more thorough picture of growth patterns resulting from insect defoliation. The new approach detected the defoliation via leaf area caused by the gypsy moths and revealed subsequent growth losses during the same year. The crown perforation foliation parameter can describe the defoliation or even the vitality status of a single tree based on only one scanning campaign, whereas our leaf area determination method needs at least two. Since it is impossible to scan every single entire leaf of a crown, robust and simple methods are required that work even if not all the leaves in the crown are scanned. Still, robust and ready-to-use software for TLS data post-processing is not available, so the ability to program is necessary.

Author contribution statement

MJ: conceptualization, data collection, data curation, TLS processing, formal analysis, investigation, methodology, resources, software, validation, visualization, writing-original draft, writing-review and editing. TH: conceptualization, data collection, data curation, methodology, visualization, writing—review and editing. BMLL: conceptualization, methodology, writing—review and editing. SK: conceptualization. HL: conceptualization, writing—review and editing. JM: supervision, conceptualization, resources, writing—review and editing. WWW: supervision, conceptualization, resources, writing—review and editing. HP: supervision, conceptualization, methodology, resources, writing—original draft, writing—review and editing.

Appendix

See Table 4.

Table 4 Stand characteristics of the 44 plots in Franconia-Bavaria, Germany

Plot	n (ha^{-1})	dq (cm)	hq (m)	BA ($m^2\ ha^{-1}$)	Standing stock ($m^3\ ha^{-1}$)
AHC	713	20.2	15.9	27.5	218.3
AHM	339	27.7	19.6	23.5	230.2
ALC	603	20.7	17.2	27.8	239.1
ALM	476	23.5	17.6	30.1	265.0
BHC	314	27.5	18.8	22.5	211.1
BHM	459	26.3	20.6	30.5	313.5
BLC	406	25.1	19.5	23.8	232.4
BLM	622	23.2	20.2	30.3	305.2
DHC	615	23.8	18.2	40.1	364.6
DHM	357	26.5	18.6	27.7	258.0
DLC	753	21.6	17.2	38.9	334.1
DLM	744	19.9	15.7	35.3	276.4
FHC	243	31.1	21.2	22.7	240.3
FHM	467	25.1	19.0	36.4	345.8
FLC	200	40.9	26.8	27.8	373.3
FLM	244	36.4	24.4	29.0	353.0
GHC	438	23.8	16.0	28.8	230.5
GHM	261	33.5	21.8	27.7	301.0
GLC	513	22.0	17.2	30.1	258.3
GLM	632	19.4	16.1	29.0	233.3
HHC	437	29.1	22.0	33.6	369.5
HHM	528	24.9	19.1	31.5	300.7
HLC	503	26.5	21.0	29.0	305.2
HLM	640	24.7	20.2	34.3	346.3
JHC	552	25.5	19.8	35.2	348.4
JHM	718	20.8	19.0	29.7	281.3
JLC	382	26.7	22.1	25.8	284.8
JLM	294	31.7	22.3	31.9	356.5
MHC	512	27.2	21.2	41.7	443.0
MHM	323	30.2	22.1	28.7	317.7
MLC	503	27.7	20.7	39.1	404.8
MLM	369	30.2	19.5	35.1	342.2
NHC	475	25.0	17.8	28.6	254.4
NHM	359	25.6	18.2	25.1	228.1
NLC	433	25.1	18.1	30.1	272.5
NLM	293	29.1	19.9	24.9	247.1
OHC	394	27.0	18.5	29.0	267.1
OHM	672	23.2	17.1	36.1	309.2
OLC	214	33.9	23.2	23.8	275.7
OLM	190	33.3	22.4	20.5	230.5
SHC	296	31.7	21.5	32.6	349.7
SHM	325	28.6	20.8	30.1	313.0
SLC	312	30.1	23.3	26.9	313.6
SLM	298	29.2	23.2	26.3	305.4

The parameters were calculated based on TLS point clouds using 5280 trees (six-tree subplots). The plots are characterised by block/defoliation risk/treatment

n number of trees, *dq* quadratic mean diameter, *hq* height corresponding to dq, *BA* basal area

Table 5 Overview of the RIEGL VZ-400i (RIEGL 2019), summarising the main characteristics

Laser measurement system (LMS) LMS		RIEGL VZ-400i
Range[a]	m	800
Effective measurement rate[b]	meas./sec	500,000
Accuracy[c,d]	mm	5
Precision[d,e]	mm	3
Vertical field of view		100
Pulse mode		Multiple target capability
Registration		Automatic
Laser beam divergence	mrad	0.35[f]

[a]Typical values for average conditions. Maximum range is specified for flat targets with size in excess of the laser beam diameter, perpendicular angle of incidence, and for atmospheric visibility of 23 km. In bright sunlight, the max. Range is shorter than under overcast sky

[b]Rounded values

[c]Accuracy is the degree of conformity of a measured quantity to its actual (true) value

[d]One sigma at 100 m range under RIEGL test conditions

[e]Precision, also called reproducibility or repeatability, is the degree to which further measurements show

[f]Measured at the 1/e2 points. 0.35 mrad corresponds to an increase of 35 mm of beam diameter per 100 m distance

Defoliation risk index (Leroy et al. 2021)

The defoliation risk index (DRI) was calculated as:

$$\mathrm{DRI} = \frac{\mathrm{MEM}}{\mathrm{CEM_c}}$$

MEM is the average number of egg masses per stem, while CEMc is the corrected critical egg-mass density for the focal survey transect. Stands with a defoliation risk index > 1 had a high risk of defoliation, while a defoliation risk index < 0.5 was considered low risk. The results were extrapolated to the surrounding areas to identify candidate sites for the experiment, i.e., stands with high DRI (> 1) and low DRI (0.5) that were close enough to one another to be grouped into experimental blocks (maximum inter-plot distance within-block of 10 km).

TLS procedure of data acquisition and parameter extraction

Scanner configuration and settings

The RIEGL VZ-400i (RIEGL 2019) laser measurement system was used. An overview of the main scanner characteristics is provided in Table 5.

We used a laser pulse repetition rate of 1200 kHz. One horizontal 360° scan was performed for each scan position with a 100° vertical field of view. In our practical experience, the horizontal angular resolution was set to 0.04°, which in our practical experience, achieves a reasonable trade-off between scan-time (45 s per scan) and the risk of disturbances due to tree movement through wind. Due to the angular measurement scheme of the scanner, which operates from the ground, the point density naturally decreases towards the top of the canopy. Furthermore, the laser beam is usually unable to penetrate tree compartments to perform measurements behind obstacles. These two effects result in rather sparse measurement densities in the upper crown and stem regions, especially if the crown parts near the scanner are dense (Hilker et al. 2010). Using the pulsed time-of-flight method for laser range measurements, the RIEGL LMS VZ-400i determines the range to all targets with which a single laser pulse interacts ("multi-target capability"). Depending on the measurement program used, the maximum number of targets that can be detected varies (typically 4–15). The RIEGL LMS VZ-400i can generate 4–15 points per laser beam.

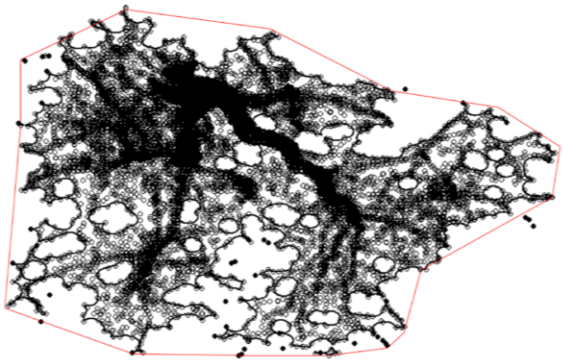

Fig. 6 A top view of an oak tree. By way of illustration of the different methods for calculating the leaf area and crown perforation within the R package "alphahull". Choosing an α-value of 1 (red polygon), a projection area similar to the traditional crown projection area was derived. Choosing an α-value of 0.1 (black polygon), the polygon framed the crown tightly

Data post-processing

We did not focus on three-dimensional tree features. Instead, our crown target variables (leaf area and crown perforation) were two-dimensional to take into account that not every individual leaf within the crown can be scanned. This was done to exclude errors occurring in the three-dimensional analysis due to non-scanned areas of the upper crown region, respectively. Using the software RiSCAN PRO version 2.0.2 (http://www.riegl.com/products/software-packages/riscan-pro/), all scan positions per plot were co-registered. The new automatic registration of the LMS VZ-400i was used so that

artificial reference targets were no longer needed. Automatic registration and filtering were performed using the software RiSCAN PRO version 2.8.2.

Tree detection and isolation

To detect individual-tree positions, we used the density-based spatial clustering algorithm with noise (dbscan) function in the dbscan package of R (Hahsler and Piekenbrock 2017). The function relied on a density-based notion of clusters, which was designed to discover clusters of arbitrary shape (Ester et al. 1996). Only the x- and y-axes were used as input data, thereby pushing all points belonging to the z-axis to one height level. The consequence was a higher point density per tree stem. Now dbscan is automatically able to find each tree as a cluster. This meant that each recognized cluster (stem) now received a unique number and could be processed individually. Additionally, non-vertically grown trees were detected at the lower part of the stem. Ground points were recognized by dbscan as noise points because of their horizontal structure in contrast to the vertically grown stems. For each stem cluster, stem base points were determined. The median values of the x- and y-coordinates and the minimum value of the z-axis of the stems were calculated. The stem base points now serve to extract the original points of the entire tree. The isolation of each single tree from the TLS point cloud was performed using the dbscan algorithm within the R programming environment (R Core Team 2016). With the application of dbscan, the entire point cloud was classified into clusters. Now each cluster is individually queried, which stem base cluster is closest in distance and whether this distance is close enough to be classified as associated points. After this step, each tree was visually checked for completeness. If necessary, unrecognised tree parts were added manually, and artefacts that did not belong to the tree were removed using the software RiSCAN PRO (http://www.riegl.com/products/software-packages/riscan-pro/).

Tree parameter extraction

The total tree height is calculated by determining the z-axis minimum and maximum points of the isolated tree. The minimum value is subtracted from the maximum value, and the output is the height. Wang et al. (2019) reported that TLS underestimated the height of big trees, which may be due to occlusion of crown and stem parts. The occlusion problem might be mainly resolved by choosing a sufficient number of different scan positions. On the other hand, TLS height measurements on Norway spruce trees in forest stands that covered a broad density range were found to be more accurate than common height measurements with the Vertex, a hand-held device based on the trigonometrical principle (Jacobs et al. 2020). Regarding our study, the total tree heights were obtained from the pointclouds in a leaf-off condition in winter. The number of scan positions per plot varied from 80 to 110 depending on stand density. Therefore, the occlusion problem should be reduced to an absolute minimum. The procedure applied for diameter calculation was introduced in Jacobs et al. (2020).

Acknowledgements The site selection was supported by Peter Aichmüller, Ludwig Albrecht, Elfi Raunecker and Stephan Thierfelder, and local district rangers from the regional forest administration of Franconia (AELF Kitzingen, Uffenheim, Würzburg and Schweinfurt). We want to thank Ralf Petercord, Ludwig Strasser, Peter Eichel, Ingrid Oberle, Britta Hausknecht and Alois Zollner for the critical contribution in planning and coordinating the spray operations. We want to thank for the permission to conduct research in their private forest stands of 33 anonymous landowners and communities.

Funding Open Access funding enabled and organized by Projekt DEAL. This research was supported by grant number Z073 administered by the Bavarian State Ministry for Food, Agriculture and Forests (Bayerischen Staatsministerium für Ernährung, Landwirtschaft und Forsten).

Availability of data and materials All data and materials support the published claims and comply with field standards. The datasets generated during and/or analysed during the current study are available from the corresponding author on reasonable request.

Code availability Not applicable.

Declarations

Conflict of interest The authors declare that they have no known competing financial interests or personal relationships that could have appeared to influence the work reported in this paper.

Ethical approval Not applicable.

Consent to participate All authors obtained consent to participate.

Consent for publication All listed authors have approved the manuscript before submission.

References

Bayer D, Seifert S, Pretzsch H (2013) Structural crown properties of Norway spruce (*Picea abies* [L.] Karst.) and European beech (*Fagus sylvatica* [L.]) in mixed versus pure stands revealed by terrestrial laser scanning. Trees 27:1035–1047. https://doi.org/10.1007/s00468-013-0854-4

Blank R (1997) Ringporigkeit des Holzes und häufige Entlaubung durch Insekten als spezifische Risikofaktoren der Eichen. Forst Und Holz 52:235–242

Bradshaw CJA, Leroy B, Bellard C, Roiz D, Albert C, Fournier A, Barbet-Massin M, Salles J-M, Simard F, Courchamp F (2016) Massive yet grossly underestimated global costs of invasive insects. Nat Commun 7:12986. https://doi.org/10.1038/ncomms12986

Calders K, Adams J, Armston J, Bartholomeus H, Bauwens S, Bentley LP, Chave J, Danson FM, Demol M, Disney M, Gaulton R, Krishna Moorthy SM, Levick SR, Saarinen N, Schaaf C, Stovall A, Terryn L, Wilkes P, Verbeeck H (2020) Terrestrial laser scanning in forest ecology: expanding the horizon. Remote Sens Environ 251:112102. https://doi.org/10.1016/j.rse.2020.112102

Dietze MC, Matthes JH (2014) A general ecophysiological framework for modelling the impact of pests and pathogens on forest ecosystems. Ecol Lett 17:1418–1426. https://doi.org/10.1111/ele.12345

Dobbertin M (2005) Tree growth as indicator of tree vitality and of tree reaction to environmental stress: a review. Eur J Forest Res 124:319–333. https://doi.org/10.1007/s10342-005-0085-3

Dobbertin M, Brang P (2001) Crown defoliation improves tree mortality models. For Ecol Manag 141:271–284. https://doi.org/10.1016/S0378-1127(00)00335-2

Dobbertin M, Hug C, Waldner P (2009) Kronenverlichtung, Sterberaten und Waldwachstum in Langzeitstudien – Welche Indikatoren beschreiben den Waldzustand am besten? Forum für Wissen 7–20

Eckmüllner O, Sterba H (2000) Crown condition, needle mass, and sapwood area relationships of Norway spruce (*Picea abies*). Can J for Res 30:1646–1654

Elling W, Heber U, Polle A, Beese F (2007) Schädigung von Waldökosystemen: Auswirkungen anthropogener Umweltveränderungen und Schutzmaßnahmen. Elsevier, Spektrum Akad. Verlag

Elseberg J, Borrmann D, Nüchter A (2013) One billion points in the cloud – an octree for efficient processing of 3D laser scans. ISPRS J Photogramm Remote Sens 76:76–88. https://doi.org/10.1016/j.isprsjprs.2012.10.004

Ester M, Kriegel HP, Sander J, Xu X (1996) A density-based algorithm fordiscovering clusters in large spatial databases with noise. In kdd 96(34):226–231

Fajvan MA, Wood JM (1996) Stand structure and development after gypsy moth defoliation in the Appalachian Plateau. For Ecol Manag 89:79–88. https://doi.org/10.1016/S0378-1127(96)03865-0

Fajvan MA, Rentch J, Gottschalk K (2008) The effects of thinning and gypsy moth defoliation on wood volume growth in oaks. Trees 22:257–268. https://doi.org/10.1007/s00468-007-0183-6

Ferretti M, Bacaro G, Brunialti G, Calderisi M, Croisé L, Frati L, Nicolas M (2021) Tree canopy defoliation can reveal growth decline in mid-latitude temperate forests. Ecol Ind 127:107749. https://doi.org/10.1016/j.ecolind.2021.107749

Forrester DI, Guisasola R, Xea T (2014) Using a stand-level model to predict light absorption in stands with vertically and horizontally heterogeneous canopies. For Ecosyst 1:1–19

Forrester DI, Rodenfels P, Haase J, Härdtle W, Leppert KN, Niklaus PA, von Oheimb G, Scherer-Lorenzen M, Bauhus J (2019) Tree-species interactions increase light absorption and growth in Chinese subtropical mixed-species plantations. Oecologia 191:421–432. https://doi.org/10.1007/s00442-019-04495-w

Gieger T, Thomas FM (2002) Effects of defoliation and drought stress on biomass partitioning and water relations of *Quercus robur* and *Quercus petraea*. Basic Appl Ecol 3:171–181. https://doi.org/10.1078/1439-1791-00091

Gninenko YI, Orlinskii AD (2003) Outbreaks of *Lymantria dispar* in Russian forests during the 1990s. EPPO Bull 33:325–329

Hahsler M, Piekenbrock M (2019) dbscan: density based clustering of applications with noise (DBSCAN) and related algorithms. J Stat Soft. https://doi.org/10.18637/jss.v091.i01

Hilker T, van Leeuwen M, Coops NC, Wulder MA, Newnham GJ, Jupp DLB, Culvenor DS (2010) Comparing canopy metrics derived from terrestrial and airborne laser scanning in a Douglas-fir dominated forest stand. Trees 24:819–832. https://doi.org/10.1007/s00468-010-0452-7

Huo L, Zhang N, Zhang X, Wu Y (2019) Tree defoliation classification based on point distribution features derived from single-scan terrestrial laser scanning data. Ecol Indic 103:782–790

Innes JL (1993) Forest health: its assessment and status. CAB International

Jacobs M, Rais A, Pretzsch H (2020) Analysis of stand density effects on the stem form of Norway spruce trees and volume miscalculation by traditional form factor equations using terrestrial laser scanning (TLS). Can J for Res 50:51–64. https://doi.org/10.1139/cjfr-2019-0121

Jacobs M, Rais A, Pretzsch H (2021) How drought stress becomes visible upon detecting tree shape using terrestrial laser scanning (TLS). For Ecol Manag 489:118975. https://doi.org/10.1016/j.foreco.2021.118975

Kaasalainen S, Hyyppä J, Karjalainen M, Krooks A, Lyytikäinen-Saarenmaa P, Holopainen M, Jaakkola A (2010) Comparison of terrestrial laser scanner and synthetic aperture radar data inthe study of forest defoliation. In: Wagner W, Székely B (eds) ISPRS TC VII Symposium – 100 Years ISPRS, Vienna, Austria, July 5–7, 2010, IAPRS, Vol. XXXVIII, Part 7A

Lecigne B, Delagrange S, Messier C (2018) Exploring trees in three dimensions: VoxR, a novel voxel-based R package dedicated to analysing the complex arrangement of tree crowns. Ann Bot 121(4):589–601. https://doi.org/10.1093/aob/mcx095

Leroy BML, Lemme H, Braumiller P, Hilmers T, Jacobs M, Hochrein S, Kienlein S, Müller J, Pretzsch H, Stimm K, Seibold S, Jaworek J, Hahn WA, Müller-Kroehling S, Weisser WW (2021) Relative impacts of gypsy moth outbreaks and insecticide treatments on forest resources and ecosystems: an experimental approach. Ecol Solut Evid. https://doi.org/10.1002/2688-8319.12045

Liebhold AM, Halverson J, Elmes G (1992) Quantitative analysis of the invasion of gypsy moth in North America. J Biogeogr 19:513–520

Logan JA, Régnière J, Powell JA (2003) Assessing the impacts of global warming on forest pest dynamics. Front Ecol Environ 1:130–137

McManus M, Csóka G (2007) History and impact of gypsy moth in North America and comparison to recent outbreaks in Europe. Acta Silv Lignaria Hung 3:47–64

Montgomery ME, Wallner WE (1988) Dynamics of forest insect populations. Plenum Press

Müller-Edzards C, Vries WD, Erisman JW (1997) Ten years of monitoring forest condition in Europe. Studies on temporal development, spatial distribution and impacts of natural and anthropogenic stress factors. UN/ECE

Naidoo R, Lechowicz MJ (2001) Effects of gypsy moth on radial growth of deciduous trees. For Sci 47:338–348

Nakajima H (2015) Defoliation by gypsy moths negatively affects the production of acorns by two Japanese oak species. Trees 29:1559–1566. https://doi.org/10.1007/s00468-015-1237-9

Orozumbekov AA, Liebhold AM, Ponomarev VI, Tobin PC (2009) Gypsy moth (*Lepidoptera*: *Lymantriidae*) in Central Asia. Am Entomol 55:258–265. https://doi.org/10.1093/ae/55.4.258

Pasquarella VJ, Elkinton JS, Bradley BA (2018) Extensive gypsy moth defoliation in Southern New England characterized using Landsat satellite observations. Biol Invasions 20:3047–3053. https://doi.org/10.1007/s10530-018-1778-0

Piper FI, Gundale MJ, Fajardo A (2015) Extreme defoliation reduces tree growth but not C and N storage in a winter-deciduous species. Ann Bot 115:1093–1103. https://doi.org/10.1093/aob/mcv038

R Core Team (2016) R: a language and environment for statistical computing. R Foundation for Statistical Computing, Vienna, Austria

Rais A, Pretzsch H, van de Kuilen J-WG (2020) European beech log and lumber grading in wet and dry conditions using longitudinal vibration. Holzforschung. https://doi.org/10.1515/hf-2019-0227

RIEGL (2019) Laser measurement system. (http://www.riegl.com,http://www.riegl.com/uploads/tx_pxpriegldownloads/RIEGL_VZ-400i_Datasheet_2020-10-06.pdf. Accessed 10 Nov2021

Rodriguez-Casal A, Pateiro-Lopez B (2019) alphahull: generalization of the convex hull of a sample of points in the plane. R package version 2.2. https://CRAN.R-project.org/package=alphahull

Rolland C, Baltensweiler W, Petitcolas V (2001) The potential for using Larix decidua ring widths in reconstructions of larch budmoth (*Zeiraphera diniana*) outbreak history: dendrochronological estimates compared with insect surveys. Trees 15:414–424. https://doi.org/10.1007/s004680100116

Roussel JR, de Boissieu F (2019) rlas: read and write "las" and "laz" binary file formats used for remote sensing data. R package version 1.3.4

Sato H, Itoh A, Kohyama T (2007) SEIB–DGVM: a new dynamic global vegetation model using a spatially explicit individual-based approach. Ecol Model 200:279–307. https://doi.org/10.1016/j.ecolmodel.2006.09.006

Seidel D, Schall P, Gille M, Ammer C (2015) Relationship between tree growth and physical dimensions of *Fagus sylvatica* crowns assessed from terrestrial laser scanning. iForest 8:735–742. https://doi.org/10.3832/ifor1566-008

Seidl R, Schelhaas M-J, Lexer MJ (2011) Unraveling the drivers of intensifying forest disturbance regimes in Europe. Glob Chang Biol 17:2842–2852. https://doi.org/10.1111/j.1365-2486.2011.02452.x

Smethurst P, Baillie C, Cherry M, Holz G (2003) Fertilizer effects on LAI and growth of four *Eucalyptus nitens* plantations. For Ecol Manag 176:531–542. https://doi.org/10.1016/S0378-1127(02)00226-8

Thomas FM, Blank R, Hartmann G (2002) Abiotic and biotic factors and their interactions as causes of oak decline in Central Europe. For Pathol 32:277–307. https://doi.org/10.1046/j.1439-0329.2002.00291.x

Villemant C, Ramzi H (1995) Predators of *Lymantria dispar* egg masses: spatio-temporal variation of their impact during the 1988–89 pest generation in the mamora cork oak forest (Morocco). Entomophaga 40:441–456

Wang Y, Pyörälä J, Liang X, Lehtomäki M, Kukko A, Yu X, Kaartinen H, Hyyppä J (2019) In situ biomass estimation at tree and plot levels: what did data record and what did algorithms derive from terrestrial and aerial point clouds in boreal forest. Remote Sens Environ 232:111309. https://doi.org/10.1016/j.rse.2019.111309

Waring RH (1987) Characteristics of trees predisposed to die. Bioscience 37:569–574

Watanabe Y, Ohno Y (2020) Severe insect defoliation at different timing affects cell wall formation of tracheids in secondary xylem of *Larix kaempferi*. Trees 34:931–941. https://doi.org/10.1007/s00468-020-01971-2

Wilkes P, Lau A, Disney M, Calders K, Burt A, Gonzalez de Tanago J, Bartholomeus H, Brede B, Herold M (2017) Data acquisition considerations for terrestrial laser scanning of forest plots. Remote Sens Environ 196:140–153. https://doi.org/10.1016/j.rse.2017.04.030

Wulff S (2002) The accuracy of forest damage assessments–experiences from Sweden. Environ Monit Assess 74:295–309

C. Supplement material

Supplementary A

Topic I - Stem form variation and volume miscalculation due to competition

Forest yield overview

In the Tables A1 – A3, a detailed forest yield overview is given.

Table A1 Forest yield overview for plots of the stand space test of Block 1. Plots differ in initial planting densities. (NDF = thinning from below, Z = thinning from above, N/ha = trees per hectare, hq = height of mean basal area stem (m), dq = diameter of mean basal area stem (cm), BA = basal area (m²), V = Standing volume ($m^3\ ha^{-1}$)). Thinning regime 1 was never thinned. Thinning regime 2 was late thinned. Thinning regime 3 was moderately thinned. Thinning regime 4 early thinned.

					Remaining stand					Released stand				
Treatment	**Plot**	**Year**	**Thinning**	**Thinning regime**	**N/ha**	**hq**	**dq**	**G**	**V**	**N/ha**	**hq**	**dq**	**BA**	**V**
Spacing test	1	1974	/	2	4000	/	/	/	/	/	/	/	/	/
Treatment 1		1992	(NDF,Z)		3110	9.8	11.2	30.9	162	385	9.1	9.3	2.6	14
		1996	(NDF,Z)		1484	12.5	15.3	27.3	175	1626	11	11.3	16.4	99
		2001	/		1462	15.7	18.9	40.8	317	22	9.2	7.6	0.1	1
		2006	(Z)		1165	19.3	21.2	41.1	385	297	18.8	19.3	8.7	81
		2014	(NDF,Z)		703	23	24.8	33.9	369	462	22.4	22.7	18.7	202
Spacing test	2	1974	/	2	400	/	/	/	/	/	/	/	/	/
Treatment 1		1992	/		389	7	14.2	6.2	24	/	/	/	/	/
		1996	(Z)		311	9.8	22.8	12.7	60	78	7.6	14.3	1.3	5
		2001	/		311	13.1	29.2	20.8	26	/	/	/	/	/
		2006	(NDF)		200	17.7	36.2	20.6	161	111	16	28.8	7.3	54
		2014	/		200	22	42.5	28.4	267	/	/	/	/	/
Spacing test	3	1974	/	2	10000	/	/	/	/	/	/	/	/	/
Treatment 1		1992	(NDF,Z)		4978	10	11.2	30.9	162	385	7.8	9.3	2.6	14
		1996	(NDF,Z)		2511	12.6	15.3	27.3	175	1626	10.9	11.3	16.4	99
		2001	/		2467	15.5	18.9	40.8	317	22	8.7	7.6	0.1	1
		2006	(Z)		1978	18.8	21.2	41.1	385	297	18	19.3	8.7	81
		2014	(NDF,Z)		1000	22.4	24.8	33.9	369	462	20.6	22.7	18.7	202
Spacing test	6	1974	/	2	2500	/	/	/	/	/		/	/	/
Treatment 1		1992	/		2080	9.4	12.3	24.7	123	45	1.4	1	/	/
		1996	(NDF,Z)		966	12.6	16.9	21.8	138	1114	11.5	13	14.8	90
		2001	/		955	15.9	21	33	255	11	4.3	2.2	/	/
		2006	(Z)		773	19.5	23.9	34.7	322	182	19.2	22.7	7.3	68
		2014	(Z)		500	23.7	28.8	325	356	273	22.6	24.4	12.8	138

Table A2 Forest yield overview for plots of the thinning test of Block 1. Plots differ in thinning regimes. (NDF = thinning from below, Z = thinning from above, N/ha = trees per hectare, hq = height of mean basal area stem (m), dq = diameter of mean basal area stem (cm), BA = basal area (m²), V = Standing volume (m³ ha^{-1})). Thinning regime 1 was never thinned. Thinning regime 2 was late thinned. Thinning regime 3 was moderately thinned. Thinning regime 4 early thinned.

					Remaining stand					**Released stand**				
Treatment	**Plot**	**Year**	**Thinning**	**Thinning regime**	**N/ha**	**hq**	**dq**	**G**	**V**	**N/ha**	**hq**	**dq**	**BA**	**V**
Thinning test	7	1974	/	1	2500	/	/	/	/	/	/	/	/	/
Treatment 2		1992	/		1943	9	12.9	25.6	122	46	1.3	1	/	/
		1996	/		1864	11.9	15.8	36.5	221	79	4.4	3.9	0.1	/
		2001	/		1761	15	18.3	46.3	346	103	7.6	6	0.3	1
		2006	/		1545	18.7	21	53.5	488	216	12.3	8.6	1.3	9
		2014	/		1409	22	23.7	62.3	657	136	16.6	2.1	1.6	14
Thinning test	8	1974	/	3	2500	/	/	/	/	/	/	/	/	/
Treatment 2		1992	/		1614	8.8	13.3	22.4	104	68	1.3	1	/	/
		1996	(NDF,Z)		886	12	17.3	20.9	126	728	11.5	15.4	13.5	80
		2001	/		830	15.4	22.1	31.8	237	56	6.5	5.4	0.1	1
		2006	(NDF,Z)		670	19.1	25.1	33.2	300	160	18.7	23.3	6.8	61
		2014	(Z)		602	23	29.6	41.4	439	68	18.3	17.6	1.7	16
Thinning test	9	1974	/	2	2500	/	/	/	/	/	/	/	/	/
Treatment 2		1992	(NDF,Z)		1195	10.5	14.4	19.5	106	680	9.6	11.5	7.1	38
		1996	(NDF,Z)		680	13.8	19.3	19.9	135	515	12.1	15.1	9.3	60
		2001	/		680	17	24	30.8	248	/	/	/	/	/
		2006	/		636	20.9	27.6	37.9	368	44	19.1	20.8	1.5	14
		2014	/		636	24.2	31.2	48.7	537	/	/	/	/	/
Thinning test	10	1974	/	4	2500	/	/	/	/	/	/	/	/	/
Treatment 2		1992	(NDF,Z)		1216	9.9	14.3	19.6	100	409	9.3	12.1	4.7	24
		1996	/		1216	13	18.1	31.4	204	/	/	/	/	/
		2001	/		1136	16.7	21.8	42.3	341	80	7.1	6.2	0.2	1
		2006	(Z)		875	20.3	24.4	41.1	396	261	19.7	22.1	10.1	96
		2014	(Z)		705	23.6	27.6	42	463	170	23.6	27.4	10.1	111
Thinning test	11	1974	/	4	2500	/	/	/	/	/	/	/	/	/
Treatment 2		1992	(NDF,Z)		1261	9.8	14.1	19.8	100	421	9.1	11.5	4.4	21
		1996	/		1261	12.4	17.4	30.1	189	/	/	/	/	/
		2001	/		1170	16	21.2	41.5	325	91	4.9	5.5	0.2	1
		2006	(Z)		864	19.9	23.4	37.1	354	301	19.5	21.8	11.5	109
		2014	(Z)		693	23.9	27	39.8	445	171	23.4	25.3	8.5	95

Table A3 Forest yield overview for plots of the thinning test of Block 2. Plots differ in thinning regimes. (NDF = thinning from below, Z = thinning from above, N/ha = trees per hectare, dq = quadratic mean diameter (cm), hq = height corresponding to dq, BA = basal area (m^2), V = Standing volume ($m^3\ ha^{-1}$)). Thinning regime 1 was never thinned. Thinning regime 2 was lately thinned. Thinning regime 3 was moderately thinned. Thinning regime 4 early thinned.

					Remaining stand					Released stand				
Treatment	**Plot**	**Year**	**Thinning**	**Thinning regime**	**N/ha**	**hq**	**dq**	**G**	**V**	**N/ha**	**hq**	**dq**	**BA**	**V**
Thinning test	17	1974	/	2	2500	/	/	/	/	/	/	/	/	/
Treatment 2		1992	/		1162	10.4	14.1	18.2	98	867	9	10.4	7.3	37
		1996	(NDF,Z)		691	13.3	19	19.7	129	471	12.1	15.6	9	56
		2001	/		691	16.9	24	31.4	251	/	/	/	/	/
		2006	(NDF,Z)		680	20.3	27.1	39.2	370	11	19.7	24.7	0.5	5
		2014	(Z)		669	23.5	30.5	49	527	11	16.2	9.7	0.1	1
Thinning test	18	1974	/	3	2500	/	/	/	/	/	/	/	/	/
Treatment 2		1992	/		2171	10.4	13	28.7	158	33	5.8	3.7	/	/
		1996	(NDF,Z)		1228	13.3	16.8	27.2	182	943	12.2	13.4	13.4	87
		2001	/		1228	16.7	20.3	39.7	325	/	/	/	/	/
		2006	(Z)		877	20.2	22.6	35.2	343	351	20	22	13.3	129
		2014	(Z)		702	23.5	26.6	39.1	430	175	23	25.2	8.8	95
Thinning test	20	1974	/	3	2500	/	/	/	/	/	/	/	/	/
Treatment 2		1992	/		2116	10.2	12.5	25.9	140	66	7.5	6.6	0.2	1
		1996	(NDF,Z)		1151	12.9	16.7	25.2	164	965	11.5	12.6	12	74
		2001	/		1151	16.3	20.3	37.4	299	/	/	/	/	/
		2006	(Z)		877	19.6	22.9	36.1	342	274	18.9	21	9.5	88
		2014	(Z)		702	23.1	27.4	41.3	447	175	21.5	22.5	7	73
Thinning test	21	1974	/	3	2500	/	/	/	/	/	/	/	/	/
Treatment 2		1992	/		1711	10.2	13.6	24.9	132	54	1.4	1	/	/
		1996	(NDF,Z)		1064	12.6	17.2	24.6	156	647	12.1	15.7	12.5	78
		2001	/		1064	16.4	20.7	35.8	287	/	/	/	/	/
		2006	(NDF,Z)		822	19.9	23.9	37	351	242	18.2	18.8	6.7	61
		2014	(Z)		702	23.5	28.5	44.7	488	120	19.5	17.9	3	30

Workflow - Technical description

1. Scan acquisition

The RIEGL LMS-Z420i (RIEGL 2010) laser-scanning system was used for data acquisition in late summer of 2017. Five scan positions were realized per plot. For each scan position, two scans (horizontal and vertical) were performed. The scan positions formed an approximate rectangle around each plot, with four scan positions at each corner and one central scan position in the middle of the plot. The vertical and horizontal angular resolution was set to 0.05° in order to achieve a reasonable trade-off between scan-time and risk of disturbances due to tree movement through wind. Due to the angular measurement scheme of the scanner that operates from the ground, the point density naturally decreases to the top of the trees. Furthermore, the laser beam is usually not able to penetrate tree compartments in order to perform measurements behind obstacles. These two effects result in rather sparse measurement densities in the upper crown and stem regions, especially if the crown parts near the scanner are dense, like those of conifers (Hilker et al. 2010). The RIEGL distance-measurement mode called “last-pulse” or “last-target” was used to counteract these effects by recording the deepest points within a footprint, thus gaining a higher proportion of returns from inner crown regions compared to first-pulse mode. The data of all scan positions per plot were co-registered using the software RiSCAN PRO. The co-registration was based on artificial targets (reflectors). The result was a “Plot Point Cloud Raw” (PPC-R).

2. Stem detection

After all scans per plot were referenced to each other, the data was exported as a .LAS file. The LAS file format is a binary file format for the fast interchange of three-dimensional data between data users. After import, the complete processing was done within the programming environment of R (R Core Team 2016). The rlas package (Roussel and Boissieu 2019) was used for data import in R.

2.2 Median-centring in PPC-R

To enable a fast analysis of the data, a sample by selecting random rows from the rough-point-cloud table was taken. The data of one plot was minimized by random sampling from approximately 50 to exactly one million points to give a faster computing time. The central position is derived as the median value of x- and y-coordinates of these five scan positions.

2.3 Median-centring and Square selection of points in the centred PPC-R

Before detecting individual tree positions, plot centering was done. This was achieved by calculating the median value of the x- and y-coordinates. The coordinates of the central position were set to x = 0, y = 0, and z = 0. That means, all x-, y-, and z-Coordinates were subtracted by their median values. All points with x <= 25 & x >= -25, and y <= 25 & y >= -25, were kept. The result was a square (50 m x 50 m) Plot Point Cloud (PPC). Although the actual plot size was 30 x 30 m, the larger size of the PPC ensured that all trees of the actual plot were within it. Otherwise, rotations around the x-axis would have been necessary to cut out the exact boundaries of the plots. At the end of this step, the coordinates of the central position were set to the initial values so that the coordinates of the PPC match the PPC-R.

2.4 Data thinning (point density reduction)

Since dbscan is limited in analysing point patterns which vary spatially in point density, it is useful to create a more homogeneous spatial distribution of the three-dimensional points. Therefore, the x- and y-axes were divided into classes with an interval of 1 m. In the end, there should be 50 x 50 classes which gives 2500 squares. Each square is 1 x 1 m in size. To achieve a homogeneous point density, a maximum sample of 15000 points per square was taken. If fewer points were found, they were all used.

2.5 Density based spatial clustering algorithm with noise

To detect individual tree positions, the dbscan function from the dbscan R package was used (Hahsler and Piekenbrock 2019). The function relies on a density-based notion of clusters, which is designed to discover clusters of arbitrary shape (Ester et al. 1996). Only the x- and y-axes were analyzed. Thereby, all points belonging to the z-axis were pushed down one level. The consequence is a higher point density per tree stem. Now dbscan is able to find each tree as a cluster automatically. This means that each recognized cluster (stem) now receives a unique number and can be processed individually. Non-vertically grown trees were also detected at the lower part of the stem. Ground points were recognized by dbscan as noise points, because these have a horizontal structure in contrast to the vertically grown stems and therefore a low density in the two dimensional analysis (x, y). In Figure A1, you can see the result of this whole sequence of steps. For each stem cluster, stem base points were determined. The median of the x- and y-coordinates as well as the minimum value of the z-axis of the stems were calculated. The stem base points now serve to extract the original points of the entire stem from the PPC-R in the form of a cylinder. In the filtered and reduced PPC, the stem base points was determined to extract the original information of the stems from the PPC-R.

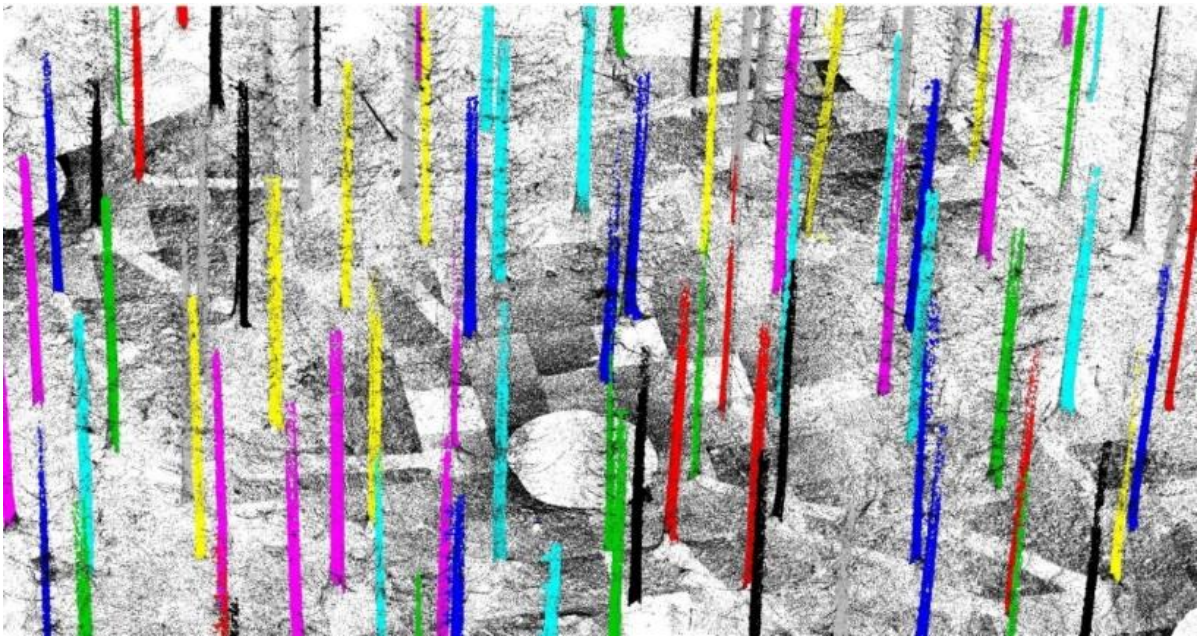

Figure A1 Automatically generated output of one plot with the density-based spatial clustering algorithm with noise (DBSCAN). Each recognized colored (bold) cluster received a unique number. Some trees had the same color due to the repeating color sequence. Noise points were colored black (not bold).

3. Stem isolation

3.2 Cylinder subset

The PPC-R now serves as a database. The trees were cut out in a radius of 1 m from the stem base point. The result is a three-dimensional point cloud in the form of a cylinder which contains all the individual tree information obtained by TLS. The point cloud size per tree differs from 30000 to 300000 points due to the scan acquisition, heterogeneous stand densities, shading, and the varying height of the crown base. The studies of DeConto (2016) and Raumonen et al. (2013) suggest that reduced point clouds can already provide precise estimates. DeConto (2016) used point clouds with reduced spatial resolution with not more than 300000 points per tree, and good accuracy was still achieved. In this study, this is the maximum size of a point cloud per tree. The average size is approximately 70000 points per tree. Not every detected tree was involved in the estimation of the stem form. Due to the heterogeneous density of the point cloud, a threshold for a minimum amount of points per tree was used. The number of points was determined for each tree silhouette. The lowest 5 % were removed, as they were either juvenile or poorly covered by TLS. Some trees were detected, but the amount of points was too low to measure stem form precisely. This is caused by occlusion. This phenomenon can be reduced by the use of more scans by plots. Therefore, the occlusion problem is mainly a consequence of a reduced number of scans.

3.3 Hough transformation for stem isolation

For stem isolation, the Hough transformation, adapted by Olofsson et al. (2014) was used. It is already implemented in the R package TreeLS (DeConto 2016). DeConto (2016) found that the Hough transform presented the best overall performance for most species, including Norway spruce. The result was an isolated stem without ground, branch and crown points. The visual result of stem isolation (blue points) can be observed in Figure A2.

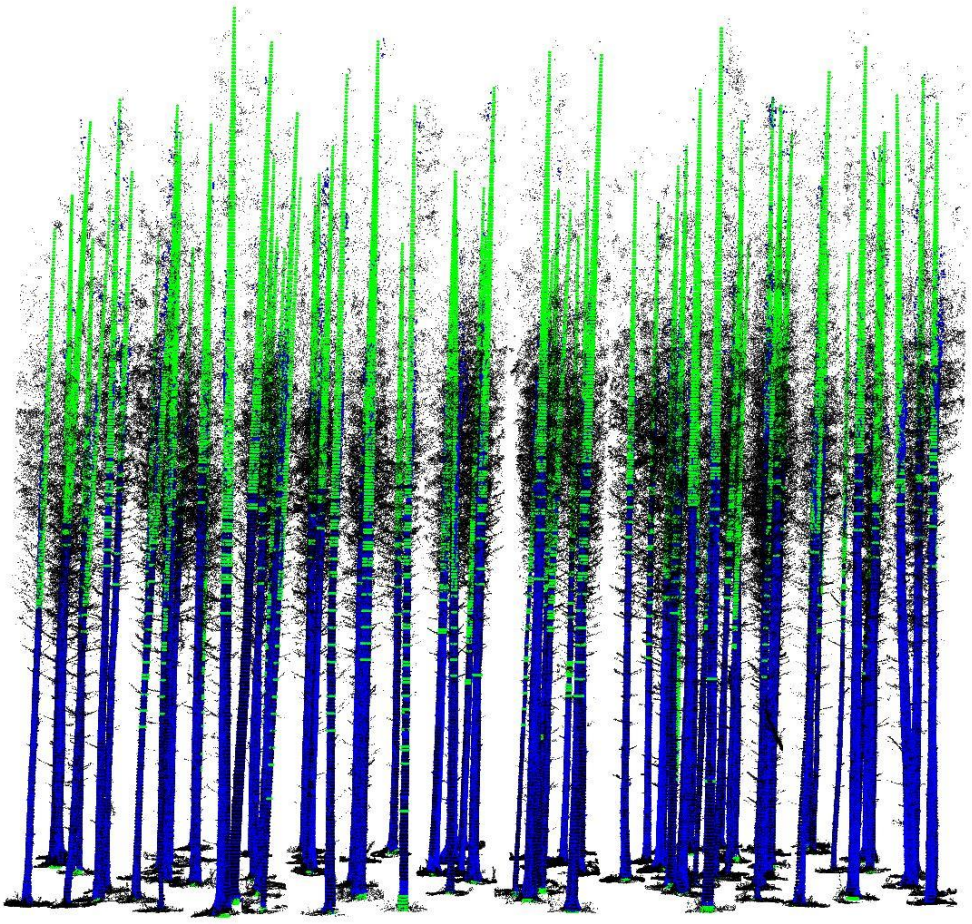

Figure A2 Visual result of TLS method (plot 3). The black points belong to the cylinder subsets of each tree. The isolated stems are colored in blue, and the green points, which are circles, are calculated for all height sections for which stem information was not available due to occlusion problems. The circle diameter calculation was done by the stem curve function (Pain and Boyer 1996). The green circles serve for the three-dimensional stem reconstruction; however, they were calculated up to the height at which the diameter was higher than 7 cm (stem wood).

4. Height determination depending on competition situation

As already mentioned the point density naturally decreases to the top of the trees, because the scanner operates from the ground. Furthermore, the laser beam is usually not able to penetrate tree compartments in order to perform measurements behind obstacles. These effects result in rather sparse measurement densities in the upper crown and stem regions, especially if the crown parts near the scanner are dense, like those of conifers (Hilker et al. 2010). Therefor, the isolated stems cannot not be used to determine the total tree height, as the stems can only be measured up to a limited height. This can be observed visually in Figure A2. The cylinder subsets that were calculated in Section 3.2 were used to determine total tree heights. As already mentioned, each tree was cut out around its stem base point in a radius of 1m. In this cylinder subset were also parts of the branches as well as the uppermost part of the crown. The highest point was then determined in this cylinder. In addition, the stem that was isolated in the previous step (3.3) was used to determine the lowest stem point. The difference between the highest and lowest point (max(z) - min(z)) resulted in the total tree height. However, this form of calculation caused errors with regard to the competition situation. The crowns of dominant trees in particular overshadow small trees underneath them. The cylinder subset contained not only the uppermost crown part, but also parts of the crowns of competing trees. As a result, the total tree height was overestimated.

The total height of trees where $d_{1.3}$ is greater than 20 cm (more dominant trees) was detected by determining the z-axis minimum and maximum point of the cylinder. The minimum value was subtracted from the maximum value. The output is the height.

The height of trees where $d_{1.3}$ is greater than 14 cm and lower than 20 cm was detected by determining the z-axis minimum and maximum point of the cylinder. The cylinder has a smaller size due to a radius of 0.1 m. Before this, the highest point of the stem isolation result was set as the central position of the cylinder. The minimum value was subtracted from the maximum value. The output is the height.

The height of trees where $d_{1.3}$ is lower than 14 cm was detected by determining the z-axis minimum and maximum point of the stem point cloud. Dominant trees surrounded these dominated trees. The advantage is that the stem in the upper region is more visible. The minimum value was subtracted from the maximum value. The output is the height.

There are findings available which confirm that TLS reaches the top of the canopy easily, where TLS-derived tree height has been compared to true tree height measured using destructive techniques (Calders et al. 2015).

5. Diameter calculation

At first, each isolated stem was divided into height classes with intervals of 0.1 m. Every 0.1 m, a diameter was measured. To ensure a sufficient number of points per height class for ellipse-fitting, every point 0.1 m below and 0.1 m above the certain height were involved in diameter computation. As a result, each section has a vertical size of 20 cm (Example: 1.30 m = 1.20 m to 1.40 m). After this, the center of the stem section was calculated by a geometric circle fit (Späth 1996) using the R package conicfit (Gama and Chernov 2015). The distances from the center to all points were computed. Ellipses were fitted, using the method of, Fitzgibbon and Fisher (1996), which is extremely robust and efficient, as it incorporates the ellipticity constraint into the normalisation factor, and as it can be solved naturally by a generalized eigensystem. The circle and ellipse fit were implemented in the R-package conicfit (Gama and Chernov 2015). Before ellipse-fitting, preparation or filtering of the stem section data is necessary due to possible noise points of branches or needles. This filtering was done in section 6.3.2 by the Hough transformation. Only ellipse fitting without filtering would lead to a deviation comparing manual and TLS measurements, especially for small tree diameters with estimations tending to be more upwardly biased for stem segments smaller than 10 cm in diameter (DeConto 2016).

After this step, the ellipse can be fitted. The ellipse was converted into a polygon. The perimeter was derived from the surface area of the polygon. Finally, the diameter was derived by the perimeter of the stem section. The diameters calculated as described in this section were used to fit the stem curves in section 2.2.4.

6. Tree by tree comparison

To compare the estimations based on data obtained from TLS vs. estimations based on traditional inventory data, it was necessary to identify each particular study tree (n = 868) on each PPC. In order to identify the trees in the field database and in the TLS point cloud, the two tree spatial maps obtained from traditional inventory data and TLS were manually rotated and merged.

Supplementary B

Topic II - Tree vitality indicator responses to severe drought stress

Scan acquisition

Two different laser-scanning systems were used for the two surveys: RIEGL LMS-Z420i (RIEGL 2010) for winter 2012/2013 and RIEGL VZ-400i (RIEGL 2019) for winter 2018/2019. An overview of the two scanners, summarizing the main characteristics, is provided in Table B1. For both dates, multiple scans were consecutively taken around the plots. In winter 2012/2013, two scans (horizontal and vertical) were performed for each scan position. The vertical and horizontal angular resolution was set to 0.05°, which in my practical experience, achieves a reasonable trade-off between scan-time and risk of disturbances due to tree movement through wind.

Table B1 Overview of both scanners, RIEGL LMS-Z420i (RIEGL 2010), and RIEGL VZ-400i (RIEGL 2019), summarizing the main characteristics.

Laser Measurement System (LMS)		RIEGL Z420i	RIEGL VZ-400i
Range[1)]	m	1000	800
Effective measurement rate[2)]	meas./s	11000	500000
Accuracy[3)4)]	mm	10	5
Precision[4)5)]	mm	4	3
Vertical field of view	°	80	100
Pulse mode		last-pulse	multiple target capability
Registration		artificial targets	automatic
Laser beam divergence	Mrad[6)]	0.25	0.35

1) Typical values for average conditions. Maximum range is specified for flat targets with size in excess of the laser beam diameter, perpendicular angle of incidence, and for atmospheric visibility of 23 km. In bright sunlight, the maximum range is shorter than under overcast sky.

2) Rounded values.

3) Accuracy is the degree of conformity of a measured quantity to its actual (true) value.

4) One sigma at 100 m range under RIEGL test conditions.

5) Precision, also called reproducibility or repeatability, is the degree to which further measurements show.

6) Measured at the 1/e2 points. 0.25/0.35 mrad corresponds to an increase of 25/35 mm of beam diameter.

In the winter of 2018/2019, the resolution was chosen so that the scans were comparable to the TLS recordings in the winter of 2012/2013. Due to the angular measurement scheme of the scanners, which operate from the ground, the point density naturally decreases towards the top of the canopy. Furthermore, the laser beam is usually unable to penetrate tree compartments in order to perform measurements behind obstacles. These two effects result in rather sparse measurement densities in the upper crown and stem regions, especially if the crown parts near the scanner are dense (Hilker et al. 2010). Regarding the RIEGL LMS-Z420i, I attempted – with the RIEGL distance-measurement mode called "last-pulse" or "last-target" – to counteract these effects and record the deepest points within a footprint, thus gaining a higher proportion of returns from inner-crown regions compared to first-pulse mode. Utilizing the pulsed time-of-flight method for laser range measurements, the RIEGL LMS VZ-400i enables the determination of the range to all targets a single laser pulse is interacting with ("multi-target capability"). Depending on the measurement program used, the maximum number of targets, which can be detected, varied. In summary, the RIEGL LMS Z-420i in the last-target setting generates one deep point per laser beam, while the RIEGL LMS VZ-400i can generate 4 – 15 points per laser beam. Due to this difference between the two scanners, I did not focus on three-dimensional tree features. Instead, the crown target variables (*cpa*, transparency and roughness) were two-dimensional to take into account the ability of the newer scanner to generate more points inside the crown space. This was done to exclude errors occurring in the three-dimensional analysis due to non-scanned areas of the upper crown region. In winter 2012/13, artificial reference targets (reflectors) distributed in the scanned forest scenes enabled the co-registration of the scans. The data of all scan positions per plot were co-registered using the software RiSCAN PRO version 2.0.2 (http://www.riegl.com/products/software-packages/riscan-pro/). In winter 2018/19, the new automatic registration of the LMS VZ-400i was used so that artificial reference targets were no longer needed. Automatic registration and filtering were performed using the software RiSCAN PRO version 2.8.2. The entire point cloud was reduced using an octree to enable fast point-cloud processing without accuracy loss (Elseberg et al. 2013). This distributes the data evenly in space, whereby each cube with an edge length of 5 cm contains on average only one measuring point, which is set according to the center of gravity of the original points in the cube. Both point clouds, from winter 2012/2013 and winter 2018/2019, were post-processed via the software Cloudcompare, using the fine registration feature to register both clouds in the same project coordinate system.

Supplementary C

Topic III - Tree growth responses to insect induced defoliation

The detailed stand characteristics can be seen in Table C1.

Table C1 Stand characteristics of the 44 plots in Franconia-Bavaria, Germany. The parameters were calculated based on TLS point clouds using 5280 trees (six-tree subplots). The plots are characterized by block/defoliation risk/treatment.

Plot	n (ha^{-1})	dq(cm)	hq(m)	BA (m^2 ha^{-1})	Standing stock (m^3 ha^{-1})
AHC	713	20.2	15.9	27.5	218.3
AHM	339	27.7	19.6	23.5	230.2
ALC	603	20.7	17.2	27.8	239.1
ALM	476	23.5	17.6	30.1	265.0
BHC	314	27.5	18.8	22.5	211.1
BHM	459	26.3	20.6	30.5	313.5
BLC	406	25.1	19.5	23.8	232.4
BLM	622	23.2	20.2	30.3	305.2
DHC	615	23.8	18.2	40.1	364.6
DHM	357	26.5	18.6	27.7	258.0
DLC	753	21.6	17.2	38.9	334.1
DLM	744	19.9	15.7	35.3	276.4
FHC	243	31.1	21.2	22.7	240.3
FHM	467	25.1	19.0	36.4	345.8
FLC	200	40.9	26.8	27.8	373.3
FLM	244	36.4	24.4	29.0	353.0
GHC	438	23.8	16.0	28.8	230.5
GHM	261	33.5	21.8	27.7	301.0
GLC	513	22.0	17.2	30.1	258.3
GLM	632	19.4	16.1	29.0	233.3
HHC	437	29.1	22.0	33.6	369.5
HHM	528	24.9	19.1	31.5	300.7
HLC	503	26.5	21.0	29.0	305.2
HLM	640	24.7	20.2	34.3	346.3

JHC	552	25.5	19.8	35.2	348.4
JHM	718	20.8	19.0	29.7	281.3
JLC	382	26.7	22.1	25.8	284.8
JLM	294	31.7	22.3	31.9	356.5
MHC	512	27.2	21.2	41.7	443.0
MHM	323	30.2	22.1	28.7	317.7
MLC	503	27.7	20.7	39.1	404.8
MLM	369	30.2	19.5	35.1	342.2
NHC	475	25.0	17.8	28.6	254.4
NHM	359	25.6	18.2	25.1	228.1
NLC	433	25.1	18.1	30.1	272.5
NLM	293	29.1	19.9	24.9	247.1
OHC	394	27.0	18.5	29.0	267.1
OHM	672	23.2	17.1	36.1	309.2
OLC	214	33.9	23.2	23.8	275.7
OLM	190	33.3	22.4	20.5	230.5
SHC	296	31.7	21.5	32.6	349.7
SHM	325	28.6	20.8	30.1	313.0
SLC	312	30.1	23.3	26.9	313.6
SLM	298	29.2	23.2	26.3	305.4

Note: n, number of trees; dq, quadratic mean diameter; hq, height corresponding to dq; BA, basal area.

Defoliation risk index (Leroy et al. 2021)

The defoliation risk index (DRI) was calculated as:

$$DRI = \frac{MEM}{CEM_c}$$

MEM is the average number of egg masses per stem, while CEMc is the corrected critical egg-mass density for the focal survey transect. Stands with a defoliation risk index > 1 had a high risk of defoliation, while a defoliation risk index < 0.5 was considered low risk. The results

were extrapolated to the surrounding areas in order to identify candidate sites for the experiment, i.e., stands with high DRI (> 1) and low DRI (0.5) that were close enough to one another to be grouped into experimental blocks (maximum inter-plot distance within-block of 10 km).

TLS procedure of data acquisition and parameter extraction

1. Scanner configuration and settings

The RIEGL VZ-400i (RIEGL 2019) laser measurement system was used. An overview of the main scanner characteristics is provided in Table C2.

Table C2 - Overview of the RIEGL VZ-400i (RIEGL 2019), summarizing the main characteristics.

Laser Measurement System (LMS)		RIEGL VZ-400i
Range[1)]	m	800
Effective measurement rate[2)]	meas./s	500000
Accuracy[3)4)]	mm	5
Precision[4)5)]	mm	3
Vertical field of view	°	100
Pulse mode		multiple target capability
Registration		automatic
Laser beam divergence	Mrad[6)]	0.35

1) Typical values for average conditions. Maximum range is specified for flat targets with size in excess of the laser beam diameter, perpendicular angle of incidence, and for atmospheric visibility of 23 km. In bright sunlight, the max. range is shorter than under overcast sky.

2) Rounded values.

3) Accuracy is the degree of conformity of a measured quantity to its actual (true) value.

4) One sigma at 100 m range under RIEGL test conditions.

5) Precision, also called reproducibility or repeatability, is the degree to which further measurements show.

6) Measured at the 1/e2 points. 0.25/0.35 mrad corresponds to an increase of 25/35 mm of beam diameter.

A laser pulse repetition rate of 1200 kHz was used. One horizontal 360° scan was performed for each scan position with a 100° vertical field of view. The horizontal angular resolution was set to 0.04°, which in my practical experience, achieves a reasonable trade-off between scan-time (45 seconds per scan) and the risk of disturbances due to tree movement through wind.

Due to the angular measurement scheme of the scanner, which operates from the ground, the point density naturally decreases towards the top of the canopy. Furthermore, the laser beam is usually unable to penetrate tree compartments in order to perform measurements behind obstacles. These two effects result in rather sparse measurement densities in the upper crown and stem regions, especially if the crown parts near the scanner are dense (Hilker et al. 2010). Using the pulsed time-of-flight method for laser range measurements, the RIEGL LMS VZ-400i determines the range to all targets with which a single laser pulse interacts ("multi-target capability"). Depending on the measurement program used, the maximum number of targets that can be detected varies. The RIEGL LMS VZ-400i can generate 4 – 15 points per laser beam.

2. Data post-processing

The focus was not on three-dimensional tree features. Instead, the crown target variables (leaf area and crown perforation) were two-dimensional to take into account that not every individual leaf within the crown could be scanned. This was done to exclude errors occurring in the three-dimensional analysis due to non-scanned areas of the upper crown region, respectively. Using the software RiSCAN PRO version 2.0.2 (http://www.riegl.com/products/software-packages/riscan-pro/), all scan positions per plot were co-registered. The new automatic registration of the LMS VZ-400i was used so that artificial reference targets were no longer needed. Automatic registration and filtering were performed using the software RiSCAN PRO version 2.8.2.

3. Tree detection and isolation

To detect individual-tree positions, the density-based spatial clustering algorithm with noise (dbscan) function in the dbscan package of R was used (Hahsler and Piekenbrock 2017). The function relied on a density-based notion of clusters, which was designed to discover clusters of arbitrary shape (Ester et al. 1996). Only the x and y axes were used as input data, thereby pushing all points belonging to the z-axis to one height level. The consequence was a higher point density per tree stem. Now dbscan is automatically able to find each tree as a cluster. This means that each recognized cluster (stem) now received a unique number and could be processed individually. Additionally, non-vertically grown trees were detected at the lower part of the stem. Ground points were recognized by dbscan as noise points because of their horizontal structure in contrast to the vertically grown stems. For each stem cluster, stem base points were determined. The median values of the x and y coordinates and the minimum values of the z-axis of the stems were calculated. The stem base points now serve to extract the original

points of the entire tree. The isolation of each single tree from the TLS point cloud was performed using the dbscan algorithm within the R programming environment (R Core Team 2016). With the application of dbscan, the entire point cloud was classified into clusters. Now each cluster is individually queried, which stem base cluster is closest in distance and whether this distance is close enough to be classified as associated points. After this step, each tree was visually checked for completeness. If necessary, unrecognised tree parts were added manually, and artifacts that did not belong to the tree were removed using the software RiSCAN PRO (http://www.riegl.com/products/software-packages/riscan-pro/).

4. Tree parameter extraction

The total tree height is calculated by determining the z-axis minimum and maximum points of the isolated tree. The minimum value is subtracted from the maximum value, and the output is the height. Wang et al. (2019) reported that TLS underestimated the height of big trees, which may be due to occlusion of crown and stem parts. The occlusion problem might be mainly resolved by choosing a sufficient number of different scan positions. On the other hand, TLS height measurements on Norway spruce trees in forest stands that covered a broad density range were found to be more accurate than common height measurements with the Vertex, a hand-held device based on the trigonometrical principle (Jacobs et al. 2020). Regarding this study, the total tree heights were obtained from the pointclouds in a leaf-off condition in winter. The number of scan positions per plot varied from 80 to 110 depending on stand density. Therefore, the occlusion problem should be reduced to an absolute minimum. The procedure applied for diameter calculation was introduced in Jacobs et al. (2020).